



<https://theses.gla.ac.uk/>

Theses digitisation:

<https://www.gla.ac.uk/myglasgow/research/enlighten/theses/digitisation/>

This is a digitised version of the original print thesis.

Copyright and moral rights for this work are retained by the author

A copy can be downloaded for personal non-commercial research or study, without prior permission or charge

This work cannot be reproduced or quoted extensively from without first obtaining permission in writing from the author

The content must not be changed in any way or sold commercially in any format or medium without the formal permission of the author

When referring to this work, full bibliographic details including the author, title, awarding institution and date of the thesis must be given

Enlighten: Theses

<https://theses.gla.ac.uk/>
research-enlighten@glasgow.ac.uk

**Structure and Function Studies of the
Filarial Nematode Excretory-
Secretory Glycoprotein ES-62.**

by

Claire Jennifer Ackerman



**UNIVERSITY
of
GLASGOW**

A thesis submitted for the degree of Doctor of Philosophy in
The Faculty of Science, University of Glasgow

ProQuest Number: 10390632

All rights reserved

INFORMATION TO ALL USERS

The quality of this reproduction is dependent upon the quality of the copy submitted.

In the unlikely event that the author did not send a complete manuscript and there are missing pages, these will be noted. Also, if material had to be removed, a note will indicate the deletion.



ProQuest 10390632

Published by ProQuest LLC (2017). Copyright of the Dissertation is held by the Author.

All rights reserved.

This work is protected against unauthorized copying under Title 17, United States Code
Microform Edition © ProQuest LLC.

ProQuest LLC.
789 East Eisenhower Parkway
P.O. Box 1346
Ann Arbor, MI 48106 – 1346



12877

copy. 2.

Declaration

This thesis has been written in accordance with the University of Glasgow regulations, has not been presented for a degree at any other university and is original except where indicated otherwise by reference in the text. The work contained within is the author's own except where work was done in collaboration as indicated.

© Claire Jennifer Ackerman; 3rd September 2002

Signed

Date

.....

~~03.09.02~~

Claire Jennifer Ackerman

03.09.02

Abstract

ES-62 is a filarial nematode excretory secretory glycoprotein of mass 57.8 kDa, from the rodent filarial nematode *Acanthocheilonema viteae*. ES-62 has been shown to possess immunomodulatory capabilities, some of which can be attributed to the phosphorylcholine moieties that are attached to certain of the carbohydrate chains of ES-62. Studies of the effects of ES-62 on B lymphocytes have shown that ES-62 downregulates B lymphocyte activation by selectively targeting protein kinases, such as ErkMAPKinase, downstream of the B cell receptor resulting in immunosuppression of the host immune system. ES-62 has been shown to have a similar effect in T lymphocytes.

This thesis describes the search for structural information about ES-62. Three main techniques were employed to characterise the low resolution structure of ES-62; bioinformatics, analytical ultracentrifugation (AUC) and small angle X-ray scattering (SAXS). Bioinformatics techniques identified six proteins homologous to ES-62 on the basis of primary structure and six proteins homologous on the basis of secondary structure. Homology modelling of ES-62 in its entirety was not possible due to a lack of structural information about the six proteins homologous to ES-62 on the basis of amino acid sequence. However, residues 252-343 of ES-62 were modelled due to the homology of this region with residues 74-168 of a leucyl aminopeptidase from *Aeromonas proteolytica* for which the structure is known.

AUC and SAXS techniques demonstrated that ES-62 exists mainly in a tetrameric state and is slightly elongated in structure. A low resolution structure of ES-62 was also obtained using DAMMIN (Svergun, 1999), a computer program which allows the *ab initio* determination of a three-dimensional structure from the small angle scattering curve of a protein.

In addition, this thesis describes the establishment of two recombinant ES-62 expression systems, one of which was unsuccessful due to the aggregation of the expressed protein and the other, while producing rES-62, was contaminated by the presence of a compound absorbing at 260 nm resulting in the rES-62 produced being unsuitable for biochemical or biophysical studies.

The search for the receptor through which ES-62 interacts with cells and the fate of ES-62 following this interaction are also discussed. These studies demonstrate that ES-62 binds to specific proteins on the surface of different immune system cells but unfortunately attempts to identify these proteins have not so far yielded a definitive answer. ES-62 has also been shown to locate to both the nucleus and cytoplasm following interaction with cells and appears to be present in different forms in these two locations. This demonstrates that ES-62 is internalised following receptor binding and may induce some of its immunomodulatory effects through interactions with intracellular proteins. Its presence in the nucleus of cells could explain the modulation of transcription factors shown to occur in B lymphocytes following exposure to ES-62.

Acknowledgements

I would like to thank a number of people for their help and assistance throughout my PhD.

I thank both my supervisors; Dr Olwyn Byron and Dr Maggie Harnett for all their enthusiasm, helpful comments and never ending optimism during the course of this PhD. I am also indebted to Dr W. Harnett and his lab at Strathclyde University, especially Dawn Rose and Dr Katrina Houston for supplying the ES-62 and providing much assistance in the development of a purification strategy. I would also like to thank Johanne Matheson in Dr W. Cushley's lab for all her help in setting up a baculovirus expression system. My thanks go also to Dr Dmitri Svergun, Dr Michel Koch and Dr Günter Grossmann for their assistance in small X-ray scattering studies. In addition, I would like to thank Dr Sharon Kelly for performing the circular dichroism experiments reported herein. Further, I would like to extend my thanks to Lisa McIver of Edinburgh University for assistance in performing the inductively coupled plasma atomic emission spectroscopy.

My thanks go also to all the members of my lab; Nithin Rai, Sandra Scatter, Kathy Watson, Catriona Moss, Derek Blair, Caroline Lord, Helen Goodridge, Elad Katz, Stephen Gauld and especially Maureen Deehan and Kirsty Brown for all their patience in listening to wedding chat, helpful advice and for making the last three years fun.

Finally I would like to thank my family, my mum and dad for all the love and support they have always given me and for always believing in me. My (little !) brother Graham for making me laugh and being my big brother on more than one occasion and my husband, Russell, for all his love, patience and support without which I would have given up long ago.

Abbreviations

APC – Antigen presenting cell

APOC – African programme for onchocerciasis control

AUC – Analytical ultracentrifuge

BcR – B cell receptor

BSA – Bovine serum albumin

BSS – Balance salt solution

CTD – Control of tropical disease

CD - Circular dichroism

CFA – Circulating antigen

DAG - Diacylglycerol

DC – Dendritic cell

DEC - Diethylcarbamazine

dMM - Deoxymannojirimycin

DNA – Deoxyribonucleic acid

DNase - Deoxyribonuclease

dNTP – Deoxynucleotide triphosphate

DTT - Dithiothreitol

EDTA – Ethylene diamine tetra acetate

EGTA – Ethylene glycol-bis (β -aminoethyl ether) N, N, N', N'-tetraacetic acid

ELISA – Enzyme-linked immunosorbent assay

EMSA – Electromobility shift assay

ES – Excretory-secretory

EST – Expressed sequence tag

F_b – Buoyant force

F_f – Frictional force

FITC – Fluorescein isothiocyanate

F_s – Sedimenting force

GAP – GTPase activating protein

GlcNAc – N-acetyl glucosamine

HEPES – N-[2-hydroxyethyl]piperazine-N'ethanesulfonic acid

ICP-AES – Inductively coupled plasma atomic emission spectroscopy

IEF – Isoelectric focusing

IFN – Interferon

Ig - Immunoglobulin

IKK - I- κ B kinase

IL - Interleukin

IP₃ – Inositol triphosphate

IPTG – Isopropyl- β -D-thiogalactoside

IRAK - IL-1 Receptor associated kinase

ITAM – Immunoreceptor tyrosine-based activation motif

JNK - Jun N-terminal kinase

K_a – Association constant

K_d – Dissociation constant

LBP – LPS binding protein

DDAO – Lauryldimethylamine oxide

LPS - Lipopolysaccharide

mAb – Monoclonal antigen

MAP – Mitogen activated protein

MAPK – Mitogen activated protein kinase

MAPKK – MAP kinase kinase

mf - Microfilariae

MHC – Major histocompatibility complex

MIF – Macrophage inhibitory factor

mIg – Membrane immunoglobulin

MKK – MAP kinase kinase

MOI – Multiplicity of infection

M_{w, app} – Apparent whole-cell weight-average molecular mass

NIK - NK- κ B inducing kinase

NK cells – Natural killer cells

NO – Nitric oxide

OCP – Onchocerciasis control programme

OEPA – Onchocerciasis elimination programme in the Americas

PAF – Platelet activating factor

PBS – Phosphate buffered saline
PC – Phosphorylcholine
PCR – Polymerase chain reaction
PKC – Protein kinase C
PLC – Protein lipase C
PMSF – Phenylmethanesulphonylfluoride
PTK – Protein tyrosine kinase
PVDF – polyvinylidene difluoride
Q – Scattering vector
rES-62 – Recombinant ES-62
R_g – Radius of gyration
SAXS – Small angle X-ray scattering
SDS PAGE – Sodium dodecyl sulphate polyacrylamide gel electrophoresis
SE – Sedimentation equilibrium
sIg – Surface immunoglobulin
SOD – Superoxide dismutase
SV – Sedimentation velocity
TAB-1 – TAK-1 binding protein
TAK-1 – TGF- β activating kinase
TcR – T cell receptor
TEMED – N, N, N', N'-tetramethyl-ethylenediamine
TGF – Tumour growth factor
TLR – Toll-like receptor
TNF – Tumour necrosis factor
TRAF-6 – TNF receptor associated factor 6
UV – Ultra violet
W.H.O. – World Health Organisation
X-Gal – 5-bromo-4-chloro-3-indolyl-b-D-galactoside

Table of Contents

ABSTRACT	i
ACKNOWLEDGEMENTS	iii
ABBREVIATIONS	iv
TABLE OF CONTENTS	vii
LIST OF FIGURES	xii
LIST OF TABLES	xvii
LIST OF EQUATIONS	xviii
 1. INTRODUCTION.....	 1
1.1. TROPICAL DISEASES.....	1
1.2. FILARIASIS	3
1.2.1. <i>Lymphatic Filariasis</i>	5
1.1.1.1. Clinical Manifestations.....	7
1.1.1.1.1. Brugian Filariasis.....	7
1.1.1.1.2. Bancroftian Filariasis	8
1.1.2. <i>Onchocerciasis</i>	9
1.1.1.1. Clinical Manifestations.....	10
1.3. FILARIAL ANTIGENS.....	11
1.3.1. <i>Surface Antigens</i>	12
1.3.2. <i>Excretory-Secretory Antigens</i>	13
1.4. FILARIAL NEMATODE MODULATION OF HOST IMMUNE RESPONSE	15
1.1.1. <i>Th1/Th2 Polarisation</i>	17
1.1.2. <i>Antibody Responses</i>	18
1.1.3. <i>Cytokines</i>	18
1.1.4. <i>The Role of Phosphocholine</i>	20
1.1.5. <i>Secondary Effects of Infection with Filarial Parasites</i>	21
1.1.6. <i>Protective Immunity</i>	22
1.5. ACANTHOCEILONEMA VITEAE.....	22
1.6. ES-62.....	24
1.6.1. <i>Biochemical Characteristics of ES-62</i>	24
1.6.2. <i>Effects of ES-62 on the Immune System</i>	30
1.6.3. <i>Mechanism of Immunomodulatory Effects on B cells</i>	31
1.6.3.1. B Cell Signalling.....	31
1.6.1.2. Effects of ES-62 on B Cell Signalling	35
1.6.4. <i>Mechanism of Immunomodulatory Effects on T cells</i>	38
1.6.5. <i>Mechanism of Immunomodulatory Effects on Dendritic and Macrophage Cells</i>	39
1.6.6. <i>Ex Vivo Studies on Effects of ES-62 on Immune System Cells</i>	39

1.7.	APPROACHES TO CONTROL OF FILARIASIS.....	41
1.7.1.	<i>Lymphatic Filariasis</i>	41
1.7.1.1.	Clinical Diagnosis.....	41
1.7.1.2.	Vector Control	43
1.7.1.3.	Chemotherapy	43
1.7.2.	<i>Onchocerciasis</i>	45
1.7.2.1.	Clinical Diagnosis	45
1.7.2.2.	Vector Control	46
1.7.2.3.	Chemotherapy	47
1.8.	AIMS	48
2.	MATERIALS AND METHODS FOR BIOCHEMICAL ANALYSIS AND EXPRESSION SYSTEMS.....	51
2.1.	ISOLATION OF WILD TYPE ES-62.....	51
2.2.	CELL CULTURE.....	51
2.2.1.	<i>SF9 Cell Culture</i>	51
2.2.2.	<i>Culture of Cell Lines</i>	52
2.3.	PCR.....	52
2.3.1.	<i>Primer Design</i>	52
2.3.1.1.	pET 19b.....	53
2.3.1.2.	pAcGP67-B.....	53
2.3.2.	<i>Program Design</i>	54
2.4.	RESTRICTION DIGESTS	55
2.5.	CLONING	57
2.5.1.	<i>Cloning for Initial Sequence Identification</i>	57
2.5.2.	<i>Cloning for Expression in a Bacterial Expression System</i>	57
2.5.2.1.	Ligation.....	57
2.5.2.1.1.	pGEM-T Easy.....	57
2.5.2.1.2.	pET 19b.....	57
2.5.2.2.	Transformation.....	58
2.5.2.2.1.	pGEM-T Easy.....	58
2.5.2.2.2.	pET 19b.....	58
2.5.2.3.	Minipreps.....	59
2.5.2.4.	Glycerol Stocks.....	60
2.5.3.	<i>Cloning for Expression in Insect Expression System</i>	60
2.5.3.1.	Ligation.....	61
2.5.3.1.1.	pGEM-T Easy.....	61
2.5.3.1.2.	pAcGP67-B.....	61
2.5.3.2.	Transformation.....	61
2.5.3.2.1.	pGEM-T Easy.....	61
2.5.3.2.2.	pAcGP67-B.....	61
2.6.	SEQUENCING.....	62
2.7.	HOMOLOGOUS RECOMBINATION.....	63
2.8.	AMPLIFICATION	63
2.9.	PLAQUE ASSAYS	63
2.10.	EXPRESSION OF RECOMBINANT ES-62	64
2.10.1.	<i>Bacterial Expression System</i>	64
2.10.2.	<i>Baculovirus Expression System</i>	66
2.11.	REFOLDING OF INSOLUBLE BACTERIAL RECOMBINANT ES-62.....	67

2.12.	PURIFICATION.....	68
2.12.1.	<i>Affinity Chromatography</i>	68
2.12.2.	<i>Ion Exchange</i>	70
2.12.3.	<i>Gel Filtration</i>	70
2.12.4.	<i>Filtration</i>	71
2.13.	AGAROSE GEL ELECTROPHORESIS.....	72
2.14.	SDS POLYACRYLAMIDE GEL ELECTROPHORESIS (SDS-PAGE).....	72
2.15.	POLYACRYLAMIDE GEL ELECTROPHORESIS.....	72
2.16.	WESTERN BLOTTING.....	73
2.16.1.	<i>Antibodies</i>	73
2.17.	FAR WESTERN BLOTTING.....	74
2.18.	SLOT BLOTTING.....	74
2.19.	GEL STAINING.....	74
2.19.1.	<i>Silver Stain</i>	75
2.19.2.	<i>Zinc Stain</i>	75
2.19.3.	<i>Coomassie Stain</i>	75
2.20.	PREPARATION OF SPLENIC MONONUCLEAR CELLS.....	76
2.21.	PREPARATION OF SPLENIC B CELLS.....	76
2.22.	CELL COUNTING.....	77
2.23.	PREPARATION OF WHOLE CELL LYSATES.....	77
2.24.	BIOTINYLATION OF CELLS.....	77
2.25.	PREPARATION OF BIOTINYLATED CELLULAR MEMBRANES.....	78
2.26.	PREPARATION OF CELLULAR CYTOSOLIC & NUCLEAR FRACTIONS....	78
2.27.	SYNTHETIC OLIGONUCLEOTIDE DNA LABELLING.....	79
2.28.	ELECTRO-MOBILITY SHIFT ASSAY (EMSA).....	79
2.29.	INCUBATION OF CELLS WITH NATIVE AND RADIOLABELLED NATIVE ES-62.....	80
2.30.	IMMUNOPRECIPITATION WITH A FITC CONJUGATE OF ES-62.....	80
2.31.	CIRCULAR DICHROISM.....	81
2.32.	INDUCTIVELY COUPLED PLASMA ATOMIC EMISSION SPECTROSCOPY (ICP-AES).....	81
2.33.	DETERMINATION OF THE ISOELECTRIC POINT OF ES-62.....	82
2.34.	MONOMERISATION OF WILD TYPE ES-62.....	82
2.35.	CALCULATION OF THE EXTINCTION COEFFICIENT FOR ES-62.....	83
2.36.	SPECTROSCOPY OF BSA AND BSA CONJUGATED TO PC.....	83
2.37.	SUPPLIERS.....	84
3.	BIOINFORMATICS	86
3.1.	IDENTIFICATION OF HOMOLOGOUS PROTEINS.....	88
3.1.1.	<i>Primary Sequence Homology</i>	88
3.1.2.	<i>Secondary Structure Homology</i>	89
3.2.	SECONDARY STRUCTURE PREDICTION.....	92
3.2.1.	<i>Jpred</i>	92
3.2.2.	<i>PIID</i>	95
3.2.3.	<i>Circular Dichroism</i>	95
3.3.	PREDICTION OF THE SPATIAL ORIENTATION OF SECONDARY STRUCTURE ELEMENTS.....	96
3.3.1.	<i>TOPS</i>	96
3.3.2.	<i>Plotcorr</i>	97

3.4.	TERTIARY STRUCTURE PREDICTION.....	99
3.4.1.	SWISS-MODEL.....	99
3.4.2.	DRAGON.....	100
3.5.	RESULTS.....	103
3.5.1.	Primary Sequence Analysis.....	103
3.5.1.1.	Motif Searches.....	105
3.5.2.	Secondary Structure Homology.....	107
3.5.2.1.	sss_align.....	107
3.5.3.	Secondary Structure Prediction.....	109
3.5.4.	Experimental Determination of Secondary Structure Content...	114
3.5.5.	Spatial Orientation of Secondary Structure Elements.....	115
3.5.6.	Tertiary Structure Prediction.....	117
3.5.6.1.	DRAGON.....	117
3.5.6.2.	SWISS-MODEL.....	120
3.6.	DISCUSSION.....	122
3.6.1.	Secondary Structure.....	127
4.	STRUCTURAL STUDIES ON NATIVE ES-62.....	135
4.1.	ANALYTICAL ULTRACENTRIFUGATION (AUC).....	136
4.1.1.	Sedimentation Equilibrium Analysis.....	139
4.1.1.1.	Data Analysis.....	140
4.1.2.	Sedimentation Velocity Experimentation.....	141
4.1.2.1.	Data Analysis.....	142
4.1.3.	The Analytical Ultracentrifuge.....	142
4.1.4.	Analytical Ultracentrifugation of ES-62.....	147
4.1.5.	Results and Discussion.....	151
4.1.5.1.	Sedimentation Equilibrium.....	151
4.1.5.2.	Sedimentation Velocity.....	158
4.2.	SMALL ANGLE X-RAY SCATTERING.....	160
4.2.1.	Scattering Theory.....	161
4.2.2.	Synchrotron Radiation.....	164
4.2.3.	Detector and Camera.....	165
4.2.4.	Data Analysis.....	165
4.2.5.	Results and Discussion.....	167
4.3.	STRUCTURAL MODELLING.....	170
4.3.1.	DALAI.....	170
4.3.2.	DAMMIN.....	172
5.	EXPRESSION AND PURIFICATION OF RECOMBINANT ES-62.....	178
5.1.	EXPRESSION IN A BACTERIAL SYSTEM.....	179
5.1.1.	Cloning, Ligation and Transformation.....	181
5.1.2.	Sequencing of the ES-62 Insert.....	186
5.1.3.	Expression.....	187
5.1.4.	Refolding.....	191
5.1.4.1.	Dialysis Temperature.....	194
5.1.4.2.	Buffer Constituents.....	194
5.1.4.3.	Denaturing Agents.....	195
5.1.4.4.	Protein Concentration.....	196
5.1.5.	Purification using Affinity Chromatography.....	196

5.2.	EXPRESSION IN A BACULOVIRUS SYSTEM.....	200
5.2.1.	<i>Cloning, Ligation and Transformation</i>	202
5.2.2.	<i>Sequencing of the ES-62 Insert</i>	204
5.2.3.	<i>Optimisation of Infection</i>	204
5.2.4.	<i>Purification</i>	206
5.2.4.1.	<i>Ion Exchange</i>	206
5.2.4.2.	<i>Gel Filtration</i>	209
5.2.4.3.	<i>Filtration</i>	214
5.2.5.	<i>Testing Recombinant ES-62</i>	220
5.3.	CONCLUSIONS.....	221
6.	MAMMALIAN CELL RESPONSE TO ES-62	225
6.1.	PLATELET ACTIVATING FACTOR RECEPTOR	229
6.2.	TOLL-LIKE RECEPTORS	231
6.3.	RESULTS.....	235
6.3.1.	<i>Receptor Binding</i>	235
6.3.1.1.	<i>Integrins</i>	244
6.3.1.2.	<i>Toll-Like Receptors</i>	248
6.3.2.	<i>ES-62 Effects on Erk, JNK and p38</i>	251
6.3.3.	<i>ES-62 Modulates Transcription Factor Activity</i>	253
6.3.4.	<i>Subcellular Localisation</i>	258
6.4.	DISCUSSION.....	265
7.	CONCLUSIONS	269
7.1.	A PROPOSED MECHANISM OF ACTION OF ES-62.....	270
7.1.1.	<i>Tetrameric Nature of ES-62</i>	270
7.1.2.	<i>Identification of the Receptor of ES-62</i>	271
7.1.3.	<i>The Fate of ES-62 Following Receptor Binding</i>	272
7.2.	FUTURE WORK	277
8.	REFERENCES.....	279
APPENDIX 1.....	307	
APPENDIX 2.....	309	
APPENDIX 3.....	315	

List of Figures

FIGURE 1-1: CAUSES OF DEATH IN THE DEVELOPED AND DEVELOPING WORLD.....	2
FIGURE 1-2: WORLDWIDE PREVALENCE OF LYMPHATIC FILARIASIS	5
FIGURE 1-3: LIFECYCLE OF PARASITES RESPONSIBLE FOR LYMPHATIC FILARIASIS OR ONCHOCERCIASIS.	6
FIGURE 1-4: SWELLING OF THE LIMBS AND MALE GENITALIA IN LYMPHATIC FILARIASIS	8
FIGURE 1-5: PREVALENCE OF ONCHOCERCIASIS IN AFRICA.....	9
FIGURE 1-6: DNA AND DERIVED AMINO ACID SEQUENCE OF ES-62.....	27
FIGURE 1-7: THE 3 CLASSES OF N-GLYCAN STRUCTURES IDENTIFIED ON ES-62.	28
FIGURE 1-8: INHIBITION OF α -MANNOSIDASE I BY (dMM).....	29
FIGURE 1-9: THE KENNEDY PATHWAY	30
FIGURE 1-10: THE B CELL RECEPTOR WITH ITS ACCESSORY MOLECULES.....	32
FIGURE 1-11: THE B CELL RECEPTOR AND ITS DOWNSTREAM SIGNALLING PATHWAYS.	34
FIGURE 1-12: ABORTIVE ACTIVATION AND BCR DESENSITISATION BY ES-62.....	36
FIGURE 3-1: OUTPUT SCREEN FROM PLOT CORR.	98
FIGURE 3-2: MULTIPLE ALIGNMENT OF ES-62.....	104
FIGURE 3-3: DNA AND AMINO ACID SEQUENCE OF ES-62.....	106
FIGURE 3-4: THEORETICAL SCATTERING CURVES.....	109
FIGURE 3-5: JPRED SECONDARY STRUCTURE PREDICTION FOR ES-62.....	113
FIGURE 3-6: A FAR - UV CIRCULAR DICHROISM SPECTRUM FOR ES-62	114
FIGURE 3-7: TOPS CARTOON FOR CHAIN B OF THE CARBON MONOXIDE DEHYDROGENASE FROM <i>PSEUDOMONAS CARBOXYDOFORANS</i>	116
FIGURE 3-8: 3-DIMENSIONAL MODELS OF RESIDUES 252-343 OF ES-62.....	117
FIGURE 3-9: PDB FILES OF THE OUTPUTS FROM MULTIPLE ITERATIONS OF DRAGON MODELLING OF ES-62 IN ITS ENTIRETY.	118
FIGURE 3-10: HIGHEST RANKED ES-62 MODEL GENERATED BY DRAGON.....	120

FIGURE 3-11: MULTIPLE ALIGNMENTS OF ES-62 AND THE SIX HOMOLOGOUS PROTEINS IDENTIFIED BY PSI-BLAST	123
FIGURE 3-12: PHYLOGENETIC TREE OF ES-62	124
FIGURE 3-13: ALIGNMENT OF ES-62 WITH HOMOLOGOUS PROTEINS.....	129
FIGURE 3-14: SEQUENCE ALIGNMENT OF ES-62 WITH THE LEUCYL AMINOPEPTIDASE FROM <i>A. PROTEOLYTICA</i>	132
FIGURE 3-15: MODELS OF RESIDUES 74-168 OF THE LEUCYL AMINOPEPTIDASE FROM <i>A. PROTEOLYTICA</i> AND RESIDUES 252-343 OF ES-62	133
FIGURE 4-1: THE THREE FORCES ACTING ON A SOLUTE PARTICLE OF MASS M.....	137
FIGURE 4-2: A TYPICAL PLOT OF ABSORBANCE AGAINST RADIUS	144
FIGURE 4-3: SCHEMATIC DIAGRAM OF THE OPTICAL SYSTEM OF THE BECKMAN OPTIMA XL-A ANALYTICAL ULTRACENTRIFUGE	145
FIGURE 4-4: EXPLODED VIEW OF AN AUC CELL.	146
FIGURE 4-5: CROSS-SECTIONS OF TWO AND SIX CHANNEL CENTREPIECES.....	147
FIGURE 4-6: OPTIMUM SPEEDS FOR SE RUNS.....	149
FIGURE 4-7: PRIMARY SE DATA FITTED WITH EQUATION 4-8.....	152
FIGURE 4-8: $M_{w, app}$ PLOTTED AS A FUNCTION OF ES-62 MONOMER LOADING CONCENTRATION.....	153
FIGURE 4-9: FITS OF THE DIMER-TETRAMER AND MONOMER-TETRAMER MODEL TO THE SE PRIMARY DATA.....	155
FIGURE 4-10: DISSOCIATION CONSTANT (K_D) OBTAINED FROM FITTING A DIMER- TETRAMER MODEL AND A MONOMER-TETRAMER MODEL.....	157
FIGURE 4-11: SEDIMENTATION COEFFICIENT AS A FUNCTION OF ES-62 MONOMER LOADING CONCENTRATION.	158
FIGURE 4-12: A TYPICAL SOLUTION SCATTERING CURVE.....	162
FIGURE 4-13: DIAGRAMMATIC REPRESENTATION OF A SYNCHROTRON RADIATION SOURCE.....	164
FIGURE 4-14: DIAGRAMMATIC REPRESENTATION OF THE CAMERA SETUP FOR SAXS EXPERIMENTATION.....	165
FIGURE 4-15: SCATTERING CURVE FOR THE MERGED DATA COLLECTED AT CAMERA LENGTHS OF 3.4 AND 1.9 M.	167
FIGURE 4-16: RADIUS OF GYRATION (R_G) OF ES-62	168

FIGURE 4-17: DIAGRAMMATIC OVERVIEW OF DALAI	171
FIGURE 4-18: COMPOSITE SCATTERING PATTERNS FROM ES-62.....	175
FIGURE 4-19: LOW RESOLUTION DUMMY ATOM MODEL OF ES-62	176
FIGURE 5-1: STRATEGY FOR ESTABLISHING BACTERIAL EXPRESSION OF RES-62 .	180
FIGURE 5-2: pBLUESCRIPT VECTOR MAP.....	181
FIGURE 5-3: 1 % AGAROSE GEL SHOWING 1.5 KB PCR PRODUCT.....	182
FIGURE 5-4: pET 19B VECTOR MAP.....	183
FIGURE 5-5: pGEM-T EASY VECTOR MAP	184
FIGURE 5-6: DIAGNOSTIC RESTRICTION DIGEST OF COLONIES OBTAINED FROM THE LIGATION OF pET 19B WITH ES-62 AND SUBSEQUENT TRANSFORMATION INTO NOVABLUCE CELLS.....	185
FIGURE 5-7: AMINO ACID CHANGE FROM ASPARTIC ACID TO GLUTAMIC ACID.....	186
FIGURE 5-8: PRE- AND POST-INDUCTION SAMPLES	188
FIGURE 5-9: THE PELLETT OBTAINED DURING CLARIFICATION, THE WASH THROUGH AND THE ELUATE FROM PURIFICATION OF ES-62	188
FIGURE 5-10: POST INDUCTION SAMPLES OF THE PELLETT AND CELL LYSATE.....	190
FIGURE 5-11: pH STABILITY OF WILD TYPE ES-62.	192
FIGURE 5-12: A TYPICAL AFFINITY PURIFICATION TRACE FROM THE PURIFICATION OF RES-62.....	198
FIGURE 5-13: AFFINITY PURIFICATION OF EXPRESSED RES-62	198
FIGURE 5-14: A TYPICAL AFFINITY PURIFICATION TRACE FROM THE PURIFICATION OF REFOLED RES-62.	199
FIGURE 5-15: BACULOVIRAL EXPRESSION OF ES-62	201
FIGURE 5-16: DIAGNOSTIC RESTRICTION DIGESTS OF pAcGP67-B/ES-62 CONSTRUCTS USING BAM HI AND ECO RI..	202
FIGURE 5-17: pAcGP67-B VECTOR MAP	203
FIGURE 5-18: OPTIMISATION OF INFECTION LEVELS	205
FIGURE 5-19: DETERMINATION OF THE PI OF ES-62.....	207
FIGURE 5-20: FRACTIONS FROM A TYPICAL ANION EXCHANGE PURIFICATION	208
FIGURE 5-21: WILD TYPE ES-62 AND FRACTIONS ELUTED FROM ANION EXCHANGE PURIFICATION OF BACULOVIRALLY PRODUCED RES-62.....	210
FIGURE 5-22: GEL FILTRATION PURIFIED RES-62.....	211
FIGURE 5-23: ANION EXCHANGE AND GEL FILTRATION PURIFIED RES-62.	212

FIGURE 5-24: GEL FILTRATION PURIFIED RES-62.....	213
FIGURE 5-25: FILTRATION PURIFICATION OF RES-62.....	214
FIGURE 5-26: CONDITIONS TESTED FOR BACULOVIRUS EXPRESSION OF RES-62..	216
FIGURE 5-27: INFECTION OF SF9 CELLS WITH RECOMBINANT BACULOVIRUS AT MOIs OF 1 & 10 IN CELL CULTURE MEDIA AT pH 6.2 & 7.....	218
FIGURE 5-28: INFECTION OF SF9 CELLS WITH RECOMBINANT BACULOVIRUS AT MOIs OF 1 & 10 AND AT pH 6.2 & 7.....	219
FIGURE 5-29: RECOGNITION OF rES-62 BY MONOCLONAL ANTI-ES-62.	220
FIGURE 6-1: BIACORE TECHNOLOGY.....	226
FIGURE 6-2: BIACORE ANALYSIS OF THE BINDING OF MEMBRANES OF U937 (MONOCYTIC) CELLS, B CELLS AND JURKAT T CELLS TO ES-62.....	227
FIGURE 6-3: PAF-R STRUCTURE.....	229
FIGURE 6-4: SIGNALLING CASCADE OF TLRs.....	233
FIGURE 6-5: BINDING OF ES-62 TO PROTEINS FROM SPLENIC B CELLS, U937 CELLS AND JURKAT CELLS.....	236
FIGURE 6-6: BINDING OF ES-62 TO PROTEINS FROM WHOLE CELL LYSATES OF SPLENIC B CELLS, WEHI CELLS, DAUDI CELLS, RAMOS CELLS, NALM 6 CELL, 207 CELL, 697 CELL AND REH CELLS.....	239
FIGURE 6-7: THE DEVELOPMENTAL PATHWAY OF B CELLS.....	240
FIGURE 6-8: IMMUNOPRECIPITATION OF BIOTINYLATED MEMBRANE PROTEINS THAT BIND ES-62 FROM U937 MONOCYTIC CELLS AND WEHI-231 IMMATURE B CELL MEMBRANES FRACTIONS.....	242
FIGURE 6-9: EFFECTS OF PHOSPHORYLCHOLINE, FUCOSE, RGDS AND RGES PEPTIDES ON BINDING OF ES-62 TO MEMBRANE PROTEINS FROM WEHI-231 B CELLS.....	247
FIGURE 6-10: POTENTIAL IDENTIFICATION OF THE P82 PROTEIN OF B CELLS THAT BINDS ES-62 AS ONE OR MORE TOLL-LIKE RECEPTORS.....	250
FIGURE 6-11: ES-62 CAUSES AN INITIAL ACTIVATION OF ERK AND JNK FOLLOWED BY A RAPID DEACTIVATION.....	252
FIGURE 6-12: ACTIVATION OF NF κ B AND ITS SUBSEQUENT TRANSLOCATION TO THE NUCLEUS TO INDUCE GENE TRANSCRIPTION.....	254
FIGURE 6-13: EMSA FOR NF κ B OR E ₂ F IN WEHI-231 B CELLS.....	255

FIGURE 6-14: ES-62 STIMULATION OF WEHI-231 B CELLS ALTERS THE LEVELS
OF THE P65 AND P50 SUBUNITS OF NFκB.....256

FIGURE 6-15: ES-62 IS INTERNALISED BY MACROPHAGES FOLLOWING RECEPTOR
BINDING AND IS LOCATED IN BOTH THE NUCLEUS AND CYTOSOL OF
THESE CELLS.....259

FIGURE 6-16: LOCALISATION OF ES-62 IN WEHI-231 B CELLS FOLLOWING
RECEPTOR BINDING.....264

FIGURE 7-1: PROPOSED MECHANISM OF ACTION OF ES-62.....276

List of Tables

TABLE 1-1: CHARACTERISTICS OF THE VARIOUS SPECIES OF FILARIAL NEMATODE ..	4
TABLE 2-1: SEQUENCES OF THE PCR PRIMERS	53
TABLE 2-2: PCR PROTOCOLS	55
TABLE 2-3: GROWTH AND INDUCTION CONDITIONS FOR EXPRESSION TRIALS	65
TABLE 2-4: PROTOCOL FOR AFFINITY PURIFICATION	69
TABLE 2-5: SILVER STAINING PROTOCOL.....	75
TABLE 3-1: SSS_ALIGN PARAMETERS.	90
TABLE 3-2: INPUT FILES AND PARAMETERS FOR DRAGON.....	101
TABLE 3-3: PROTEINS WITH A HIGH DEGREE OF PRIMARY SEQUENCE IDENTITY TO ES-62.....	103
TABLE 3-4: PROTEINS WITH HIGH SECONDARY STRUCTURE IDENTITY TO ES-62 ..	108
TABLE 3-5: SECONDARY STRUCTURE CONTENT OF WILD TYPE ES-62 FROM CD. .	114
TABLE 3-6: PERCENTAGE IDENTITY BETWEEN ES-62 AND THE SIX HOMOLOGOUS PROTEINS IDENTIFIED BY PSI-BLAST.....	125
TABLE 3-7: COMPARISON OF EXPERIMENTALLY DETERMINED SECONDARY STRUCTURE CONTENT OF ES-62 WITH THE PREDICTED SECONDARY STRUCTURE CONTENT.....	130
TABLE 5-1: GROWTH AND INDUCTION CONDITIONS.....	189
TABLE 5-2: ICP-AES RESULTS FOR WILD TYPE ES-62.....	195

List of Equations

EQUATION 4-1: DEFINITION OF THE SEDIMENTATING FORCE, F_s	137
EQUATION 4-2: DEFINITION OF THE BOUYANT FORCE, F_b	137
EQUATION 4-3: DETERMINATION OF THE MASS OF FLUID DISPLACED BY A MOLECULE	138
EQUATION 4-4: DEFINITION OF THE FRICTIONAL FORCE, F_f	138
EQUATION 4-5: ATTAINMENT OF EQUILIBRIUM.....	138
EQUATION 4-6: THE SVEDBURG EQUATION.....	138
EQUATION 4-7: DETERMINATION OF THE MASS OF THE SOLUTE FOR A SINGLE IDEAL NON-ASSOCIATING SPECIES	139
EQUATION 4-8: EQUILIBRIUM DISTRIBUTION OF A SINGLE IDEAL SPECIES	140
EQUATION 4-9: EQUILIBRIUM DISTRIBUTION OF A SELF-ASSOCIATING SYSTEM ...	140
EQUATION 4-10: DETERMINATION OF THE SEDIMENTATION COEFFICIENT.....	141
EQUATION 4-11: CONVERSION OF THE SEDIMENTATION COEFFICIENT TO STANDARD CONDITIONS	142
EQUATION 4-12: DETERMINATION OF THE TIME TAKEN TO REACH EQUILIBRIUM.	143
EQUATION 4-13: CONVERSION OF ASSOCIATION CONSTANTS TO UNITS OF CONCENTRATION.....	156
EQUATION 4-14: DETERMINATION OF THE DISSOCIATION CONSTANT	156
EQUATION 4-15: BRAGG'S LAW	162
EQUATION 4-16: DEFINITION OF THE SCATTERING VECTOR.....	163
EQUATION 4-17: THE DEBYE EQUATION.....	163
EQUATION 4-18: DETERMINATION OF RADIUS OF GYRATION.....	168
EQUATION 4-19: DETERMINATION OF MASS AT INFINITE DILUTION	169
EQUATION 4-20: DETERMINATION OF THE DISCREPANCY OF THE FUNCTION THAT FORMS THE BASIS OF DAMMIN.....	172

1. Introduction

1.1. *Tropical Diseases*

Tropical diseases kill 17.3 million people annually worldwide (W.H.O., 1997) and hinder the development, socially and economically, of the countries affected. Figure 1-1 shows the deaths attributable to tropical diseases compared with those caused by a number of other diseases. The majority of those affected by tropical diseases live in the developing world, where the numbers affected are increasing due to urbanisation and industrialisation, which provide ripe breeding grounds for the vectors of these tropical diseases. However, the developed world is currently facing an increasing risk of infection as international travel makes contact with these diseases increasingly likely.

To aid countries affected by tropical diseases in their fight against infection and in their activities to minimise the suffering of those affected, the World Health Organisation (W.H.O.) has set up the division for Control of Tropical Diseases (CTD). The CTD mandate is to eradicate or control a number of tropical diseases including Chagas disease, lymphatic filariasis, malaria, African trypanosomiasis, leishmaniasis, schistosomiasis, intestinal parasites, dengue and dengue haemorrhagic fever (W.H.O., 1998). In this regard, the CTD has had some success in achieving a limited level of control of many of these diseases. However, the situation regarding infection and disease treatment remains serious.

This thesis focuses on the excretory-secretory protein ES-62, from the filarial parasite *Acanthocheilonema viteae*, a rodent filarial parasite used in the study of human filariasis. Filariasis is one of the few tropical diseases classified as potentially eradicable (W.H.O., 1999b).

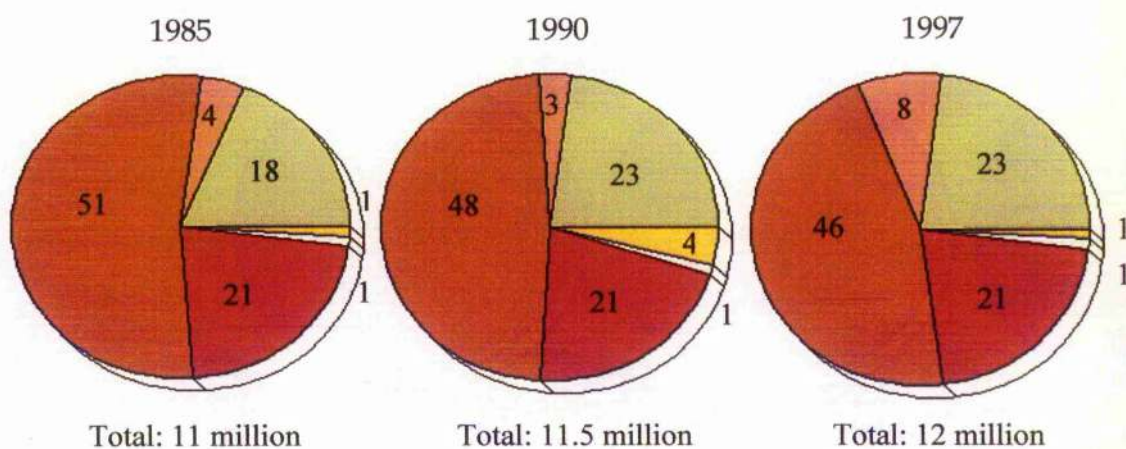
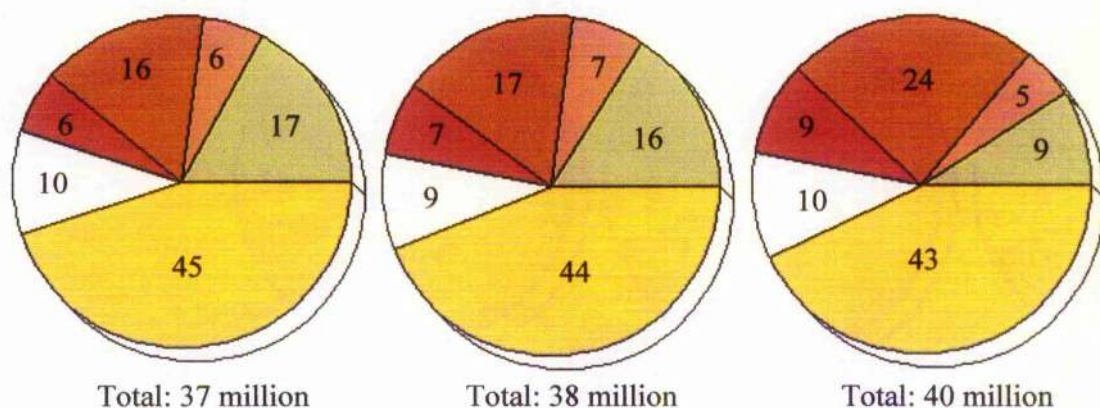
Developed World**Developing World**

Figure 1-1: Causes of death in the developed and developing world in 1985, 1990 and 1997. Deaths classified as due to infectious/parasitic disease (■), perinatal/maternal causes (□), cancer (■), circulatory system diseases (■), respiratory system diseases (■) or other/unknown causes (■). Source: World Health Organisation; <http://www.who.org/whr>

1.2. Filariasis

Filariasis is the name given to the range of diseases caused by filarial nematodes. There are eight distinct species of filarial nematode which give rise to filariasis in humans; *Wuchereria bancrofti*, *Brugia malayi*, *Brugia timori*, *Onchocerca volvulus*, *Loa loa*, *Dipetalonema streptocerca*, *Mansonella ozzardi* and *Mansonella perstans* (Evered *et al.*, 1987). Table 1-1 shows the characteristics of these eight species. Three of these species, *W. bancrofti*, *B. malayi* and *O. volvulus*, are the major causes of morbidity in the tropics (W.H.O., 1995b).

Currently approximately 150 million people demonstrate clinical symptoms of infection with filarial nematodes including skin lesions, elephantiasis and blindness. The clinical manifestations of filarial diseases vary not only between species of filarial nematode, but can also vary between people infected with the same parasite species (Kazura *et al.*, 1993). In addition to those displaying clinical symptoms there are many more people infected who display no clinical symptoms while a further billion people are estimated to be at risk of contracting filarial diseases (W.H.O., 1998). Despite the large numbers of people affected by filariasis there are few effective treatments available for filarial infection and presently no hope for a vaccine.

Human filarial infections demonstrate a number of common features. Firstly, the filarial parasites all result in long term/chronic infection (Vanamail *et al.*, 1996) wherein the adult worms are able to survive and reproduce sexually within the host's lymphatic vessels or tissues for ten years or longer. This is thought to be achieved through immunomodulation of the host immune system. Secondly, the immune response mounted by the host against the parasite is complex. This is due to the chronic nature of infection and also to the multicellular nature of filarial parasites, which gives rise to a vast array of antigens being presented to the host immune system. This complex immune response is believed to be responsible for the majority of the clinical manifestations of filarial diseases and could explain the differences observed in clinical manifestations between people infected with the same parasitic species. Finally, the parasites are incapable of

completing an entire lifecycle within the host; an anthropod intermediate vector is required (Kazura *et al.*, 1993).

Species	Vector	Disease Caused	Symptoms
<i>Wuchereria bancrofti</i>	Mosquitoes: Culex fatigans, Aedes, & Anopheles	Bancroftian filariasis	Fever, lymphangitis, lymphadenitis, lymphocele, abscess formation, elephantiasis
<i>Brugia malayi</i>	Mosquitoes: Mansonia, Anopheles & Aedes	Malayan filariasis	Fever, lymphangitis, lymphadenitis, lymphocele, abscess formation, elephantiasis
<i>Brugia timori</i>	Mosquitoes: Anopheles & Barbistrois	Malayan filariasis	Fever, lymphangitis, lymphadenitis, lymphocele, abscess formation, elephantiasis
<i>Onchocerca volvulus</i>	Black Fly: Simulium	Onchocerciasis	Nodule formation, acute inflammatory response, pruritis, onchodermatitis, blindness, lymphedema
<i>Loa loa</i>	Mango flies: Chrysops	Loiasis	Edema of conjunctiva & lids, localised subcutaneous edema,
<i>Dipetalonema streptocerca</i>	Midges: Culicoides	Dermatitis	Pruritic dermatitis, hypopigmented macules, inguinal adenopathy
<i>Mansonella ozzardi</i>	Midges: Culicoides	Non-pathogenic	Some cases of allergic symptoms, but generally non-pathogenic
<i>Mansonella perstans</i>	Midges: Culicoides	Non-pathogenic	Some cases of allergic symptoms, but generally non-pathogenic

Table 1-1: Characteristics of the various species of filarial nematode that infect humans.

1.2.1. Lymphatic Filariasis

Lymphatic filariasis is attributable to infection with the lymphatic dwelling parasites, *Wuchereria bancrofti*, *Brugia malayi* and *Brugia timori*. Over 120 million people are affected by lymphatic filariasis, 90 % of whom are infected with *W. bancrofti*. Figure 1-2 highlights the areas where lymphatic filariasis is prevalent. Approximately one third of those affected live in India, one third in Africa and the remainder in south-east Asia, the Pacific and the Americas (W.H.O., 1998). Urbanisation in these areas has led to an increase in the number of affected individuals. It is expected that the number of infected individuals will continue to rise due to the continuing rapid and unplanned growth of cities, which creates breeding sites for the mosquitoes that transmit the disease.

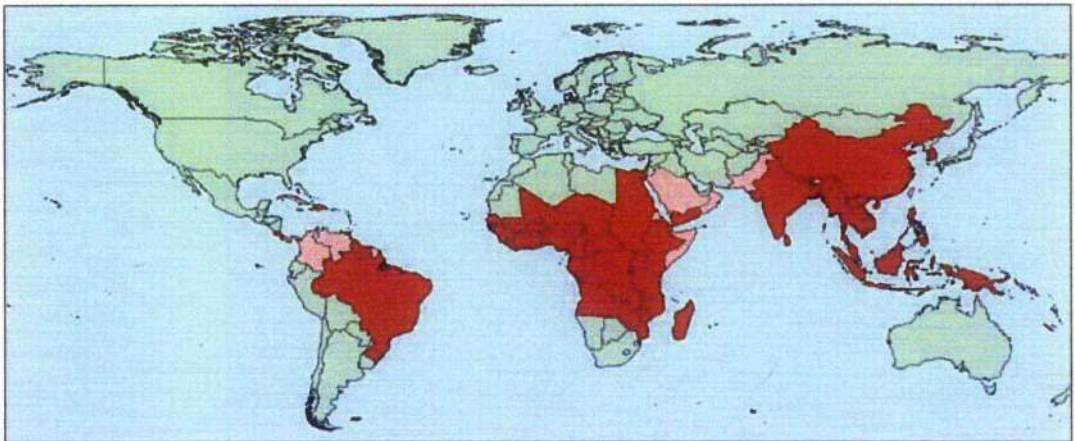


Figure 1-2: Worldwide prevalence of lymphatic filariasis [image from W.H.O. web site, <http://www.who.int/ctd/filariasis/library/countries4.html>]
Red areas show endemic regions, pink areas show areas of uncertain status and green areas show non endemic areas.

Transmission of the parasite species responsible for lymphatic filariasis is achieved via the female mosquitoes of the Anopheles, Aedes, Culex and Mansonia species. These mosquitoes are the anthropod intermediate vector, which is essential for completion of the lifecycle of the parasite and acts to transmit the parasite from one host to another. There are 4 stages of parasite development that occur specifically in either the host or the vector. The final stage of which is the development of adult parasitic worms within the host

(Evered *et al.*, 1987). These adult worms live within the lymphatics of the mammalian host, most frequently within the lymphatics of the lower extremities and are approximately 40-100 mm in length and 0.1-0.3 mm in diameter. Sexual reproduction of the adult worms leads to the release of thousands of microfilariae (mf, first stage larvae or L1) by the female adult worms into the bloodstream of the mammalian host. These microfilariae are approximately 250 μm in length and possess an acellular sheath. The mf can then be ingested via a bloodmeal into the mosquito vector where they exsheath to form the L2 stage of parasitic development and penetrate the midgut of the mosquito. From here they migrate to the thoracic musculature and finally into the mouthparts of the mosquito as third stage larvae (L3). The development from L1 to L3 within the female mosquito takes approximately 10-14 days. The larvae can then be transmitted to another mammalian host when the mosquito takes a bloodmeal. Following transmission to a mammalian host the L3 larvae migrate into the lymphatics where they undergo two further molts to form fourth stage larvae (L4) and adult worms respectively. Sexually mature adult worms appear after 9-12 months (Kazura *et al.*, 1993). A diagrammatic representation of the lifecycle of the parasites responsible is shown in Figure 1-3.

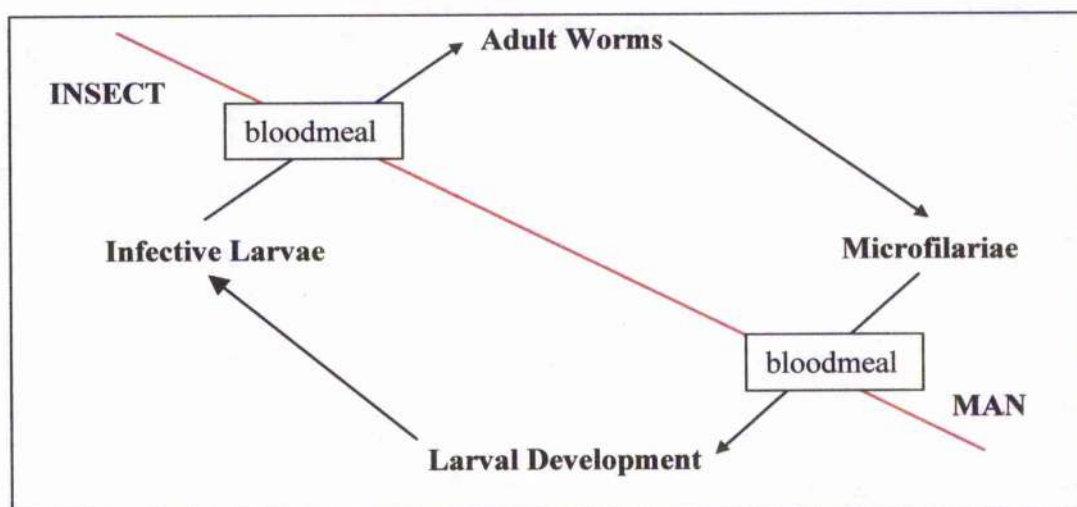


Figure 1-3: Lifecycle of parasites responsible for lymphatic filariasis or onchocerciasis. These constitute three main parasites that infect humans; *W. bancrofti*, *B. malayi* and *O. volvulus*. Insect is the mosquito in the case of lymphatic filariasis and the blackfly in the case of onchocerciasis.

1.2.1.1. Clinical Manifestations

Lymphatic filariasis can be divided into two distinct groups. The first, termed lymphatic filariasis, is caused by adult or developing adult worms in the lymphatics of the host. The second, termed occult filariasis, is caused by host immune hyper-responsiveness to microfilariae. A general pattern of the clinical symptoms showing the sequence of events following infection can be discerned as prepatent period, asymptomatic microfilaraemia and acute and chronic clinical filariasis. The timescale of this sequence depends on the species of parasite with which the individual is infected (Evered *et al.*, 1987). As discussed, three parasites are responsible for causing lymphatic filariasis. Those individuals infected with *Brugia malayi* or *Brugia timori* are classified as suffering from Brugian filariasis while those infected with *Wuchereria bancrofti* suffer from Bancroftian filariasis.

1.2.1.1.1. Brugian Filariasis

The acute clinical manifestations of Brugian filariasis often initiate with lymphadenitis in the inguinal region. This is usually self-healing but can develop into retrograde lymphangitis in which the lymph node becomes infected, spreading to the whole thigh or even limb. This can lead to lymphoedema of the foot and ankle and the infected lymph node may form an abscess and deteriorate into an ulcer. Although these ulcers heal spontaneously they typically leave scarring. For patients infected with *B. timori* the symptoms are as above, but the node affected can move from the inguinal node which is the first to be affected to other lower nodes in subsequent attacks (Evered *et al.*, 1987), (UNDP *et al.*, 1997).

Recurrence of these acute symptoms leads to incomplete resolution of the lymphoedema and the disease progresses to the chronic stage. Chronic clinical manifestations include lymphoedema of the leg below the knee and, less frequently, of the arm below the elbow. The affected limb usually swells to approximately twice its normal size and the skin may become thickened, as shown in Figure 1-4 (a).

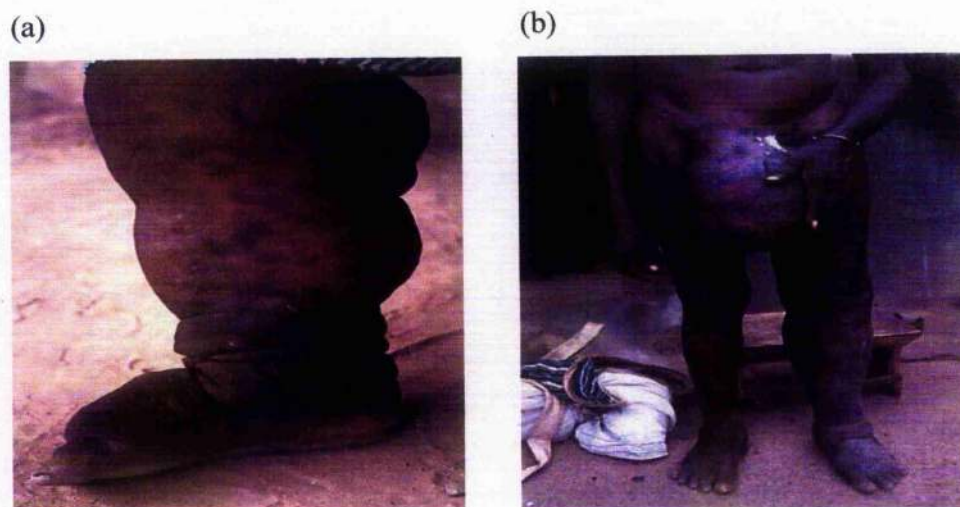


Figure 1-4: Swelling of the limbs (a) and the male genitalia (b) occurs in lymphatic filariasis [images from the W.H.O. web page, TDR image library; <http://www.who.int/tdr/media/image.html>, (a) image number: ID9902948, credit line: WHO/TDR/Crump, (b) image number: ID9902980, credit line: WHO/TDR/Crump]

1.2.1.1.2. Bancroftian Filariasis

The acute phase of bancroftian filariasis is marked by swelling of the male genitalia due to the effects of *W. bancrofti* on the lymphatics of this region. Symptoms include tenderness, pain which may be excruciating and possibly fever. The extent of the swelling of the male genitalia is shown in Figure 1-4 (b).

The chronic phase of bancroftian filariasis occurs when the acute attacks fail to completely heal and in time a hydrocele develops. This can develop further to scrotal elephantiasis, but this is a rare occurrence (Evered *et al.*, 1987; UNDP *et al.*, 1997). Lymphoedema and elephantiasis can also occur in bancroftian filariasis but with less frequency than in brugian filariasis.

The chronic stages of lymphatic filariasis are surprisingly painless. However, the psychological effects are in some ways far worse especially as those severely affected become a burden to their families and community. There is also an

asymptomatic form of lymphatic filariasis, which is characterised by the presence of millions of microfilariae in the bloodstream and adult worms in the lymphatics but no clinical symptoms. However, these outwardly healthy individuals often have kidney and lymphatic damage (UNDP *et al.*, 1997).

1.2.2. Onchocerciasis

Onchocerciasis is an immune-mediated disease caused by the filarial parasite *Onchocerca volvulus*. Onchocerciasis is the world's second major infectious cause of blindness and presents its largest public health problem in Africa, where 99 % of the 20 million people infected worldwide are located and a further 100 million are at risk of infection (W.H.O., 1995a). Figure 1-5 highlights the areas in Africa affected by onchocerciasis.

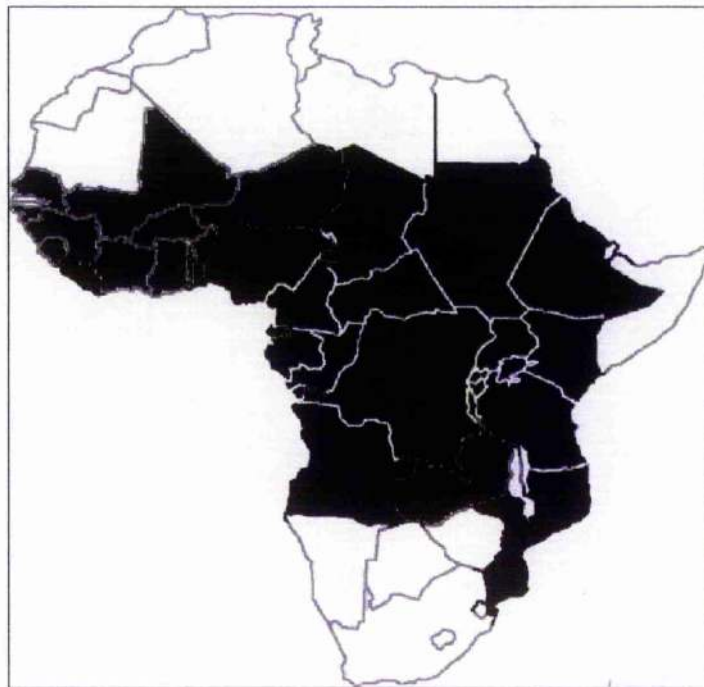


Figure 1-5: Prevalence of onchocerciasis in Africa [image from the W.H.O. web site, <http://www.who.int/ocp/slides/SetE/d0025.htm>, Credit line: OCP/APOC/WHO]

Onchocerciasis is transmitted between mammalian hosts by the female blackfly (*Simulium damnosum* species) which, in a similar way to the mosquitoes responsible for transmitting lymphatic filariasis, requires a bloodmeal after mating. The adult worms of *O. volvulus* when sexually mature form spherical bundles consisting of 2-3 female worms (23-70 mm in length and 275-325 μm in diameter) and 1-2 male worms. These bundles are found in subcutaneous nodules called onchocercomata. Following mating, the female *O. volvulus* worms release millions of microfilariae that migrate out of the nodule through the host tissue and congregate in the dermis of the host. The microfilariae may then be ingested during a bloodmeal by the blackfly. The ingested microfilariae migrate within the vector to the thoracic muscles and mature into infective larvae over the course of approximately 6-8 days. The infective larvae (440-700 μm in length, 12-19 μm in diameter) then migrate to the head of the blackfly where they can be transmitted to a new host when the vector takes a bloodmeal. It takes between 7 and 34 months from infection of the mammalian host with the infective larvae for adult worms to develop and secrete microfilariae. The lifecycle of filarial parasites, including *O. volvulus*, is shown in Figure 1-3 (Kazura *et al.*, 1993).

1.2.2.1. Clinical Manifestations

The clinical manifestations of *O. volvulus* are thought to be associated with the destruction of the microfilariae of *O. volvulus* in the skin and eye tissues. These manifestations include nodule formation, rashes, lesions, intense itching, depigmentation of the skin and lymphadenitis, resulting in hanging groin and genital elephantiasis (Evered *et al.*, 1987). Clinical manifestations arise in individuals 1-3 years after infection with *O. volvulus*. Early stages of onchocerciasis in the skin can be identified by the localisation of inflammatory cells around the adult worms forming an onchocercomata, a fibrous structure that encases the worms, and an increase in dermal fibroblasts and mast cells. The onchocercomata are visible, 0.5 –10 cm in diameter, but rarely cause pain. Later stages of the disease include onchocercal dermatitis. This involves recruitment of inflammatory cells to the dermis where the microfilariae are located and leads to loss of elastic fibres and eventually advanced atrophy of the epidermis. Localised

onchocerciasis (Sowda) can also occur due to a severe inflammatory reaction to the microfilariae. It occurs mostly in young men and consists of an increase in pigmentation of the skin, generally of the legs (Evered *et al.*, 1987).

Onchocerciasis in the ocular tissues follows a similar course with the infiltrate of plasma cells, eosinophils and mast cells followed by vessel dilation and thickening leading to blindness. This occurs most commonly in males, who tend to have heavier infections. Three types of ocular lesions can occur: the first is punctate keratitis (opaqueness of the cornea) which rarely affects vision. The second is sclerosing keratitis, an immune reaction to microfilariae in the cornea, leading to vascularisation of the cornea and blindness. The third is chorioretinitis, a non-granulomatous inflammatory reaction to microfilariae, which also causes blindness (Evered *et al.*, 1987). All of the symptoms mentioned suggest the presence of a chronic inflammatory response to the presence of the parasite in the host tissues and this is why onchocerciasis is believed to be an immune-mediated disease.

1.3. Filarial Antigens

A comprehensive overview of filarial parasitic antigens and the research carried out in this area is given by Harnett & Parkhouse, (1995).

Filarial parasitic antigens, which are very immunogenic, have been classified into three groups; surface antigens, somatic antigens and excretory-secretory antigens (Harnett & Parkhouse, 1995). Although some antigens can be classified into more than one of these groups, most are unique to one. Filarial parasites proceed through several developmental stages on their way to adulthood. The surface antigens vary in their stage specificity - some antigens are only exposed at certain developmental stages whereas others are exposed continually (Harnett & Parkhouse, 1995). The level of expression can also vary with development (Maizels *et al.*, 1983; Phillipp *et al.*, 1980). In addition, the antigens exposed can vary depending on the sex of the parasite (this is the case for *A. viteae* (Baschong, 1985)) and is thought to be due to different environmental

requirements of the different sexes. Study of filarial antigens to determine immunoprophylactic and immunodiagnostic antigens has been confined to surface antigens, which are more viable potential vaccines due to their direct exposure to the immune system. Surface antigens are also more successful in diagnostic assays than somatic and ES antigens as these latter classes of antigen demonstrate cross-reactivity between human filarial species (Caberra *et al.*, 1989; Harnett & Parkhouse, 1995; Phillipp *et al.*, 1984). However, ES antigens, antigenic during infection, are now starting to be considered as an alternative to the more traditional source of vaccine material.

1.3.1. Surface Antigens

Surface molecules of filarial parasites are antigenic during infection. Analysis of these antigens has revealed that some are cross-reactive but usually only between closely related species (Harnett & Parkhouse, 1995; Maizels *et al.*, 1985b). The range of surface antigens on many of the filarial parasites has been identified, but as yet they have not been characterised in terms of function. Surface antigens may be identified by radiolabelling of surface molecules (e.g. via radioiodination) followed by separation of the labelled molecules using sodium dodecyl sulphate polyacrylamide gel electrophoresis (SDS-PAGE) (Harnett & Parkhouse, 1995; Selkirk *et al.*, 1990; Tamashiro *et al.*, 1986). Often one or two main molecular weight species can be identified, but this may be due to the different ways in which the molecules react to the radiolabelling rather than a measure of abundance. Two cloned and sequenced antigens of *O. volvulus* have been screened against the sequence databanks but no match has been found. Hence although screening of sequences of antigens against the databank may be successful in some cases and is a more rapid method of identifying function, in some cases it may be necessary to characterise each individually. In addition to the surface antigens of filarial parasites, various host molecules have also been detected at the parasitic surface (Egwang *et al.*, 1988; Forsyth *et al.*, 1984a; Harnett & Parkhouse, 1995). It is thought that these host molecules may play a role in masking the parasite from the host immune system (Harnett & Parkhouse, 1995). For example, the host protein albumin, found on the surface of blood and

skin microfilariae, is thought to be involved in inhibiting eosinophil peroxidase mediated oxidative damage (Forsyth *et al.*, 1984b).

Some of the surface antigens of filarial parasites have been shown to be glycosylated. This is most often observed in adult parasite surface antigens in comparison with those from microfilariae. The location of expression of the carbohydrate moiety has been found to vary with the sex of the parasite and is only found on the copulatory bell of adult male worms compared to a more general distribution in females (Ortega-Pierres *et al.*, 1986).

1.3.2. Excretory-Secretory Antigens

The excretory-secretory (ES) products of filarial parasites are released by the parasite via the excretory or anal pore, mouth, female reproduction tract or the cuticle (Harnett & Parkhouse, 1995), into the bloodstream of the parasitised host and can be isolated from the blood or urine of an infected individual. ES products are highly antigenic. Similarly to surface antigens, ES antigens are both stage- and sex-specific (Harnett *et al.*, 1986; Parkhouse & Clark, 1983). This stage specificity is demonstrated by many parasites, for example *A. viteae* (Harnett *et al.*, 1989). ES products are now starting to be considered as a potential source of vaccine material. ES products can be identified by SDS-PAGE with 2D electrophoresis yielding the most accurate identification.

Examination of ES products of a range of parasites has revealed a high degree of glycosylation of these products. For example, one ES product from *A. suum* possesses 22 % carbohydrate by mass (Stromberg, 1979). The presence of carbohydrate on these molecules can be demonstrated by chemical analysis, carbohydrate staining using dyes specific for carbohydrate, use of sugar cleavage enzymes or use of biosynthetic labelling of the ES products with [^3H] glucosamine (Harnett *et al.*, 1990; Kwan-Lim *et al.*, 1989; Meghji & Maizels, 1986). Many of the ES products of filarial parasites have also been demonstrated to contain phosphorylcholine using a radioimmunoassay employing two anti-PC monoclonal antibodies, TEPC-15 as capture and Bp1, labelled with [^{125}I], as an

indicator (Harnett *et al.*, 1990). The PC moiety has been shown to be attached to the carbohydrate molecules of the glycosylated ES products although the method of attachment is currently unknown (Harnett *et al.*, 1993; Houston *et al.*, 1997; Houston & Harnett, 1996). A considerable amount of cross-reactivity occurs between species, this is thought to be attributable to PC being a common epitope associated with a large range of parasitic ES products. Carbohydrate is also a common epitope and contributes to the cross-reactivity observed between different species of filarial parasite. Host molecules such as albumin and immunoglobulin have also been identified in the ES products of filarial parasites (Kaushal *et al.*, 1982; Maizels *et al.*, 1985a; Ngu *et al.*, 1981). It is thought that the host molecules may be ingested at some point in the parasitic lifecycle and are then secreted, as they are not needed.

ES products of many filarial parasites have been studied in some detail and to date a function has been determined only for a few of these molecules. These ES products include proteinases that digest proteins, trypsin-like proteins (*A. simplex*) (Matthews, 1982) and collagenases with a metal requirement (*B. malayi* and *O. volvulus*) (Petalanda *et al.*, 1986). The role of the proteinases is thought to be related to tissue penetration and migration (Hinsk & Ivey, 1976; Knox & Kennedy, 1988; Petralanda *et al.*, 1986). This hypothesis is substantiated by the reduced presence or absence of these proteinases in the non-migratory stages of the parasite (Petalanda *et al.*, 1986). Acetylcholinesterase is also secreted by a range of parasitic nematodes. The possible function of this ES product is to interfere with the host immune system by degrading acetylcholine. Acetylcholine increases the release of histamine, which in turn exacerbates inflammatory immune responses, which form part of the Th1 immune response. Degradation of acetylcholine by parasitic products would lead to a decrease in the levels of histamine and thus a decrease in the inflammatory response which forms part of the Th1 immune response (Rang *et al.*, 1998). This may provide a survival advantage to the parasite by promoting the bias of the host immune response to parasite to a Th2 response. People with chronic parasitic infection demonstrate a Th2 bias in their immune response (Allen & Macdonald, 1998; Stewart *et al.*, 1999). Other functions of ES products identified include superoxide dismutase,

to detoxify the contents of neutrophils and eosinophil granules (Rhoads, 1983; Walter *et al.*, 1987), interaction with complement to aid parasite survival by fixing complement at a site distant from the parasite (Staniunas & Hammerberg, 1982), release of a chemotactic agent to attract neutrophils away from the parasites (Bruschi *et al.*, 1989; Harnett & Parkhouse, 1995) and interference with the lymphocytic response of the host immune system inhibiting responses to antigen (Faubert, 1976; Harnett & Harnett, 1999a). The role of ES products in immunomodulation of the host immune response can be further highlighted by their suppressive effects on T cell proliferation (Allen & Macdonald, 1998; Lal *et al.*, 1990). Peripheral blood lymphocytes from people infected with filarial nematodes are known not to proliferate in response to parasitic antigen, while proliferation responses to other antigens are unimpaired (Allen & Macdonald, 1998; Nutman *et al.*, 1987a). Injection of ES products into mice results in a similar decrease in T cell proliferation thus suggesting that it is the ES products that induce this effect in the case of filarial infection (Allen & Macdonald, 1998).

1.4. Filarial Nematode Modulation of the Host Immune Response

Immune responses to pathogens are mediated by a range of immune system cells. These cells originate from pluripotent haemopoietic stem cells in the bone marrow and divide to produce lymphoid stem cells and myeloid stem cells. The lymphoid stem cells give rise to T and B lymphocytes which are distinguishable by their site of differentiation and their antigen receptors (Janeway & Travers, 1996).

T cells, which differentiate in the thymus, are responsible for the cellular arm of the immune system. The activation of these cells in the draining lymphoid organs forms the first step in the adaptive immune response. This activation takes the form of the recognition of a specific antigen:MHC complex which leads to the production of armed antigen specific effector T cells (Janeway & Travers, 1996). During the initial activation of naïve CD4 T cells, differentiation occurs leading

to the cells becoming either Th1, inflammatory, effector cells or Th2, helper, effector cells. This differentiation is influenced greatly by the cytokines present at the early stages of this immune response (Janeway & Travers, 1996). The differing capabilities for pathogens to interact with the different cells of the innate immune response influences the cytokines present and thus can influence the form that the adaptive immune response takes. IL-12 and IFN γ , produced by macrophages and NK cells in the early stages of immune responses, promote Th1 cell differentiation. In addition, IFN γ inhibits proliferation of Th2 cells. IL-4 and IL-10, produced by, amongst others, mast cells and macrophages and B1 B cells, lead to the differentiation of T cells into Th2 cells. IL-4 promotes this differentiation while the combination of IL-4 and IL-10 inhibits generation of Th1 cells. The nature and amount of antigen also affects the differentiation of CD4 T cells. A large amount of antigen or strongly interacting antigen induces a Th1, inflammatory response, while a small amount of antigen or weakly interacting antigen leads to a Th2 bias (Janeway & Travers, 1996).

B cells, which differentiate in the bone marrow, are responsible for the humoral arm of the immune system and on activation differentiate into antibody secreting plasma cells. The antigen receptors of B cells are membrane bound versions of the antibodies they secrete when activated. On binding antigen, the B cell antigen receptors transmit a signal to the cell interior and deliver antigen to intracellular sites where it can be processed and presented by MHC class II molecules on the B cell surface. This complex of antigen with MHC molecule can then be recognised by helper T cells which assist in the differentiation of B cells to plasma cells (Janeway & Travers, 1996).

Some pathogens have evolved to exploit the immune system by generating an immune response that is beneficial to them rather than to the host. Filarial parasites are one such example and have developed specific techniques to counter the immune defences of the host. These techniques involve the excretory-secretory products of the parasites, identified as including proteinases, protease inhibitors and antioxidants (Pastrana *et al.*, 1998). It is thought that these ES products aid the misdirection of the immune system to yield a Th2/anti-

inflammatory response. This response is characteristic of filarial infection and appears to allow the establishment of chronic infection (Mahanty & Nutman, 1995; Winkler *et al.*, 1998). Treatment of parasitic diseases with DEC or ivermectin leads to a re-establishment of the Th1 response in infected individuals resulting in clearance of the parasites and microfilariae (Dikshit *et al.*, 1995).

1.4.1. Th1/Th2 Polarisation

Downregulation of the host immune response and Th1/Th2 polarisation is a marker of filariasis (Allen & Macdonald, 1998; Elkhaila *et al.*, 1991; Nutman *et al.*, 1987a). Amicrofilaremic individuals exhibit a Th1 response to the filarial parasite that leads to a strong T cell response and is characterised by IL-2 and IFN γ cytokines. It is thought that this Th1 response, an inflammatory response, is responsible for the symptoms, such as limb swelling and skin lesions (Pastrana *et al.*, 1998; Soboslay *et al.*, 1999), exhibited by amicrofilaremic individuals. The majority of infected individuals however, are asymptomatic microfilaremic and demonstrate a polarisation in the Th1/Th2 balance in favour of a Th2 response (Soboslay *et al.*, 1999). This appears to provide a survival advantage to the parasite, which can survive for greater than ten years in the host. The Th2 response is characterised by the presence of IL-4, IL-5 and IL-10 cytokines and also high IgG4 and IgE levels (Soboslay *et al.*, 1999).

The decreased or abrogated Th1 response observed in asymptomatic microfilaremic patients could arise via a number of mechanisms; tolerance, immunosuppression, genetic factors in the host, imbalance of antigen-specific Th1/Th2 subpopulations or a combination of two or more of these (Mahanty & Nutman, 1995). The tolerance hypothesis is considered unlikely if tolerance is considered only to be clonal deletion, however, tolerance can also be defined as T-cell anergy that can occur in a mature immune system (Maizels & Lawrence, 1991). Responses to parasite antigens have been shown to be restored following treatment thus it is unlikely that a deletion of cells specific for parasitic antigens is occurring, whether T cell anergy is a possible alternative is yet to be determined. One possible exception to this is in the case of children born of a

mother who is positive for the presence of microfilariae. These children possess a decreased response to parasitic antigen (Kazura *et al.*, 1993), and may be an example of tolerance in the form of clonal deletion rather than T cell anergy. This exception occurs as a result of the neo-natal exposure of the children's immune system to the parasitic antigens and thus more closely resembles elimination of self-reactive T cells which occurs by clonal deletion than tolerance induced following exposure of a mature immune system to parasitic antigen.

1.4.2. Antibody Responses

Antibody responses to filarial disease depend on the parasitological status of the individuals and not on clinical symptoms. All infected individuals exhibit B cell hyporesponsiveness to the parasite while B cell responses to other immune challenges remains unchanged (Kurniawan-Atmadja *et al.*, 1998; Marley *et al.*, 1995; Nicolas *et al.*, 1999; Nutman *et al.*, 1987b). Individuals with detectable levels of adult worms possess higher filarial specific IgG4 and lower IgG3 and IgE levels than individuals free of adult worms. IgG4 is unable to fix complement and does not interact with macrophages, other phagocytes, mast cells or basophils. IgG3 can both fix complement and bind macrophages and other phagocytes while IgE, although unable to fix complement, can bind macrophages, other phagocytes, mast cells and basophils. These factors perhaps provide a survival advantage to the parasite by limiting the pro-inflammatory immune response mounted against it. Those individuals with no adult worms but with microfilariae have low filarial specific IgG1 and IgG2 levels. Both IgG1 and 2 can fix complement, IgG1 can also bind macrophages and other phagocytes. These properties, giving a strong immune response, are perhaps responsible for the lack of adult worms.

1.4.3. Cytokines

As mentioned, infection with filarial parasites generally leads to a Th2 immune response, thus cytokines such as IL-4, IL-5 and IL-10 are induced early in infection (Pastrana *et al.*, 1998; Soboslay *et al.*, 1999). The presence of these

cytokines on activation of CD4 T cells leads to the bias of the differentiation of these cells in the direction of a Th2 response. Nitric oxide (NO) is also involved in the host response to parasitic infection. NO is cytotoxic to both microfilariae and to adult worms and it is believed to play a role in the elimination of microfilariae in infected individuals (Winkler *et al.*, 1998).

The imbalance of antigen-specific Th1/Th2 subpopulations is currently the favourite hypothesis for the survival of filarial parasites within the host. This is supported by IL-10, the cytokine secreted in a Th2 response, downregulating the Th1 response in cells (Mahanty & Nutman, 1995). Research shows that mice deficient in C1q (of the complement cascade) have a decreased clearance of parasites that can be attributable to the C1q depletion. This in turn leads to an upregulation of the levels of IFN γ , an important cytokine in the Th1 response, further demonstrating the important role cytokines play in the host response to filarial infection (Taylor *et al.*, 1998). The hyporesponsiveness of the microfilaremic individual is restricted to parasitic antigens. Responses to non-parasitic antigens are normal (Mahanty & Nutman, 1995).

Filarial parasites have also been found to secrete a homologue of the human proinflammatory cytokine macrophage inhibitory factor (MIF) (Pastrana *et al.*, 1998). This homologue is chemotactic for human immune system cells raising the question of why filarial parasites would want to attract the cells they need to avoid in order to survive. One theory is that the attraction of macrophages by filarial parasites is the first step in a process that allows alteration of the host immune response (Pastrana *et al.*, 1998). Production of homologues of host molecules involved in immune signalling with the aim of diverting the immune response, is a trick employed by a number of pathogens including poxvirus which secretes a chemokine, cytomegalovirus which interferes with Class I MHC molecule expression and EBV which secretes a IL-10 homologue.

1.4.4. The Role of Phosphorylcholine

Excretory-secretory proteins from filarial nematodes all possess a PC moiety that has been shown to be important in the immunomodulatory role which ES products are believed to play (Harnett & Parkhouse, 1995; Houston & Harnett, 1999b). Studies of PC-containing bacteria have demonstrated the ability of PC to interact with cells of the adaptive immune system independently of antigen receptors and cause polyclonal activation of the B cells. This interaction can occur via the PAF (platelet activating factor) receptor. Bacteria with PC on their surface are known to be dependent on the interaction between PC and the PAF receptor for invasion of cells (Harnett & Harnett, 1999b). Use of PAF receptor agonists, which block binding of PC-containing bacteria to the PAF receptor, have confirmed the role of the PAF receptor in the invasion of immune cells by these pathogens.

Filarial nematode PC-containing ES proteins cause a down regulation of B cell proliferation associated with ligation of the antigen receptor (Deehan *et al.*, 1998a; Harnett & Harnett, 1993). The receptors for these ES products are unknown, but recent research has demonstrated that ES-62, the model ES product employed in this thesis, can bind cell membranes from a number of cell types with receptor-like affinity and in a PC dependent manner (Harnett, M.M. & Harnett W., Unpublished). This raises the possibility of PC receptors acting as receptors for ES products. The PAF receptor, employed, as described above, by PC containing bacteria, is one possible receptor through which these ES products could be inducing their effects.

The presence of PC on a pathogen can often present a disadvantage for the pathogen, as the innate immune system is rapidly directed against PC. This acts as a crucial host protection mechanism against certain invasive pathogens (Harnett & Harnett, 1999b). However, the PC on ES products of filarial nematodes appears to have a role in promoting the longevity of filarial nematodes within the host. It would appear thus that the presence of a PC moiety on a pathogen might not always be disadvantageous.

1.4.5. Secondary Effects of Infection with Filarial Parasites

Filarial parasites can survive for ten years or more within the host. It has been suggested that the filariae induce a semi-permanent state of immunological unresponsiveness and that this results in the host becoming tolerant to the worm burden thus displaying minimal responsiveness to parasite antigens. People infected with filarial parasites who possess this tolerance to the worm burden are asymptomatic. If this tolerant state should break down, the host can mount an immune response to the parasite, which results in skin lesions, limb swelling and elephantiasis. This has implications for vaccine development, as it is necessary to ascertain that the antigens used in a vaccine will not induce these symptoms.

Infection with filarial parasites causes a variety of effects in the host immune response not all of which are solely related to the filarial infection. Filarial infection is known to induce a Th2 type response and to modulate the host immune response. Reported incidents of high levels of bacterial infections, for example lepromatous leprosy, in filarial endemic areas led to research into the effects of infection with filarial parasites in terms of bacterial infections. Many mycobacterial infections induce Th1 responses allowing the body to rid itself of infection whereas Th2 responses result in active infection. Studies have shown that infection with mycobacteria and filarial parasites causes an increase in the symptoms and severity of the mycobacterial infection. This demonstrates that filarial infection is capable of modulating the immune response to a concurrent infection (Stewart *et al*, 1999).

While immunosuppression of the host can be seen to occur upon infection with filarial parasites there is also evidence that some immune system cells are required for growth of the filarial parasites. Research has shown that host NK cells are required for the growth of the *B. malayi* parasite. This demonstrates the level of immunomodulation, achieved by filarial parasites, of the host immune response with both the downregulation of the protective branch of the immune system and the promotion of immune system cells essential for parasite growth (Babu *et al*, 1998).

1.4.6. Protective Immunity

Protective immunity is immunity to re-infection with a previously encountered pathogen and as such it is the goal of vaccine developers. Protective immunity in the case of filarial parasitic infection is stimulated by L3 larvae and demonstrates some cross reactivity between species. Dead L3 larvae do not induce this protective immunity thus the active immunogen is believed to be either secreted or produced post-infection. Protective immunity induced by L3 larvae can be achieved either by vaccination with irradiated L3 larvae or by prolonged exposure to filarial parasites. Either way this protective immunity results in a decrease in the worm burden on the infected individual (Helmy *et al.*, 2000; Maizels & Lawrence, 1991; SchrempfEppstein *et al.*, 1997). Triple vaccination with irradiated L3 larvae results in protection against infection for six months. Other parasite derived molecules can induce strong humoral responses. Superoxide dismutase (SOD) is one such molecule. Research has shown that SODs may participate in the immune evasion of filarial infection, this coupled with the strong humoral immune response that they invoke makes them an ideal target for anti-filarial vaccines (Lattmann *et al.*, 1999).

1.5. *Acanthocheilonema Viteae*

Human filarial parasites are very host specific and thus are difficult to maintain in animals (Lucius & Textor, 1995). It is therefore necessary to employ a model system. *A. viteae*, a rodent filarial nematode which dwells in the subcutaneous tissues of its host, is the parasite used in this thesis and by other groups as a model system for the study of filariasis. *A. viteae* reproduces in a narrow spectrum of rodents (Lucius & Textor, 1995), the host employed for *A. viteae* in this thesis was the jird, a Syrian hamster. *A. viteae* is employed as a model system for filariasis as it exhibits many similarities to human filarial infection.

The course of infection of *A. viteae* in jirds parallels chronic human filarial infection as the adult *A. viteae* filariae develop well in the jird, are long living and produce high levels of microfilariae which are present throughout the life of the infected host. In addition the antibody responses of the jird to *A. viteae* vary

during the period of infection (Lucius *et al.*, 1987) which parallels the human antibody response to human filarial parasites.

The similarities between *A. viteae* and human filarial parasites are not restricted to the course of infection within the respective hosts. *A. viteae* shares antigens with *O. volvulus* (Nogami *et al.*, 1986), one of the human filarial parasites. In addition, the major ES product of *A. viteae*, ES-62, is homologous to an expressed sequence tag (EST) from *O. volvulus* and *B. malayi* and also contains PC (phosphorylcholine) a common component of human filarial ES products. ES-62, in a similar fashion to the ES products of *B. malayi*, is located predominately in the gut of the parasite (Wenger *et al.*, 1988) and possesses an epitope present on the circulating antigens of *B. malayi* (Maizels *et al.*, 1987), *O. volvulus* (Harnett *et al.*, 1989) and *W. bancrofti* (Dissanayake *et al.*, 1984).

Research into the infection of golden hamsters with *A. viteae* revealed that the cellular response of the host to mitogens decreases during infection (Weiss & Tanner, 1981). This is similar to the depression of the host cellular immune system observed in some individuals infected with lymphatic filariasis and onchocerciasis (Nutman *et al.*, 1987c; Ottesen, 1984; Soboslay *et al.*, 1991).

A. viteae infection is currently used as a model system for the screening of filaricidal drugs (Zahner & Schares, 1993) and has potential for use in the characterisation and screening of candidate vaccine antigens as protection against *A. viteae* in jirds can be induced by vaccination with irradiated L3 larvae (Lucius *et al.*, 1991; Tanner & Weiss, 1981). *A. viteae* is thus a good model system for the study of human filarial infection.

1.6. ES-62

ES products are produced by the parasite whilst within its mammalian host and are secreted by both L4 stage parasites and adult worms. ES products are believed to play an immunomodulatory role in the host and the PC moiety found on these ES products supports this hypothesis as PC is a known immunomodulator.

ES-62 is the major ES product of the rodent filarial parasite *A. viteae*, located predominately in the parasite gut. It has a mass of 57.8 kDa and is employed as a model for the study of the origin, fate and action of filarial ES products. ES-62 is used as a model system for human filarial ES products for three reasons: the first is that it is readily purified in sufficient quantities for study, the second is that it contains a PC moiety that is also present on human filarial ES products (Harnett *et al.*, 1989) and finally it is a homologue of molecules secreted by human filarial nematodes, such as *B. malayi* (Harnett *et al.*, 1999a). ES-62 also possesses an epitope present on circulating antigens of *B. malayi* (Maizels *et al.*, 1987), *O. volvulus* (Harnett *et al.*, 1989) and *W. bancrofti* (Dissanayake *et al.*, 1984).

1.6.1. Biochemical Characteristics of ES-62

ES-62 has been cloned, its DNA sequenced and this sequence utilised to derive the amino acid sequence of ES-62. To provide independent confirmation of the DNA derived amino acid sequence, tryptic peptides of ES-62 were subjected to Q-TOF sequencing, a mass spectroscopy (MS) technique (Harnett *et al.*, 1999b). Figure 1-6 shows the DNA sequence and the derived amino acid sequence. The overlined portions highlight those peptides defined by MS sequencing. Gel filtration studies of native ES-62 have indicated that it is likely to be a tetramer with a molecular weight of 248 kDa (Harnett *et al.*, 1999a). A sequence motif very similar to that seen in C-reactive protein has also been identified in ES-62 and is shown in Figure 1-6. This motif in C-reactive protein binds PC non-covalently. The presence of this sequence in ES-62 suggests that it is possibly binding PC non-covalently and then transferring it to its site of attachment on the

N-glycans. Sequence homology searches have shown ES-62 to possess a region homologous to aminopeptidases as shown in Figure 1-6. Studies involving the incubation of ES-62 with leucine-7-amino-4-methylcoumarin, an aminopeptidase substrate (Acosta *et al.*, 1998), confirmed that ES-62 does possess aminopeptidase activity (Harnett *et al.*, 1999b). Recent homology searches (discussed in Chapter 3) have shown ES-62 to possess high full-length homology to haematopoietic switch 2 and switch 2-related proteins, to a murine and human aminopeptidase, a glutamate carboxypeptidase precursor and a human liver annexin-like protein. The function of the haematopoietic switch proteins is not fully known but they are known to possess carboxypeptidase activity (Chen & Talmage, 1998). The lack of available information on these proteins makes it difficult to predict the function of ES-62 on the basis of these homologies. However, the high level of aminopeptidase and carboxypeptidase activity seen in these proteins might suggest a role for peptidase activity in the function of ES-62.

Further analysis of the sequence of ES-62 has also revealed the presence of leucine rich motifs, shown in Figure 1-6, which may play a role in the interaction of ES-62 molecules with other ES-62 molecules, resulting in multimerisation. Amino acids that form two putative metal co-ordination sites have also been identified and can be seen in Figure 1-6. The residues that form the putative metal coordination sites are conserved in the six identified homologous protein mentioned above. Inductively coupled plasma atomic emission spectroscopy (discussed in Chapter 5) showed a strong magnesium signal for native ES-62 suggesting a requirement for this metal ion and substantiating the presence of possible metal co-ordination sites.

```

1      M L L N S S T F F F L V T L 14
1      ATAAATATGCTA CTCAATTCCTCG ACATTTTCTCTC TTGGTCACCCTA 48

15     T V V L G↑A A V L P D K T V A P 30
49     ACTGTCGTTTTG GGCGCAGCTGTC CTTCCGGACAAA ACTGTCGCTCCG 96

31     K N Y I Q E T F G K E V A E L I 46
97     AAGAATTATATC CAAGAAACGTTT GGAAGGAAGTT GCCGAATTAATC 144

47     Q Y I T K G E E V G L A Y Q W L 62
145    CAGTATATTACT AAAGGTGAAGAA GTTGGATTAGCT TATCAATGGCTT 192

63     S K L V D G F G H R M V G S D S 78
193    AGCAAATTGGTC GATGGCTTTGGA CATCGTATGGTT GGTTCGATAGC 240

79     L E K S I A F L E E S L K N D N 94
241    TTGGAAAAATCG ATTGCTTTCTTA GAAGAAAGCTTG AAAAATGATAAT 288

95     F D K V H T E E V P N L P H W V 110
289    TTTGATAAGGTG CACACCGAGGAA GTACCAAACCTG CCACATTGGGTT 336

111    R G N D V V E M I E P R N Q R L 126
337    CGTGGAACGAC GTTGTCGAAATG ATTGAACCACGA AATCAACGGCTC 384

127    N V L A I G G S E P A S A T G E 142
385    AATGTGCTTGCT ATTGGTGGATCT GAACCAGCTAGT GCGACCGGAGAA 432

143    V T V I Y D L D D V K P D D V R 158
433    GTGACAGTTATT TATGATCTTGAT GATGTCAAGCCT GATGATGTCCGT 480

159    G K I V V T A Q T F A G Y P L T 174
481    GGCAAGATTGTT GTGACGGCACAA ACATTTGCTGGT TATCCGTTAACG 528

175    L K Y R R S V K L F E Q L G A I 190
529    CTTAAATATCGT CGATCAGTAAAA TTATTTGAACAA TTAGGTGCCATT 576

191    G V L V K S I T S F S I N S P H 206
577    GGTGTTCTGGTC AAATCAATAACA TCATTTTCCATT AATTCACCTCAT 624

207    T G T G A E N T T I P A A C L T 222
625    ACCGGCACTGGT GCAGAAAATACA ACAATTCCTGCT GCATGTTTAAACG 672

223    I E E A E M L E R L Y R S G K K 238
673    ATTGAGGAAGCT GAAATGCTTGAA CGATTGTATAGG AGCGGCAAAAAG 720

239    I V I R M D M K S H Y E E P I N 254
721    ATCGTAATCCGA ATGGATATGAAA TCACATTATGAG GAACCTATAAAT 768

255    S S N L I F E I T G S E R P S E 270
769    TCCAGCAATCTT ATCTTTGAAATT ACCGGTAGTGAA CGACCATCTGAA 816

271    V V L L S A H V D S W D V G Q G 286
817    GTGGTACTATTA TCGGCACATGTG GACAGTTGGGAT GTTGGACAAGGA 864

287    A L D D G A G C A V V W S A L H 302
865    GCATTGGATGAT GGTGCTGGTTGT GCTGTTGTATGG AGTGCTTTGCAT 912

303    S L K K L A E R N P K F K P K R 318
913    TCATTAAAAAAA TTAGCCGAAAGA AATCCAAAATTC AAACCAAAACGG 960

319    T I R G I F W T S E E Q G Y G G 334
961    ACAATTCGAGGC ATATTTTGGACA TCGGAAGAACAA GGATATGGGGGT 1008

```


335	<u>A</u>	<u>K</u>	<u>H</u>	<u>Y</u>	<u>Y</u>	<u>I</u>	<u>T</u>	<u>H</u>	<u>K</u>	N	D	S	P	E	K	F	350
1009	G	C	A	A	A	C	A	T	T	A	C	A	C	A	T	T	1056
351	Y	F	V	S	E	T	D	T	G	T	F	K	S	T	N	W	366
1057	T	A	T	T	T	G	T	A	T	C	T	C	A	A	A	T	1104
367	L	A	H	L	S	F	S	G	D	K	K	S	M	L	R	L	382
1105	C	T	T	G	C	A	T	C	T	T	C	A	T	T	G	G	1152
383	K	E	I	T	R	L	L	S	R	N	G	I	A	L	G	L	398
1153	A	A	G	A	A	T	A	A	C	A	T	T	G	A	G	C	1200
399	I	<u>N</u>	<u>S</u>	<u>S</u>	V	Q	G	D	V	T	F	W	A	K	D	G	414
1201	A	T	A	A	A	T	A	G	C	T	C	A	G	T	G	A	1248
415	I	P	S	V	N	Y	I	P	D	K	A	V	D	Y	Y	F	430
1249	A	T	A	C	C	A	T	C	A	G	T	T	A	T	A	T	1296
431	Y	F	H	H	T	A	G	D	Y	M	T	V	L	K	D	G	446
1297	T	A	T	T	T	C	A	T	C	A	T	A	C	T	A	T	1344
447	D	L	E	Y	T	T	S	I	F	A	T	L	G	H	V	I	462
1345	G	A	T	T	A	G	A	T	A	T	A	C	A	A	T	T	1392
463	A	N	M	D	D	W	G	S	D	P	N	Q	P	Q	Q	L	478
1393	G	C	T	A	A	T	A	T	G	G	A	A	G	T	G	A	1440
479	N	S	K	Q	S	T	T	E	K	S	D	R	K	K	L		493
1441	A	A	T	T	C	C	A	A	A	C	A	A	T	T	C	T	1488

Figure 1-6: DNA and derived amino acid sequence of ES-62. The arrow marks the start of the mature protein sequence, the sequence before this is a signal sequence, which dictates that ES-62 is secreted. Bold residues show those residues that constitute the leucine rich regions, residues in bold italics show the glycosylation sites, boxed residues are those involved in the formation of metal co-ordination sites, **red residues show the region of ES-62 homologous to aminopeptidases and underlined residues show the region of ES-62 homologous to the PC binding region of C-reactive protein (residues 56-81 of human C-reactive protein (Harnett et al., 1999a)). Overlined residues show the peptides defined by MS sequencing.**

Mass spectroscopy studies have shown ES-62 to consist of 6 % carbohydrate and suggest the presence of at least 1-2 PC groups. Studies characterising the carbohydrate content of ES-62 (Haslam *et al.*, 1997) have identified three types of N-glycan structures; (1) high mannose; more analogous to fungal than bacterial PC-containing glycans, (2) those fully trimmed to the mannosyl core and fucosylated and (3) those with a trimannosyl core substituted with GlcNAcs, with or without core fucosylation. The latter of the three classes is the only one known to have PC attached (Haslam *et al.*, 1997). Figure 1-7 shows examples of the carbohydrate structures of these three classes.

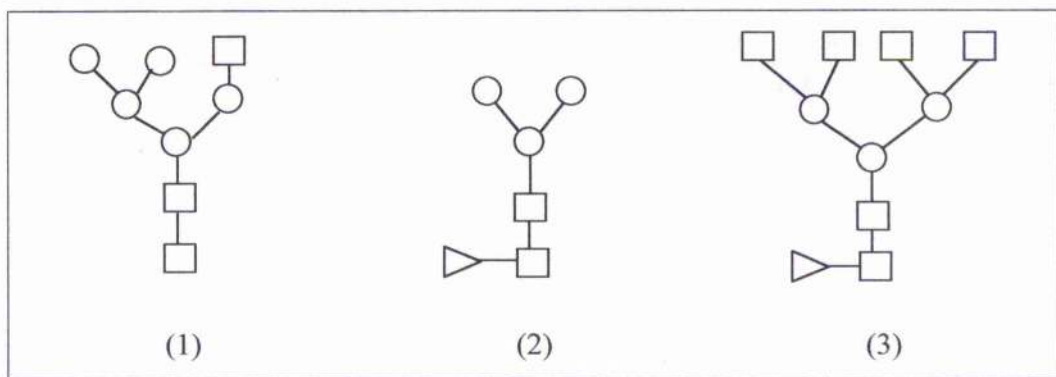


Figure 1-7: Examples of the three classes of N-glycan structures identified on ES-62 (Haslam *et al.*, 1997). (1) High mannose type structures, (2) those fully trimmed to the mannosyl core and sub-stoichiometrically fucosylated, (3) those with a trimannosyl core with or without core fucosylation and carrying 1-4 additional N-acetylglucosamine residues. The third class of N-glycan structures shown is the only class found to be substituted with phosphorylcholine. □ – N-acetylglucosamine, ▽ – Fucose, ○ – Mannose.

Studies on the processing of ES-62 through the endoplasmic reticulum and Golgi provides evidence that the PC groups are attached to the N-glycan structures in the Golgi and that this attachment occurs only if the glycan has been correctly processed. Incubation of worms with tunicamycin, an antibiotic which inhibits N-type glycosylation, results in non-glycosylated ES-62 which contains no PC and is only partially secreted. This demonstrates clearly that PC is attached to ES-62 via an N-linked glycan (Houston & Harnett, 1996). Further studies

incubating worms with brefeldin A (which inhibits transport from the ER to the Golgi), N-deoxy-1-deoxynojirimycin (dNM) (which inhibits α -glucosidase I in the ER) or 1-deoxymannojirimycin (dMM) (which inhibits α -mannosidase I in the Golgi, as shown in Figure 1-8), have also shown that PC is attached via N-linked glycans as each of these inhibitors prevents attachment of PC (Harnett *et al.*, 1993; Houston *et al.*, 1997; Houston & Harnett, 1999a). These studies also suggest that PC attachment is a post-ER event, probably occurring in the medial Golgi where the substrate for transfer is $\text{Man}_5\text{GlcNAc}_3$ or $\text{Man}_3\text{GlcNAc}_3$. This association of PC with N-linked glycans is not seen in humans and thus could represent a target for chemotherapeutic agents (Houston & Harnett, 1999a).

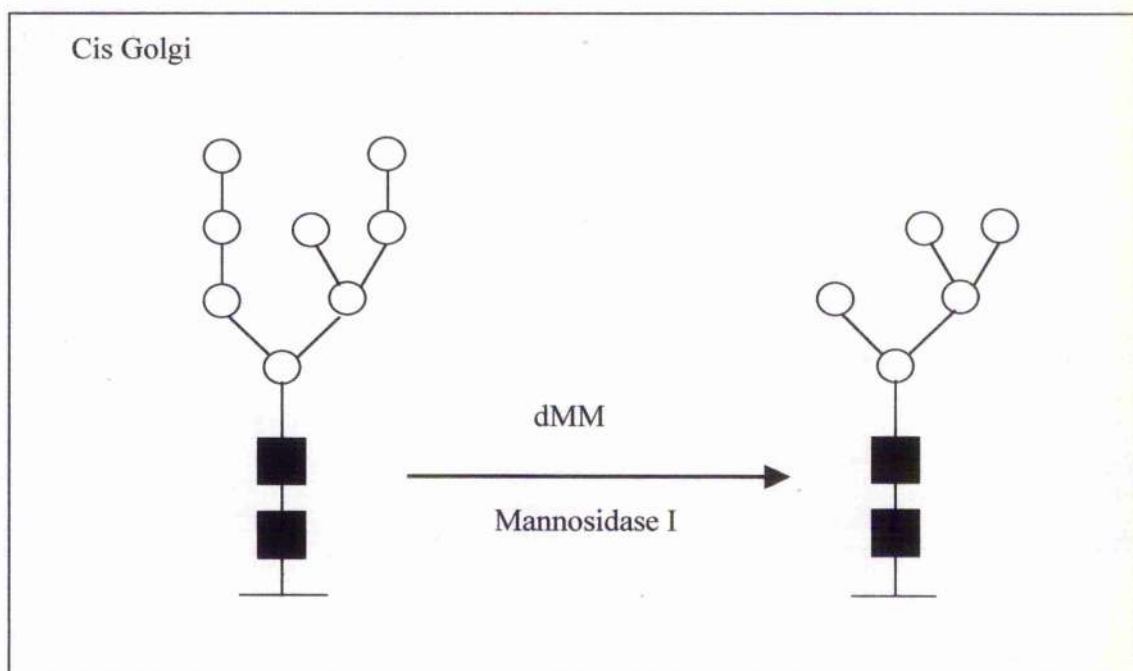


Figure 1-8: 1-deoxymannojirimycin (dMM) inhibits α -mannosidase I in the Golgi, inhibiting processing of the glycans on ES-62 and preventing the addition of PC to ES-62. ○ – Mannose, ■ – N-acetylglucosamine.

The source of the PC attached to ES products of filarial nematodes has yet to be identified (Houston & Harnett, 1999a). However, *A. viteae* filarial nematodes grown in choline-free media still produce ES-62 that possesses PC (Vanamail *et al.*, 1996). This suggests that the worms make PC by an as yet unidentified pathway rather than obtain it from the host. While the source of PC for the

worms remains elusive, studies have shown that attachment of PC is blocked by hemicholinium 3; an inhibitor of choline kinase which is the first enzyme in the Kennedy pathway. The Kennedy pathway, shown in Figure 1-9, is a metabolic pathway for the synthesis of phosphatidylcholine. Choline kinase catalyses the phosphorylation of choline as the first step in the transfer of PC from CDP-choline to DAG. This demonstrates that the phosphorylation of choline is essential for attachment of PC to ES-62 but there is no evidence that the rest of the pathway is involved (Houston & Harnett, 1999b).

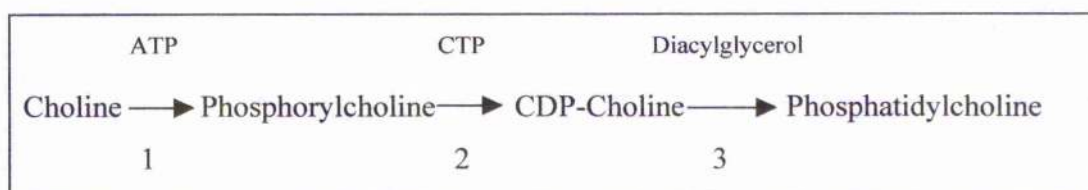


Figure 1-9: The Kennedy pathway for the metabolic synthesis of phosphatidylcholine. 1, 2 and 3 represent the three enzymes, choline kinase, phosphocholine cytidyltransferase and choline phosphotransferase respectively, that catalyse the Kennedy pathway. Hemicholinium 3, an inhibitor of choline kinase, inhibits the phosphorylation of choline , the first step in the Kennedy pathway.

1.6.2. Effects of ES-62 on the Immune System

ES-62 is immunogenic, studies have shown its systemic half-life, as estimated by clearance, to be 2-7 hours in naïve animals and 30 minutes in 4-10 week infected animals. This correlates with the clearance of antigen by antibody in the infected animals (Harnett *et al.*, 1989). The effects of ES-62 on the immune system have been studied in depth due to the finding, observed in many studies spanning several decades, that filarial infection appears to promote defects in the host immune response (Harnett & Harnett, 1993). As ES products are found circulating freely in the bloodstream they were considered a good candidate for an immunomodulatory molecule. *In vitro* studies have shown that ES-62 inhibits polyclonal activation of murine B cells and that this effect can be mimicked by PC conjugated to BSA or PC alone (Harnett & Harnett, 1993). This suggested

that the PC moiety is responsible for some of the immunomodulatory activity of ES-62 and is further substantiated by the knowledge that PC can interact with B cells via a receptor which is not the B cell receptor (Bach *et al.*, 1983). However, the protein and carbohydrate content of ES-62 must also be important for function, as not all of the effects induced by ES-62 can be mimicked by PC conjugated to BSA or PC alone. Further, whilst PC alone is immunomodulatory, it is approximately two orders of magnitude less effective than when complexed to ES-62 (Harnett & Harnett, 1993).

The PC moiety is commonly found on ES products of all filarial parasites and the data to date suggests that PC-ES molecules play an important role in the immunomodulation of T and B cells observed during filarial parasitic infection. Studies have shown definitively that host exposure to PC-ES products during the course of a filarial infection leads to the loss of ability of B cells to respond to antigen. The extent of the role of the PC moiety itself is not fully known although studies showing that PC and PC conjugated to BSA can mimic many of the effects of ES-62 in both B and T cells suggest it has a large role to play.

1.6.3. Mechanism of Immunomodulatory Effects on B cells

ES-62 elicits effects on a number of different cells of the immune system. The best studied of these is the effects of ES-62 on B cells. The normal state of B cell signalling and the effects induced by ES-62 are discussed in this section.

1.6.3.1. B Cell Signalling

Activation of B cells leads to proliferation and differentiation of these cells to form plasma cells and memory cells. These processes require many different signals from a number of immunoregulatory receptors on different cells. The antigen receptor on B lymphocytes consists of a membrane immunoglobulin (mIg) molecule and two glycoproteins, Ig α and Ig β . Ig α and Ig β form two heterodimers and are non-covalently associated with the mIg molecule. This is shown in Figure 1-10.

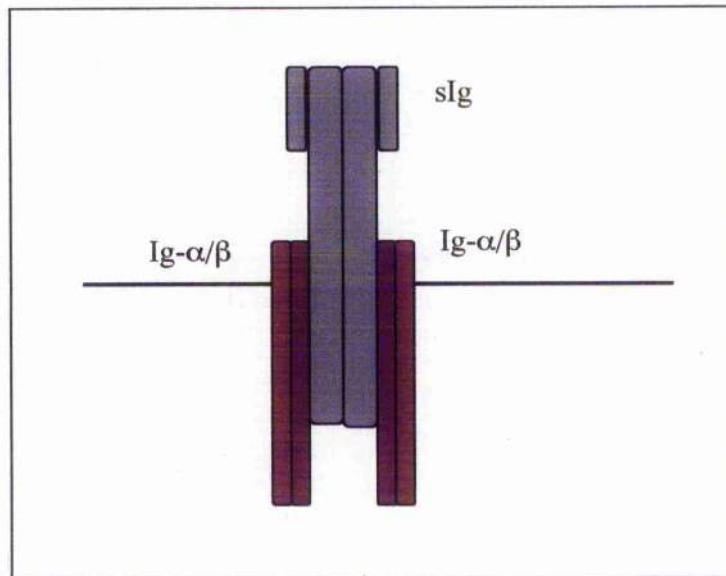


Figure 1-10: The B cell receptor with its accessory molecules $Ig\alpha$ and $Ig\beta$.

Stimulation of cells via the B cell receptor (BcR) leads to activation of second messenger systems. However, mIg has no intrinsic catalytic activity. $Ig\alpha$ and $Ig\beta$ also possess no intrinsic catalytic activity however, they do contain ITAM (Immunoreceptor Tyrosine based Activation Motif) motifs, similar to those in the CD3 complex components of the T cell receptor, which allow interaction with protein tyrosine kinases to activate downstream signalling cascades (Cambier *et al.*, 1994; Cushley & Harnett, 1993). The $Ig\alpha$ and $Ig\beta$ therefore constitute an integral part of the BcR signalling complex.

Following antigen recognition by the BcR and receptor crosslinking, the first intracellular event is activation of the src-family protein tyrosine kinases (PTK) (approximately 15 – 60 seconds after receptor ligation) resulting in tyrosine phosphorylation of the ITAM motifs of $Ig\alpha$ and $Ig\beta$. This results in recruitment of further PTKs which, once activated, tyrosine phosphorylate a variety of cellular substrates following which the BcR signalling pathway diverges into 3 major biochemical pathways (Cambier *et al.*, 1994; Cushley & Harnett, 1993). The first of these is the tyrosine phosphorylation and activation of phospholipase $C\gamma$ (PLC γ). PLC γ , once activated, hydrolyses phospholipids leading to the

formation of IP_3 (inositol trisphosphate) and DAG (diacylglycerol). IP_3 and DAG are second messengers which each activate specific protein kinase C (PKC) isoforms leading to redistribution of PKC to the plasma membrane, and influence gene transcription. In addition, IP_3 also induces release of calcium from intracellular stores and influx of extracellular calcium, which leads to modification of DNA transcription.

The second pathway is the Ras-MAPK pathway. This pathway is activated by the formation of active Ras approximately 1-2 minutes after receptor ligation. Ras is activated by transition from a GDP to a GTP bound state (Harwood & Cambier, 1993). This process is regulated by VAV, a GTPase exchange protein (Bustelo *et al.*, 1992; Gulbins *et al.*, 1993), GAP, a GTPase activating protein (Gold *et al.*, 1992), SOS, a guanine nucleotide exchange factor and Grb2, an adaptor molecule (Feig, 1993). Ras specifically regulates c-Raf, which in turn regulates serine/threonine phosphorylation of MEK and ultimately tyrosine/threonine phosphorylation of MAPK. MAPK is known to influence gene expression due to its ability to activate Fos and Myc – proteins involved in regulation of gene expression. Thus activation of this pathway in response to antigen recognition influences gene expression within the B cell.

The third pathway involves the activation of phosphatidylinositol 3-kinase (PI3K) via tyrosine phosphorylation by the PTK Lyn. PI3K, once activated, phosphorylates inositol phospholipids. This induces a variety of downstream effects including the activation of PKC ζ , which is not activated by either IP_3 or DAG. PKC ζ can directly affect gene transcription but also acts as an alternative pathway through which MAPK can be activated. Figure 1-11 shows diagrammatically the complex nature of signalling within B cells.

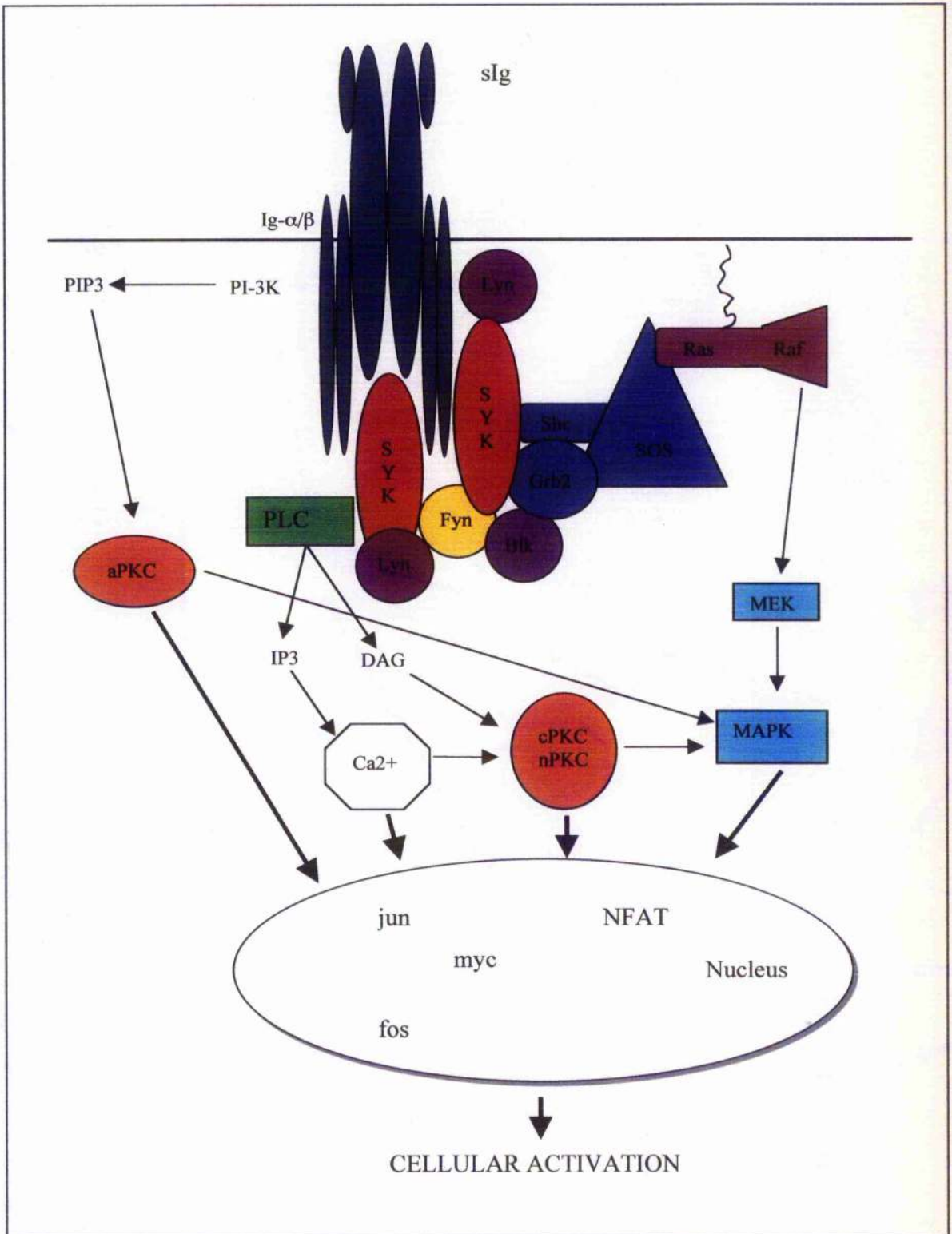


Figure 1-11: The B cell receptor and its downstream signalling pathways.

1.6.3.2. Effects of ES-62 on B Cell Signalling

Studies have shown that ES-62 can elicit weak mitogenic effects on resting B cells but this effect can be achieved only at concentrations far in excess of physiological concentrations (Harnett *et al.*, 1999a). At physiological concentrations of ES-62, an abortive, non-productive activation of certain signalling molecules is induced leading to desensitisation of subsequent sustained proliferation signalling both *in vitro* and *in vivo* (Deehan *et al.*, 1998a). The effects induced by ES-62 are specific. ES-62 induces tyrosine phosphorylation activation of Lyn, Syk and Blk protein tyrosine kinase but not the protein tyrosine kinase, Fyn (Deehan *et al.*, 1998a). It also induces phosphorylation and activation of the Erk2 isoform of MAP kinase (MAPK) (Deehan *et al.*, 1998a) and decreases the total level and activity of cellular protein kinase C (PKC) by modulation of expression of PKC isoforms (Deehan *et al.*, 1998b; Harnett & Harnett, 1993). ES-62 does not affect LPS induced activation of B cells nor does it modulate phosphatidyl-phospholipase C (PtdCho-PLC), -phospholipase D (-PLD) or choline-specific sphingomyelinase activity (Deehan *et al.*, 1998a; Harnett & Harnett, 1993). Figure 1-12 shows diagrammatically the abortive activation induced by ES-62.

The activation of protein tyrosine kinases and MAPK induced by ES-62 does not lead to polyclonal activation of B cells and subsequent proliferation but instead desensitises the cells to subsequent activation of PI3K, PKC and RasMAPK pathways and thus to cellular proliferation via the BcR (Harnett *et al.*, 1999a). This desensitisation is achieved by the recruitment of protein tyrosine phosphatases, such as SHP-1 and PAC-1, to sites of protein tyrosine kinase and MAPKinase activity.

As discussed in section 1.6.3.1, crosslinking of the BcR leads to protein tyrosine kinase activity and subsequent tyrosine phosphorylation of the ITAM motifs on the Ig α and β chains of the BcR. This in turn leads to activation of a number of downstream signalling cascades; the tyrosine phosphorylation and activation of PLC γ , the RasMAPK cascade and the activation of PI3K. ES-62 affects only the RasMAPK cascade and activation of PI3K. Activation of PLC γ is unaffected.

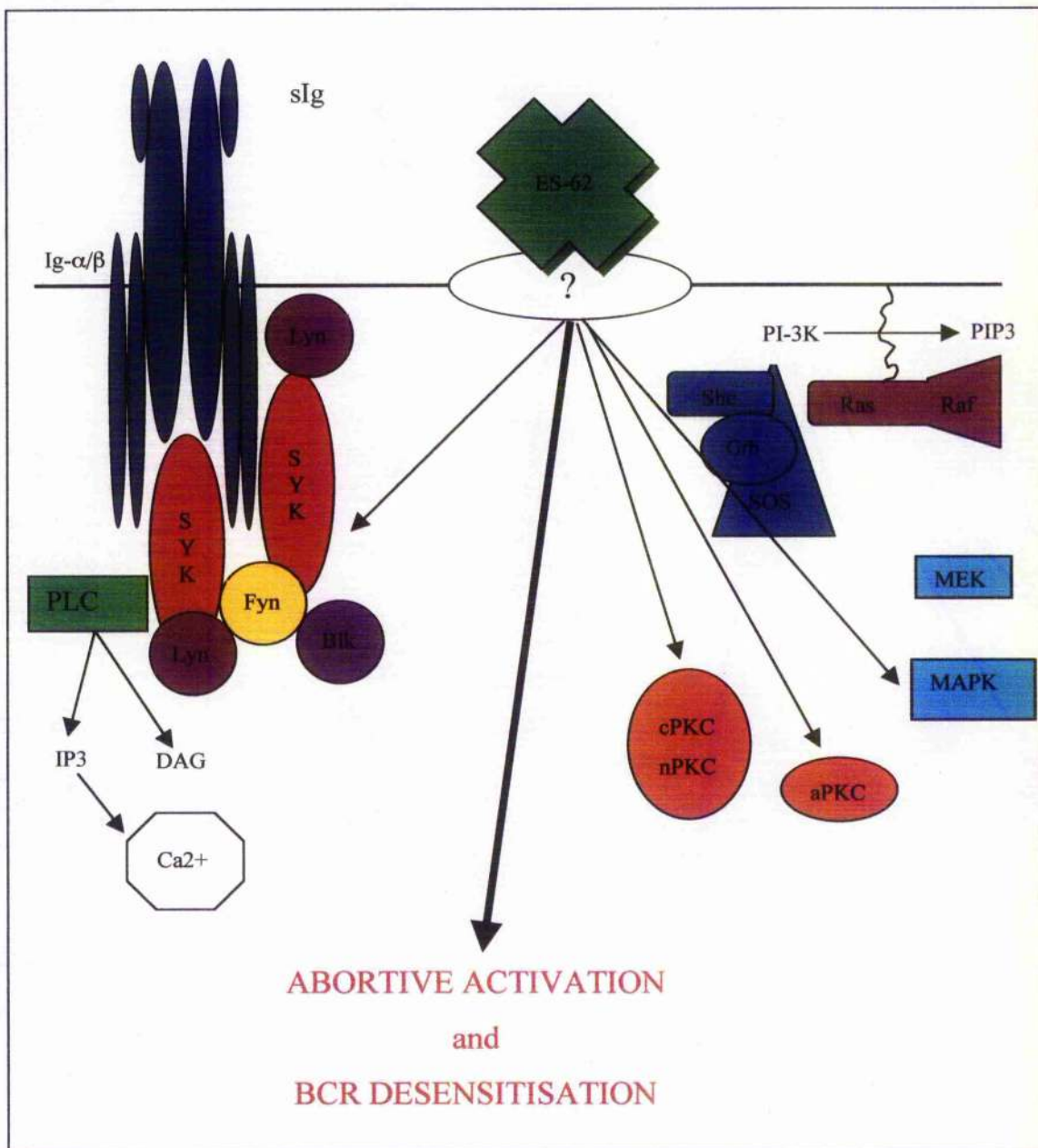


Figure 1-12: Abortive activation and BcR desensitisation by ES-62.

ES-62 polyclonally activates certain protein tyrosine kinases (PTKs) and MAP kinase signal transduction elements in B lymphocytes. This activation does not lead to proliferation of the B lymphocytes, instead it desensitises the cells to subsequent activation via the antigen receptor.

ES-62 alone doesn't induce activity of either PI3K or Ras despite activating Lyn, Syk and Blk. This suggests that either the activity induced is insufficient for downstream signalling or that ES-62 also recruits unidentified signals that negatively modulate Ras and PI3K activity (Deehan *et al.*, 1998a). For example, ES-62 has also been found to increase activity of GAP, a GTPase protein which catalyses the conversion of GTP to GDP. This protein acts to convert the active form of Ras (Ras-GTP) to its inactive form (Ras-GDP) which in turn blocks activation of the MAPK pathway and hence Erk activation. Pre-treatment of B cells with ES-62 followed by anti-Ig stimulation caused a decrease in BcR-coupled PI3K and Ras activity (Deehan *et al.*, 1998a). Erk MAPK is also desensitised by ES-62 due to recruitment of PAC-1, as mentioned above. Thus ES-62 invokes a two-pronged attack on the RasMAPK signalling cascade. The role of Erk in B cell proliferation is well characterised and this is one of the main methods ES-62 employs to inhibit proliferation in B cells (Deehan *et al.*, 1998a; Harnett *et al.*, 1999a).

ES-62 as mentioned earlier decreases the total level and activity of cellular PKC and selectively modulated expression of the PKC isoforms (Deehan *et al.*, 1998b; Harnett & Harnett, 1993). PKC isoforms are classed into three groups. The first of these is the conventional PKC isoforms (α , β and γ) which are calcium, DAG and phospholipid dependent and as such are potential downstream targets of phospholipid derived second messengers. The second group is the novel PKC isoforms (δ , ϵ , μ and ϕ) which are DAG dependent. The third group is the atypical PKC isoforms (ζ and ι/λ) which transduce PI3K mediated signals and are a downstream target of PI3K.

The effects on PKC isoform expression are only observed following pre-exposure of B cells to ES-62 followed by subsequent anti-Ig stimulation. Treatment with ES-62 alone causes only a very slight decrease in PKC expression and activity. ES-62 downregulates the α , β , δ , ζ and ι/λ PKC isoforms and inhibits the nuclear translocation of these isoforms which is essential for activation. ES-62 upregulates the γ and ϵ isoforms. The differential sensitivity of PKC isoforms to downregulation may reflect their distinct

subcellular locations and functional properties. The downregulatory effects of ES-62 on PKC isoforms are achieved by proteolysis. Studies have shown that PMSF and leupeptin, protease inhibitors, reduce PKC downregulation by ES-62.

Incubation of ES-62 pretreated cells with IL-4 prevents the downregulation of PKC α and ι/λ isoforms. IL-4 can also act synergistically with ES-62 to produce B cell activation, raising the question as to whether B cells *in vivo* which encounter ES-62 in the presence of IL-4 are activated. Hyporesponsive filarial patients show greatly elevated levels of IgE and IgG4 which are both regulated by IL-4. These data suggest a role for IL-4 in the modulation of the immune response to filarial parasites.

1.6.4. Mechanism of Immunomodulatory Effects on T cells

The above section discusses the effects of ES-62 on B cells, this section discusses the effects ES-62 has on T cells. T cell signalling is similar to that of B cells and the effects induced by ES-62 are also similar. It is known from studies of patients infected with *B. malayi* that the PC-containing molecules of *B. malayi* inhibit the response of T cells to mitogens (Lal *et al.*, 1990). Recent studies have shown that ES-62 can render T cells anergic to activation by the T cell receptor (TcR) (Harnett *et al.*, 1998). It achieves these effects in T cells in a similar way to its actions in B cells. ES-62 modulates the activity of the PTKs; Fyn, Lck and ZAP-70 in T cells in the same way that it modulates the activity of Syk and Blk in B cells (Harnett *et al.*, 1999a). This acts to disrupt the coupling of the T cell receptor to the downstream signalling cascades of phospholipase D, PKC, PI3K and Ras/MAPK (Harnett *et al.*, 1998) in a similar fashion to the disruption of the PI3K, PKC and Ras/MAPK pathways in B cells. These findings suggest a role for ES-62 in the induction of T cell hyporesponsiveness, which is a key characteristic of filarial infection.

1.6.5. Mechanism of Immunomodulatory Effects on Dendritic and Macrophage Cells

B and T cells are not the only immune system cells to be affected by ES-62. ES-62 also modulates macrophage and dendritic cell function (Whelan *et al.*, 2000). Recent work, (Goodridge *et al.*, 2001), has shown that macrophages treated with ES-62 cannot subsequently be fully activated by LPS, causing decreases in IL-12, IL-6 and TNF- α cytokine production but no alteration in nitric oxide (NO) production. This has implications for the Th1/Th2 balance of T cells produced. IL-12, IL-6 and TNF- α promote a Th1 bias in the Th1/Th2 balance thus a decrease in these cytokines results in a Th2 bias. This is, as mentioned previously, the bias typically seen in infected individuals displaying no pathological signs of disease.

Similarly, recent work on dendritic cells (Whelan *et al.*, 2000) has demonstrated that ES-62 also has an effect on these cells. Dendritic cells can, by process of specific maturation, drive the immune response to a Th1 or Th2 type response. Maturation of dendritic cells occurs following exposure to microbial agents when dendritic cells produce immunostimulatory cytokines and up-regulate expression of MHC I, MHC II and costimulatory molecules. This results in the dendritic cells becoming more efficient antigen presenting cells (APCs) and provides crucial elements for selective activation of T cells to drive a Th1 or Th2 response. ES-62 can induce the maturation of dendritic cells which have the capacity to induce a Th2 response, the classical immune response observed in those infected with filarial parasites (Whelan *et al.*, 2000).

1.6.6. Ex vivo Studies on the Effects of ES-62 on Immune System Cells

Most of the effects that ES-62 has on immune cells have been revealed by work done *in vitro*. Studies using mini-pumps to deliver ES-62 at physiological concentrations over a two week period have tried to address this (Goodridge *et al.*, 2001; Wilson *et al.*, 2002). These *ex vivo* studies, where cells are exposed to ES-62 *in vivo* but stimulated *in vitro*, have shown a decrease in proliferation in

splenic B cells and nodal cells but not in peritoneal B1 cells. Changes in expression of cell surface markers have also been observed with decreases in CD19, 40, 80 & 86 and MHC II occurring in splenic cells. These cell surface markers all act as co-receptors or co-stimulatory molecules for B cells. The observed decrease in expression of these molecules thus suggests a desensitisation of the B cells to antigen and co-stimulatory molecules and hence in the ability to be activated and to activate T cells. This correlates with the known desensitisation effect of ES-62 on B cells. Macrophages show suppressed levels of IL-12, IL-6 and TNF- α similarly to those findings from *in vitro* studies. Nitric oxide production is not found to be affected. Preliminary data from Goodridge *et al.* (unpublished) have suggested that these decreases in cytokine production, observed following ES-62 treatment, are the result of the disruption of IL-12 mRNA expression by modulation of LPS induced Erk MAPK and NF- κ B signalling by ES-62.

Studies of mitochondrial potential following ES-62 treatment have revealed that ES-62 is not inducing apoptosis, as an increase in mitochondrial potential is observed. Apoptosis is preceded by a decrease in mitochondrial potential due to the breakdown of the membrane systems within the mitochondria. Anergy is not preceded by a decrease in mitochondrial potential thus it is possible that anergy not apoptosis is induced by ES-62.

Ex vivo results corroborate the earlier *in vitro* work and reinforce the premise that cell populations respond differently to ES-62. It is therefore important to take into account the amount of ES-62 that each cell population would come in contact with in the case of filarial infection of a host when assessing the effects ES-62 has on the immune system.

1.7. Approaches to Control of Filariasis

1.7.1. Lymphatic Filariasis

There are two main strategies for treatment and control of lymphatic filariasis as outlined by the W.H.O division of Control of Tropical Diseases. These strategies are to stop the spread of infection and to alleviate suffering of infected individuals. The first of these can be split into two; treatment of entire communities for lymphatic filariasis (chemotherapy) and vector control. The second of these is aimed at educating communities, where lymphatic filariasis is a problem, about strategies that can aid those already infected (W.H.O., 1996; W.H.O., 1998).

1.7.1.1. Clinical Diagnosis

Clinical diagnosis of infected members of an endemic community has always been restricted by the sensitivity of the assays available combined with the periodicity of the filarial parasites. The assays measure circulating or urinary parasitic products with the aim of confirming infection of both symptomatic individuals and asymptomatic individuals and to attempt to identify a relationship between antigen levels and levels of infection, i.e. worm burden (Harnett *et al.*, 1990). The periodicity of the parasites means that the density of the microfilariae in the peripheral bloodstream varies over the course of the day such that it is greatest at peak biting times i.e. evening/night. For this reason, coupled with the restriction on sensitivity exhibited by the assays, night blood samples are often required when trying to assess the infected state of members of an endemic community. Night collection of samples is not an ideal situation as clinics are shut at night and those collecting the samples are exposed to infection with parasitic disease.

The assays are usually antibody-based which can present problems due to the sensitivity of these antibodies to the antigens. They are also affected by the antigen to which the antibody is specific. Parasitic surface antigens are less

cross-reactive amongst human filarial species and are thus ideal for diagnostic assays. However, many of the excretory-secretory parasitic products are also highly immunogenic and are present at much higher levels both within the bloodstream and urine of the patient, the urine being easier and less hazardous to collect. The high levels of these excretory-secretory products makes them ideal diagnostic targets. Unfortunately heavy glycosylation and the presence of phosphorylcholine moieties means that many of the antibodies raised against these products are not species specific.

During the last decade two monoclonal antibody (mAb) ELISAs have been developed which are sufficiently sensitive to detect infected individuals from blood samples collected during the day. As these mAbs are against adult worm circulating antigens (CFA), these ELISAs can detect both microfilaremic (mf+) and amicrofilaremic (mf-) individuals (Nicolas *et al.*, 1997).

The W.H.O. has also developed diagnostic and epidemiological assessment tools, which include three direct highly sensitive and specific diagnostic methods. The first involves analysis of daytime finger-prick blood samples using monoclonal antibodies specific for *W. bancrofti* antigens. The second and third methods are similar in that they both employ PCR to detect parasitic DNA, which while both specific and sensitive, requires a laboratory with a high level of quality control (W.H.O., 1999a). One of the methods is directed towards testing human blood for the presence of parasitic DNA whilst the other is concerned with testing the vector (mosquitoes) for the presence of parasitic DNA. These tests can detect *W. bancrofti*, *B. malayi* and *B. timori*. The techniques of detection described so far are targeted at detecting microfilariae in the blood or urine; however, it is also possible to visualise living adult *W. bancrofti* worms present in the scrotal area of infected individuals using ultrasound (Dreyer *et al.*, 1998; Noroes *et al.*, 1997). Live adult worms exhibit a 'dance' pattern of movement within their nests in the lymphatic vessels of the spermatic cords of infected individuals.

1.7.1.2. Vector Control

There is a range of strategies aimed at decreasing the transmission of lymphatic filariasis by targeting the vector. The most simple of these include bednets and curtains impregnated with insecticides and long-lasting indoor insecticide sprays. There is also some evidence that ivermectin can be used in vector control. Studies have shown that mosquitoes fed on ivermectin-treated mice or ivermectin/sugar mix either die themselves or the infective larvae within them die. The level of ivermectin needed to kill the mosquitoes varies between species. However, studies have shown that even at concentrations insufficient to kill the vector there is still a reduction in transmission of the parasite. This is thought to occur due to the proposed effect of ivermectin on the development of the microfilariae (Wilson, 1993).

Another method of vector control involves the use of the toxin-producing bacterium *Bacillus sphaericus*. This bacterium kills mosquito larvae and thus is an effective method of control against lymphatic filariasis. However, the bacteria do not act on blackfly larvae and thus cannot be used against onchocerciasis (Cheong & Yap, 1985; Hougard *et al.*, 1993). The survival of these bacteria has been shown to be increased by the presence of polluted as opposed to clean water, which makes it eminently useable, in the countries affected by filariasis. The bacteria also have the environmental benefit of being harmless to non-target organisms. This method of vector control has been employed in the clearance of lymphatic filariasis from Japan, South Korea, Taiwan and China.

1.7.1.3. Chemotherapy

Chemotherapy of communities in areas of endemic lymphatic filariasis has one main aim; to decrease the level of circulating microfilariae so that transmission rates are reduced and symptoms of those affected are relieved. For the past five decades diethylcarbamazine (DEC), a microfilaricidal compound, has been used to treat lymphatic filariasis (W.H.O., 1996; W.H.O., 1998). Unfortunately its use is contra-indicated for areas where onchocerciasis and loiasis are also present as it can induce severe and dangerous adverse reactions by rapidly killing the

Onchocerca or *Loa loa* microfilariae (Ottesen *et al.*, 1997). Recent studies have shown ivermectin, a microfilaricide used in treatment of onchocerciasis (Shan *et al.*, 2001), and albendazole to be successful in treatment of lymphatic filariasis. DEC, ivermectin and albendazole all cause reductions in microfilariae levels although the timescale over which this occurs and the length of time that the effects last varies.

DEC treatment of lymphatic filariasis suppresses microfilaremia and appears to have some macrofilaricide effects. Treatment with ivermectin is more rapid than treatment with DEC and is as successful in lowering the microfilariae level. However, ivermectin has no macrofilaricide effects. Combined treatment of lymphatic filariasis with DEC and ivermectin is more successful in lowering microfilariae levels than either individually, but co-administration of ivermectin with DEC appears to interfere with the macrofilaricidal action of DEC (Dreyer *et al.*, 1998).

Albendazole, a potent broad-spectrum antihelminthic agent, has already been shown to have antifilarial activity in onchocerciasis and loiasis (Ismail *et al.*, 1998) and studies have recently been carried out to assess its effects on lymphatic filariasis both alone and in conjunction with DEC or ivermectin. These studies indicated that multiple doses of albendazole have both micro- and macrofilaricidal activity and that combined treatment of ivermectin and albendazole was the most successful treatment in terms of rapid and sustained clearance of microfilariae from the bloodstream (Ismail *et al.*, 1998). Mass use of a single dose of albendazole in conjunction with ivermectin would have many benefits; not only does this combination treat lymphatic filariasis, but it would be safe to use in areas where onchocerciasis and loiasis are also present. The broad-spectrum effect of albendazole means it would also act to reduce the prevalence and intensity of intestinal worms in the community. Although further studies to assess the adverse effects, safety, cost and availability in endemic areas are still required, this new combination of antifilarial drugs could be the new strategy to aid eradication of filariasis.

As well as chemotherapy the W.H.O. have identified the need to educate endemic communities about the benefits to be gained from rigorous local hygiene of affected limbs. Studies have shown that much of the progression of symptoms such as elephantiasis and hydrocele are due to bacterial and fungal infections of the tissues with compromised lymphatic function. Rigorous hygiene of these areas can reduce or even eliminate the infections thus easing the symptoms and alleviating suffering of the affected individual (W.H.O., 1999a).

1.7.2. Onchocerciasis

The Onchocerciasis Control Programme (OCP) launched in 1975 and covering eleven West African countries, has the sole objective of eliminating onchocerciasis, a public health and socio-economic problem. Onchocerciasis is currently under full control in the OCP area, although outside this area there are an estimated 15 million people infected with *O. volvulus*.

1.7.2.1. Clinical Diagnosis

Clinical diagnosis of onchocerciasis relies on antibody-based assays which, due to the lack of circulating antigen and poor specificity of antibodies, are inaccurate and unreliable. Development of recombinant antigens has led to antibody assays based on these antigens which are more sensitive and specific for identification of human onchocerciasis infection than earlier assays based on mixes of native antigens.

At present diagnosis of onchocerciasis infection is based on identification of microfilariae in skin snips. Unfortunately this method is incapable of identifying individuals with low levels of microfilariae in their skin and also prevents early detection of infection for rapid treatment. Further to the diagnostic problems associated with skin snips, this method also presents problems in that the equipment required is expensive and carries a risk of transmission of blood-borne viruses between patients. Alternative diagnostic procedures include topical application of a DEC cream with examination of the skin 48 hours later

(localised papular reaction indicates death of microfilariae in the skin) (Weil *et al.*, 2000) and use of PCR technology. PCR detection of *O. volvulus* presents the same problems as those discussed for PCR detection of *W. bancrofti*, *B. malayi* and *B. timori* and has the further disadvantage that skin snips are still required to obtain the samples for diagnosis (Chandrashekar *et al.*, 1995).

Development of a rapid, sensitive diagnostic assay, which does not require the collection of samples via skin snips, is desperately needed. Recently, a rapid format card test has been developed which detects IgG4 antibodies to recombinant *O. volvulus* antigen Ov16. Initial trials of this diagnostic test have proved encouraging with a sensitivity of 90.6 % and a high level specificity for *O. volvulus*. It is hoped this test signals an end to the collection of skin snips (Weil *et al.*, 2000).

1.7.2.2. Vector Control

Initially the OCP was based solely on vector control of *Simulium damnosum*, the blackfly vector of *O. volvulus*. Larvae were destroyed by the widespread aerial spraying of larvicides on the breeding sites of the blackfly, along the banks of fast flowing rivers. The reasoning behind this use of larvicide was that if the transmission of the parasite could be interrupted for longer than adult parasites can survive in the host then onchocerciasis could be eliminated.

Vector control faced two main obstacles; the first was that the border of the OCP area was invaded by infective blackflies from outwith the OCP. This problem was overcome by extending the borders to allow the core area to be protected. The second obstacle was that the blackfly became resistant to the initial insecticide used. This was overcome by identifying seven insecticides, one of which is a biological insecticide, that are used in rotation.

1.7.2.3. Chemotherapy

In 1987 the pharmaceutical company Merck, Sharp and Dohme offered ivermectin free of charge for 'as long as needed'. This allowed the OCP to adopt a two-pronged approach to the elimination of onchocerciasis and also allowed clinicians in endemic areas outside the OCP to treat infected people. Ivermectin has been shown to have prophylactic activity against *O. volvulus* if given on the day of infection (Chandrashekar *et al.*, 1995). However, this action is of little use in treating those already infected although it does provide strong support for early treatment of onchocerciasis and provision of ivermectin for those in endemic areas who do not display clinical symptoms as yet. A study on the effects of large scale ivermectin treatment on the transmission of *O. volvulus* demonstrated that after eight annual treatments the prevalence and intensity of *O. volvulus* infection had decreased by 90 % despite the lack of vector control in the study area. This study also demonstrated that ivermectin acted on the adult worms, decreasing their reproductive capability by approximately 92 % (Boussinesq *et al.*, 1997).

At present ivermectin is used within the OCP in conjunction with vector control programmes and outwith the OCP on its own. The OCP has treated 1.5 million infected people, prevented 125,000-200,000 people from going blind, protected 30 million people at risk of infection and made 25 million hectares of land available for settlement. The OCP is due to come to conclusion in 2002 and the two related projects; OEPA (Onchocerciasis Elimination Programme in the Americas) and the APOC (African Programme for Onchocerciasis Control) are expected to allow the global elimination of onchocerciasis as a public health problem by 2008. Recently a breakthrough has been made concerning the treatment of onchocerciasis. Research has shown that there are bacteria abundantly present in the tissues of *O. volvulus* worms (Werren, 1997). Killing of these bacteria through treatment with antibiotics, such as tetracyclin, has been shown to result in the death of the parasite as well (Kennedy & Harnett, 2001). Trials are currently underway in Ghana which, if successful, could result in treatment becoming available in 2002.

1.8. Aims

The aim of this thesis was to employ a combination of techniques, from biophysics to cellular signalling, to obtain structural information about the filarial nematode excretory-secretory glycoprotein ES-62 and to attempt to identify its receptor on cells of the immune system.

Structural information about a filarial nematode excretory-secretory protein would allow the rational design of drugs to target these proteins and thus be used to treat filariasis and drugs which could mimic excretory-secretory proteins and be used as immunosuppressants to treat transplant patients and in inflammatory diseases. Structural information about ES proteins could also potentially aid receptor identification and further understanding of the interaction of these proteins with cells of the immune system. In addition vaccine development could be aided by the structural characterisation of a potential vaccine molecule. Identification of the receptor for ES-62 would allow further elucidation of the mechanism of action of ES-62 which can then be related to the mechanism of action of ES proteins of human filarial species. Identification of the receptor for ES-62 would also aid the development of chemotherapeutic agents for the treatment of human filariasis and would allow study of the native agonists of this receptor and its cellular role. As discussed in section 1.7, lymphatic filariasis and onchocerciasis are targets for elimination by the World Health Organisation (W.H.O.). Currently there is no effective vaccine available for these diseases and few effective treatments, thus the development of new chemotherapeutic agents and vaccines are imperative.

ES-62 was employed in this thesis as a model for the ES proteins of human filariasis. ES-62, as discussed previously, shows many similarities to these proteins and is the major ES protein of *A. viteae*, the rodent filarial parasite employed as a model system for the study of human filariasis. The effects of ES-62 on B cell signalling have been studied in detail aiding identification of potential receptors.

ES-62, as previously discussed, is a glycoprotein and is only available in relatively small quantities, these factors make it a difficult target for structural determination by crystallography. It was thus decided to use a different approach to obtain structural information about ES-62 and three main techniques were employed.

The first of these was the use of bioinformatic programs to identify homologous proteins, predict the secondary structure of ES-62 and attempt to model its tertiary structure. Bioinformatic programmes were employed as the first step to obtaining structural information as the identification of a homologous protein would be extremely useful for modelling the structure of ES-62 and could also potentially provide functional information about ES-62. Bioinformatic programmes could be employed in the structural characterisation of ES-62 as the DNA and amino acid sequences are known (Harnett *et al.*, 1999b) as is the structure of the carbohydrate chains of ES-62 (Haslam *et al.*, 1997). A number of biophysical techniques, such as circular dichroism (CD) and inductively coupled plasma atomic emission spectroscopy (ICP-AES), were employed to obtain experimental structural data about ES-62 which could then be used to assess the accuracy of the data obtained from the bioinformatic programmes. CD studies of ES-62 provided information about the secondary structure content of ES-62 which was used to assess the predicted secondary structure of ES-62. ICP-AES determines the presence of metal ions within a protein and this information was then used to assess the accuracy of predictions regarding putative metal co-ordination sites within ES-62.

The second approach used was analytical ultracentrifugation (AUC) to establish the stoichiometry and self-interaction constant for native ES-62. AUC was employed as it requires small quantities of protein for analysis and can analyse glycoproteins easily. AUC also analyses the proteins in a solution state as opposed to a crystal state, and thus provides data on the low resolution shape and size of a protein in a physiologically relevant environment.

The third technique employed was small angle X-ray scattering (SAXS). This technique was used to obtain information about the overall shape of ES-62 and to perform tertiary structure modelling, based on the experimentally obtained scattering curve, using the programme DAMMIN (Svergun, 1999). SAXS complements the information obtained from AUC studies and again requires small quantities of the protein for analysis. Similarly to AUC, SAXS analyses proteins in solution rather than in a crystal state.

ES-62 is glycosylated and possesses phosphorylcholine moieties. In order to investigate the contribution that each of the components of ES-62 (protein, carbohydrate and PC) make to the immunomodulatory potential of ES-62, the establishment of two different expression systems was attempted. The first of these was a bacterial expression system in *E. coli* to allow the study of the protein component of ES-62 alone. The second was a baculovirus expression system in SF9 insect cells to allow the study of glycosylated ES-62 without its phosphorylcholine moieties. The establishment of recombinant expression systems would also allow crystallographic studies of ES-62 in the future by alleviating the limiting factor of the production of milligram quantities of ES-62 and in the case of bacterial expression removing the problematic carbohydrate moieties. The structural information obtained from future crystallographic studies could be used to examine any differences between the solution and crystalline structure of ES-62.

Finally an attempt was made to identify the receptor for ES-62 on a number of immune system cells to further aid understanding of the way in which ES-62 induces its immunomodulatory effects. This information could be used to aid both the development of vaccines and chemotherapeutic agents for treatment of filarial disease and in the development of immunomodulatory drugs.

2. Materials and Methods for Biochemical Analysis and Expression Systems

2.1. Isolation of Native ES-62

Native ES-62 was obtained by sacrificing infected jirds and harvesting the adult *A. viteae* worms. The harvested worms were then kept in tissue culture flasks containing RPMI 1640 (GIBCO BRL, Paisley, UK) complete medium at 37 °C in an atmosphere of 5 % CO₂ / 95 % air, where they secreted ES-62 into the media. To obtain the secreted ES-62 the media was collected and filtered through a 0.22 µm membrane filter to remove the adult worms. The media was then concentrated and transferred to PBS (5.5 mM potassium chloride, 145 mM sodium chloride, 8 mM disodium hydrogen orthophosphate, 1.5 mM sodium dihydrogen orthophosphate) pH 7.0 using an ultrafiltration cell (Amicon) with a 10 kDa cut-off membrane (PM10). To further concentrate the ES-62, centrifugal concentrators (Amicon) with a 100 kDa cut-off membrane were used. This concentrated sample was then subjected to FPLC purification using a Superose 6 column. Elution of the Superose 6 column with PBS pH 7.0 produced a single peak on the FPLC spectrophotometer trace (recorded at 280 nm). Analysis of the eluted samples by SDS PAGE and Western blotting determined that 95 % of the protein eluted was ES-62 (Harnett & Harnett, 1993).

2.2. Cell Culture

2.2.1. SF9 Cell Culture

The insect cell line, SF9, was cultured following the manufacturers instructions (PharMingen, 1999) using TMN-FH and protein free insect media (PharMingen, BD Biosciences, Cowley, Oxford)) supplemented with penicillin (100 U ml⁻¹) (GIBCO BRL, Paisley, UK) and streptomycin (100 µg ml⁻¹) (GIBCO BRL,

Paisley, UK). Cells were transferred from fully supplemented to protein free media following manufacturers instructions (PharMingen, 1999).

2.2.2. Culture of Cell Lines

U937, WEHI, Daudi, Jurkat, REH, 207, 697, Ramos and Nalm 6 cell lines were cultured in RPMI 1640 supplemented with 5 % (v/v) heat inactivated fetal calf serum, penicillin (100 U ml⁻¹) and streptomycin (100 µg ml⁻¹) at 37°C in 5 % CO₂/95 % humidified air.

2.3. PCR

PCR, polymerase chain reaction, is a technique used to amplify minute quantities of specific DNA using primers (Saiki *et al.*, 1985). PCR can also be used to add small sequences of DNA, such as restriction digestion sites, to the ends of target DNA. In this study PCR was used to amplify the ES-62 sequence within the pBluescript (Stratagene) vector and add appropriate restriction digestion sites to the ends of the sequence to allow cloning of ES-62 into either the pET 19b or pAcGP67-B vector. In order to perform PCR some knowledge of the sequence of the DNA to be amplified is required such that suitable primers can be designed.

2.3.1. Primer Design

PCR primers are usually between 15 and 30 bases in length, and are designed to bind to the DNA on either side of the region of interest. The primers usually have no greater than 50 % G+C content and should not contain sequences that could flip back on themselves forming secondary structure. In addition the primers should also not contain complementary regions in order to avoid the formation of primer dimers. All of the primers discussed below were obtained from Oswel (Oswel DNA Service, Lab 5005, Medical and Biological Sciences Building, University of Southampton, Boldrewood, Bassett Crescent East, Southampton SO16 7PX).

2.3.1.1. pET 19b

To clone ES-62 into pET 19b, ES-62 needed to be amplified from pBluescript (Stratagene) and Nde I and Bam HI restriction digestion sites had to be added onto the ends of ES-62. As the sequence of ES-62 was known, primers were designed to include the Nde I and Bam HI restriction digest site at either the N or C terminal regions. The sense primer, ES-62 sense, consisted of 14 bases of the N-terminal of ES-62 starting after the secretion signal with the restriction digest site for Nde I preceding it and 7 random bases. The antisense primer, ES-62 anti, consisted of the last 15 bases of the C-terminal of ES-62 with the restriction digest site for Bam HI attached to the end and six random bases. The sequences of the two primers are shown in Table 2-1.

2.3.1.2. pAcGP67-B

To clone ES-62 into pAcGP67-B, the vector used in overexpression in Sf9 cells, its DNA sequence needed to be amplified from pBluescript (Stratagene) and Bam HI and Eco RI restriction digest sites added onto the ends. PCR primers were designed that would add these restriction digest sites onto the appropriate ends of ES-62. The sense primer, BAC sense, consisted of the first fourteen bases of the N-terminal of ES-62, starting after the secretion signal, preceded by the sequence for the Bam HI restriction digest site and seven random bases. The antisense primer, BAC antisense, consisted of the last fifteen bases of ES-62 with the sequence for the restriction digest site for Eco RI attached to the end followed by six random bases. These two primers are shown in Table 2-1.

ES-62 sense	CGTCGTCCATATGGCAGCTGTCCTTCC
ES-62 anti	GCATTTTTTCGATATTCCTAGGACGACC
BAC sense	CGTCGTCCGATCCGCAGCTGTCCTTCC
BAC antisense	GCATTTTTTCGATATTCCTTAAGACGACC

Table 2-1: Sequences of the PCR primers used to amplify the ES-62 sequence and add restriction digestion sites to allow cloning of ES-62 into pET 19b and pAcGP67-B.

2.3.2. Program Design

PCR reactions involve the use of a number of components. The template for the amplification of ES-62 in both PCR reactions was the pBluescript construct containing the ES-62 insert. Other vital components for the reaction are 10x buffer (containing 500 mM potassium chloride, 100 mM Tris-HCl (pH 9.0) and 1 % Triton X-100), $MgCl_2$ (essential as divalent cations are cofactors for Taq polymerase with magnesium the best source of divalent cations for this purpose), deoxyribonucleotide triphosphates (dNTPs) and Taq polymerase (a thermostable DNA polymerase that replicates DNA at an optimal temperature of 74 °C). 25 pmol of each relevant primer was used in each PCR reaction. The annealing temperature of the primers, supplied in the data sheet from Oswel, is of vital importance, as this is required to design the PCR program, discussed below.

There are three steps to PCR; the first is a denaturation step to yield single stranded DNA, the second is an annealing step during which the primers bind to the single stranded DNA and the final step is the extension step during which time the DNA is amplified. For the PCR amplification of ES-62 a low initial annealing temperature was employed for two cycles to increase the starting material without imposing too stringent criteria for binding. The annealing temperature was then raised to 5 °C below the lowest of the annealing temperatures supplied with the two primers.

PCR reactions were set up as follows: 20-40 ng of template DNA was mixed with 1 µl of 25 pmol/µl primers (either ES-62 sense and antisense or BAC sense and antisense), 2.5 µl of 10x PCR buffer (Promega), 1 µl of 10 mM dNTPs (Promega), 1.5 µl of 25 mM $MgCl_2$ and 0.5 µl Taq (Promega) in a total volume of 25 µl. The reactions were pipetted to mix and then run in a thermocycler using the relevant program, depending on the primers used, described in Table 2-2.

Step	Time (minutes)	Temperature (°C) ES-62 sense and antisense	Temperature (°C) BAC sense and antisense	
1	1	94	94	2 cycles
2	1	37	37	
3	2	72	72	
1	1	94	94	25 cycles
2	1	53	53	
3	2	72	72	

Table 2-2: PCR protocols for the thermocycler for both sets of primers.

2.4. Restriction Digests

Restriction digests were performed to allow ligation to be carried out and also to allow identification of vector constructs containing the ES-62 insert. Restriction digests performed for the purpose of ligation of ES-62 into pET 19b were carried out as follows. Two reactions were set up, one containing 3 µg of ES-62/pGEM-T Easy construct DNA and the second containing 3 µg of pET 19b vector DNA along with 3 µl 10x buffer B (Boehringer Mannheim) and 10 U BamHI (Boehringer Mannheim) in a total volume of 30 µl made up with dH₂O. The mixture was incubated at 37 °C for 20 minutes and then 10 U of NdeI (Boehringer Mannheim) was added. The reaction was incubated at 37 °C for a further hour and then a further 5 U of NdeI was added to each tube. The reaction was then incubated at 37 °C for a further 2 hours. 1 µl shrimp alkaline phosphatase (Promega) was then added to the Eppendorf tube containing the pET 19b digested DNA to remove the 5' phosphate to prevent recircularisation of the pET 19b vector. DNA loading buffer was added to the reactions and they were run on 1 % low melt agarose gels.

Restriction digests performed for the purpose of ligation of ES-62 into AcGP67-B were carried out as follows. Two reactions were set up, one containing 3 µg of ES-62/pGEM-T Easy construct DNA and the second containing 3 µg pAcGP67-B vector DNA along with 2.5 µl 10x buffer B and 10 U Bam HI in a total volume of 25 µl made up with dH₂O. The mixture was incubated at 37 °C for 1 hour and then 10 U of Eco RI (Boehringer Mannheim) was added. The reaction was then incubated at 37 °C for a further 3 hours. DNA loading buffer was added to the reactions and they were run on 1 % low melt agarose gels.

Restriction digests performed for the identification of positive colonies of ES-62 in pET 19b were performed as follows; 20 µl DNA from a miniprep of the colony of interest was incubated with 3 µl 10x buffer B, 10 U Bam HI, 10 U Nde I and dH₂O to a total volume of 30 µl. The reaction was incubated at 37 °C overnight and then run on a 1 % agarose gel to identify colonies in which the restriction digestion had led to the release of an insert the correct size for ES-62.

Restriction digests performed for the identification of positive colonies of ES-62 in pAcGP67-B were performed as follows; 5 µl DNA from a miniprep of the colony of interest was incubated with 2.5 µl 10x buffer B (Boehringer Mannheim), 10 U Bam HI (Boehringer Mannheim), 10 U Eco RI (Boehringer Mannheim) and dH₂O to a total volume of 25 µl. The reaction was incubated at 37 °C for 3 hours and then run on a 0.7 % agarose gel to identify colonies in which the restriction digestion had led to the release of an insert of the correct size for ES-62.

2.5. Cloning

2.5.1. Cloning for Initial Sequence Identification

ES-62 was cloned into pBluescript (Stratagene) as described by Harnett *et al.* (1999) for sequencing purposes by W. Harnett *et al.*.

2.5.2. Cloning for Expression in a Bacterial Expression System

In order to clone ES-62 into the pET 19b bacterial expression vector (Novagen) it was necessary to attach the appropriate restriction enzyme cleavage sites to the ends of the ES-62 sequence. This was achieved using PCR (as detailed in section 2.3). To overcome the problems of digesting restriction digest sites at the ends of fragments of DNA, the PCR product was first ligated into pGEM-T Easy (Promega) before cloning into pET19b.

2.5.2.1. Ligation

2.5.2.1.1. pGEM-T Easy

The ES-62 PCR fragment, obtained from pBluescript, was blunt end ligated into pGEM-T Easy. 1 µl of 10x ligation buffer (Promega) was mixed with 1 µl of pGEM-T Easy vector (50 ng), 3 µl of PCR fragment (150 ng), 1 µl of T4 DNA ligase (Promega) (3 Weiss units) and 4 µl of deionised water. The reaction was incubated overnight at 4 °C.

2.5.2.1.2. pET 19b

The insert from pGEM-T Easy, isolated by restriction enzyme digestion as detailed in section 2.4, was ligated into the pET19b vector, which had been subject to restriction enzyme digestion by Nde I and Bam HI as detailed in section 2.4. The digested pGEM-T Easy and pET 19b vectors were run on a low

melt agarose gel (1 %). The bands representing the ES-62 fragment from the pGEM-T Easy vector and the digested pET 19b vector were cut out of the gel and placed in Eppendorf tubes. The Eppendorf tubes were centrifuged briefly to collect the gel slices at the base of the tubes. The gel slices were then heated to 65 °C until melted and again centrifuged briefly to collect the gel at the base of the tubes. The ligation reaction was then set up as follows; 2 µl of low salt 10x buffer (Boehringer Mannheim) was mixed with 0.5 µl of pET vector band, 3 µl of ES-62 band and 11.5 µl deionised water. 1 µl T4 DNA ligase and 2 µl 10 mM ATP (Promega) were added to the reaction after the gel had cooled. The reaction was incubated at 16 °C overnight.

2.5.2.2. Transformation

2.5.2.2.1. *pGEM-T Easy*

The ligation reaction was transformed into JM109 (Promega) competent cells. 1 µl of the ligation reaction was gently mixed, by flicking, with 50 µl of competent cells. The cells were left on ice for 20 minutes to allow the DNA to complex with calcium and deposit on the cells and also to aid membrane ruffling which increases ease of uptake of DNA into the cells. The cells were then heat shocked for 45 seconds at 42 °C to induce uptake of DNA into the cells. The cells were then returned to ice for 2 minutes. 950 µl of room temperature SOC medium (Promega) was added to the cells and the cells incubated for 1.5 hours at 37 °C with shaking. The cells were then pelleted by centrifuging briefly and most of the supernatant decanted leaving ~100 µl remaining. The pellet was resuspended in the remaining 100 µl and then plated out onto an L broth/IPTG/ampicillin/X-Gal agar plate to allow for selection of recombinant transformants using blue/white screening.

2.5.2.2.2. *pET 19b*

Transformation of the pET 19b constructs was performed as described in section 2.5.2.2.1 except Novablue (Novagen) competent cells were used in place of

JM109 competent cells and the Novablue competent cells were plated out onto L broth/ampicillin (50 µg/ml) agar plates. Positive colonies were identified by growing small cultures of some of the colonies, minipreping to isolate the vector DNA and performing restriction digests with Nde I and Bam HI to establish whether the vector contained the ES-62 insert. Six positives were selected for expression purposes and transformed into BL21 (DE3) cells (Novagen), as described for transformation of the pET 19b construct into Novablue competent cells.

2.5.2.3. Minipreps

Minipreps were carried out using a QIAprep Spin Miniprep kit (Qiagen) and the following protocol. Buffers P1, P2, N3, PB, PE and EB are supplied as part of the kit. An overnight culture was obtained by inoculating 5 ml L broth containing 5 µl 100 mg ml⁻¹ ampicillin with the colony of interest and growing overnight at 37 °C in a shaking incubator. Following incubation 3 ml of the overnight culture was spun (1.5 ml at a time) in an Eppendorf tube at 13500 rpm for 10 minutes in a bench top centrifuge. The pellet was resuspended in 250 µl of buffer P1 which contains RNase A to remove any RNA contaminants. The cells were then subjected to alkaline lysis by addition of 250 µl of buffer P2 and the Eppendorf tube gently inverted 4-6 times. The sample was then neutralised by addition of 350 µl of buffer N3, which also contains a high salt concentration that causes precipitation of denatured proteins, chromosomal DNA and cellular debris, and the Eppendorf tube inverted 4-6 times. The mixture was next centrifuged at 13500 rpm for 10 minutes in a bench top centrifuge to pellet the precipitated proteins, chromosomal DNA and cellular debris. The supernatant, containing the plasmid DNA, was added to a QIAprep spin column, the column was centrifuged for 30-60 seconds at 13500 rpm in a bench top centrifuge and the flow through was discarded. In those cells with high nuclease activity or high carbohydrate content (i.e SOLR strain used in initial cloning with pBluescript and JM109 cells used in the blunt end cloning step into the pGEM-T Easy vector, but not Novablue or BL21 (DE3) cells) a further step was including at this point. This further step involved the addition of 500 µl of buffer PB to the column, which

removes any endonucleases. The column was then spun again for 30-60 seconds at 13500 rpm in a bench top centrifuge and the flow through discarded. The next step, for all cell lines, was to add 750 μ l of buffer PE to the column and again centrifuge for 30-60 seconds at 13500 rpm in a bench top centrifuge. This step removes the salts from the sample. The flow through was discarded and the column spun for a further minute at 13500 rpm in a bench top centrifuge to remove residual wash buffer. The Qiaprep column was then placed into an Eppendorf tube and 50 μ l of buffer EB was added to the centre of the column. The column was left to stand for 1 minute and then spun for a minute at 13500 rpm in a bench top centrifuge. The Qiaprep column was then discarded and 1/10 volume of the eluate volume of 2 M sodium acetate and 2 volumes of the eluate volume of ethanol were added to the Eppendorf tube containing the eluate from the column. The sample was then stored at -20°C for a minimum of 30 minutes. Following incubation at -20°C the sample was centrifuged for 30 minutes at 13500 rpm at 4°C . The supernatant was discarded and the pellet washed in 70 % ethanol. The wash supernatant was then discarded and the pellet air dried and resuspended in 30 μ l of TE buffer (10 mM Tris pH 7.5 and 1mM EDTA).

2.5.2.4. *Glycerol Stocks*

Glycerol stocks of the cultures were made by mixing 500 μ l sterile 80 % glycerol with 500 μ l of culture medium from the overnight culture in sterile capped Eppendorf tubes. Glycerol stocks were stored at -70°C .

2.5.3. Cloning for Expression in Insect Expression System

The restriction enzyme digestion sites at the ends of the insert in pET 19b were not suitable for cloning into the pAcGP67-B vector for baculovirus expression. Thus PCR was carried out as described in section 2.3 using primers which contained appropriate restriction digest sites for cloning into pAcGP67-B (PharMingen). As with cloning in pET 19b, the PCR insert was cloned first into PGEM-T Easy, and in this case sequenced, before being cloned into pAcGP67-B.

2.5.3.1. Ligation

2.5.3.1.1. *pGEM-T Easy*

The ES-62 PCR fragment was ligated into pGEM-T Easy as detailed in section 2.5.2.1.1.

2.5.3.1.2. *pAcGP67-B*

The insert from pGEM-T Easy, isolated by restriction enzyme digestion as detailed in section 2.4, was ligated into the pAcGP67-B vector, which had been subject to restriction enzyme digestion by Eco RI and Bam HI as detailed in section 2.4. The digested pGEM-T Easy and pAcGP67-B were run on a low melt agarose gel (1 %). The bands representing the ES-62 fragment from the pGEM-T Easy vector and the digested pAcGP67-B were cut out of the gel and placed in Eppendorf tubes. The Eppendorf tubes were centrifuged briefly to collect the gel slices at the base of the tubes. The gel slices were then heated to 65 °C until melted and again centrifuged briefly to collect the gel at the base of the tubes. The ligation reaction was then set up as follows; 2 µl of low salt 10x buffer was mixed with 2 µl of the pAcGP67-B vector band, 2 µl of the ES-62 band and 11 µl deionised water. 1 µl of T4 DNA ligase and 2 µl of 10 mM ATP were added to the reaction after the gel cooled. The reaction was incubated at 16 °C overnight.

2.5.3.2. Transformation

2.5.3.2.1. *pGEM-T Easy*

The pGEM-T Easy ligation with ES-62 was transformed into JM109 competent cells as detailed in section 2.5.2.2.1.

2.5.3.2.2. *pAcGP67-B*

The pAcGP67-B ligation with ES-62 was transformed into Novablue competent cells. 1.7 µl of a 1:20 dilution of β-mercaptoethanol was added to 100 µl of

Novablue cells on ice. The cells were incubated on ice for 10 minutes swirling every 2 minutes. After the 10 minute incubation, 1 μ l of ligation reaction mix was added to the cells and they were incubated on ice for 30 minutes. Cells were then heat shocked for 50 seconds at 42°C followed by 2 minutes incubation on ice. 900 μ l of SOC medium, preheated to 37 °C, was added to the cells and they were incubated for 1 hour at 37 °C with shaking. The cells were then spun at 4000 rpm for 10 minutes and the supernatant removed. The pellet was resuspended in the residual media, plated onto an L broth/ampicillin (100 μ l/ml) agar plate and incubated at 37 °C overnight.

Following successful cloning of ES-62 into pAcGP67-B, as determined by restriction digestion with Bam HI and Eco RI, the next step was to make recombinant virus. This was achieved by homologous recombination of the pAcGP67-B vector containing the insert with BaculoGold DNA (PharMingen) (for method see section 2.7). The BaculoGold DNA has been modified such that if homologous recombination with the vector does not occur then the viral DNA cannot form infectious particles as it is missing vital genes that are present on the vector along with the insert of interest. Thus any infectious viral particles which form following homologous recombination must contain the vector and therefore the insert as well.

2.6. Sequencing

The ES-62 inserts from the pET 19b and pAcGP67-B vector constructs were sequenced to ensure no errors had arisen from the PCR amplification of ES-62. The ES-62 insert from pET 19b was sequenced whilst in pET 19b while the ES-62 insert from pAcGP67-B was sequenced whilst in pGEM-T Easy. Sequencing in both cases was carried out using the T7 forward primer and some internal primers used to sequence ES-62 initially (Harnett et al., 1999). 100 μ l of 63 ng μ l⁻¹ of the pET 19b and the pGEM-T Easy vector constructs were sent to PNACL (Protein and Nucleic Acid Chemistry Laboratory, CMHT, Hodgkin Building, University of Leicester, Leicester) along with 10 μ l of 1 pmol μ l⁻¹ of four of the internal ES-62 primers and of the T7 promoter and terminator primers.

2.7. Homologous Recombination

Homologous recombination is the method by which the pAcGP67-B vector that has been identified as containing an ES-62 insert, is combined with baculovirus DNA to enable formation of recombinant virus particles. As mentioned previously the baculovirus DNA with which the vector is combined has been genetically manipulated such that it can only form virus particles if it combines with the vector DNA. Homologous recombination of the vector containing ES-62 and the BaculoGold DNA was performed according to manufacturers instructions (PharMingen, 1999).

2.8. Amplification

Amplification of the viral stock to obtain larger quantities of high titre virus was performed according to the manufacturer's instructions (PharMingen, 1999), with the exception that the cells were incubated for 5 days instead of 3 and that the cellular debris were spun out at 5000 x g instead of 10000 x g.

2.9. Plaque Assays

The method detailed in the manufacturers instructions (PharMingen, 1999) was complicated to set up and unsuccessful in determining the titre of the amplified stocks, thus a modified version of this plaque assay was employed as detailed below. 1×10^6 cells were plated in each well of a 6 well plate and allowed to attach for 30 minutes at room temperature. The media was then removed from the cells and 1 ml of fresh TMN-FH media added to each well. 1 ml of virus was added to the first well and mixed well, 100 μ l was then taken from this well and added to the next well and so on to give serial dilutions of 10^4 , 10^5 , 10^6 , 10^7 and 10^8 with one well containing no virus. The cells were then incubated for 1 hour at room temperature, rocking gently. 12 ml of 1.6 % Agarplaque (PharMingen) in protein free media, per 6 well plate, was prepared and kept at 42 °C. 12 mls of TMN-FH media, per 6 well plate, was also warmed to 42 °C. After 1 hour incubation the same volume of TMN-FH media was added to the 1.6 % Agarplaque solution (i.e. 12 ml media to 12 ml Agarplaque) to give a 0.8 %

Agarplaque solution. The solution was mixed well and kept at 42 °C. The inoculum was removed from each well of the 6 well plate and the cells in each well overlaid, carefully, with 3 ml of 0.8 % Agarplaque. The plates were rocked gently to prevent formation of a fluid layer under the Agarplaque from any residual media and then wrapped in Saran wrap and incubated at 27 °C for 4-5 days. After 4-5 days each well was overlaid with 1 ml neutral red dye solution (9 ml 0.8 % Agarplaque in protein free media, 1 ml filtered neutral red dye per 6 well plate) and incubated overnight at 27 °C. The plaques were clearly visible the following day. The viral titre was determined by counting the number of plaques in a well containing approximately 50 plaques. The viral titre was then expressed as pfu ml⁻¹ of original stock. e.g. if 48 plaques were counted in the 10⁵ dilution well then the viral titre was 4.8 x 10⁶ pfu ml⁻¹.

2.10. Expression of Recombinant ES-62

2.10.1. Bacterial Expression System

Once colonies that contained the ES-62 insert within the pET 19b vector had been identified and glycerol stocks made of these colonies, as detailed in section 2.5.2.4, the next step was to see if recombinant ES-62 was being produced. 5 ml L broth containing ampicillin at 100 µg ml⁻¹ was inoculated with a stab from a glycerol stock and grown at 37 °C in a shaking incubator until the optical density at 600 nm in a 1 cm pathlength cuvette was 0.6. IPTG was then added at a final concentration of 1 mM and the culture left to grow for 3 hours. Cells were pelleted by centrifuging at 6000 x g for 10 minutes and the pellets resuspended in 2x loading buffer, run on a SDS PAGE gel and Coomassie Blue stained (sections 2.14 & 2.19).

Once expression of recombinant ES-62 was established, a larger scale expression was performed and cells were lysed to ascertain whether the recombinant protein was soluble or insoluble. Further, in order to establish the start of the log phase of growth of the bacteria, which is the point at which expression should be induced by addition of IPTG, a growth curve for BL21 (DE3) cells transfected

with the pET 19b/ES-62 construct was obtained. This growth curve showed that the log phase of growth for these cells started when the optical density at 600 nm was approximately 0.7. Large scale bacterial expression of ES-62 was then performed as follows; an overnight culture was obtained by inoculating 20 ml L-broth containing ampicillin at 100 $\mu\text{g ml}^{-1}$ with a stab from the glycerol stock and growing overnight at 37 °C in a shaking incubator. 1 L of L-broth containing ampicillin at 100 $\mu\text{g ml}^{-1}$ was inoculated with the 20 ml overnight culture and then grown at 37 °C in a shaking incubator for approximately 2 hours until the optical density at 600 nm was 0.7. IPTG was then added at a final concentration of 1 mM and the culture allowed to grow for a further 3 hours. The cells were then pelleted by centrifugation at 6000 x g for 10 minutes and lysed using sonication (6 x 30 s bursts) or cell disruption. The lysed cells were then centrifuged at 6000 x g for 10 minutes and a sample of both the cell pellet (which contains nuclear and membrane material along with inclusion bodies that contain any insoluble proteins) and the supernatant (which contains soluble proteins from the cytosol of the cells) run on a SDS-PAGE gel.

A number of different growth conditions, as listed in Table 2-3, were attempted using the expression protocol above to optimise expression of soluble recombinant ES-62.

Growth Temperature (°C)	IPTG concentration (mM)	Induction time (hours)
37	1, 0.5, 0.25, 0.1	3
30	1, 0.5, 0.25, 0.1	4
25	1, 0.5, 0.25, 0.1	5
16	1, 0.5, 0.25, 0.1	~18

Table 2-3: Growth and induction conditions for expression trials of bacterial recombinant ES-62. Cells were grown in L broth containing 100 $\mu\text{g ml}^{-1}$ ampicillin at 37 °C until an optical density at 600 nm of 0.7 was reached. IPTG was then added at the appropriate concentration and the growth temperature altered accordingly.

In all expression trials, the BL21 (DE3) cells were grown at 37 °C until induction (addition of IPTG) and then the temperature was adjusted as detailed in Table 2-3. The quantity of soluble expressed recombinant ES-62 produced was assessed by lysing the cells and running samples of both the pellet and supernatant on a SDS-PAGE gel. In addition to the above conditions leaky expression was also tested for by growing uninduced cells for 48 hours at 20 °C. The cells were then harvested and the quantity of expressed recombinant ES-62 produced assessed as detailed above.

From the expression conditions tested, optimal expression of soluble recombinant ES-62 was found to occur when the BL21 (DE3) cells, containing the ES-62/pET 19b construct, were grown at 37 °C, induced using IPTG at a final concentration of 0.1 mM then incubated at 25 °C for a further 4-5 hours. The bacterial cells were then harvested as described previously.

2.10.2. Baculovirus Expression System

Once colonies that contained the ES-62 insert within the pAcGP67-B vector had been identified, homologous recombination performed to obtain recombinant virus particles containing the DNA for ES-62 and the virus particles amplified to a sufficiently high titre as advised in the manufacturers instructions (PharMingen, 1999), SF9 cells were infected with different amounts of the recombinant virus, known as different multiplicities of infection (MOI). The MOI is calculated by dividing the number of virus particles by the number of cells infected. SF9 cells were infected at MOIs of 3, 7 and 10 to determine the optimum MOI for expression of recombinant ES-62.

From the conditions tested, optimal expression of recombinant ES-62 was achieved when cells were infected at an MOI of 10. To obtain recombinant ES-62, 2×10^7 SF9 cells grown in protein free media were seeded onto a 150 mm tissue culture flask in a total of 30 ml of protein free media. The cells were allowed to bed down for 1 hour and then infected with high titre recombinant baculovirus at an MOI of 10. Cells were incubated at 27 °C for 2 days and the

supernatant then harvested, as the pAcGP67-B vector in which ES-62 was cloned has a secretion signal and thus the recombinant protein will be secreted. Any cells present in the supernatant were pelleted by centrifugation at 5000 x g for 5 minutes. The supernatant was then cleared further by centrifugation at 10000 x g for 10 minutes. The virus particles present in the supernatant were then removed by centrifugation of the supernatant at 50000 x g for 1 hour. Recombinant ES-62 was isolated from the supernatant by purification techniques discussed in section 2.12.

2.11. Refolding of Insoluble Bacterial Recombinant ES-62

The insolubility of the bacterial recombinant ES-62 (section 5.1.3) resulted in the development of a protocol to refold the protein. Many different refolding protocols were tried, the method described here was the most successful method identified for refolding of ES-62.

Cells from 1 L of bacterial culture, grown and induced as described in section 2.10.1, were pelleted by centrifugation at 6000 x g for 10 minutes. The pellet was resuspended in 50 ml buffer 1 (50 mM sodium acetate, 5 mM EDTA, 5 % (w/v) sucrose), frozen and thawed twice, and then sonicated (6 x 30 s bursts) in 10 ml aliquots to lyse the cells. The lysed cells were then centrifuged at 6000 x g for 10 minutes and the pellet, containing the insoluble material, washed once in 50 ml buffer 2 (50 mM sodium acetate, 5 mM EDTA, 0.1 % (v/v) Triton X-100), twice in 50 ml buffer 3 (50 mM sodium acetate, 5 mM EDTA, 2 M urea) and once in 50 ml dH₂O. The pellet was then solubilised by addition of 20-25 ml buffer 4 (100 mM sodium acetate, 8 M urea, 10 mM DTT) followed by incubation at 37 °C for 1 hour in a shaking incubator (250 rpm). The solubilised pellet was then diluted to 0.01 – 0.5 mg ml⁻¹, in buffer 5, (100 mM sodium acetate, 5 mM EDTA, 8 M urea), as assessed by a Bradford protein assay. The solubilised protein solution was then dialysed against 100 volumes of buffer 6 (100 mM sodium acetate, 50 mM sodium chloride). Modifications to this protocol are discussed in Chapter 5.

2.12. Purification

Purification of recombinant protein depends on the characteristics of the protein in question and on whether or not it has been expressed with a tag e.g. a GST or 5 –histidine tag. If the protein is known to have a substrate for which it has a reasonably high affinity or if it has been expressed with a tag then affinity chromatography is usually the purification method of choice. However, if there is no known substrate or tag then other purification methods based on the physical characteristics of the protein are used.

2.12.1. Affinity Chromatography

This method was used to purify the bacterial recombinant ES-62. The bacterial expression system employed for production of recombinant ES-62 attached a cleavable histidine tag to the N-terminal of the protein. The histidine tag shows strong affinity towards divalent cations (such as nickel, zinc and copper) and this affinity was exploited to allow purification of the recombinant material. After harvesting the cells by centrifugation as discussed in section 2.10, the cells were resuspended in 20 mM imidazole, 50 mM sodium acetate, 300 mM sodium chloride and lysed using sonication (6 x 30 s bursts). The lysed cells were then centrifuged at 13000 x g for 25 minutes, the supernatant filtered, adding DNase (Promega) if the supernatant was very viscous, and then loaded onto the metal chelate column for purification. Unbound proteins were washed off and the target protein recovered by elution with imidazole. Imidazole binds tightly to divalent cations and thus competes with the histidine tags for binding to the divalent cations on the column, dislodging the tags and allowing elution of the recombinant protein. A UV detector was used to monitor elution of the proteins from the column. This method was employed to purify both the soluble recombinant protein and the refolded recombinant material. Table 2-4 shows the steps in the purification protocol and the buffers employed at each stage. The method described in Table 2-4 was altered as detailed in the figure legend only during optimisation of the purification protocol. A further alteration to this protocol was to include LDAO, a mild detergent, in all the buffers at concentrations of either 0.01, 0.05 or 0.1 % (v/v).

Loading of greater than 5 ml of lysed crude bacterial preparation was achieved by adding in multiple repeats of steps 6 and 7 until the appropriate volume was loaded. This is not recommended if the crude bacterial preparation has a high concentration of expressed protein as the column will be overloaded.

Step	Description	Solutions loaded onto column
1	Clean column to regenerate	480 mM NaCl 100 mM EDTA
2	Wash column	dH ₂ O
3	Charging of column with divalent cations	100 mM NiSO ₄
4	Removal of unbound divalent cations	1. dH ₂ O 2. 480 mM NaCl 3. 500 mM imidazole
5	Equilibrate column	500 mM NaOAc 480 mM NaCl 20 mM imidazole
6	Load sample	5 ml of crude bacterial preparation
7	Wash to remove unbound sample	500 mM NaOAc 480 mM NaCl 60 mM imidazole
8	Elution of bound material	500 mM NaOAc 480 mM NaCl 500 mM imidazole
9	Clean column to regenerate	480 mM NaCl 100 mM EDTA

Table 2-4: Protocol for affinity purification of bacterially expressed recombinant ES-62. Note that at step 8, elution of the bound proteins was also attempted using an imidazole gradient from 60 mM to 500 mM or with 2 steps, first to 20 mM imidazole and then to 750 mM imidazole. Elution from the column was monitored using an inline UV detector.

2.12.2. Ion Exchange

Ion exchange chromatography was used to purify baculovirus expressed recombinant ES-62. The pI of wild type ES-62 and recombinant ES-62 was determined experimentally (section 2.33) to be approximately 5.6. Thus the recombinant protein has a negative charge when in PBS (5.5 mM potassium chloride, 145 mM sodium chloride, 8 mM disodium hydrogen orthophosphate, 1.5 mM sodium dihydrogen orthophosphate) at pH 7.2, the buffer condition in which wild type ES-62 is stable. Anion exchange was therefore performed on the crude baculovirus preparation with the aim that the recombinant ES-62 would bind to the column and could be eluted in a pure state by increasing salt concentration. The crude baculovirus supernatant from infected cells was concentrated in an ultrafiltration stirred cell (Amicon) and dialysed overnight into pH 7.0 phosphate buffer (3.2 mM potassium chloride, 9.6 mM disodium hydrogen orthophosphate, 1.9 mM potassium dihydrogen orthophosphate) prior to loading on to the column. The column used was a POROS 20HQ column (PerSeptive Biosystems). The column was equilibrated in 10 column volumes of phosphate buffer, 5 ml of the sample was loaded and then the column washed with 10 column volumes of 45 mM NaCl to remove any unbound material. The two steps of loading and washing were repeated 3 or 4 times. Following the removal of any unbound material, elution of proteins from the column was achieved using a salt gradient starting at 45 mM NaCl and running to 300 mM NaCl. A UV detector was used to monitor the elution of proteins from the column. The fractions collected were tested for the presence of ES-62 by Western blotting (section 2.16) to identify the salt concentration at which recombinant ES-62 was eluted. The column was cleaned to allow reuse by washing with a salt gradient starting at 300 mM NaCl, finishing at 1.5 M NaCl.

2.12.3. Gel Filtration

Gel filtration was used to attempt to separate tetrameric ES-62 from monomeric ES-62 after the anion exchange purification step. A Superose 12 (HR10/30) (Pharmacia Biotech) column with a bed volume of 24 ml was attached to a Pharmacia Biotech FPLC pump. The column was equilibrated at 0.4 ml min^{-1}

with filtered and degassed phosphate buffer pH 7.0 (50 mM disodium hydrogen orthophosphate, 50 mM potassium dihydrogen orthophosphate, 150 mM NaCl). 200 μ l of sample was then loaded onto the column and 30 ml phosphate buffer pH 7.0 run through the column at 0.4 ml min⁻¹. 0.5 ml fractions were collected starting immediately after the sample was loaded. Each fraction passed through an inline detector and the absorbance trace at 280 nm was plotted on a chart recorder. The fractions constituting each peak detected were pooled, filtered and then tested for the presence of recombinant ES-62 using Western blotting procedures (section 2.16).

2.12.4. Filtration

An ultrafiltration stirred cell (Amicon) with 30 kDa (YM 30) and 100 kDa (YM 100) cut-off membranes was used to attempt to concentrate and partially purify recombinant ES-62 from cleared baculovirus supernatant from infected SF9 insect cells (recombinant ES-62 should be the major protein secreted into the media). The cleared supernatant was spun through the YM 100 membrane first until only 15-20 ml were remaining and the filtrate collected. The YM 100 membrane is a 100 kDa cut off membrane, thus all proteins below 100 kDa in mass should pass through it leaving only proteins greater than 100 kDa retarded by the membrane. The aim of this procedure was to enable the separation of tetrameric recombinant ES-62 from monomeric recombinant ES-62. The 15-20 ml retarded by the membrane were washed with PBS pH 7.0 (5.5 mM potassium chloride, 145 mM sodium chloride, 8 mM disodium hydrogen orthophosphate, 1.5 mM sodium dihydrogen orthophosphate). PBS was added to the sample increasing the volume to 120 ml and the sample then spun down again to 15-20 ml, the filtrate again being collected. This process was repeated once more and the 15-20 ml remaining then removed from the stirred cell, filtered and stored, sterile, at 4 °C. The collected filtrate from the YM 100 membrane was placed in a stirred cell and spun through a YM 30 membrane until only 15-20 ml was remaining. The YM 30 membrane allows proteins smaller than 30 kDa in mass to pass through it and retards those greater than 30 kDa enabling small molecular weight, <30kDa, contaminants of the sample to be removed. The 15-20 ml

sample retarded by the membrane was washed in PBS as before and then removed from the stirred cell, filtered and stored, sterile, at 4 °C. The samples were tested for the presence of ES-62 using Western blotting techniques (section 2.16).

2.13. Agarose Gel Electrophoresis

Low melt agarose (Boehringer Mannheim) was dissolved by heating in TAE buffer (40 mM tris base, 5.51 % (v/v) glacial acetic acid, 1 mM EDTA, pH 8) at an appropriate percentage (w/v) for the DNA fragments to be visualised. Ethidium bromide ($1.5 \mu\text{g ml}^{-1}$) was added to the solution once it had cooled slightly. The gel mixture was then poured immediately using agarose gel electrophoresis equipment (BioRad) according to manufacturer's guidelines. Samples were run at 100 volts until sufficiently separated. Samples were visualised using a UV light source and photographs were taken of the images obtained.

2.14. SDS Polyacrylamide Gel Electrophoresis (SDS-PAGE)

Tris-glycine SDS polyacrylamide gels for gel electrophoresis of proteins were prepared and run using the solutions and protocols as described by Harlow & Lane, (1988), Laemmli, (1970) and Sambrook *et al.*, (1989).

2.15. Polyacrylamide Gel Electrophoresis

Tris-glycine polyacrylamide gels for gel electrophoresis of proteins under non-denaturing and non-reducing conditions were prepared and run as described in section 2.14 except SDS and β -mercaptoethanol were excluded from all the buffers used and the samples were not boiled prior to loading.

2.16. Western Blotting

Gels were transferred to either nitrocellulose or PVDF membrane (activated in methanol) using gel transfer apparatus (Biorad). Transfer was achieved either overnight at 40 mA or for 1 hour at 100 volts and variable current in transfer buffer (200 mM glycine, 25 mM tris in 800 ml dH₂O, 200 ml methanol).

Membranes were blocked in 10 % skimmed powdered milk or 1 % BSA for a minimum of 1 hour, but preferably overnight. Antibody dilutions were made up in 1 % skimmed milk powder or 0.1 % BSA in TBS-T (500 mM sodium chloride, 20 mM tris, 0.001 % Tween-20). Antibody incubations were typically left for 3 hours at room temperature or overnight at 4°C for primary antibodies, and 1 hour at room temperature for secondary antibodies. Membranes were washed between the antibody incubations and after the secondary antibody incubation twice for 15 minutes and 3 times for 5 minutes with TBS-T.

Membranes were developed using Amersham ECL visualisation technology for secondary antibodies that were HRP conjugates and using NBT BCIP substrate tablets (Sigma) for secondary antibodies that were alkaline phosphatase conjugates. BSA or skimmed milk powder was used depending on the recommendation supplied on the antibody data sheet.

2.16.1. Antibodies

The following antibodies were used in Western blotting;

Antibody	Supplier	Concentration
Rabbit anti-ES-62	W. Harnett	100 µg ml ⁻¹
Anti-rabbit-HRP	Sigma	1:3000 dilution
Anti-rabbit-HRP	Amersham Pharmacia	1:2000 dilution
Anti-rabbit-alkaline phosphatase	Amersham Pharmacia	1:30000 dilution
TEPC-15 (anti-PC)	Sigma	10 µg ml ⁻¹
Anti-mouse IgA-alkaline phosphatase	Amersham Pharmacia	1:30000 dilution
Anti-TLR2-biotin	Insight Technology	1 µg ml ⁻¹
Anti-TLR-4-biotin	Insight Technology	1 µg ml ⁻¹
Anti-biotin	New England Biolabs	1:2000 dilution
Anti-mouse-HRP	Amersham Pharmacia	1:4000 dilution

Anti p65 and p50 (NFκB subunits)	Santa Cruz technology	1:1000 dilution
Anti phospho p44/42 MAPK (Erk)	New England Biolabs	1:1000 dilution
Anti phospho JNK	Promega	1:1000 dilution
Anti phospho p38	Santa Cruz	1:1000 dilution
Anti P44/p42 MAPK	New England Biolabs	1:1000 dilution
Anti SAPK/JNK	New England Biolabs	1:2000 dilution

2.17. Far Western Blotting

Far Western blotting was carried out as described for Western blotting in section 2.16, except that a biotin conjugate of ES-62 was used in place of the primary antibody. A secondary antibody, anti-biotin conjugated to HRP (horse-radish peroxidase) was used as normal.

2.18. Slot Blotting

Slot blots were performed using slot blotting apparatus (Scotlab, UK) connected to a vacuum pump. The apparatus was set up according to manufacturer's guidelines with nitrocellulose, pre-wetted in transfer buffer (200 mM glycine, 25 mM tris in 800 ml dH₂O, 200 ml methanol), as the membrane onto which the proteins were transferred. Blocking of the nitrocellulose and antibody incubations were performed as described in section 2.16.

2.19. Gel Staining

A variety of methods can be used to stain SDS polyacrylamide gels in order to visualise the protein bands. Tris glycine SDS polyacrylamide gels were run as detailed in section 2.14. Staining of the gels was then performed using one of the three following methods. Silver staining (the most sensitive gel staining protocol), zinc staining or Coomassie Blue staining (least sensitive).

2.19.1. Silver Stain

Silver staining of SDS-PAGE gels was accomplished with the ten steps detailed in Table 2-5.

Step	Time (minutes)	Treatment
1	30	20 % (v/v) trichloroacetic acid (TCA)
2	10	50 % (v/v) methanol; 10 % (v/v) acetic acid
3	20	20 % (v/v) methanol; 5 % (v/v) acetic acid
4	10	8 % (v/v) gluteraldehyde
5	2 x 2	dH ₂ O
6	20	0.25 % (w/v) silver nitrate
7	2 x 1	dH ₂ O
8	2-10	2.5 % (w/v) sodium carbonate; 0.1 % (v/v) formaldehyde
9	30	10 % (v/v) glycerol; 5 % (v/v) acetic acid
10	~60	Gel drier at 80 °C

Table 2-5: Silver staining protocol

2.19.2. Zinc Stain

SDS-PAGE gels were zinc stained using the BioRad zinc stain and destain kit for electrophoresis. The gel was incubated in the buffers supplied according to manufacturers guidelines. The stained gel was then dried using a gel drier for 45 minutes at 80 °C.

2.19.3. Coomassie Stain

SDS-PAGE gels were incubated in Coomassie blue dye (50 % (v/v) methanol, 10 % (v/v) acetic acid, 0.05 % (v/v) Coomassie Blue (R250)) for 1 hour and destained (50 % (v/v) methanol, 10 % (v/v) acetic acid) until a clear background was obtained. The stained gel was then dried using a gel drier for 45 minutes at 80 °C.

2.20. Preparation of Splenic Mononuclear Cells

Spleens from Balb/c mice were pressed through mesh in 9 ml red cell removal buffer (0.168 M ammonium chloride) per 3 spleens. The cell suspension was transferred to a 15 ml tube (Falcon), underlaid with 1 ml fetal calf serum (FCS) (GIBCO BRL, Paisley, UK) and incubated on ice for 7 minutes. The supernatant was then removed to a 15 ml tube, underlaid with 1 ml FCS and spun at 1500 rpm for 7 minutes at 4 °C. The supernatant was discarded and the pellet resuspended in 9 ml (per 3 spleens) dead cell removal buffer (DCRB) (250 mM sorbitol, 38.5 mM glucose, 12.5 % (v/v) balanced salt solution (BSS) (200 mM sodium chloride, 5 mM potassium chloride, 3 mM calcium chloride, 1.68 mM magnesium sulphate, 3.36 mM potassium dihydrogen orthophosphate, 2.24 mM dipotassium hydrogen orthophosphate, 20 mM HEPES, pH 7.2)). BSS containing 5 % (v/v) FCS was added to dead cell removal columns (glass pipettes with small cotton wool plug) during the final centrifugation step to pre-wet the columns. The cells in DCRB were passed through the dead cell removal columns (1 column per 3 spleens) into 1 ml of BSS containing 5 % FCS on ice. The cell suspension was then centrifuged at 1500 rpm for 7 minutes at 4 °C and the pellet resuspended in 5 ml BSS containing 5 % (v/v) FCS and kept on ice.

2.21. Preparation of Splenic B Cells

Splenic cells were prepared as described above (section 2.20) and the total number of cells obtained determined as described in section 2.22. The splenic cells were pelleted by centrifugation at 1400 rpm for 5 minutes at 4 °C and then resuspended in cold MACS (5.5 mM potassium chloride, 145 mM sodium chloride, 8 mM disodium hydrogen orthophosphate, 1.5 mM sodium dihydrogen orthophosphate, 0.5 % w/v bovine serum albumin, 2 mM EDTA) buffer at a concentration of 2×10^8 cell / ml. 100 μ l CD43 positive beads / 2×10^8 cells were added to the resuspended cells and the cells incubated for a minimum of 20 minutes at 4 °C. To prepare the CS depletion column (Miltenyi Biotec Ltd) for use the column was washed via the side syringe using 10 ml cold MACS buffer. A sheathed needle (No. 23 gauge) with the end of the sheath removed was then attached to the column and 50 ml MACS buffer passed through the column and

discarded. 1 ml MACS buffer was then added to the splenic cell / bead mix, the mix passed through nitex gauze, loaded onto the CS depletion column and the eluate collected. The CS depletion column was then washed with 40 ml cold MACS buffer and the eluate collected. The eluates were then pooled and the cells were counted (section 2.20). The cells were then pelleted by centrifugation at 1400 rpm for 10 minutes at 4 °C, resuspended in RPMI media at the required concentration for the experiment and allowed to rest at 4 °C before being used in experiments.

2.22. Cell Counting

Cells were counted in a haemocytometer (Neubauer, Assistant, Germany). 10 µl of the cell suspension was added to 10 µl of trypan blue and the solution loaded onto the haemocytometer. The number of cells, in two blocks of 16 squares, was counted. This gave the number of cells $\times 10^4$ per ml of sample. Multiplication of this value by the total volume of the sample gave the total number of cells.

2.23. Preparation of Whole Cell Lysates

Cells were pelleted by centrifugation at 1200 rpm for 10 minutes and the pellet resuspended in 150 µl of 2x lysis buffer pH 7.5 (100 mM tris base, 300 mM sodium chloride, 4 % (v/v) NP40, 0.5 % (v/v) sodium deoxycholate, 2 mM EDTA) containing 1 µg ml⁻¹ of chymostatin, leupeptin, antipain and pepstatin A and 1 mM sodium orthovanadate and 10 mM PMSF. The solution was transferred to an Eppendorf tube, vortexed well and left on ice for 20 minutes. The solution was then centrifuged at 10000 rpm for 10 minutes at 4 °C to remove cellular debris. The supernatant was removed and stored at -20 °C.

2.24. Biotinylation of Cells

1×10^8 cells were pelleted by centrifugation at 1200 rpm for 8 minutes. The pellet was washed 3 times in ice cold PBS (5.5 mM potassium chloride, 145 mM sodium chloride, 8 mM disodium hydrogen orthophosphate, 1.5 mM sodium

dihydrogen orthophosphate) pH 7.2 and then resuspended in 0.5 ml PBS in a foil wrapped universal tube. 1.5 ml of freshly prepared NHS-biotin solution (Pierce) at 4 mg ml⁻¹ was added to the cells and they were incubated at room temperature for 30 minutes on a rocking platform. The cells were then pelleted by centrifugation at 1200 rpm for 8 minutes and washed 3 times in ice cold PBS to remove any unbound biotin.

2.25. Preparation of Biotinylated Cellular Membranes

Cells were biotinylated as described in section 2.24, pelleted by centrifugation at 1500 rpm for 5 minutes and then resuspended in 1.5 ml of ice cold extraction buffer (50 mM HEPES pH 7.4, 5 mM calcium chloride, 140 mM sodium chloride, 1 % (v/v) octyl- β -D-glucopyranoside, 1 mM PMSF, 1 mM aprotinin, 1 mM leupeptin) and snap frozen in liquid nitrogen. The sample was then thawed, homogenised in a glass homogeniser (20-30 strokes) and incubated on ice for 1 hour. The extract was then centrifuged at 2000 rpm for 10 minutes, to pellet the nuclei and unbroken cells, and the pellet discarded. The supernatant was then centrifuged at 45000 x g for 1 hour at 4 °C and the supernatant retained as the membrane extract.

2.26. Preparation of Cellular Cytosolic and Nuclear Fractions

Cells were washed twice with 10 ml ice cold TBS pH 7.6 (20 mM tris, 136 mM sodium chloride), pelleted by centrifugation at 1500 x g for 5 minutes and washed with 1 ml TBS before being transferred to an Eppendorf tube and pelleted again by centrifugation at 1500 x g for 5 minutes. The pellet was then resuspended by gentle pipetting in 400 μ l of ice cold buffer A (10 mM HEPES pH 7.9, 10 mM potassium chloride, 1.5 mM magnesium chloride, 0.1 mM EDTA, 0.1 mM EGTA, 0.5 mM DTT, 0.15 mM spermine, 0.75 mM spermidine, 1 μ g ml⁻¹ leupeptin, 1 μ g ml⁻¹ aprotinin, 1 μ g ml⁻¹ PMSF, 100 μ M sodium orthovanadate) and the cells left to swell on ice for 15 minutes. 25 μ l of 10 % NP-40 was then added, the samples vortexed vigorously for 10 s and centrifuged

at 13000 x g for 30 s to pellet the nuclear material. The supernatant (cytosolic fraction) was removed and stored at -20°C . The nuclear pellet was vortexed, resuspended in 50 μl ice cold buffer B (20 mM HEPES pH 7.9, 25 % (v/v) glycerol, 0.4 mM sodium chloride, 1 mM EDTA, 1 mM EGTA, 1 mM DTT, 1 $\mu\text{g ml}^{-1}$ leupeptin, 1 $\mu\text{g ml}^{-1}$ aprotinin, 1 $\mu\text{g ml}^{-1}$ PMSF) and then mixed vigorously on a rocking platform for 15 minutes on ice. The nuclear extract was then centrifuged at 13000 x g for 5 minutes at 4°C , the pellet discarded and the supernatant stored at -20°C .

2.27. Synthetic Oligonucleotide DNA Labelling

A probe labelling mix (32 μl dH_2O , 5 μl 10x buffer H (Promega), 6 μl dNTP mix (Promega), 4 μl ds DNA (probe), 2 μl ^{32}P - α -ATP (Amersham), 1 μl Klenow (DNA polymerase 2 U μl^{-1} Boehringer Mannheim)) was prepared and incubated at 37°C for 3 hours. 6 μl of DNA loading buffer (0.25 % (w/v) bromophenol blue, 40 % (w/v) sucrose) was then added to the probe mix and the probe mix run on a 8 % polyacrylamide gel (11 ml 30 % (w/v) polyacrylamide, 4 ml 5x TBE (446 mM tris base, 444 mM boric acid, 10 mM EDTA, pH 8.0), 25 ml dH_2O , 100 μl 30 % (w/v) ammonium persulphate, 34 μl TEMED) in 0.5x TBE at 20 mA for 1-2 hours. The labelled probe was then identified by autoradiography, cut out of the gel, placed in an Eppendorf tube and incubated overnight in T/E buffer (10 mM tris pH 8.0, 1 mM EDTA) at 37°C to allow elution of the labelled probe from the gel.

2.28. Electro-Mobility Shift Assay (EMSA)

A binding assay mix (10 μg sample protein, 10 μl 4x buffer (80 mM HEPES pH 7.9, 4 mM magnesium chloride, 0.4 mM EDTA, 2 mM dithiothreitol, 40 % (v/v) glycerol), 2 μl poly-dIdC (1 mg ml^{-1} Pharmacia), 1 μl ^{32}P -labelled probe made up to 40 μl in dH_2O) was prepared for each sample, including a control containing no protein, and incubated at room temperature for 30 minutes. 3 μl DNA loading buffer (0.25 % (w/v) bromophenol blue, 40 % (w/v) sucrose) was then added to each sample binding assay mix and the samples run on a 6 % polyacrylamide gel

(8 ml 30 % (w/v) polyacrylamide, 4 ml 5x TBE (446 mM tris base, 444 mM boric acid, 10 mM EDTA, pH 8.0), 28 ml dH₂O, 100 µl 30 % (w/v) ammonium persulphate, 34 µl TEMED) in 0.5x TBE at 20 mA until the dye front neared the end of the gel. One gel plate was then removed and the gel fixed in fixing solution (2 methanol : 1 acetic acid : 1 glycerol : 6 water (v/v)) for 20 minutes. The gel was then dried in a gel drier for 1-2 hours at 80 °C and developed using autoradiography.

2.29. Incubation of Cells with Native and Radiolabelled

Native ES-62

1×10^7 cells per timepoint were placed into a well of a 24 well plate in 1 ml of RPMI 1640 medium supplemented with 5 % (v/v) heat inactivated fetal calf serum, penicillin (100 U ml⁻¹) and streptomycin (100 mg ml⁻¹). ES-62 (2 µg ml⁻¹) was added to each well and the cells incubated at 37 °C in 5 % CO₂/95 % humidified air for the appropriate times. After each timepoint cells were added to 14 ml RPMI 1640 medium supplemented as before and pelleted by centrifugation at 1500 rpm for 5 minutes. Nuclear and cytosolic fractions were then made from the cells as described in section 2.26.

2.30. Immunoprecipitation with a FITC Conjugate of

ES-62

Whole cell lysate preparations were pre-cleared by the addition of 50 µl of 50 % protein L washed slurry followed by incubation for 1 hour at 4 °C on a rotator. Samples were then centrifuged at 13000 rpm for 10 minutes, the pellet discarded and ES-62-FITC (5 µg ml⁻¹) added to the supernatant. The sample (wrapped in tin foil because ES-62-FITC is light sensitive) was then incubated for 2 hours at 4 °C on a rotator. 50 µl of washed protein L slurry was incubated with 1 µg of anti-FITC antibody (Sigma-Aldrich) for 2 hours at 4 °C on a rotator concurrently. The anti-FITC/protein L slurry was then centrifuged (13000 rpm for 7 minutes) to pellet the beads and the beads then washed in PBS pH 7.2 and added to the

membrane sample that had been incubated with ES-62-FITC. The sample was then incubated overnight at 4 °C on a rotator before being centrifuged to pellet the beads. The beads were then washed 3 times in PBS pH 7.2, resuspended in 50 μ l of 2 x gel loading buffer and boiled to release the immunoprecipitated proteins from the beads. The beads were then pelleted by centrifugation and the supernatant loaded onto a SDS-PAGE gel.

2.31. Circular Dichroism

Far - UV circular dichroism spectra for native ES-62 at 1.0 mg ml⁻¹ in 10 mM, pH 7.0 sodium phosphate, 150 mM sodium fluoride were obtained on station 3.1 at the Synchrotron Radiation Source, Daresbury Laboratory and for native ES-62 at 0.33 mg ml⁻¹ in 150 mM, pH 7.0 phosphate buffer in a 0.02 cm pathlength quartz cell on a JASCO J-600 spectropolarimeter at the Scottish CD Facility, University of Glasgow.

2.32. Inductively Coupled Plasma Atomic Emission

Spectroscopy (ICP-AES)

ICP-AES uses high energy plasma to atomise the sample. High energy plasma is used in preference to a flame as a higher temperature can be obtained which reduces chemical and matrix interference. The precise nature of the high energy plasma compared to flames, which can vary greatly depending on conditions, means that the spectra of several elements can be measured simultaneously if the protein contains multiple elements and that elements can be detected at much lower concentrations than when a flame is employed.

An inductively coupled plasma emission spectrum for wild type ES-62 at 1 μ M, based on the monomeric mass of ES-62, in PBS (5.5 mM potassium chloride, 145 mM sodium chloride, 8 mM disodium hydrogen orthophosphate, 1.5 mM sodium dihydrogen orthophosphate) pH 7.0, was obtained at the Department of Chemistry, University of Edinburgh on a Thermo Jarrell Ash IRIS inductively coupled plasma atomic emission spectrometer. Standards containing iron,

sulphur, zinc, copper, manganese, magnesium, potassium, cobalt and nickel at 100, 10, 5, 1, 0.5, 0.1, 0.05 and 0.01 ppm (parts per million) were used to calibrate the spectrometer prior to running the sample.

2.33. Determination of the Isoelectric Point of ES-62

The isoelectric point of ES-62 was determined by running a sample of ES-62 on a series of isoelectric focusing gels, initially with a pI range of pI 3 to pI 9 and then on a gel with a narrower pI range of pH 4 to pH 6.5. The gels and gel equipment used were the PhastGels and PhastSystem from Amersham Pharmacia Biotech. Gels were run according to manufacturers guidelines.

2.34. Monomerisation of Wild Type ES-62

Wild type ES-62 was monomerised by sequential dialysis into buffers of decreasing pH. Wild type ES-62 at 570 $\mu\text{g ml}^{-1}$ in PBS (5.5 mM potassium chloride, 145 mM sodium chloride, 8 mM disodium hydrogen orthophosphate, 1.5 mM sodium dihydrogen orthophosphate) pH 7.0 was dialysed into 0.1 M sodium phosphate pH 6.0, 0.1 M sodium acetate pH 5.5, 0.1 M sodium acetate pH 5.0 and finally into 0.1 M sodium phosphate pH 7.0. Each dialysis step was carried out for 3 hours and a 2 μg (4 μl) sample taken at each pH. Samples were mixed with 4 μl 2 x loading buffer (100 mM Tris pH 6.8, 20 % (v/v) glycerol, bromophenol blue) and loaded, without pre boiling, onto an 8 % (w/v) non-denaturing polyacrylamide gel (contains no SDS). The gel was run until the dye front reached the bottom of the gel. The gel was then removed and stained with Coomassie blue dye (50 % (v/v) methanol, 10 % (v/v) acetic acid, 0.05 % (v/v) Coomassie Blue (R250)) and destained (50 % (v/v) methanol, 10 % (v/v) acetic acid). The stained gel was then dried using a gel drier for 45 minutes at 80 °C.

2.35. Calculation of the Extinction Coefficient for ES-62

A Coomassie protein assay was carried out using BSA protein standards at 0.125, 0.25, 0.5, 0.75, 1, 1.5 and 2 mg ml⁻¹ to obtain a standard curve. The concentration of an aliquot of a sample of ES-62 was determined from the standard curve. The absorbance of the sample at 277 nm was measured and the extinction coefficient determined using the equation $A = Ecl$, where A is the absorbance at 277 nm, E the extinction coefficient (cm² mg⁻¹), c is the concentration (mg ml⁻¹) and l is the pathlength of the spectrophotometer (cm).

2.36. Spectroscopy of BSA and BSA Conjugated to PC

Absorption spectra of denatured BSA, 0.67 mg ml⁻¹, and BSA with PC conjugated to it, 0.5 mg ml⁻¹, were obtained using a wavelength scan from 150 nm to 400 nm in a UNICAM UV/VIS spectrometer. Denatured BSA was used as the control as BSA has to be denatured before PC can be conjugated to it.

2.37. Suppliers

Supplier	Materials
PharMingen: BD Biosciences, 21 Between Towns Rd, Cowley, Oxford	SF9 insect cell line TMN-FH medium Protein-free insect cell medium PAcGP67-B vector BaculoGold DNA Agarplaque
Novagen: CN Biosciences (U.K.) Ltd, Boulevard Industrial Park, Padge Rd, Beeston, Nottingham	PET 19b vector SOC medium Novablue competent cells BL21 (DE3) competent cells
Gibco BRL: Paisley, U.K.	All cell culture reagents
BioRad: BioRad House, Maylands Ave., Hemel Hempstead	Zinc Stain Gel transfer apparatus, Agarose gel electrophoresis apparatus
Promega: Delta House, Chilworth Research Centre, Southampton	PGEM-T Easy vector Ligation buffer T4 DNA ligase ATP JM109 competent cells SOC medium 10 x PCR buffer dNTPs Taq Shrimp alkaline phosphatase 10x Buffer H
Boehringer Mannheim: Roche Diagnostics Ltd, Bell Lane, Lewes, East Sussex	Low salt 10x buffer Eco RI Nde I Bam HI Buffer B

Boehringer Mannheim: Roche Diagnostics Ltd, Bell Lane, Lewes, East Sussex	Low melt agarose Klenow
Qiagen: Boundary Court, Gatwick Rd, Crawley, West Sussex	QiaPrep spin miniprep kit
Amicon: Millipore (U.K.) Ltd, Units 3 & 5, The Courtyards, Halvers Lane, Watford	Ultrafiltration cell YM 100 membranes YM 30 membranes
Applied Biosystems: Lingley House, 120 Birchwood Boulevard, Warrington	POROS purification columns (PerSeptive Biosystems) Superose 12 (HR 10/30) (Pharmacia Biotech) Poly dIdC (Pharmacia Biotech) PhastGels (Pharmacia Biotech) ³² P- α -ATP (Amersham Pharmacia)
Sigma-Aldrich: Dorset, England	Anti-FITC Antibody NBT-BCIP substrate

3. Bioinformatics

There has been considerable research into the effects of ES-62 on the immune system (Dechan *et al.*, 1998a; Dechan *et al.*, 1998b; Harnett & Harnett, 1999a; Harnett *et al.*, 1995; Harnett *et al.*, 1999a; Harnett & Harnett, 1993) and into the constituents of the carbohydrate chains and phosphorylcholine moieties that form part of ES-62 (Harnett *et al.*, 1994; Harnett *et al.*, 1993; Haslam *et al.*, 1999; Haslam *et al.*, 1997; Houston *et al.*, 1997; Houston & Harnett, 1999a; Houston & Harnett, 1999b). However, at the start of this PhD project the only structural information available for ES-62 were the amino acid and DNA sequences and the hypothesis that it existed in a tetrameric state. One of the aims of this PhD was to obtain structural information about ES-62 with the objective of identifying homologous proteins to aid elucidation of the function of ES-62 and to ultimately allow rational drug design both for the treatment of filarial diseases and for the development of immunosuppressive drugs. Three techniques were employed in the course of this PhD to obtain structural information about ES-62. The first of these techniques, bioinformatics, is discussed in this chapter. The discussion of bioinformatic techniques is further supplemented by a web page, written as part of this PhD, which discusses the techniques employed (<http://crick.chem.gla.ac.uk/~clairea/bioinformatics/123.html>). In addition, a CD is included as part of this thesis containing the program RasMol (Sayle & Milner-White, 1995) and the PDB (Protein Data Bank) files for the structures of ES-62 obtained from bioinformatic techniques. Appendix 1 provides details of how to view these structures. The other two techniques employed, AUC and SAXS, are discussed in Chapter 4.

Bioinformatics is a computer-based method of obtaining information about a protein or gene of interest from the many protein and DNA databases available on the internet and from prediction programs, such as motif and secondary structure prediction programs, also available on the internet. The amino acid sequence of ES-62 was the starting point for the bioinformatics search for structural information about ES-62.

Proteins fold to enter a low energy state, believed to be fuelled by the need to pack hydrophobic residues into the interior of the molecule, away from contact with water (Rost, 1998). Chaperone proteins play a role in the folding of proteins ensuring that correct folding occurs and correcting misfolds. As the protein folds to enter a low energy state, predicting the tertiary structure of a protein from its primary sequence simply by identifying the structure with the lowest energy should be possible. However, the difference in energy between a folded and unfolded protein is only $\sim 1 \text{ kcal mol}^{-1}$ (Rost, 1998). This small energy difference coupled with the complexities of protein folding, means that the determination of the folding of a protein solely from its primary amino acid sequence exceeds current computing power. That is not to say it is impossible to predict the tertiary structure of a protein from its amino acid sequence, simply that it is necessary to obtain further information about the protein, such as secondary structure information, homologous proteins or protein motifs present within the amino acid sequence, before the tertiary structure prediction can be performed.

Homology modelling is the prediction of the tertiary structure of a protein, based on the known structure of a homologous protein and has been utilised to predict the tertiary structure of between 10 and 30 % of protein sequences within the many protein databanks. Proteins that share at least 25-30 % pairwise sequence identity are highly likely to fold into similar structures (Rost, 1998; Rost & Valencia, 1996). Thus the identification of a homologous protein can allow an accurate 3-dimensional model for a protein of interest to be generated. While the prediction of the tertiary structure of a protein from its amino acid sequence and other information obtained through bioinformatics is rarely successful, the prediction of the secondary structure, solvent accessibility of constituent amino acids and the presence of transmembrane helices, binding sites and motifs within a protein are widely performed and in the most part are reliable.

3.1. Identification of Homologous Proteins

3.1.1. Primary Sequence Homology

The first step in the search for structural information about ES-62 was the identification of homologous proteins. This was achieved through the use of databanks that contain the amino acid sequences of proteins and other relevant information, such as DNA sequence, protein function, protein family and the PDB file name of the 3-dimensional structure if this is known. One example of such a databank is Entrez (<http://www.ncbi.nlm.nih.gov/Entrez/>), a molecular biology database and retrieval system developed by the NCBI (National Centre for Biotechnology Information).

A number of programs, such as PSI-BLAST, BLAST and Gapped BLAST (<http://www.ncbi.nlm.nih.gov/BLAST/index.html>) (Altschul & Koonin, 1998; Altschul *et al.*, 1997), are available on the internet and can be used to search protein and DNA databases for sequence similarities (Altschul *et al.*, 1997). PSI-BLAST was used to identify proteins homologous to ES-62, as this is the most sensitive of the three programs. The iterative methodology it implements allows identification of distant homologues to the protein of interest (Altschul & Koonin, 1998). PSI-BLAST works by using Gapped BLAST to generate gapped sequence alignments, comparing the amino acid sequence of the protein of interest with a protein database. The proteins identified as homologous by the Gapped BLAST algorithm are then aligned in a multiple alignment with the original sequence serving as a template. A profile is generated, representing the original sequence and taking into account differences between it and the proteins identified as homologous. This profile can then be re-compared to the protein database to see if any new proteins are identified and the whole process of generating a profile repeated. This process can be repeated either a set number of times or until convergence is reached, where convergence is defined as the identification of no new proteins.

For the initial identification of proteins homologous to ES-62 default settings in PSI-BLAST were employed and all protein databases were searched. The default settings employed in PSI-BLAST were nr (non redundant) database, Blosum62 matrix and Gap costs of 11 for existence and 1 for extension. The results obtained were presented as a graphical display and as a list of homologous proteins. Further iterations, a vital part of PSI-BLAST, were performed, again using the default settings.

A multiple alignment of the homologous proteins identified by PSI-BLAST was then generated to allow easy identification of highly conserved regions. In addition, many of the secondary structure prediction programs use these multiple alignment files as input. Multiple alignments of ES-62 with the proteins identified as homologous by PSI-BLAST were performed using MultAlin (Corpet, 1998) (<http://prodes.toulouse.inra.fr/multalin/multalin.html>). The sequences of the proteins identified as homologous were obtained from the links to the protein sequence entries in PSI-BLAST. These sequences, in FASTA format, were submitted to MultAlin along with the sequence for ES-62, taking care to avoid use of the word 'protein' in the header line of the sequences. This is essential as although use of 'protein' in the header line will not affect the generation of a multiple alignment, it will result in a serious error in the program Plotcorr (used downstream of MultAlin), which will subsequently fail to run due to a misreading of the sequence header line as the designation of the secondary structure definition block. All optional parameters were left at the default settings except for the maximum line length option, which was set to 70 amino acids. The output was saved both as a gif file, by clicking on the graphic itself and selecting 'save image as', and in msf format by selecting the 'results in text format' option, copying this information to a blank file and saving as a .msf file.

3.1.2. Secondary Structure Homology

It is possible to identify homologues of the protein of interest on the basis of secondary structure using programs such as sss_align (Sturrock & Dryden, 1997) (http://www.icmb.ed.ac.uk/sss_align/sss_align.html). sss_align aligns proteins on

the basis of secondary structure enabling the identification of proteins with similar secondary structure but little sequence identity. *sss_align* bases its predictions on the parameters described in Table 3-1.

Parameter	Description
-infile <i>filename</i>	This compulsory parameter takes the form of a PHD output file, a FASTA format sequence or SWISS/EMBL output file.
-pams <i>1-500</i>	Specifies the Dayhoff PAM table to use. 1 specifies the strictest scoring, 500 the most relaxed.
-gapopen <i>1-100</i>	This specifies the penalty for a single gap. The optimum value varies with the PAM table being used. The program will select an appropriate value automatically if one is not specified.
-gapextend <i>0-gapopen</i>	This specifies the penalty for extending an open gap. The program will select an appropriate value, based on the PAM table selected and the gapopen value, if one is not specified.
-qval <i>0-100</i>	<i>sss_align</i> has 2 scoring systems, a PAM table and a log odds table relating to the reliability of the predicted structure. This value allows the percentage use of each system to be specified. 100 is all sequence, 0 is all secondary structure.
-summary <i>0-max</i>	Specifies the number of hits in the output summary list.
-align <i>0-max</i>	Specifies the number of sequences used in an alignment.
-dbname <i>file_name</i>	Allows the specification of a user-defined database to search against. If none is supplied the default database is used which consists of 2000 sequences.

Table 3-1: *sss_align* parameters. The only compulsory parameter is *-infile* but use of the *-pams* and *-qval* parameters is recommended in the program manual to increase the accuracy of the search. Wording in italics under the parameters heading indicates information that is supplied by the user.

The first step in identifying proteins homologous to ES-62 using these criteria was to generate a secondary structure prediction for ES-62 using the secondary structure prediction program, PHD (Rost, 1996; Rost *et al.*, 1995; Rost & Sander, 1993; Rost & Sander, 1994a; Rost & Sander, 1994b) (<http://www.embl-heidelberg.de/predictprotein/predictprotein.html>). The predicted secondary structure of ES-62 was then compared with the secondary structure of over 2000 proteins for which the tertiary structure is known and homologous proteins, on the basis of secondary structure, identified. A Dayhoff PAM value of 250 and a qval value of 75 were used. No gapopen or gapextend values were supplied and the default database, as supplied with sss_align, was employed. The tertiary structures of the homologous proteins were then used to provide some insight into the possible tertiary structure of ES-62.

Dayhoff PAM 250 is one of many amino acid scoring schemes. These schemes are an essential part of protein sequence alignment and database scanning. The most commonly used matrices are the Dayhoff matrix for 250 PAMS, as used in sss_align and BLOSUM 62. The Dayhoff matrix is based on the likelihood of any amino acid mutating to any other amino acid and thus consists of the average ratio of the number of changes a particular amino acid underwent to the number of amino acids of that type in the database for each amino acid (Barton, 1996). PAM is the percentage of acceptable point mutations per 10^8 years. A PAM of 250, as used in sss_align, means 1 amino acid in 5 remains unchanged. The amino acids vary in mutability thus 48 % of tryptophans, 41 % of cysteines, 20 % of histidines and only 7 % of serines would remain unchanged. A PAM value of 250 lies near the limit of detection of distant relationships (Barton, 1996). BLOSUM, **blocks substitution matrix**, is a matrix derived from ungapped alignments of short regions of related sequence. The sequences are clustered into groups within which the sequences are similar at a threshold value. The commonly used BLOSUM matrix, BLOSUM 62, is used in PSI-BLAST, where sequences are clustered into groups demonstrating 62 % identity. Substitution frequencies for each amino acid within each group are then calculated and these form the matrix from which amino acids can be scored (Barton, 1996).

3.2. Secondary Structure Prediction

Prediction of the secondary structure of a protein from its primary amino acid sequence is a reliable method of gaining structural information about the protein of interest. There are a number of prediction programs available that use different algorithms to generate the predictions. The question thus arises as to which of the prediction programs to use. Ideally, the solution to this question would be to generate a prediction using each of the different programs available and then compare the predictions obtained. It would be hoped that adopting this strategy would result in the generation of a number of similar predictions from which a consensus could be drawn, ideally providing increased accuracy. Unfortunately the input and output requirements for each of the prediction programs generally differs and thus this strategy is not easy to adopt. Jpred

(<http://jura.ebi.ac.uk:8888/>) overcomes these problems and allows predictions to be generated by a number of different prediction programs in a user friendly manner.

3.2.1. Jpred

Jpred (<http://jura.ebi.ac.uk:8888/>) (Cuff & Barton, 1999; Cuff *et al.*, 1998a) is a consensus secondary structure prediction internet web server. It standardises the input and output requirements of six of the most commonly used prediction programs (Cuff *et al.*, 1998b; Cuff *et al.*, 1998a); PHD (Rost, 1996; Rost & Sander, 1993; Rost *et al.*, 1994), PREDATOR (Frishman & Argos, 1996; Frishman & Argos, 1997), NNSSP (Salamov & Solovyev, 1995), DSC (King & Sternberg, 1996), Mulpred (Barton, 1994) and Zpred (Zvelebil *et al.*, 1987). The results from all of the programs are then displayed adjacent to each other along with a computer generated consensus thus allowing a consensus prediction to be gained from either a single amino acid sequence or a multiple alignment of homologous sequences. Tests performed have shown that the Jpred consensus prediction is 1 % more accurate in predicting the correct secondary structure than PHD, which has an accuracy of 71.9 % (Cuff *et al.*, 1998b).

The six secondary structure prediction programs that form Jpred are based on different algorithms and strategies for predicting secondary structure. NNSSP is based on a nearest neighbour algorithm which assumes that the secondary structure of a primary sequence is the same as that of the closest primary sequence to it of known secondary structure (King, 1996; Salamov & Solovyev, 1995). PREDATOR is also based on a nearest neighbour algorithm but incorporates information from multiple sequence alignments, such as hydrogen bonding propensities, to enhance the predictions (Frishman & Argos, 1996; Frishman & Argos, 1997; King, 1996). PHD (described in more detail in section 3.2.2) is based on jury decision neural networks. Neural networks consist of processing units which are connected. The weights of these connections are altered during the learning phase when correct information about classification is supplied. These connections are adjusted until a good input-output mapping is obtained which can predict the test set reliably. PHD obtains two network predictions and enters these into a third network to obtain a jury decision (King, 1996; Rost, 1996; Rost & Sander, 1993; Rost *et al.*, 1994). DSC employs a method of linear discrimination. This combines information from multiple alignments about the composition of the amino acid sequence with a set of concepts, which allow prediction of secondary structure. The information is processed using linear statistics (Heringa, 2000). MULPRED uses the consensus single sequence combination method. This consists of utilising a number of single sequence prediction methods, such as Lim (King, 1996; Lim, 1974) and GOR (Garnier *et al.*, 1978; King, 1996), to obtain prediction profiles from which a consensus is taken. Finally Zpred generates a conservation number weighted prediction. The consensus prediction generated by Jpred is obtained by a 'majority wins' methodology between NNSSP, PHD, PREDATOR and DSC as these four are the most modern and accurate prediction methods. If the majority wins method fails due to a tie then the prediction from PHD for that amino acid is used as PHD has the highest accuracy of these four programs for prediction of correct secondary structure.

As mentioned Jpred can generate a prediction from either a single amino acid sequence or from a multiple alignment in the form of a .msf file. Multiple

alignments have long been known to increase the accuracy of a secondary structure prediction thus if a single amino acid sequence is submitted, Jpred rapidly generates a multiple alignment by searching the sequence against the OWL (Bleasby *et al.*, 1994) database using BLAST, filtering the results and then generating a multiple alignment.

For prediction of the secondary structure of ES-62, a .msf file was submitted to Jpred and 'aligned multiple sequences in msf format' was selected as the file format parameter. The msf requirements by Jpred are strict and so the consensus line at the bottom of the .msf file from MultAlin had to be deleted before submission. In order to increase the accuracy of the prediction, NNSSP was selected to run. The default setting is to predict the secondary structure without running NNSSP. To override the default setting there is a small button at the bottom of the page that can be selected. As it was known that the proteins homologous to ES-62 had no known structures from which to obtain information about ES-62, the option to perform an 'autoscan of Brookhaven database' was deselected.

The output from Jpred gives a list of viewing options. The results were viewed by selecting either the Jalview (Java alignment viewer/editor) option or the html format option. To download the output to a Silicon Graphics Unix operating system workstation, option 8 'Gzipped tar file' was selected. This saves the output as a .tar.gz file which was unzipped (using the command; `gunzip filename`) and then 'untared' (using the command; `tar xf filename`). This process gave a large list of files from which those of importance could be selected. The files important for future steps in the bioinformatics process were the .ps (.amas.ps), .hssp and .phd files. These files were renamed and the remainder deleted. The .ps file, a postscript file containing the secondary structure prediction output from Jpred in graphical format, was viewed using the program ghostview. The .phd file is the secondary structure prediction from the secondary structure prediction program PHD. This file was used as input for the programs sss_align and Plotcorr.

3.2.2. PHD

PHD (<http://www.embl-heidelberg.de/predictprotein/predictprotein.html>) (Rost, 1996; Rost & Sander, 1993; Rost *et al.*, 1994) is a secondary structure prediction program that uses jury decision neural networks. The program is 'trained' using groups of amino acid sequences for which the secondary structure is known. As well as providing a secondary structure prediction, PHD also predicts the solvent accessibility for each amino acid residue and the likelihood that the residue will lie within a transmembrane helix. In conjunction with these three predictions PHD also scans the submitted protein sequence using the PROSITE database (Bairoch *et al.*, 1997; Hofmann *et al.*, 1999), which identifies any functional sequence motifs such as glycosylation sites and phosphorylation sites, and the ProDom database which identifies any domains within the protein that are homologous to domains detected in the SWISS-PROT database (Corpet *et al.*, 1998; Rost, 1996; Rost & Sander, 1998).

For the prediction of the secondary structure of ES-62, PHD was run as part of Jpred. In order to check that Jpred did not alter the running of PHD in any way PHD was also run separately from Jpred using all the default settings. The secondary structure prediction for ES-62 obtained by PHD run within Jpred was very similar to that obtained from PHD run in isolation. Therefore, the PHD output file (.phd) from Jpred was used as the input file for Plotcorr.

3.2.3. Circular Dichroism

Circular dichroism (CD) was carried out to allow comparison of the predicted secondary structure content of ES-62 with the experimentally determined secondary structure content. In addition to being a method used to determine the secondary structure content of a protein, CD is also a powerful tool for following conformational changes in proteins e.g. upon denaturation (Kelly & Price, 1997; Price, 1995). CD measures the differential absorption of right and left circularly polarised light. This difference in absorption gives distinctive spectra for α -helices, β -sheets and random coils. The spectra obtained from the protein of interest can be broken down to determine the percentage of α -helices, β -sheets

and random coil constituting the protein (Kelly & Price, 1997; Price, 1995). CD experiments were carried out on ES-62 as described in Chapter 2.

3.3. Prediction of the Spatial Orientation of Secondary Structure Elements

3.3.1. TOPS

TOPS (Gilbert *et al.*, 1999; Westhead *et al.*, 1999) is a protein topology server available on the internet (<http://www3.ebi.ac.uk/tops/>). This program converts the information in a PDB (<http://www.rcsb.org/PDB/>) file into a pictorial list, known as a TOPS cartoon, showing the secondary structure from N to C termini. The TOPS cartoon describes the type of secondary structure element i.e. helix or strand, where it is located on the protein backbone, its orientation and what other secondary structure elements it lies close to in 3-dimensional space. This information is essential for the prediction of the tertiary structure of a protein using the tertiary structure prediction program DRAGON. As TOPS generates these cartoons from the PDB files of proteins with known structures, the program itself is of little use for ES-62. However, it can be used to obtain a TOPS cartoon for a protein identified as homologous to the protein of interest on the basis of secondary structure (as discussed in 3.1.2). This cartoon can then be used as a template for the manually constructed TOPS diagram of the protein of interest.

To obtain a TOPS cartoon for the proteins identified as homologous to ES-62 on the basis of secondary structure, the PDB files for each homologous protein were downloaded from the Brookhaven database. The option 'generate your own topology cartoons' was selected on the input page followed by 'submit a protein structure for cartoon calculation'. The PDB file for the protein for which a TOPS cartoon was desired (e.g. 1QJ2) was then uploaded from the computer and a TOPS cartoon was generated for that protein.

3.3.2. Plotcorr

Plotcorr (Goebel *et al.*, 1994) is a program that predicts the spatial proximity of pairs of amino acids within a protein of interest. For this thesis the program was downloaded from <http://www.pdg.cnb.uam.es/pazos/plotcorr.html> and run on a Silicon Graphics O2 workstation running IRIX 6. Recently a web-based version of Plotcorr has been developed and can be accessed at http://www.pdg.cnb.uam.es:8081/pdg_contact_pred.html. By predicting which amino acids in a protein are likely to lie close together in 3-dimensional space the user can then postulate which secondary structures lie close to each other in space and manually construct a TOPS cartoon. Unfortunately for large proteins the number of possible pairs of amino acids is extremely large and as a result the information obtained from Plotcorr is hard to decipher thus vastly increasing the difficulties in determining which secondary structures lie close to one another.

The input for Plotcorr is secondary structure information and a multiple alignment of the protein of interest. For ES-62 the secondary structure information was in the form of a PHD output file. The multiple alignment, required in hssp file format, was generated from the PHD file using the 'to_hssp' program supplied with Plotcorr. This program is invoked using the command 'to_hssp *PHDfilename* *outputfilename.hssp*'. Terms in italics are specified by the user and correspond to the respective files. Once the two input files were obtained, Plotcorr was run by supplying it with the names of the two input files i.e. 'plotcorr *outputfilename.hssp* *PHDfilename*'.

The output from Plotcorr, shown in Figure 3-1, takes the form of the amino acid sequence of the protein of interest displayed around the outside of a circle on the left hand side of the screen with lines connecting residues that Plotcorr has predicted to lie close to each other in 3-dimensional space. Selecting a point on the outside of the circle displays the residue, holding down the shift key allows more than 1 residue to be displayed at once. The four bars on the right hand side of the screen can be varied and alter the graphical display. The last two bars control residue variability and secondary structure prediction and thus do not

affect the assessment of correlation between two amino acids. The first two bars on the right hand side of the output screen are the minimum and maximum values for the correlation coefficient. These values can be altered and lines will appear and disappear on the graphical display as only residues with a correlation value between the set maximum and minimum values will be displayed.

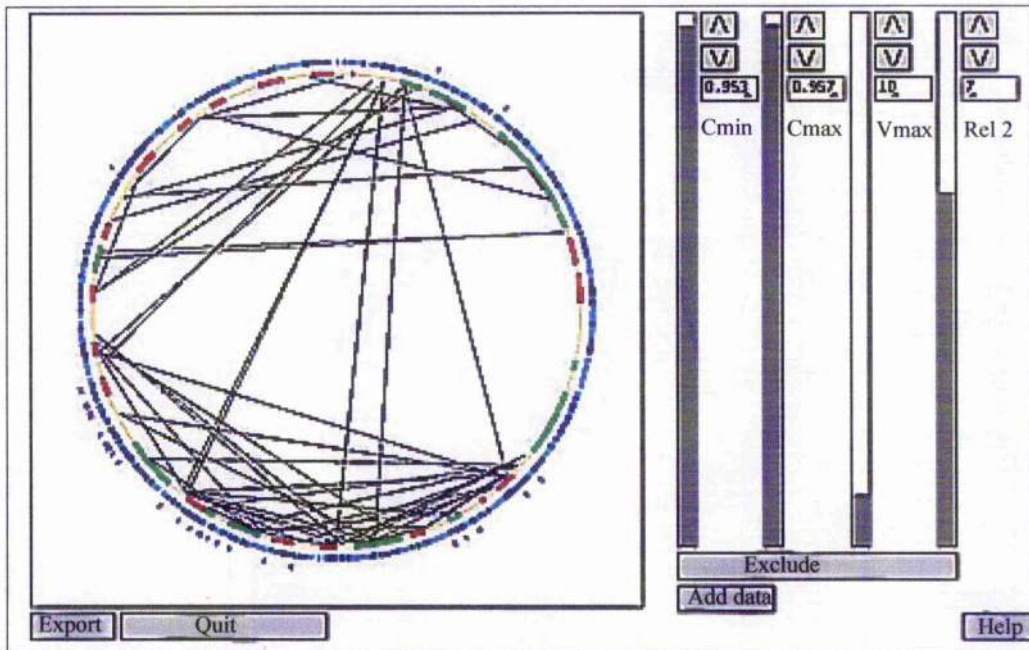


Figure 3-1: Output screen from Plotcorr. On the left hand side is the amino acid sequence of ES-62 displayed on the outside of a circle. Lines within this circle link pairs of amino acids that lie close to one another. The four bars represent, from left to right, minimum correlation coefficient, maximum correlation coefficient, residue variability and secondary structure prediction.

The information obtainable from this program needs to be used in conjunction with the information from secondary structure predictions. The secondary structure prediction provides the order and type of secondary structure elements from the N to C terminus, along with residue numbers for the start and finish of each individual secondary structure feature. By using the predictions of Plotcorr

as to which residues lie close together in space it is possible to establish the possible orientation of secondary structure features with respect to each other. This information is required for DRAGON, a tertiary structure prediction program used in this project.

3.4. Tertiary Structure Prediction

As mentioned previously, successful *de novo* prediction of tertiary structure from the primary sequence of a protein is not possible without further information about the protein, such as secondary structure information or amino acid accessibility. The success rate and accuracy of these predictions with this information is greatly dependent on the amount and type of information available. The greater the amount of structural information that can be supplied for the protein that is being modelled the greater the accuracy of the prediction. A more successful method for generating a model of the tertiary structure of a protein is homology modelling. However, this requires a high level of homology between the protein of interest and a protein of known structure.

3.4.1. SWISS-MODEL

SWISS-MODEL (<http://www.expasy.org/swissmod/SWISS-MODEL.html>) (Peitsch, 1996) is an internet-based tertiary structure homology modelling program which has a good success rate in predicting the tertiary structure of proteins provided that there is a minimum of 25 % identity between the amino acid sequence of the protein of interest and that for a protein for which the structure is known. The small section of ES-62 (residues 252-343) which is homologous to a region (residues 74-168) of the leucyl aminopeptidase from *Aeromonas proteolytica* (PDB code 1AMP) (Chevrier *et al.*, 1996; Chevrier *et al.*, 1994; Schalk *et al.*, 1992), was modelled using SWISS-MODEL by providing the amino acid sequence for this section of ES-62 and a modified version of the 1AMP PDB file, containing only information about residues 74-168, as the template (this region shows 35 % identity to ES-62).

3.4.2. DRAGON

DRAGON (Aszodi & Taylor, 1994a; Aszodi & Taylor, 1994b; Taylor & Aszodi, 1994) is a protein tertiary structure modelling program which can predict the tertiary structure of a protein from its amino acid sequence together with other structural information. The greater the amount of information supplied to DRAGON, such as solvent accessibility, secondary structure content, distance constraints and even homologous structures (although this is not a requirement of DRAGON), the more likely it is that the program will be able to predict a tertiary structure and the more accurate the resultant prediction. DRAGON was downloaded from <http://mathbio.nimr.mrc.ac.uk/rmunro/dragon.html> and installed on a Silicon Graphics O2 workstation running IRIX 6 for this project however, it can no longer be downloaded from this or any other site.

The files and parameters required as input for DRAGON are described in Table 3-2. Essential input files are `Alnfnm`, `Sstrfnm`, `Masterno`, `Graph` and `Outfnm`. The additional files serve to increase the reliability of the structural prediction if the information supplied is accurate. DRAGON requires other default files and values as input, but these are not altered in any way by the user and are supplied with the program. It is essential to ensure that these default files are located in the correct directory. A commands file, that takes the form of a list of the input parameters, directs DRAGON to all the information it requires to perform the prediction.

The commands file used to predict the tertiary structure of ES-62 was as follows;

Accfnm ES-62.accfnm

Alnfnm ES-62.msf

Graph 1

Masterno 1

Outfnm ES-62b.out

Restrfnm JPREDES-62.restr

Sstrfnm JPRED2.sstrfnm

Text in bold font is the parameter description, text in plain font is the user defined filename or input value. Typing 'c filename.commands' ran DRAGON. The output from this program was a PDB file which was viewed using the program Rasmol (Sayle & Milner-White, 1995).

Parameter	Description
Accfnm	A list of the residues believed to be on the surface or buried in the protein. The information can be obtained from a number of sources, the predicted accessibility obtained from the Jpred prediction is one such source.
Alnfnm	A multiple alignment file of the protein of interest with as many other similar proteins as possible.
Graph	Tells DRAGON whether to run the program with a graphical interface or not, where 1 indicates a graphical interface.
Masterno	Dictates which sequence in the multiple alignment is modelled (usually 1).
Outfnm	Tells DRAGON what to call the output file and where to store it.
Restrfnm	A distance restraints file that provides distances between amino acids pairs and a measure of the certainty of this information.
Sstrfnm	A secondary structure file - this details what the secondary structures are and how they lie in relation to each other.
Homfnm	A PDB file of a similar structure if available.

Table 3-2: Input files and parameters for DRAGON along with a brief explanation of each. Essential files and parameters are Alnfnm, Sstrfnm, Masterno, Graph and Outfnm. There are other parameters and files that DRAGON requires to run but they are all default files and values.

Initially, the small region (residues 252-343) of ES-62 similar to a small region (residues 74-168) of the leucyl aminopeptidase from *Aeromonas proteolytica* for which there was a PDB file available (PDB code 1AMP), was modelled using DRAGON. For this modelling a cut down version of the PDB file of the leucyl

aminopeptidase from *Aeromonas proteolytica*, containing only the information for the relevant region, was submitted as the Homfnm input file for DRAGON. In addition to this file Accfnm, Alnfnm, Outfnm, Restrfnm and Sstrfnm files were provided and values supplied for Graph and Masterno parameters. These parameters specified that the program was run with a graphical interface and that the sequence to be modelled was the first sequence in the multiple alignment. For modelling of ES-62 in its entirety there was no homology model available thus no Homfnm file was provided. Accfnm, Alnfnm, Outfnm, Restrfnm and Sstrfnm files were provided along with values for the Graph and Masterno parameters. The program was again run with a graphical interface and the sequence modelled was the first sequence in the multiple alignment.

The Accfnm files were created from the Jpred output, which provided information about the accessibility of each residue. This information was transformed into a list of amino acid residues that were predicted either to be buried or to be on the surface of the molecule. The Alnfnm files were the msf output from the PSI-BLAST search of either the small section of ES-62 (residues 252-343) which shows homology to the region of the leucyl aminopeptidase from *Aeromonas proteolytica* defined by residues 74-168, or ES-62 in its entirety. The Restrfnm files consisted of distance constraints between amino acids. These values were obtained using either the 1AMP PDB file for the small region of ES-62 modelled or one of the protein structures identified by sss_align as similar in secondary structure content to ES-62. The Sstrfnm files consisted of a list of the secondary structure elements of ES-62 and how they relate to each other e.g. the strands that make up a sheet and whether they lie parallel or antiparallel to each other. The information for these files was obtained from a combination of the information obtained from Plotcorr and the TOPS diagrams for the protein structures identified by sss_align as homologous to ES-62 on the basis of secondary structure. The contents of these files can be seen in Appendix 2.

3.5. Results

3.5.1. Primary Sequence Analysis

The protein sequence of ES-62 was submitted to PSI-BLAST and the default setting used to search the non-redundant databases for proteins with amino acid sequence similarity to ES-62. PSI-BLAST identified six proteins with full length homology to ES-62; plasma glutamate carboxypeptidase (human) [GenBank sequence number: 5174627] (Gingras *et al.*, 1999), aminopeptidase (human) [GenBank sequence number: 7706387](Liu *et al.*, unpublished), hematopoietic lineage switch 2 related protein (rat) [GenBank sequence number: 3851632] (Chen & Talmage, 1998), liver annexin-like protein (rat) [GenBank sequence number: 7108713] (Servillo *et al.*, unpublished), aminopeptidase (mouse) [GenBank sequence number: 5442032] (Liu *et al.*, unpublished) and hematopoietic lineage switch 2 protein (mouse) [GenBank sequence number: 9055234] (Chen & Talmage, 1998), which showed sequence similarity to ES-62. The level of similarity between these proteins and ES-62 is between 37 and 39 % as shown in Table 3-3. The multiple alignment of these proteins, performed using MultAlin, can be seen in Figure 3-2 and further highlights the level of similarity between the six proteins and ES-62.

Protein	GenBank Sequence Number	% Homology with ES-62
Plasma glutamate carboxypeptidase (human)	5174627	38
Aminopeptidase (human)	7706387	37
Hematopoietic lineage switch 2 related protein (rat)	3851632	37
Liver annexin-like protein (rat)	7108713	39
Aminopeptidase (mouse)	5442032	38
Hematopoietic lineage switch 2 protein (mouse)	90552341	39

Table 3-3: Proteins with a high degree of primary sequence identity to ES-62.

Figure 3-2: Multiple alignment of ES-62 with the six proteins identified as homologous by PSI-BLAST as performed by MultAlin. Plasma is the plasma glutamate carboxypeptidase (human) [Genbank sequence number: 5174627] (Gingras *et al.*, 1999), Human (amino) is the aminopeptidase (human) [Genbank sequence number: 7706387 (Liu *et al.*, unpublished), switch(rel) is the hematopoietic lineage switch 2 related protein (rat) [Genbank sequence number: 3851632] (Chen & Talmage, 1998), liver is the liver annexin-like protein (rat) [Genbank sequence number: 7108713] (Servillo *et al.*, unpublished), Mouse (amino) is the aminopeptidase (mouse) [Genbank sequence number: 5442032] (Liu *et al.*, unpublished) and Switch is the hematopoietic lineage switch 2 protein (mouse) [Genbank sequence number: 9055234] (Chen & Talmage, 1998). Red residues show high homology (90 %), Blue residues show low homology (10 %) and black shows neutral residues. Symbols are as follows: ! is any one of I or V; \$ is any one of L or M; % is any one of F or Y; # is any one of N, D, Q, E, B or Z.

Figure 3-2: Multiple alignment of ES-62 with the six proteins identified as homologous by PSI-BLAST, as performed by MultAlin.

In addition to the searches conducted using PSI-BLAST, searches were also performed of the nematode and filarial databases using the DNA sequence of ES-62. This identified several expressed sequence tags from *B. malayi* and *O. volvulus* that are homologous to ES-62.

3.5.1.1. Motif Searches

Motif searches carried out using Prosite identified a number of putative sites for glycosylation, phosphorylation, myristoylation and amidation. The four sites identified by Prosite as glycosylation sites are known to be glycosylated on wild type ES-62. A number of phosphorylation sites were identified by Prosite; eleven protein kinase C phosphorylation sites, nine casein kinase and three tyrosine kinase phosphorylation sites. Seven putative myristoylation sites and a putative amidation site were also identified. The identified Prosite motifs are shown in Figure 3-3.

1 M L L N S S T F F F L V T L 14
1 ATAAATATGCTA CTCAATTCCTCG ACATTTTCTTC TTGGTCACCCTA 48

15 T V V L G A A V L P D K T V A P 30
49 ACTGTCGTTTTG GGC GCAGCTGTC CTTCCGACAAA ACTGTCGCTCCG 96

31 K N Y I Q E T F G K E V A E L I 46
97 AAGAATTATATC CAAGAAACGTTT GGAAGGAAGTT GCCGAATTAATC 144

47 Q Y I T K G E E V G L A Y Q W L 62
145 CAGTATATTACT AAAGGTGAAGAA GTTGGATTAGCT TATCAATGGCTT 192

63 S K L V D G F G H R M V G S D S 78
193 AGCAAATTGGTC GATGGCTTTGGA CATCGTATGGTT GGTTCGATAGC 240

79 L E K S I A F L E E S L K N D N 94
241 TTGGA AAAATCG ATTGCTTCTTA GAAGAAAGCTTG AAAAATGATAAT 288

95 F D K V H T E E V P N L P H W V 110
289 TTTGATAAGGTG CACACCGAGGAA GTACCAAAGCTTG CCACATTGGGTT 336

111 R G N D V V E M I E P R N Q R L 126
337 CGTGGAAACGAC GTTGTGCAAAATG ATTGAACCACGA AATCAACGGCTC 384

127 N V L A I G G S E P A S A T G E 142
385 AATGTGCTTGCT ATTGGTGGATCT GAACCAGCTAGT GCGACCGGAGAA 432

143 V T V I Y D L D D V K P D D V R 158
433 GTGACAGTTATT TATGATCTTGAT GATGTCAAGCCT GATGATGTCCGT 480

159 G K I V V T A Q T F A G Y P L T 174
481 GGCAAGATTGTT GTGACGGCACAA ACATTTGCTGGT TATCCGTTAACG 528

175 L K Y R R S V K L F E Q L G A I 190
529 CTTAAATATCGT CGATCAGTAAAA TTATTTGAACAA TTAGGTGCCATT 576

191 G V L V K S I T S F S I N S P H 206
577 GGTGTTCTGGTC AAATCAATAACA TCATTTTCCATT AATTCACCTCAT 624

207 T G T G A E N T T I P A A C L T 222
625 ACCGGCACTGGT GCAGAAAATACA ACAATTCCTGCT GCATGTTTAAACG 672

223 I E E A E M L E R L Y R S G K K 238
673 ATTGAGGAAGCT GAAATGCTTGAA CGATTGTATAGG AGCGGCAAAAAG 720

239 I V I R M D M K S H Y E E P I N 254
721 ATCGTAATCCGA ATGGATATGAAA TCACATTATGAG GAACCTATAAAT 768

255 S S N L I F E I T G S E R P S E 270
769 TCCAGCAATCTT ATCTTTGAAATT ACCGGTAGTGAA CGACCATCTGAA 816

271 V V L L S A H V D S W D V G Q G 286
817 GTGGTACTATTA TCGGCACATGTG GACAGTTGGGAT GTTGGACAAGGA 864

287 A L D D G A G C A V V W S A L H 302
865 GCATTGGATGAT GGTGCTGGTTGT GCTGTTGTATGG AGTGCTTTGCAT 912

303 S L K K L A E R N P K F K P K R 318
913 TCATTA AAAAAA TTAGCCGAAAGA AATCCAAAATTC AAACCAAAACGG 960

319 T I R G I F W T S E E Q G Y G G 334
961 ACAATTCGAGGC ATATTTTGGACA TCGGAAGAACAA GGATATGGGGGT 1008

335	A	K	H	Y	Y	I	T	H	K	N	D	S	P	E	K	F	350
1009	G	C	A	A	A	C	A	T	T	A	C	A	C	A	T	T	1056
351	Y	F	V	S	E	T	D	T	G	T	F	K	S	T	N	W	366
1057	T	A	T	T	T	T	G	T	A	T	C	T	A	C	A	A	1104
367	L	A	H	L	S	F	S	G	D	K	K	S	M	L	R	L	382
1105	C	T	T	G	C	A	T	C	T	T	C	A	G	T	G	G	1152
383	K	E	I	T	R	L	L	S	R	N	G	I	A	L	G	L	398
1153	A	A	G	A	A	T	A	A	C	A	G	A	T	G	G	T	1200
399	I	N	S	S	V	Q	G	D	V	T	F	W	A	K	D	G	414
1201	A	T	A	A	T	A	G	C	T	C	A	G	T	G	A	C	1248
415	I	P	S	V	N	Y	I	P	D	K	A	V	D	Y	Y	F	430
1249	A	T	A	C	C	A	T	C	A	G	T	T	A	T	A	T	1296
431	Y	F	H	H	T	A	G	D	Y	M	T	V	L	K	D	G	446
1297	T	A	T	T	T	C	A	T	C	A	T	A	T	T	C	A	1344
447	D	L	E	Y	T	T	S	I	F	A	T	L	G	H	V	I	462
1345	G	A	T	T	T	A	G	A	T	A	T	A	C	A	A	T	1392
463	A	N	M	D	D	W	G	S	D	P	N	Q	P	Q	Q	L	478
1393	G	C	T	A	A	T	A	T	G	G	A	A	G	T	C	A	1440
479	N	S	K	Q	S	T	T	E	K	S	D	R	K	K	L		493
1441	A	A	T	T	C	C	A	A	C	A	A		T	C	C	A	1488

Figure 3-3: DNA and amino acid sequence of ES-62. The arrow marks the start of the mature protein sequence. Bold residues are those that constitute the leucine rich regions, residues in bold italics show the glycosylation sites, boxed residues are those involved in the formation of metal co-ordination sites, residues in the region of ES-62 homologous to aminopeptidases are underlined (____) and residues in the region of ES-62 homologous to the PC binding region of C-reactive protein (residues 56-81 of human C-reactive protein (Harnett *et al.*, 1999a)) are underlined (____). Blue residues are those predicted by Prosite to form a glycosylation site, green residues are those predicted by Prosite to form a PKC phosphorylation site, red residues (or red underlining) are those predicted by Prosite to form a casein kinase II phosphorylation site, yellow residues are those predicted by Prosite to form a tyrosine kinase phosphorylation site, cyan residues (or cyan underlining) are those predicted by Prosite to form a N-myristylation site and pink underlining shows residues predicted by Prosite to form an amidation site.

3.5.2. Secondary Structure Homology

3.5.2.1. *sss_align*

sss_align (Sturrock & Dryden, 1997) compares a secondary structure prediction of the protein of interest, typically the output from PHD (Rost, 1996; Rost & Sander, 1993; Rost *et al.*, 1994), to a database of the secondary structures of 2000 proteins. The identification of proteins similar to ES-62 in terms of secondary structure but not necessarily sequence is important in gaining structural information, such as the possible orientation of secondary structures in relation to each other, which is essential when constructing a 3-dimensional model for ES-62. *sss_align* identified ES-62 as demonstrating secondary structure similarity, but not sequence similarity, to four proteins; pyruvate ferredoxin oxidoreductase from *Desulfovibrio africanus* (PDB code 1B0P), the ectodomain of human transferrin receptor (PDB code 1CX8), endocellulase from *Clostridium cellulolyticum* (PDB code 1FCE) and carbon monoxide dehydrogenase from *Pseudomonas carboxydovorans* (PDB code 1QJ2). The structures of these proteins are shown in Table 3-4. Homologous secondary structure elements have been coloured the same in Table 3-4 (running from brown at the N-terminus to pink at the C-terminus). In all cases the homologous regions in the four proteins are smaller than ES-62. The structures shown in Table 3-4 appear to show little overall fold similarity which is surprising given that all four structures were identified as homologous to ES-62. A more objective measure of shape similarity was obtained by comparison of the solution small angle X-ray scattering curves calculated (using CRY SOL (Svergun *et al.*, 1995)) from the atomic co-ordinates for the regions of the 4 proteins found to be homologous with ES-62 (i.e. those presented in Table 3-4) as shown in Figure 3-4. By this criterion the homologous regions of 1B0P and 1CX8 appear to have quite similar solution shapes; 1QJ2 is slightly different and 1FCE is very different.


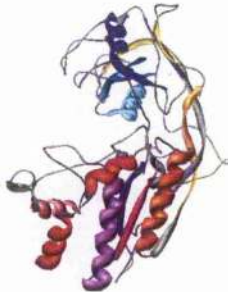

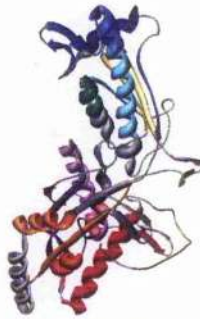
Protein	PDB accession code	Structure of homologous region
Pyruvate ferredoxin oxidoreductase from <i>Desulfovibrio africanus</i> (Rg = 26.4 Å; M = 41,958 Da)	1B0P	
Ectodomain of human transferrin receptor (Rg = 24.9 Å; M = 45,920 Da)	1CX8	
Endocellulase from <i>Clostridium cellulolyticum</i> (Rg = 22.5 Å; M = 50,799 Da)	1FCE	
Carbon monoxide dehydrogenase from <i>Pseudomonas carboxydovorans</i> (Rg = 26.5 Å; M = 44,794 Da)	1QJ2	

Table 3-4: Proteins with a high secondary structure identity to ES-62. The radius of gyration (Rg) was calculated, by *O. Byron*, from atomic co-ordinates using the program CRY SOL (Svergun *et al.*, 1995). The mass was calculated from the amino acid composition. Secondary structural elements are coloured according to their position in the primary sequence as follows:



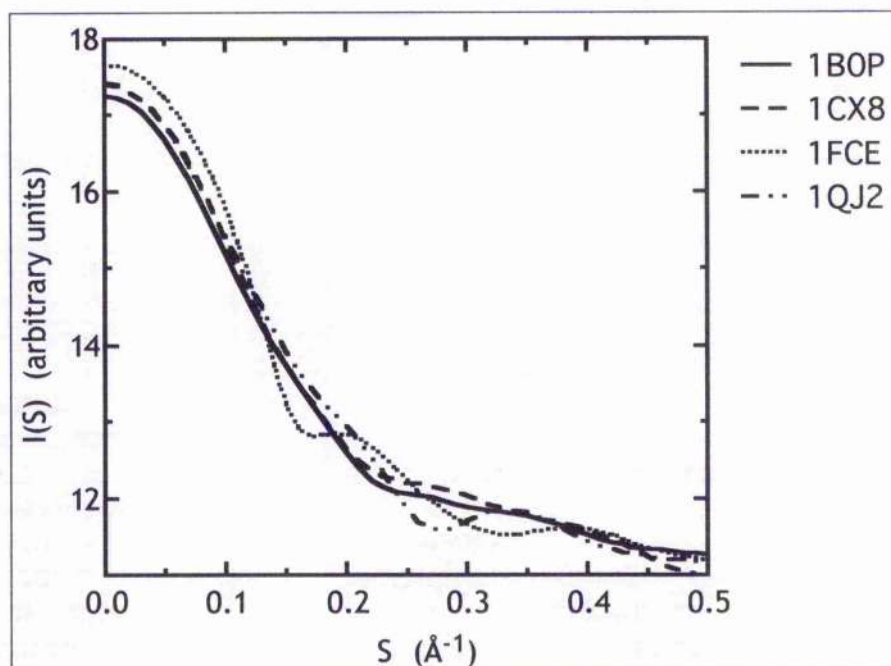
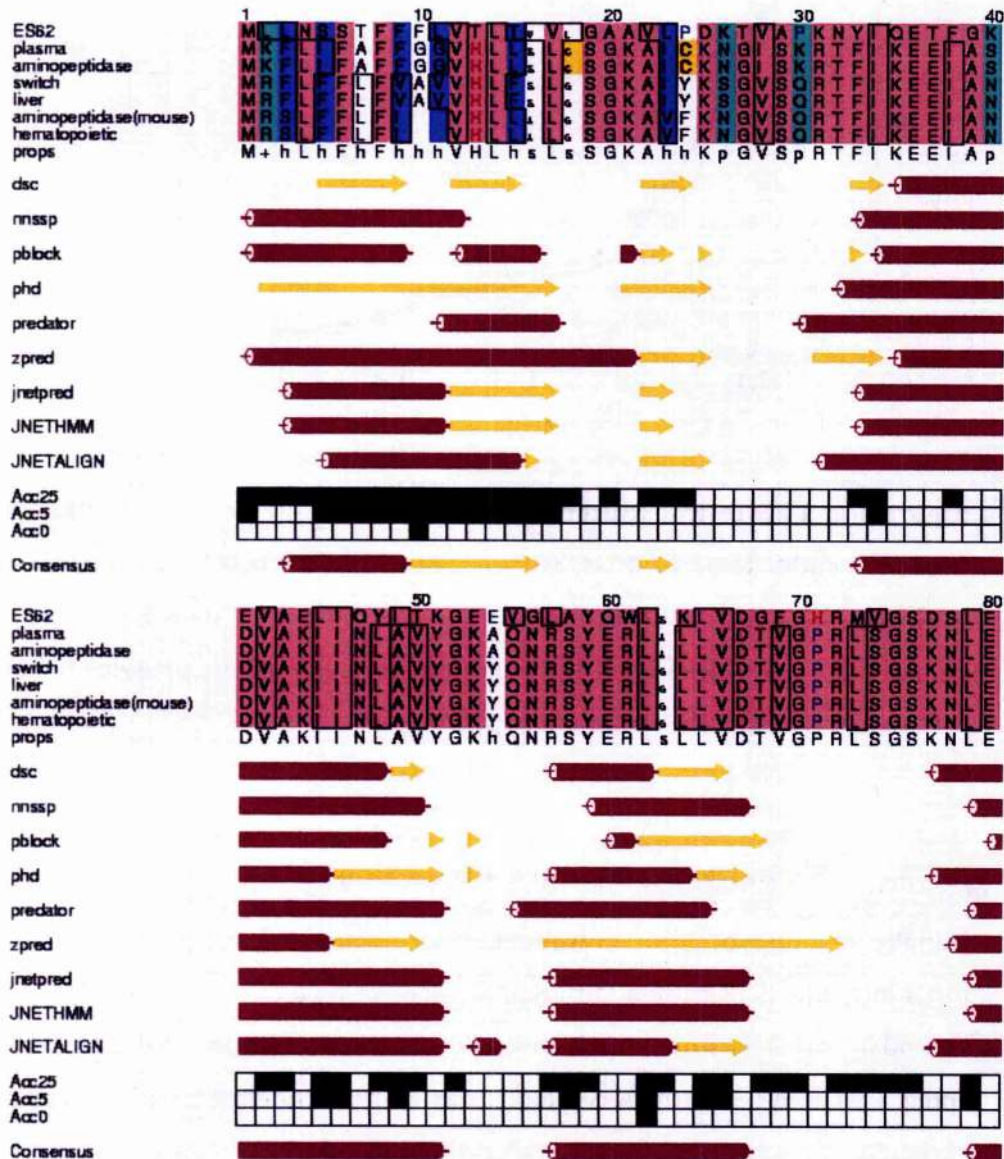
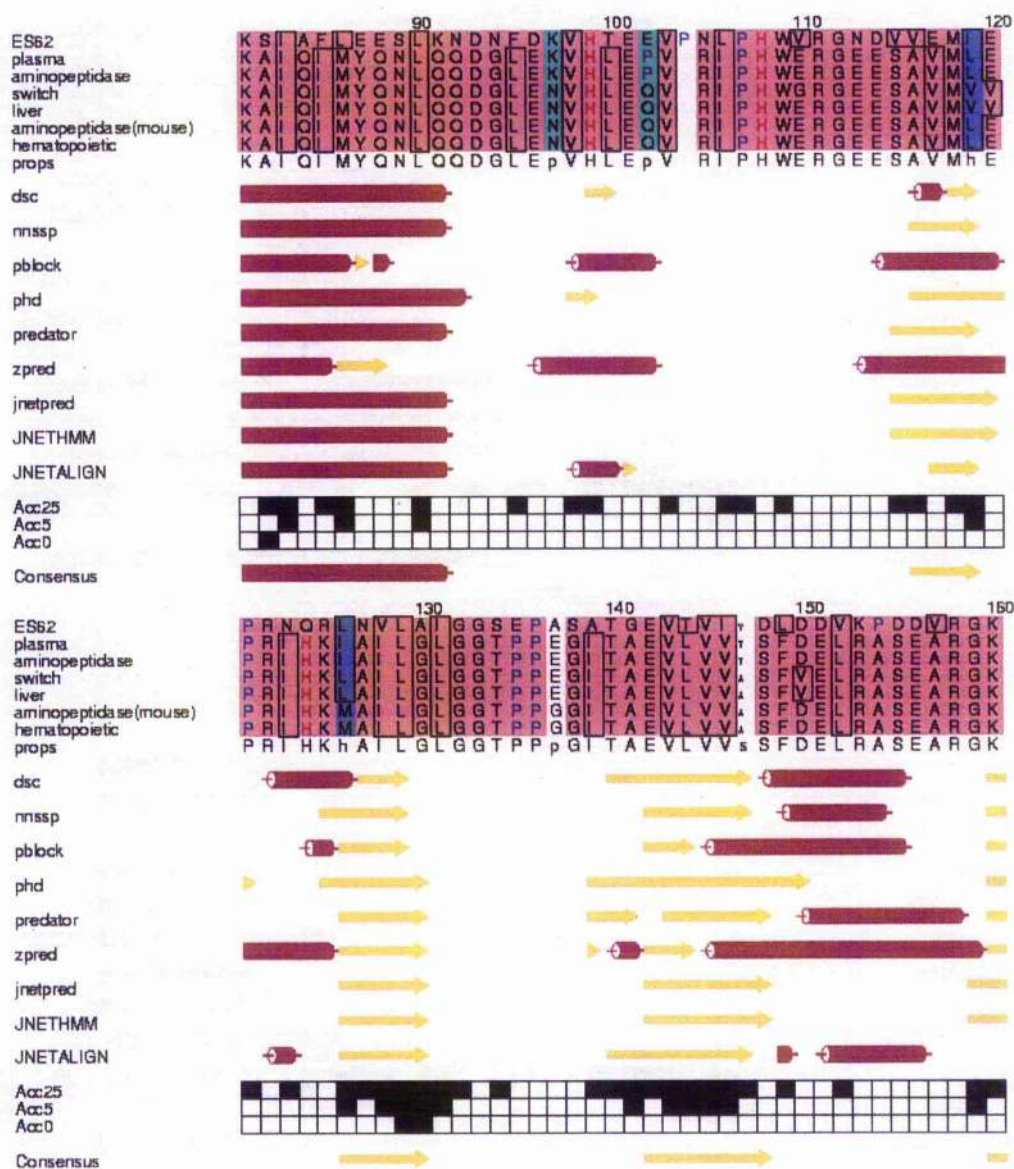


Figure 3-4: Theoretical scattering curves for the four proteins (PDB accession codes 1B0P (—); 1CX8 (---); 1FCE (.....); 1QJ2 (-.-.-)) predicted to share a high degree of secondary structure homology with ES-62. The curves were calculated from the homologous region of the proteins using the software CRY SOL (Svergun *et al.*, 1995).

3.5.3. Secondary Structure Prediction

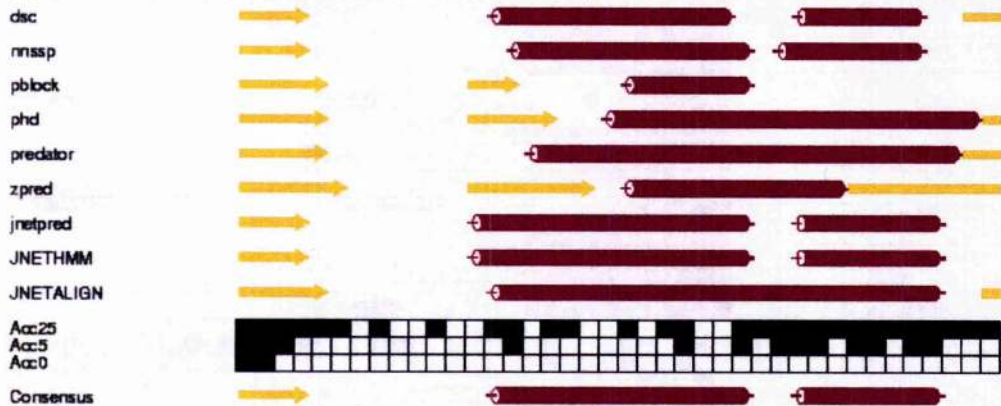
Initially a number of different web-based secondary structure prediction programs, which all employ different methods of prediction, were used to gain secondary structure information about ES-62. Ultimately, one of these programs, Jpred, was used for all the secondary structure predictions of ES-62. Jpred was chosen as it is known to give a more accurate secondary structure prediction than other secondary structure prediction programs (Cuff & Barton, 1999; Cuff *et al.*, 1998a). In addition, as discussed previously, Jpred comprises a number of different secondary structure prediction programs and supplies the outputs from each of these in addition with final Jpred output. The overall content of secondary structure elements as predicted by Jpred is 26 % alpha helix, 21 % beta sheet and 53 % other. The Jpred secondary structure prediction for ES-62 is shown in Figure 3-5.





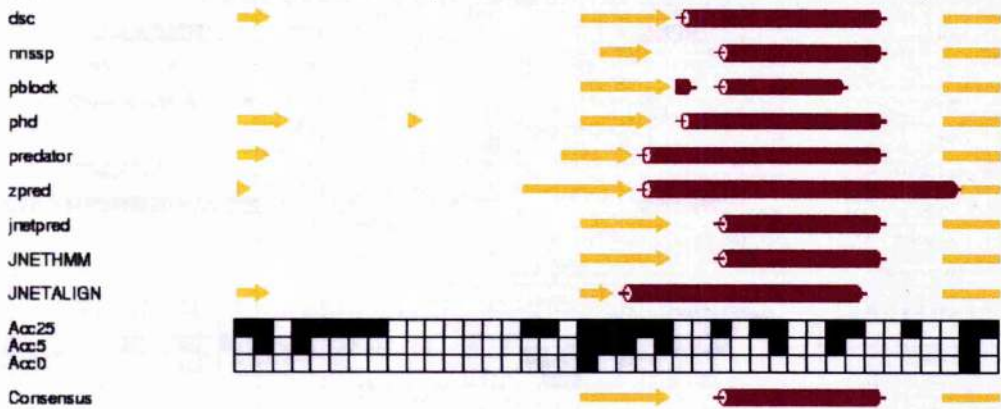
ES62
plasma
aminopeptidase
switch
liver
aminopeptidase(mouse)
hematopoietic
props

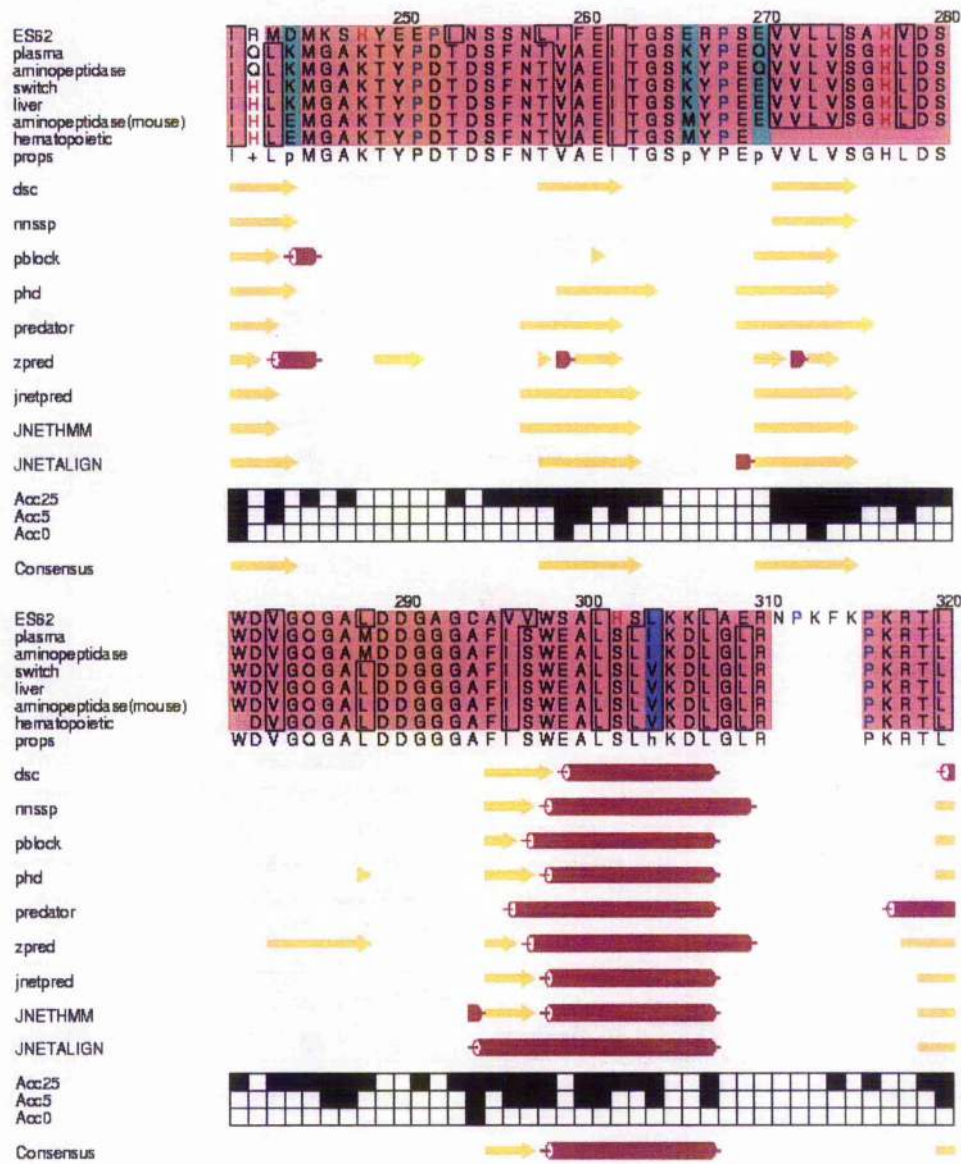
170 180 190 200
I V V Y N Q P Y s s Y s + T V Q Y R p G A V E A A K V G A h A S L I + S V A S F
V V Y N Q P Y s s Y s + T V Q Y R p G A V E A A K V G A h A S L I + S V A S F
V V Y N Q P Y s s Y s + T V Q Y R p G A V E A A K V G A h A S L I + S V A S F
V V Y N Q P Y s s Y s + T V Q Y R p G A V E A A K V G A h A S L I + S V A S F
V V Y N Q P Y s s Y s + T V Q Y R p G A V E A A K V G A h A S L I + S V A S F



ES62
plasma
aminopeptidase
switch
liver
aminopeptidase(mouse)
hematopoietic
props

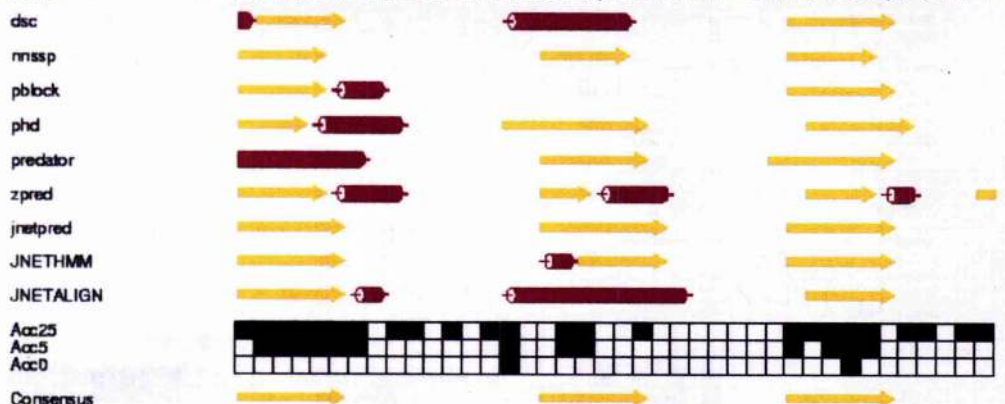
210 220 230 240
S I N S P H T G T G A E N T T I P A A C C I T T V E D A E M M S R M A S S G K K V
S I Y S P H T G T G A E N T T I P A A C C I T T V E D A E M M S R M A S S G K K V
S I Y S P H T G T G A E N T T I P A A C C I T T V E D A E M M S R M A S S G K K V
S I Y S P H T G T G A E N T T I P A A C C I T T V E D A E M M S R M A S S G K K V
S I Y S P H T G T G A E N T T I P A A C C I T T V E D A E M M S R M A S S G K K V





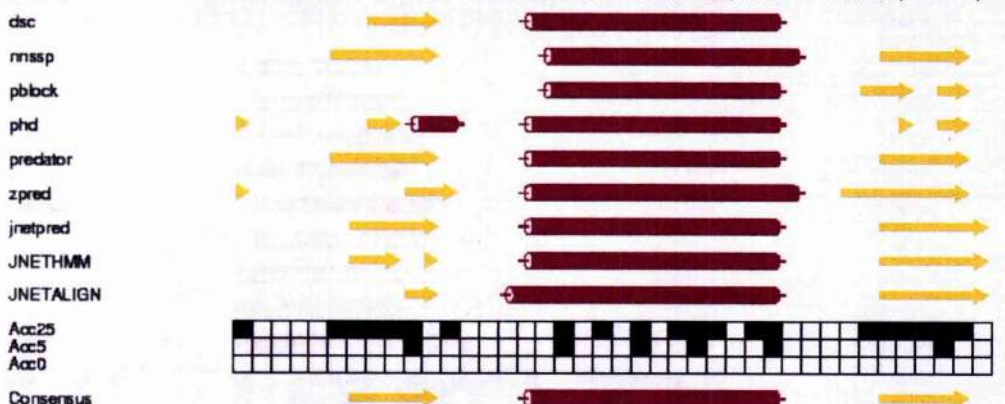
ES62
plasma
aminopeptidase
switch
liver
aminopeptidase (mouse)
hematopoietic
prosp

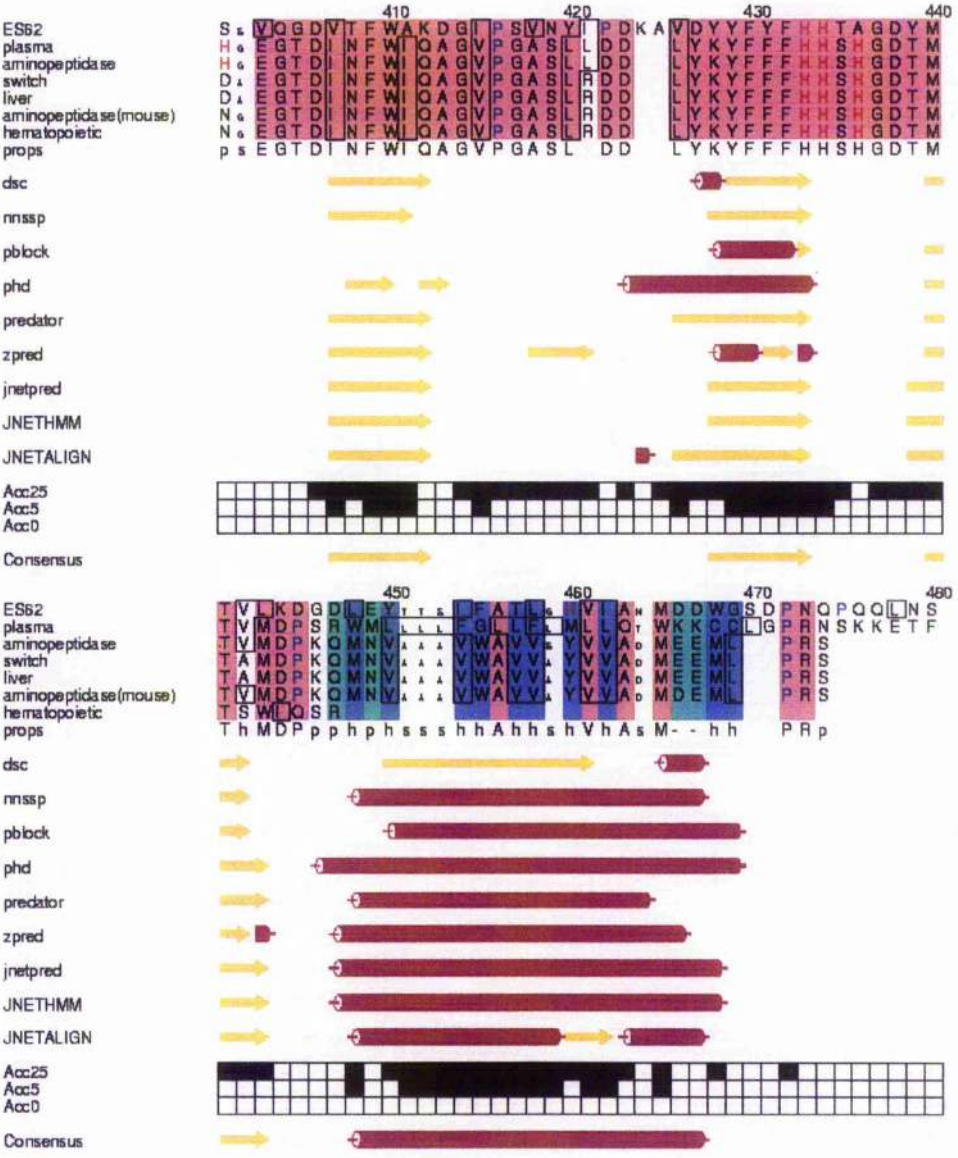
330 340 350 360
RGLFETWTSFQQGYVGAFAHYYYTQKKNDSPEKFYFVSEETDAQT
RLVLTWTAMmmmmQGGVGAFAFYQYYTQKKNVNIISNNYSLVMMEEDDAQT
RLVLTWTAMmmmmQGGVGAFAFYQYYTQKKNVNIISNNYSLVMMEEDDAQT
RLVLTWTAMmmmmQGGVGAFAFYQYYTQKKNVNIISNNYSLVMMEEDDAQT
RLVLTWTAMmmmmQGGVGAFAFYQYYTQKKNVNIISNNYSLVMMEEDDAQT
RLVLTWTAEEQGGhGAhQYYpLHKhNIISKYSLVMEsDsGT



ES62
plasma
aminopeptidase
switch
liver
aminopeptidase (mouse)
hematopoietic
prosp

370 380 390 400
FKSTNWLJAHLQFTTGSSEEDKARAIKESMIRKEIVMSLLOPLNINITITOKKGLVNS
FLPPTGFLPPTGFLPPTGFLPPTGFLPPTGFLPPTGFLPPTGFLPPTGFLPPTGFLPPTGFLPPTG
LQFTGS-KARAI-MKEVMP-LLQPLNITpVh p





3.5.4. Experimental Determination of Secondary Structure Content

The secondary structure content of ES-62 was determined experimentally by circular dichroism (CD) (as described in Chapter 2). Results from two CD experiments at different laboratories were very similar. The CD results indicate a higher percentage of α helix than β sheet in the protein with approximately 40 % α helix, 16 % β sheet and 16 % turn as shown in Table 3-5 and Figure 3-6.

	% α -helix	% β -sheet	% turn	% other
CD (Glasgow)	39.4	16.7	16.3	28.1
CD (Daresbury)	48	14	14	26

Table 3-5: Secondary structure content of wild type ES-62 from CD.

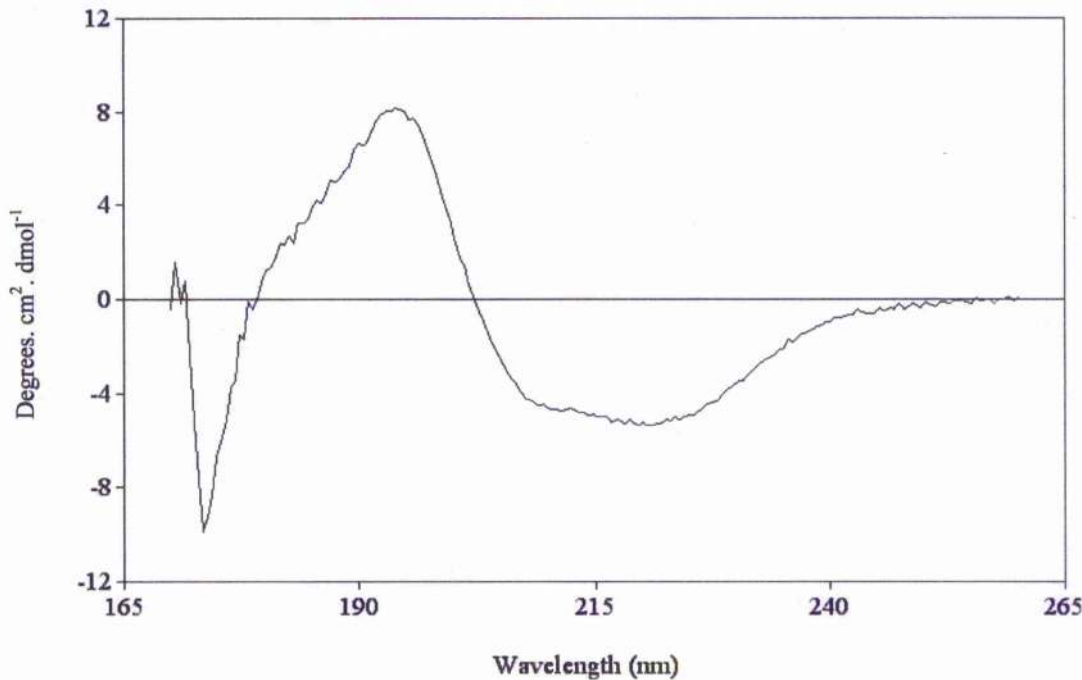


Figure 3-6: A Far - UV circular dichroism spectrum for tetrameric wild type ES-62 at 0.33 mg ml⁻¹ in 150 mM phosphate buffer in a 0.02 cm pathlength quartz cell obtained on a JASCO J-600 spectropolarimeter at the Scottish CD Facility, University of Glasgow.

3.5.5. Spatial Orientation of Secondary Structure Elements

Although Jpred predicts which secondary structural elements are present with respect to the amino acid sequence, it provides no information on the spatial orientation of these elements. Two methods were employed in an attempt to determine the orientation of the predicted secondary structural elements of ES-62 in relation to each other. Initially the program Plotcorr was used as discussed in section 3.3.2. Although the information obtained from Plotcorr was limited and often difficult to interpret due to the large size of ES-62, it did provide information about a small region of ES-62 (residues 252-343) that shows homology to residues 74-168 of the leucyl aminopeptidase from *Aeromonas proteolytica* for which there is a known structure. The information provided was sufficient to enable input files for the tertiary structure prediction program, DRAGON, to be written and this small region of ES-62 modelled. The region modelled by DRAGON was then compared to the tertiary structure of residues 74-168 of the leucyl aminopeptidase from *Aeromonas proteolytica* (see Figure 3-8).

In the second method the highest ranked protein identified by sss_align as showing secondary structure similarity to ES-62, carbon monoxide dehydrogenase from *Pseudomonas carboxydovorans*, 1QJ2, was used as a model for ES-62 to gain information as to the orientation of the secondary structural elements of ES-62. This protein (1QJ2) was submitted to the web based, Protein Topology server as discussed in section 3.3.1. The TOPS cartoon created for 1QJ2 was then used to predict which secondary structure elements in ES-62, as predicted by Jpred, might lie next to each other. The information from the TOPS cartoon was instrumental in the assembly of input files for the tertiary structure prediction program, DRAGON. The TOPS cartoon generated for 1QJ2 is shown in Figure 3-7.

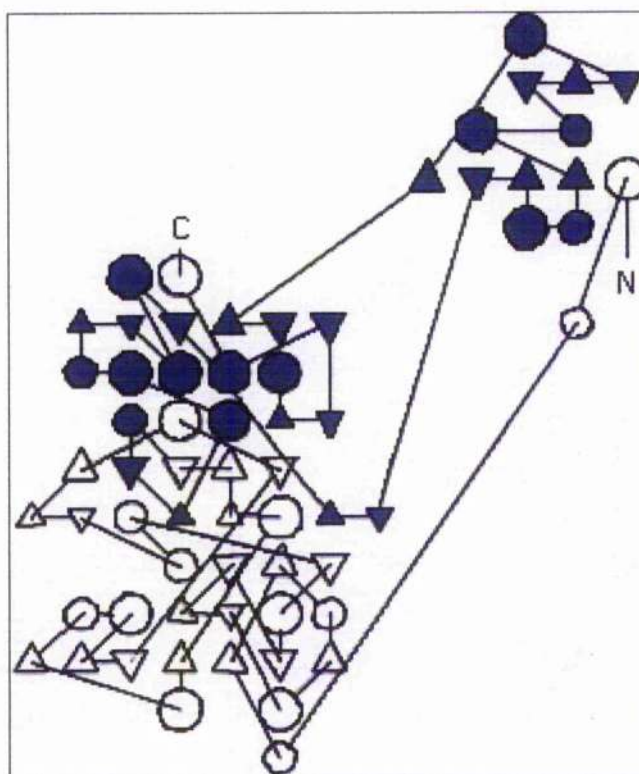


Figure 3-7: TOPS cartoon for chain B of the carbon monoxide dehydrogenase from *Pseudomonas carboxydovorans*, PDB code 1QJ2. Circles represent helices, while triangles represent strands. The different sizes of the circles and triangles represent the sizes of the helices and strands. The direction of the triangle provides information regarding the parallel or antiparallel nature of strands within a sheet. The blue circles and triangles represent the section of chain B of 1QJ2, which shows a high degree of secondary structure homology to ES-62. This was the region used as a template for the construction of a TOPS cartoon for ES-62.

Figure 3-8: 3-dimensional models of residues 252-343 of ES-62 that show homology to residues 74-168 of the leucyl aminopeptidase from *Aeromonas proteolytica*, PDB code 1AMP. Modelling was carried out using DRAGON (a) and SWISS-MODEL (b). (c) shows the 3-dimensional structure of residues 74-168 of the leucyl aminopeptidase from *Aeromonas proteolytica*, PDB code 1AMP. Structural elements in all three images are coloured yellow for sheets and pink for helices. In (b) and (c) turns are coloured light blue. In (a) glycosylation sites on ES-62 are coloured green, residues involved in metal co-ordination are coloured red and residues forming a leucine rich region are coloured blue. The PDB files for the model obtained using DRAGON and the homologous region of the leucyl aminopeptidase from *Aeromonas proteolytica* can be found on the CD included with this thesis. Details of how to view these molecules can be found in Appendix 1.

3.5.6. Tertiary Structure Prediction

3.5.6.1. DRAGON

The modelling of residues 252-343 of ES-62, similar to residues 74-168 of the leucyl aminopeptidase from *Aeromonas proteolytica*, was successful. The output from a number of runs was similar indicating the stability of the resultant model. Figure 3-8 shows the modelled structure of this small region of ES-62 obtained from DRAGON, a model of the same region obtained using SWISS-MODEL and the structure of residues 74-168 of the leucyl aminopeptidase from *Aeromonas proteolytica*.

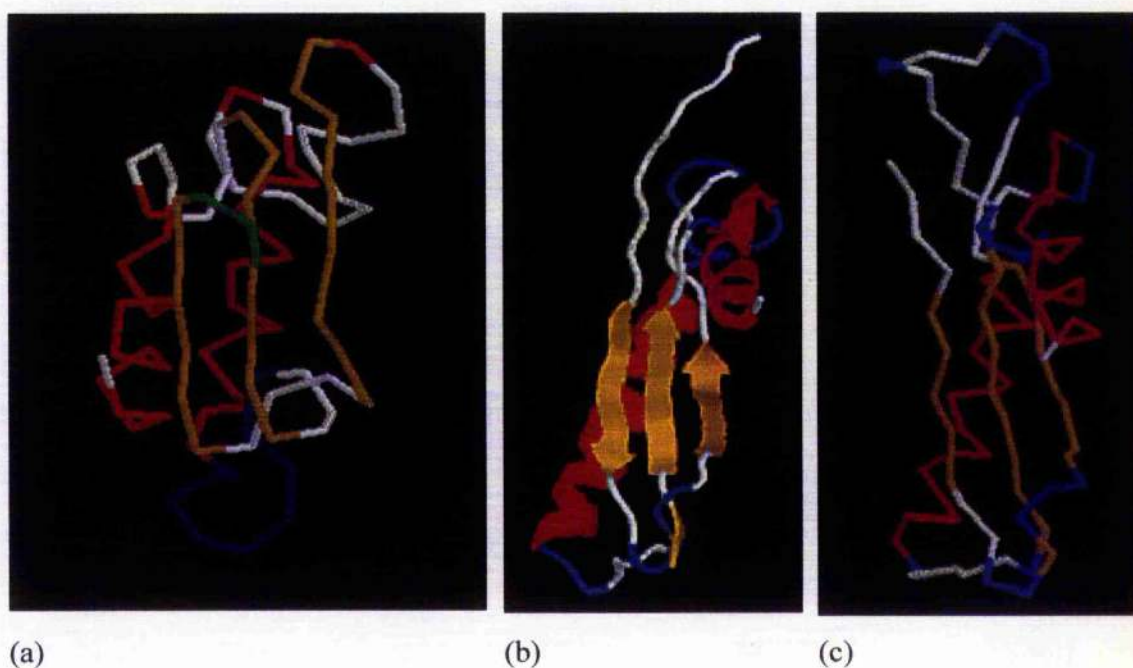


Figure 3-8: 3-dimensional models

In addition to modelling residues 252-343 of ES-62, the modelling of ES-62 in its entirety was also attempted. However, successive iterations of DRAGON did not yield similar models. Figure 3-9 shows the overlay of the models generated from successive iterations of DRAGON.

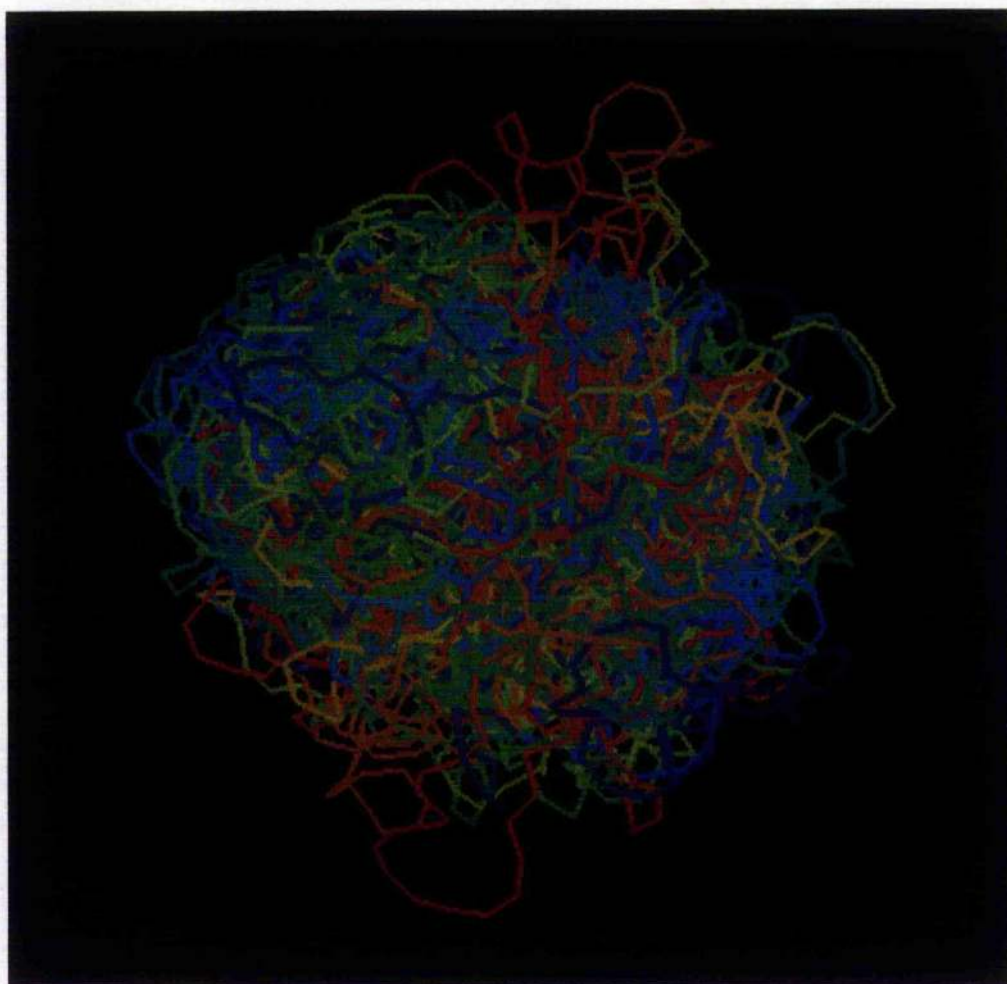


Figure 3-9: PDB files of the outputs from multiple iterations of DRAGON modelling ES-62 in its entirety. The outputs of 24 iterations are shown each coloured differently. As can be seen there is no conservation of structural elements between iterations. The PDB file for these outputs can be found on the CD included with this thesis. Details of how to view these output structures can be found in Appendix 1.

The models obtained from the different iterations were assessed and ranked using a program called rank, supplied with DRAGON. The highest ranked model for ES-62 was then examined to ascertain whether the features ES-62 is known to possess, such as glycosylation sites, were located sensibly within the model e.g. on the surface of the protein. This model with the features marked is shown in Figure 3-10.

Two of the four glycosylation sites could be located on the surface of the model with the other two sites slightly buried. Of the two leucine rich repeats, one was located on the surface and the other partially on the surface. The two cysteines in ES-62 were 24.3 Å apart in the model, although it is unknown whether a disulphide bond links these cysteines. The five residues comprising the two metal co-ordination sites postulated to be present in ES-62 (Harnett *et al.*, 1999a), did not appear to form distinct clusters as might be expected in metal co-ordination sites.



Figure 3-10: Highest ranked model generated by DRAGON for ES-62 in its entirety. β strands are coloured yellow and for α helices are coloured pink. Glycosylation sites are coloured green, leucine rich regions – blue, residues involved in metal co-ordination – orange and cysteines are coloured cyan. The PDB file for this model can be found on the CD included with this thesis. Details of how to view this structure can be found in Appendix 1.

3.5.6.2. *SWISS-MODEL*

SWISS-MODEL, as mentioned previously, requires a protein with known structure that has a high level of homology with the protein of interest in order to work. Unfortunately there is no known homologous protein with a known structure that could allow the modelling of ES-62 in its entirety. However, residues 252-343 of ES-62 that demonstrate homology to residues 74-168 of the

leucyl aminopeptidase from *Aeromonas proteolytica* for which there is a known structure, PDB code 1AMP, was a candidate for modelling using SWISS-MODEL. The model of this region of ES-62 can be seen in Figure 3-8 (b) and is very similar to the model obtained for residues 252-343 of ES-62 using DRAGON. This overall similarity suggested that the modelled structures for this region of ES-62 probably represents the actual structure of this region. As seen in Figure 3-3, residues 252-343 of ES-62 which are homologous to residues 74-168 of the leucyl aminopeptidase from *Aeromonas proteolytica* contain a known glycosylation site, three of the residues involved in metal co-ordination and one of the two leucine rich regions of ES-62. It also contains four of the putative PKC phosphorylation sites, two putative casein kinase II phosphorylation sites and two putative N-myristylation sites predicted to be present by PROSITE. The glycosylation site and leucine rich region appear to lie on the outside of the model. However, as this is only a small section of the whole protein it is not possible to determine if this section of ES-62 lies on the surface when the complete structure of ES-62 is considered.

3.6. Discussion

Analysis of ES-62 using PSI-BLAST identified six proteins with alignment scores of greater than 200 indicating very low (approximately e^{-70}) E values. The E value is a parameter which describes the number of hits that can be expected to occur by chance when searching the database, for example an E value of 1 would mean that 1 match with a similar score would be expected to occur by chance. Small E values indicate that the protein identified is truly homologous to the search protein and that the match has not occurred by chance. As shown in Figure 3-11(a), although particular regions [residues 112-119, 207-219, 230-243, 271-345] have a greater identity than others, all six of the identified proteins show similarity to ES-62 along the full length of the sequence. This level of similarity suggests that these proteins possibly have related functions and structures. Unfortunately the structures of these similar proteins are unknown thus obtaining a model of the structure of ES-62 is difficult as there is no obvious protein structure on which to base the model.

Closer examination of the six proteins identified as homologous to ES-62 reveals that these sequences show greater homology to each other than to ES-62 as shown in Figure 3-11(b). ES-62 shares 37-38 % identity with the other six proteins identified, while these proteins share between 84-99 % identity with each other. The six proteins can be further subdivided into groups, the members of these smaller groups showing greater homology with each other than to members outside these groups. This is most clearly shown when a phylogenetic tree is constructed of the six sequences as shown in Figure 3-12. More detailed analysis of the similarity of the sequences to each other is provided in Table 3-6. This suggests that although ES-62 is related to these other proteins it is a more distant relation of this family. This could be explained by the species difference, in that the six homologous proteins are mammalian proteins whereas ES-62 is a nematode protein.

[illegible]

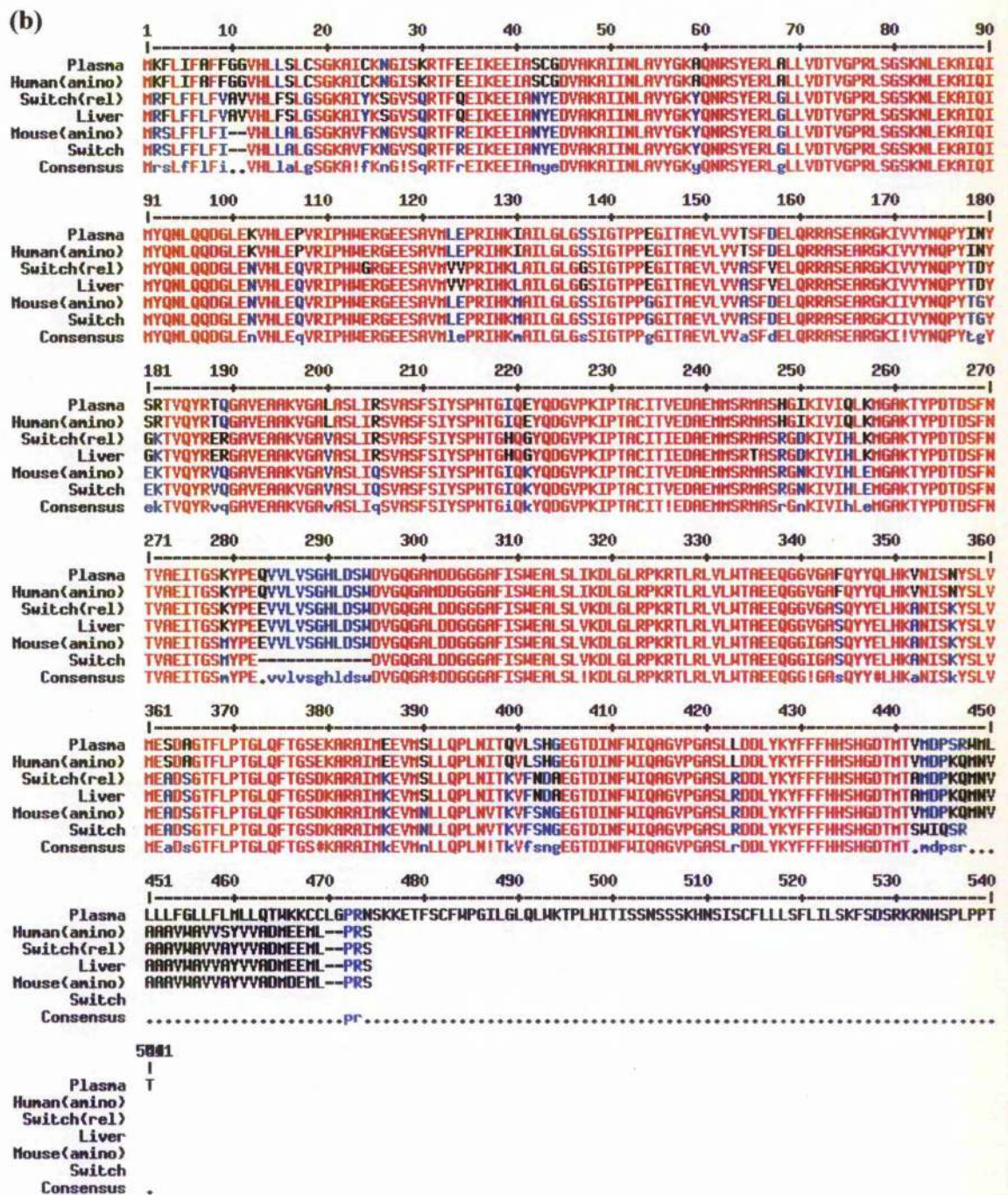


Figure 3-11: (a) Multiple alignment of ES-62 and the six homologous proteins identified by PSI-BLAST as performed by MultAlin. (b) Multiple alignment of the six proteins homologous to ES-62 alone as performed by MultAlin. Plasma is the plasma glutamate carboxypeptidase (human) [Genbank sequence number: 5174627] (Gingras *et al.*, 1999), Human (amino) is the aminopeptidase (human) [Genbank sequence number: 7706387 (Liu *et al.*, unpublished), Switch(rel) is the hematopoietic lineage

switch 2 related protein (rat) [Genbank sequence number: 3851632] (Chen & Talmage, 1998), liver is the liver annexin-like protein (rat) [Genbank sequence number: 7108713] (Servillo *et al.*, unpublished), Mouse (amino) is the aminopeptidase (mouse) [Genbank sequence number: 5442032] (Liu *et al.*, unpublished) and Switch is the hematopoietic lineage switch 2 protein (mouse) [Genbank sequence number: 9055234] (Chen & Talmage, 1998). Red residues show high homology (90 %), Blue residues show low homology (10 %) and black shows neutral residues. symbols are as follows: ! is any one of I or V; \$ is any one of L or M; % is any one of F or Y; # is any one of N, D, Q, E, B or Z.

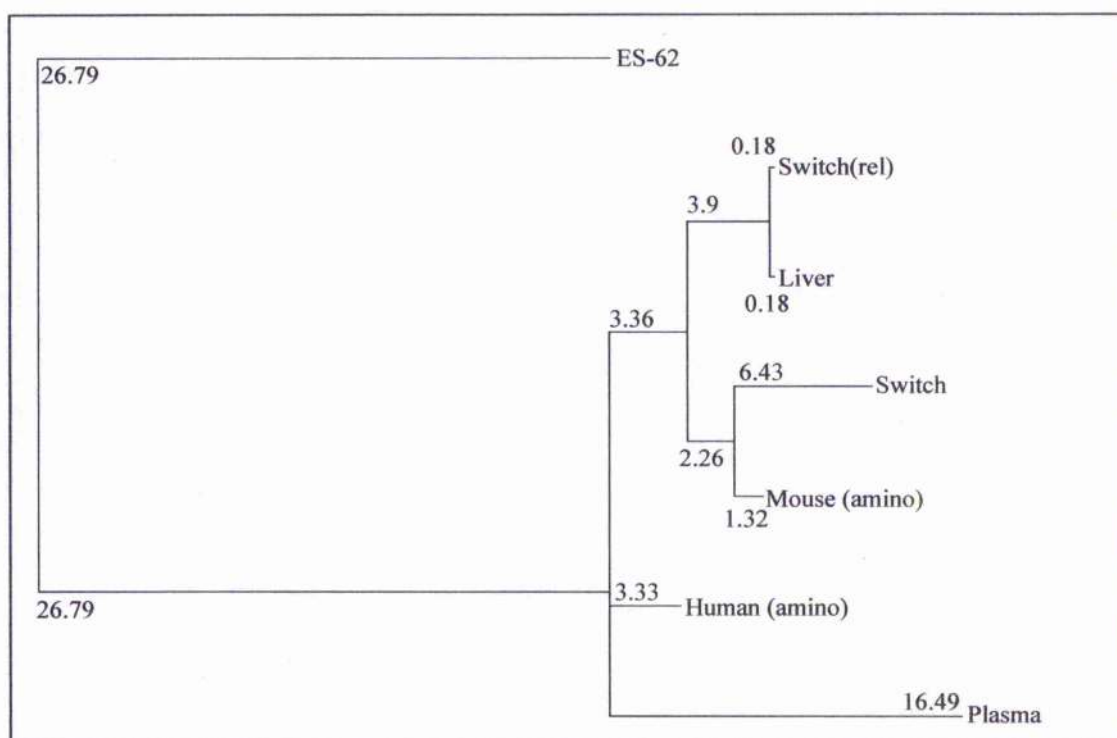


Figure 3-12: Phylogenetic tree of ES-62 and the six homologous proteins identified by PSI-BLAST constructed by clustalw (<http://jura.ebi.ac.uk:6543/cgi-bin/clustalw.cgi>). Plasma is the plasma glutamate carboxypeptidase (human), Human (amino) is the aminopeptidase (human), Switch(rel) is the hematopoietic lineage switch 2 related protein (rat), Liver is the liver annexin-like protein (rat), Mouse (amino) is the aminopeptidase (mouse) and Switch is the hematopoietic lineage switch 2 protein (mouse).

	ES-62	Plasma glutamate carboxypeptidase (human)	Aminopeptidase (human)	Hematopoietic lineage switch 2 related protein (rat)	Liver annexin-like protein (rat)	Aminopeptidase (mouse)	Hematopoietic lineage switch 2 protein (mouse)
ES-62	100	38	37	37	37	37	36
Plasma glutamate carboxypeptidase (human)	38	100	99	86	86	87	84
Aminopeptidase (human)	38	99	100	87	87	87	84
Hematopoietic lineage switch 2 related protein (rat)	38	86	87	100	99	92	89
Liver annexin-like protein (rat)	38	86	87	99	100	92	89
Aminopeptidase (mouse)	37	87	87	92	92	100	97
Hematopoietic lineage switch 2 protein (mouse)	36	84	84	89	89	97	100

Table 3-6: Percentage identity between ES-62 and the six homologous protein identified by PSI-BLAST and between each of the six homologous proteins. Percentage identities were obtained from PSI-BLAST (Altschul & Koonin, 1998; Altschul *et al.*, 1997).

The six proteins identified as homologous to ES-62 all show homology to the peptidase M20 family in the region of residues 253-376. In addition, these six proteins, with the exception of liver annexin-like protein, have all been classified as either amino or carboxypeptidases. It is possible that the liver annexin-like protein may be incorrectly classified as PSI-BLAST and Entrez searches of this sequence do not identify other annexin proteins. Further, the liver annexin-like protein shows no discernible homology to other annexin proteins. This suggests a common function for the six proteins homologous to ES-62.

ES-62 has been shown to possess aminopeptidase activity (Harnett *et al.*, 1999b). However, ES-62 has not been identified as being homologous to M20 family members. In spite of this the region of the six proteins homologous to ES-62, identified as being homologous to the M20 family members, is one of the more highly conserved regions shared by ES-62 and the six proteins identified.

The classification of the six homologous proteins as peptidases, the similarity of a region of these proteins to the M20 peptidase region and the fact that this region of the identified proteins shows high homology with ES-62, all indicate that the aminopeptidase activity identified for ES-62 is not an artefact, but has biological significance. This aminopeptidase activity may be important in promoting the immunomodulatory role of ES-62. The peptidase role for ES-62 further strengthens the hypothesis of a metal co-ordination site within ES-62 as many peptidases possess at least one metal ion often situated in the active site of the enzyme.

In addition to the six homologous proteins identified using PSI-BLAST, searching of filarial and nematode EST (expressed sequence tag) databases using the DNA sequence of ES-62 revealed several ESTs from *B. malayi* and *O. volvulus* homologous to ES-62. The ESTs identified as homologous were from female, male and microfilariae forms of the parasites. The identification of these ESTs demonstrates that while ES-62 is an excretory-secretory protein from a rodent filarial parasite, it is homologous to human filarial parasitic products. The use of ES-62 as a model for human filarial excretory-secretory products is therefore justified.

3.6.1. Secondary Structure

In an attempt to gain some information as to the possible secondary structure elements which might constitute ES-62 a range of prediction programs were used. Jpred enabled a range of predictions to be both generated and easily compared from prediction programs which use different secondary structure prediction algorithms. Examination of the results of the secondary structure predictions from each of the programs used (Figure 3-5) indicates that despite using different algorithms, in general the secondary structure predictions generated by each program are in agreement. In particular, PHD appears overall to agree with the Jpred, which has been shown to be the most accurate prediction method (Cuff *et al.*, 1998b). However, it should be noted that PHD does predict strands in some regions which are assigned as helical by Jpred. The general consensus of PHD with the other prediction programs and in particular with the Jpred consensus is of importance as the programs Plotcorr and DRAGON are used downstream of PHD and thus their accuracy depends on the reliability the PHD output. As the prediction generated by PHD was similar overall to the other programs, it is fair to suppose that the input to these downstream programs is reliable.

The proteins identified as being homologous to ES-62 on the basis of secondary structure using sss_align did not appear to be similar to one other with respect to tertiary structure thus raising doubts over the accuracy and validity of this method of identification of homologous proteins. However, examination of the secondary structure of the proteins predicted to be homologous to ES-62 clearly indicated that the proteins identified shared similar secondary structure elements and that these elements were also present in the same order. The output of sss_align indicating the secondary structure alignments with reference to ES-62 is shown in Figure 3-13.

ES-62 aligned with pyruvate ferroxin oxidoreductase from *D. africanus* (PDB code: 1B0P)

```

      EEEEEEtttttt EEeeee   HHHHHHH HHHHHHHHHH tt ee ee
1B0P  164 NVPFMHFFDGFRTSHEIQKIEVD---YADMASLVNQKALAEFRAKSMNPEHPHVRGTAQ 220
      | : . | : . . . . . : . . . . . : : : : .
ES-62  4  NSSTFFFLVTLTVLGA AVLDPKTVAPKNYIQETFGKEVAELIQYITKGEEVGL----- 57
      EEEEEEEEEEEEE EEE      HHHHHHHHHHHHHHHHHHHHH hh

```

HHHHHHHHtthhhhhhhhHHHHHHHHHHHH eeeEE tt eEEEe thh
 1B0P 221 NPDIYFQGREAA NPYLKVPGIVA EYM QKVASLTGRSYKLFDYVGAPDAERVIVSMGSSC 280
 . : : : : : : : ||.. :: : ..|: : : :
 ES-62 58 AYQWLSKLVDGFGRHMVGS D SLEKSIA FLEES LKNDNF DKVHTVEVPNLPHWVRGNDVVE 117
 hHHHHHHHH eeee HHHHHHHHHHHHH EE EEE eee

```

          hhhhhhhhhhhhttt      eEEEE EEe   hhhhhhhh  tt  EEEEE   t
1B0P  281 ETIEEVINHLAAKGEK-----IGLIKVRLYRPFVSEAFFAALPASAKVITVLDRTKEP 333
          . . . . .          . : . | . . . . . | . . . . . : . :
ES-62 118 MIEPRNQLRNVLAI GGSEPASATGEVTVI-YDLDDV-----KPDDVRGKIVVTAQTFA 169
          ee      eeeeeee      EEEEE EE      eEEEEEEEEe

```

```

t      hhhhhHHHHHHHHHt      EEEEE      HHHHHHHHHH
1B0P  334 GAPGDPLYLDVCSAFVERGEAM----PKILAGRYGLGSKEFS-----PAMVKSVD 380
      | | | | | : | : : : : : : : : : : : : : : : : :
ES-62 170 GYPLTLKYRRSVKLFELGAIGVLVKSITSFSINSPTGTGAENTTIPAACLTIIEAEML 229
      eeee  HHHHHHHH  eeeeeeeeeEEEEE  hhhHHHHHHHHH

```

		HHHtt	EE		tt	EEEEEEEEett		
1B0P	381	NMSGAKKNHFT----VGIEDDVTGTSLPVDNAFADTTTPKGTIQCFWGLGADG-----						429
		:	:	:	:	:	:	
ES-62	230	ERLYRSGKKIVIRMDMKSHYEEPINSSNLIFEITGSRPSEVVLLSAHVDSWDVQGALD						289
		HHHhh	EEeee		eeeeee	EEEEEEE		

hhHHHHHHHHHHHHHHHHHH EEEEEEE eeEEEEEEEE
 1B0P 430 -----TVGANKQAIKIIGDNTDL-----FAQGYFSYDSKSGGITISHLRFGEKPIQST 478
 . | : . : : | : : . : | | . . : : | : . : .
 ES-62 290 DGAGCAVVWSALHSLKLAERNPKFKPKRTIRGIFWTSEEQGYGGAKHYIYTHKNDSPK 349
 eeeHHHHHHHHHHHHHHHHHH EEEEEEE EEEEEEE e

		EEEE	tt	tttt	tt	eeEee	HHHHHHH	HHHHHHHHHtt	
1B0P	479	YLVNRADYVACHNPA	YVGIYDILEGIKDG	GTFLVNSPWSSLE	MDKHLPSG	IKRTIAN	KK		538
	:		..:	:	.	.	:	.. :	.. :
ES-62	350	F-----YFV	SETDTGTFKST	NWL-----	AHLSFGDKK	SMRL	RL--KEIT	RLLSRNG	393
	e	EEEEe	ee	hhhh	EE ee	HHHHHHH	HHHHHHHHH		

```

      EEEEE
1B0P  539 LKFYNID  545
      : : | :
ES-62 394 IALGLIN  400
      EEEEE

```

Alignment of ES-62 with ectodomain of human transferrin receptor (PDB code: 1CX8)

```

          HHHHHHHHHHHHt      HHHHHHt      tt HHHHHHHHHHHHHhht
1CX8  124 WDDLKRKLSEKLDSTD----FTSTIKLLNENSYPREAGSQKDENLALYVENEFREFKLS 179
          ::. .| : ::::.      :: | :.  .. ::. ::::|: |: :. .
ES-62  38 FGKEVAELIQYITKGEEVGLAYQWLSKLVDFGHRMVGSDSLEKSIAFLEESLKNDFDK 97
          HHHHHHHHHHHH      hHHHHHHHhhh  eeee  HHHHHHHHHHHHHH

          EE      EEE  EEEEEe      EEEEE      tt
1CX8  180 KVWRD-----QHF---VKIQVKDSAQNSVIIVDKNGRLVYLVEN-----PGGYVAYSKA 225
          :      |  :: ..|.  ::.  :.  .  ::.  :|  ...
ES-62  98 VHTEEVPNLPHWVRGNDVVEMIEPRNQRLNVLAIGGSEPASATGEVTVIYDLDDVKPDDV 157
          EE      EEE  EEEEE      EEEEEe      eeeeeee

          EEEEE EEE ttt ttttt      tt EEEEE
1CX8  226 ATVTGKLVHANFGTKKDFEDLY-----TPVNGSIVIVR-----AGKIT----- 263
          . .  ::. |  ::.      .. | :|  :....
ES-62  158 RGKIVVTAQTFAGYPLTLKYRRSVKLFEQLGAIGVLVKSITSFSINSPTGTGAENTTIP 217
          EEEEEeEEEE  eeee  hhhhhhhh  eeeEEEEEEEEe

          HHHHHHHHHHt      EEEE  ttt      tt
1CX8  264 -----FAEKVANAESLNAIGVLIYMDQTKFPIVNAELSFFG---HAHLGTGDPYTPGFP 314
          ...: :  ::  ::| ||  ..  . : | :  :  ::  :.
ES-62  218 AACLTIEEAEMLERLYRSGKKIVIRMDMKSHYEELINSSNLIFEITGSERPSEVLLSAH 277
          hhhhhhHHHHHHHHHh      EEEEE  eeeee  eeeeeee

          eEEE HHHHHHHHt      tt      tt EEE
1CX8  315 SFNHTQFPSPSRSSGLPNIPVQTISRAAAEKLFNGMEGDCPSDWKTDSTCRMVTSSEKNVK 374
          : .  ::. .|.  .  ::. |.  .  .  .  ::.  :....
ES-62  278 VDSWDVGQALDDGAGC---AVVWSALHSLKKLA-----ERNPKFKPKRTIRG 322
          EEEhHHHHHHHHHh      hh      eEEE

          EEE eeee  eeEEEEEE  EE      tt EEEEE      tttthhh  HHHHH
1CX8  375 LTVSNVLK---EIKILNIFGVKGFVEPDHYVVVGAQRDAWGPGAAGSGVG---TALLL 427
          : ::  :  . |  |  . |.  ... | |  :: ::.  :  ::  . :|
ES-62  323 IFWTSEEQGYGGAKHYI---THKNDSPKIFYVSETDTGTFKSTNWLHLFSFGDKKSM 380
          EEEe      EEEEE  EE      eeEEEEEE  ee  hhhhee  ee  HHHHH

          HHHHHHHHHHt      EEEE      t hhhhhhhh  tttthhhHEEEE
1CX8  428 KLAQMFSDMVLDKG-----FQPSRSIIFASWSAGDFGSGATEWLEGYLSLHLKAFTY 481
          :| ::.  :  ::      ..| : :.  :  .  :  : |
ES-62  381 RLKEITRLLSRNGIALGLINSSVQGDVTFWAKDGIPSVNY-----IPDKAVD---YYFY 431
          HHHHHHHHHHHH  eeeee  eee eEEEEe      e      EEEE

          EE tt      EEEE      HHHHHHHHt      tt      t
1CX8  482 INLDKAVLGTSNFKVSASPL----LYTLIEKTMQNVKHPVTGQFLYQDSNWASKVEKLT 537
          ::      :: ..|.  ..      :.  .  .  :  |  :  .||  ..
ES-62  432 FHH----TAGDYMTVLKGDLEYTTSIFATLGHVIANMDDWGSDPNPQQLNSKQSTTEK 487
          EEE      eEEEE  eeee  HHHHHHHHeeee

          t
1CX8  538 DN 539
          .:
ES-62  488 SD 489

```


ES-62 aligned with endocellulase from *C. cellulolyticum* (PDB code: 1FCE)

```

          tt eeHHHHHHHHHHHHHHHHHh hHHHHHHHHHHHHHt ttt hHHHtt
1FCE  43 VEAPDYGHVTTSEAMSYIMWLEAMHGRFSGDFTGFDKSWSVTEQYLIPTEKDQPNSTMSR 102
      ... . :. . :. | :: .|: .|:. | . :. : ::: ..
ES-62 23 LPDKTVAPKNYIQETFGKEVAELIQYITKGEEVGLAYQWLSKLVDGFGHRMVGSDSLEKS 82
          hhhHHHHHHHHHHHHHHHHHHH HHHHHHHHHHHH eeee HHHhh

          tt ee tt HHHHHHHH EE
1FCE 103 YDANKPATYAPEFQDPSKYPSPLDTSQPVGDRPINSQLTSAYGTSMLYGMHWIL----- 156
          : |... .. : :|
ES-62 83 -----IAFLEESLKNDNFDKVHTEEVPNLPH 108
          HHHHHHHHh EE

      Ett tt EEEE tt tt EE EE tt thhhhEE
1FCE 157 DVDNWyGFGARADGTSKPSYINTFORGEQESTWETIPQPCWDEHKFGGQYGFLLDFTKDT 216
      | . . . . : : : : : : : : : : : : : : : : : :
ES-62 109 WVRGNDVVEIEPRNQRLNLVLAIGGSE--PASATGEVTVIYDLDDVKPDDVRGKIVVTAQ 166
      Eee eeeee eEEEEe eeEEeEE eeeeeEEee

          eEEEE hHHHHHHHHhhhh hhhhhhttt HHHHH
1FCE 217 GTPAKQFKYTNPADADARAVQATYW-----ADQWAKEQGKSVSTSVG 258
      . :: :. . .... . :: :. :. :. :. :. :
ES-62 167 TFAGYPLTLKYRRSVKLFEQLGAIGVLVKSITSFSINSPTGTGAENTTIPAACTIEEA 226
      e EEEE HHHHHHHH eeeeeeeeeeee hhhHHHHHH

      HHHHHHHH tt eettEEEE EEEEE eEEE E
1FCE 259 KATKMGDYLRYSFFDKYFRKIGQPSQAGTGyDAAHYLLSWYAWGGGIDSTWSWIIGSSH 318
      . .. . : : : : : | : . . . | : :
ES-62 227 EMLERLYRSGKK-----IVIRMDMKSHYEEPINSSNLIFEITGSERPSEVV---L 273
      HHHHHHHH EEEEE EEEEEe EEE E

      EE hhhhhhhhh hhhhhHHHHHHHHHHHHHt EEE
1FCE 319 NHFGYQNPFAAWVLSTDANFKPKSSNGASDWAKSLDRQLEFYQWLQSAEGAIAAGGATNSW 378
      :: :. ....| : .:|:. :. :. . . : :
ES-62 274 LSAHVDSDW-----VGQALDDGACAVVWSALHSLKLAERNPKFKPKRTIRGI--- 323
      EEee eeeHHHHHHHHHHHHHHH eEEEE

      tttt tt EEtEEEE tt tt thhhhhHHHHHHHHHHHHH HHHHHH
1FCE 379 NGRYEAVPSTSTFYGMGYVENPVYADPGSNTWFGMQVWSMQRVAELYKYTGDAKAKLL 438
      |. . |:. | :. ::: :. . | :::|:| :. . . :|
ES-62 324 FWTSEEQGYGGAHHYIITHKNDSPKIFYFVSETDTGTGFKSTNWLHLSPSGDKKSMRLRK 383
      eee EEeEEEE eeeeeee ee HHHHee ee HHHHHHHH

      HHHHHHHHt EE tt EEEeEEEEEE ttt tt EEEEEEEe
1FCE 439 DKWAKWINGEIKFNADGTFQIPSTIDWEGQPDWTNPTQGYTGANLHVKVNYGTD 494
      : ...| :. :. ....| . :. . . :::| . ::::
ES-62 384 EITRLLSRNGIALGLINSSVQGDVTFWAKDGIPSVN--YIPDKAVDYFYFHHTAG 437
      HHHHHHHH EEeee EEE EEEEE e EEEEEEE

```

carboxydovorans (PDB code: 1QJ2)

		EEEEEEEEE	ee	tttHHHHHHHHHHHHHHHh	HHHHHH	
1QJ2	363	YDMPVAHLAVDGVYTNKASGGVAYRXSFRVTEAVYAIAERIAETLAQRLEMD---	SADLRI	419		
	 :. . :.: : . : :				
ES-62	4	NSSTFFFLVTLTVVLGAAVLDPDKTVAPKNYIQETFGEVAELI QYITKGEEVGLAYQWLS	63			
		eeeeeeeeeee eee	hhHHHHHHHHHHHHHHHHHHH	hhHHHHHH		
		HH ee tt EE	HHHHHHHHHHHHHthhhhhhHh	hhhhhhht		
1QJ2	420	KNFIQPEQFPYMAPLGWEYDSGNYPLAMKKAMD TVGYHQLRAEQK----	AKQEAFKRGET	475		
		.: :::	::.	:	:..	
ES-62	64	KLVDGFGH-----RMVGSDSLEKSIAFLEES-----LKNDNFDKVHTEEVPNLP	107			
		HHhh e EeE	HHHHHHHHHHHHH	HH	ee	
		EEEEeeEEEE	t t t Eett ee	EEEEEE tt	EEEE	
1QJ2	476	REIMGIGISFFTEIVGAGPSKNC DILG---VSMFDSA EIRIHPTGS-----VIARMGT	525			
		: :. :: : : : : . . : :				
ES-62	108	HWVRGN DVEMIEPRNQRLNVLAIGGSEPASATGEVTVIYDLDDVKPDDVRGKIVVTAQT	167			
		EEE EEEEE	eeeeeeE	EEEEEEE	eeeEEEEEEe	
		hhhhhhHHHHHHHt	EEEE ttt	tt ttttHHHHHHHHHH		
1QJ2	526	KSQGQHGHETT YAQIIATELGIPADDIMIEEGNTDTAPYGLGTYGSRSTPTAGAATAVAAR	585			
		: . . : : : : : . : . : : : . : .				
ES-62	168	FAGYPLTLKYRRSVKLF EQLG AIGVLVKSITSFSINS PHTGTGAENTTIPAACL TIEEAE	227			
		eeee HHHHHHHh	eeeEEEEeeeeee	HHHHHHHHHH		
		HHHHHHHh	hhhhht	EEE	EEEEttee	
1QJ2	586	KIKAKAQM-----IAAHMLEVHEGDLEW-----DVDRFRVKGLP-----	619			
		::. : :	: .. :	.	: : .	
ES-62	228	MLERLYRSGKKIVIRMDMKSHYE EEPINSSNLIFEITG SERPSEVLLSAHVDSWDVGQGA	287			
		HHHHHHH eeeee	EEEEee	EEEEeeEE		
		EEEEeHHHHHHHHHHH	tt	EEEEEEE	eeEEEEEEeettt	
1QJ2	620	-----EKFKTMKELAWASYNSPPPNLEPGLEAVNYDPPNM TYPF GAYFCIMDIDIDT	672			
		. : : :.. . :.: : . . : :. : : ..				
ES-62	288	LDDGAGCAVVWSALHSLKLAERNPKFKPKRTIRGIFWTSEEQGYGGAKHYI THKNDSP	347			
		EEehHHHHHHHHHHHh	EEEEEEEe	EEEEEE		
		EEEEEE	eeeEE	HHHHHHHHHHHHHHHHHHh	EE tt	
1QJ2	673	GVAKTTRF-----YALDDCGTRINPM IEGQVHGGLTEAF AVAMG---QEIRYDEQ	720			
		. . : : : : . : : . : . : . : :				
ES-62	348	EKFYFVSETDTGTGTFKSTNWLAHLSFSGDKK SMLRLKEITRLLSRGIALGLINSSVQGDV	407			
		eEEEEEE ee hhhhEE ee	HHHHHHHHHHHHHHHHH	eeee eEE ee		
		EE ttt ttt	EEEE	tt tt	tthHHHHHHHH	
1QJ2	721	GNVLGASFMDFFLPTAVETPKWETDYTVTPSPHHP IAKGVGESPHVGGVPC	772			
		. : : . : . : . : . : .				
ES-62	408	TFWAKDGIPSVNYIPDKAVDYYFYFHHTAGDYMTVLKDGDLEYTTSIFATLG	459			
		eeEE e	eeEEEEe	eeeeee	eeee HHHHHHH	

Figure 3-13: Alignment of ES-62 with homologous proteins identified on the basis of secondary structure by sss align (Sturrock & Dryden, 1997).

The analysis of the results from `sss_align` suggest that although the secondary structure prediction program `sss_align` was able to identify proteins containing similar secondary structure elements to those predicted for ES-62, the proteins identified did not share similar folds. This is perhaps not unexpected as it is clear that even when only a limited number of secondary structure elements are present, that the elements may arrange themselves in a multitude of different ways.

As discussed in section 3.5.4, the secondary structure of ES-62 was further examined by CD spectroscopy. The results obtained from CD are significantly different from those generated by the secondary structure prediction programs as shown in Table 3-7 below. This suggests either a disappointing failure of the secondary structure prediction programs to predict the secondary structure of ES-62 or serious inaccuracies in the CD studies. The CD studies were performed at two separate laboratories, both studies yielding very similar secondary structure content results. If the discrepancy between the CD results and the predicted secondary structure is taken to indicate that the predicted secondary structure is inaccurate, this finding has serious implications, as the secondary structure predictions are the basis for homologous secondary structure searches by `sss_align` and for modelling using Plotcorr and DRAGON.

	% α -helix	% β -sheet	% turn	% other
CD (Glasgow)	39.4	16.7	16.3	28.1
CD (Daresbury)	48	14	14	26
Predicted by Jpred	26	21	0	53

Table 3-7: Comparison of the experimentally determined secondary structure content of ES-62 with the predicted secondary structure content.

The differences in the CD results and the secondary structure predictions could possibly be explained by limitations in secondary structure prediction or perhaps limited refolding of ES-62 upon tetramerisation (secondary structure prediction programs do not take into account quaternary structure information). In addition

post-translational modifications to the protein (glycosylation and phosphorylcholine) may stabilise secondary structure elements which would otherwise not be predicted as being stable (i.e. by JPred). As with the phosphorylation, myristylation and amidation sites suggested by the motif recognition program Prosite it is impossible to reasonably suggest the effects such post-translation modifications may have on either the structure or the way in which ES-62 induces its signalling effects without further structural information such as high resolution crystallographic data.

Modelling of both ES62 in its entirety and of residues 252-343 of ES-62 (homologous to residues 74-168 of the leucyl aminopeptidase from *Aeromonas proteolytica*) was attempted (section 3.5.6). The modelling program DRAGON was employed to model both of these structures while SWISS-MODEL was only used to model residues 252-343 due to the lack of a suitable homologous model for the whole of ES-62. DRAGON was unable to model the structure of the monomer of ES-62, with multiple iterations of the program producing models which, by visual examination, did not appear similar.

In view of the discrepancy between the secondary structure predictions and the CD results discussed above, the failure of DRAGON may be due to inaccuracies in the secondary structure information available. In addition, ES-62 exceeds the recommended size limit for DRAGON of 300 residues (ES-62 contains 508 residues). Further, it is possible and perhaps likely, that ES-62 folds as number of domains and DRAGON is not able to model multi-domain proteins (Aszodi & Taylor, 1994a; Aszodi & Taylor, 1994b; Taylor & Aszodi, 1994). The quaternary structure of ES-62, a tetrameric structure, is also likely to influence the tertiary structure of the ES-62 monomers. DRAGON is unable to model the tertiary structure of a protein taking into account any quaternary structural influences. In contrast to modelling of the whole monomer, the models obtained from multiple iterations of DRAGON for residues 252-343 of ES-62 appeared to be similar to one another. Further, modelling of this region using the homology modelling program SWISS-MODEL yielded a model which was similar to those produced by DRAGON. Using PSI-Blast the most similar structurally

determined sequence to ES-62 identified was that of a leucyl aminopeptidase from *Aeromonas proteolytica*. A sequence alignment of this aminopeptidase with ES-62 is shown in Figure 3-14.

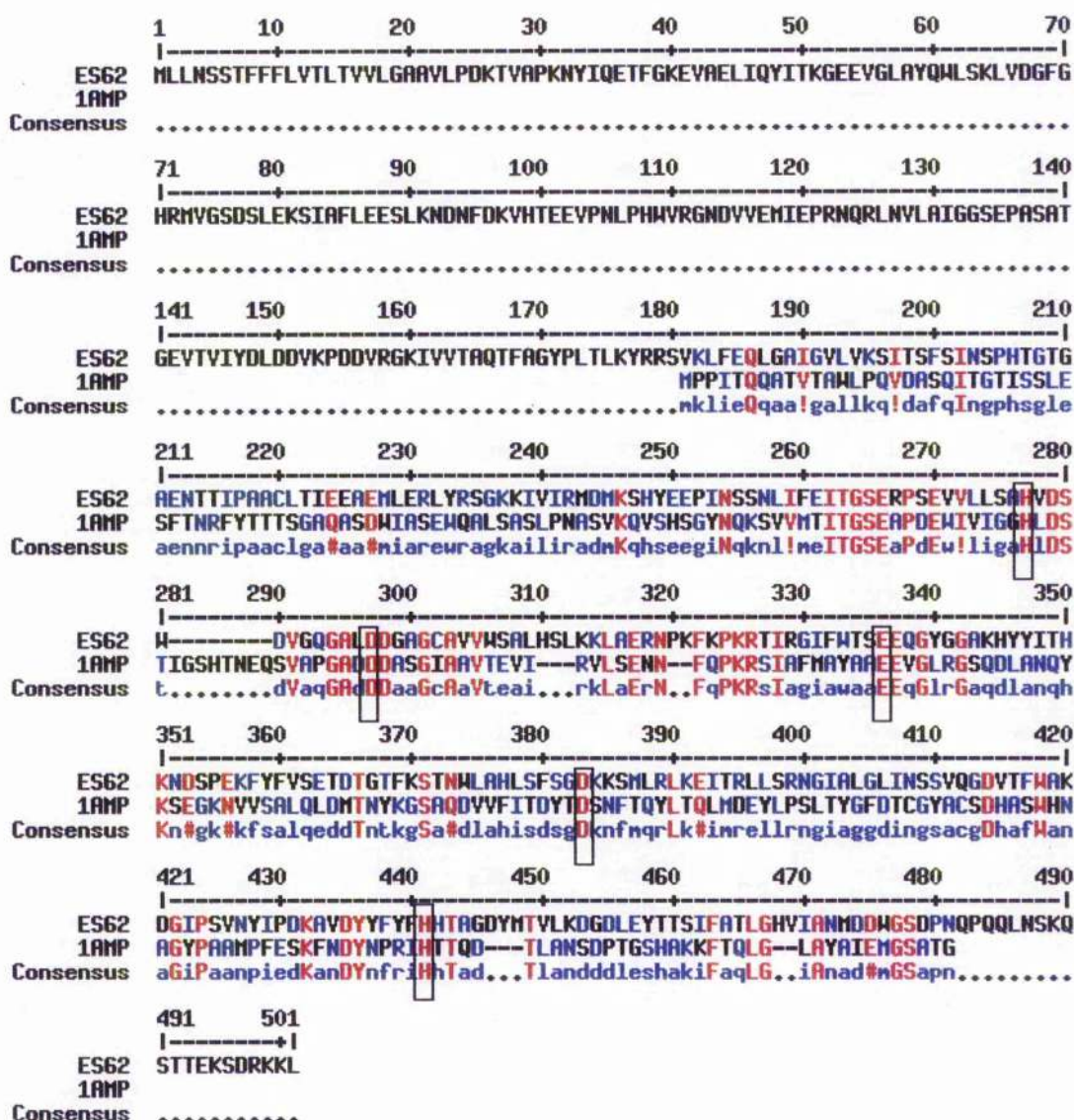


Figure 3-14: Sequence alignment performed using MultAlin of ES-62 with the leucyl aminopeptidase from *A. proteolytica*. Residues involved in metal binding in the *A. proteolytica* structure are boxed. Red residues show high homology (90 %), blue residues show low homology (10 %) and black show neutral residues. Symbols are as follows: ! is any one of I or V; \$ is any one of L or M; % is any one of F or Y; # is any one of N, D, Q, E, B or Z.

In view of the above alignment, the model of this region produced by DRAGON was compared with that of the *A. proteolytica* leucyl aminopeptidase structure. The aim in comparing the two structures was to determine if the residues shown to be involved in zinc binding in the leucyl aminopeptidase structure and conserved in the ES-62 sequence were close together in space in the modelled structure. If these conserved residues are similarly spatially arranged this would add weight to the suggestion that these residues form a metal binding site in ES-62 (it has been postulated that ES-62 contains a metal binding site (Harnett et al., 1999a)).

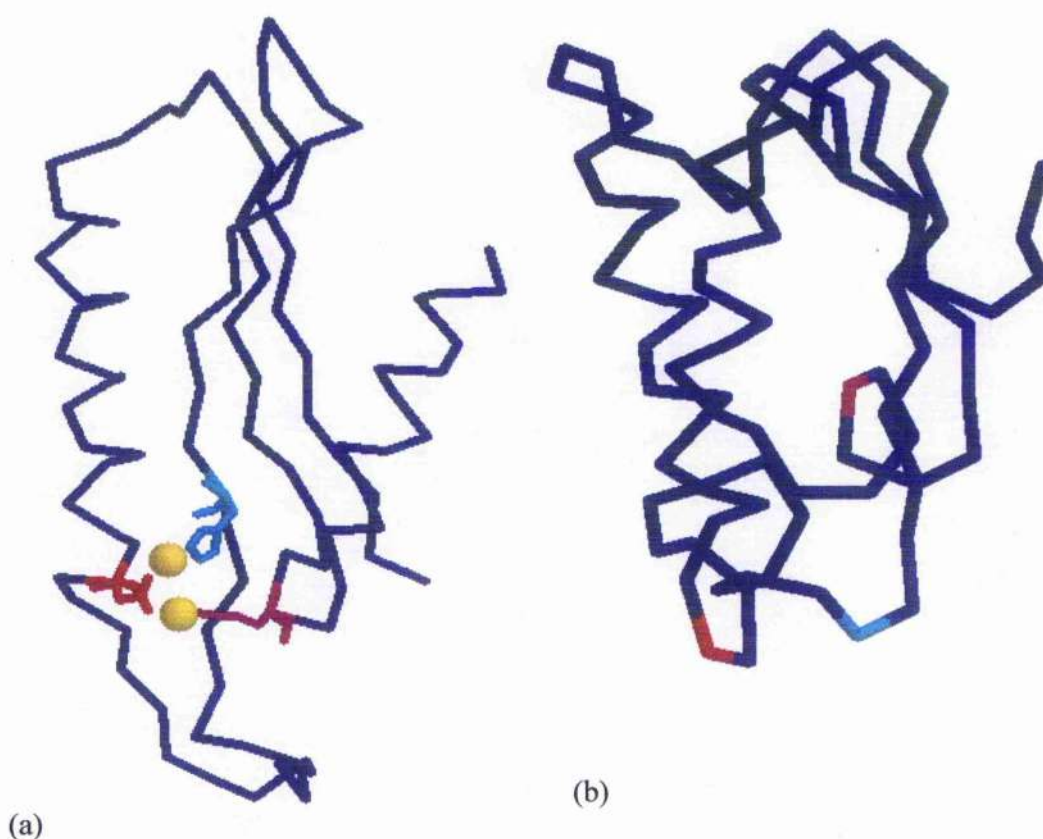


Figure 3-15: (a) Residues 74-168 of the leucyl aminopeptidase from *A. proteolytica* structure (pdb code 1AMP). Residues involved in zinc binding in this region are shown as His 97 in cyan, Asp 117 in red and Glu 152 in magenta. The two co-ordinated zinc atoms are shown in yellow. (b) Residues 252-343 of ES-62, homologous to residues 74-168 of the leucyl aminopeptidase from *A. proteolytica*, with the conserved residues His 277 in cyan, Asp 287 in red and Glu 336 in magenta. Side chain positions of the conserved residues are not shown as they are not modelled by DRAGON.

Overall the structure shown in Figure 3-15 (b) is similar to that shown in Figure 3-15 (a) in that it comprises a β -sheet region formed from three β -strands and contains two helical regions, although the orientation of the helical regions with respect to the β -sheet region is different. Examination and comparison of the models shown in Figure 3-15 suggests that the residues involved in binding and co-ordinating the zinc atoms in the *A. proteolytica* leucyl aminopeptidase structure, although grouped together in the DRAGON modelled structure, do not appear to form a metal binding region. It would appear from the C α trace produced by DRAGON that the side chains of His 277 and Glu 336 extend away from each other and possibly into solvent. However, this model is only a portion of the whole protein and thus may be surrounded by the rest of the ES-62 structure. Although DRAGON may have successfully modelled the general structure of this region of the ES-62 structure which is similar to that of the leucyl aminopeptidase from *A. proteolytica*, it is possible that the actual residue positions are not accurately provided by this model. The predicted C α positions of the conserved residues may be incorrect, as other residues in the structure may influence the folding of this region. As DRAGON modelled the region in isolation, it is possible that the lack of information from the remainder of ES-62 in the folding of this region would lead to inaccuracies in the model shown. In addition, a relatively slight movement in the predicted C α positions would cause the predicted metal co-ordinating residues to be directed away from the possible solvent region.

In order to predict more accurate models of the structure of ES-62 it would be preferable to include in the input homologous structures which have greater similarity for a larger number of residues present in ES-62. Unfortunately, there are no high resolution structures for proteins which share full-length sequence homology with ES-62.

4. Structural Studies on Native ES-62

In addition to the bioinformatics approach to gaining tertiary structural information discussed in Chapter 3, two biophysical techniques, analytical ultracentrifugation (AUC) and small angle X-ray scattering (SAXS) were employed to obtain the low resolution quaternary structure of ES-62. AUC provided an accurate value for the molecular weight for ES-62, information about its overall shape and information about the self-interaction of the monomeric form. SAXS was used to obtain a model of the overall shape of ES-62.

AUC experiments were carried out using a Beckman Optima XL-A analytical ultracentrifuge which measures the distribution of samples under gravitational force using absorbance optics. It was thus essential to calculate the extinction coefficient for ES-62 and to perform wavelength scans of the protein to determine the wavelength at which maximal absorbance occurs. A wavelength scan of ES-62 revealed that maximal absorbance occurred at a wavelength of 277 nm as opposed to 280 nm, which is a typical wavelength for protein maximal absorbance. The concentration of the sample of ES-62 was determined via a Coomassie protein assay to be 0.437 mg ml^{-1} . The absorbance at 277 nm of this ES-62 sample was 0.883 in a 1 cm pathlength cell. Using the equation $A = \epsilon cl$, where A is the absorbance at 277 nm, ϵ is the extinction coefficient ($\text{cm}^2 \text{ mg}^{-1}$), c is the concentration (mg ml^{-1}) and l is the pathlength of the spectrophotometer, in this case 1 cm, the extinction coefficient for wild type ES-62 was calculated to be $2 \text{ cm}^2 \text{ mg}^{-1}$ ($2.31 \times 10^5 \text{ cm}^2 \text{ M}^{-1}$). This is a higher extinction coefficient than might normally be expected for a protein and was postulated to be the result of phosphorylcholine (PC) moieties attached to several of the carbohydrate chains of ES-62 (Harnett *et al.*, 1994).

4.1. Analytical Ultracentrifugation (AUC)

Analytical ultracentrifugation is a biophysical technique that is utilised to obtain information about the molecular weight, homogeneity, size and shape, molecular interactions, changes in conformation and non-ideality of a macromolecule in solution. It is a definitive method for the determination of the molecular weight of a protein as it does not require standards of known molecular weights and is not complicated by interactions between the protein and a medium such as polyacrylamide gel or size exclusion matrix. A brief introduction to AUC is given in this chapter, a more detailed description is given by Ralston, (1993) which is the source of all the equations defined below.

AUC experiments can be carried out in two modes — sedimentation equilibrium (SE) and sedimentation velocity (SV). SE experiments are carried out at lower speeds whereby the molecules reach an equilibrium distribution from which information about the molecular mass and any self-interaction that is occurring can be obtained. SV experiments are performed at higher speeds and thus the molecules eventually sediment entirely to the base of the centrifugal cell. Analysis of this sedimentation leads to the determination of the sedimentation coefficient of the molecule, which is related to its overall shape. These two modes of AUC experimentation are described in more detail in sections 4.1.1 and 4.1.2. AUC studies exploit the sedimentation of molecules that occurs when they are subjected to elevated gravitational force by rotating the sample in a rotor at high speed. The molecules in solution are acted upon by three forces that influence the behaviour of the molecules. These three forces, shown in Figure 4-1, are the sedimenting or gravitational force, F_s , the buoyant force, F_b and the frictional force, F_f .

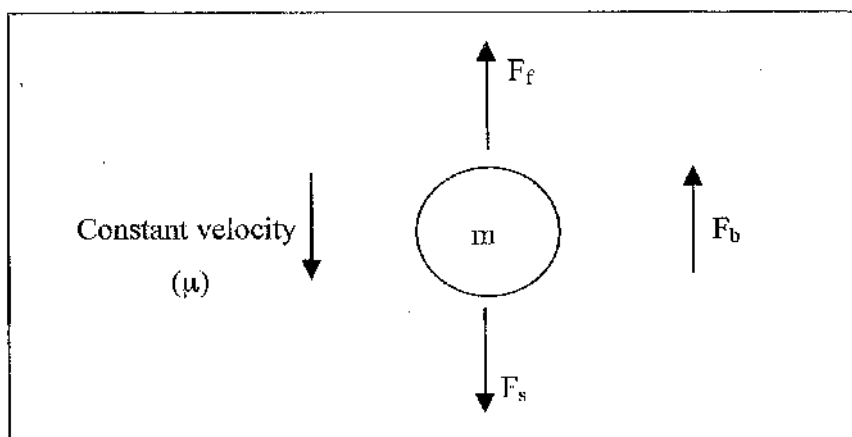


Figure 4-1: The three forces acting on a solute particle of mass m , moving with velocity μ , in a gravitational field. F_f is the frictional force acting on the particle, F_b the buoyant force and F_s the sedimenting or gravitational force.

F_s (N) is proportional to the mass and acceleration of the particle and is defined as;

$$F_s = m\omega^2 r = \frac{M}{N}\omega^2 r \quad \text{Equation 4-1}$$

where m is the mass of a single particle (g), ω is angular velocity (radians s^{-1}), r is the distance of the molecule from the centre of rotation (cm), M is the molar mass of the molecule (g mol^{-1}) and N is Avogadro's number ($6 \times 10^{23} \text{ mol}^{-1}$).

F_b (N) is related to the weight of fluid displaced by the particle and is defined as;

$$F_b = -m_o\omega^2 r \quad \text{Equation 4-2}$$

where m_o is the mass of fluid displaced by the molecule (g).

$$m_o = m\bar{v}\rho = \frac{M}{N}\bar{v}\rho \quad \text{Equation 4-3}$$

where \bar{v} is the partial specific volume, the volumetric increment produced in a solution when a unit mass of the solute is added (ml g^{-1}) and ρ is the density of the solvent (g ml^{-1}). \bar{v} can be calculated from the amino acid content of the protein (Perkins, 1986).

Provided that the density of the solute is greater than that of the solvent the particle will sediment. $F_r(N)$ is proportional to the velocity of the particle and is defined as;

$$F_f = -f\mu \quad \text{Equation 4-4}$$

where f is the frictional coefficient (g s^{-1}), dependent on the size and shape of the particle, and μ is the constant velocity with which the particle sediments (cm s^{-1}).

These three forces rapidly balance in less than 10^{-6} s as the solution reaches terminal velocity.

$$F_s + F_b + F_f = 0$$

$$\text{thus} \quad \text{Equation 4-5}$$

$$\frac{M}{N}\omega^2 r - \frac{M}{N}\bar{v}\rho\omega^2 - f\mu = 0$$

The Svedberg equation results from the equivalence in forces;

$$s = \frac{M(1 - \bar{v}\rho)}{Nf} = \frac{\mu}{\omega^2 r} \quad \text{Equation 4-6}$$

where s is the sedimentation coefficient, the velocity of the particle per unit gravitational acceleration, which usually lies within the region of $1 - 100 \times 10^{-13}$ s. Sedimentation coefficients are therefore usually expressed in Svedberg units, S, where $1 \text{ S} = 1 \times 10^{-13} \text{ s}$.

4.1.1. Sedimentation Equilibrium Analysis

Investigation of a molecule using SE analysis involves the centrifugation of a small volume of sample at lower angular velocities than are required for SV experiments. During the experiment the solute sediments, increasing the solute concentration at the cell bottom resulting in diffusion of the solute towards to the top of the cell, opposing the process of sedimentation. Eventually the two processes, sedimentation and diffusion, reach equilibrium and at this point the concentration of the solute increases exponentially towards the cell bottom and ceases to alter with time. For a single, ideal, non-associating species the mass of the solute can be determined using Equation 4-7.

$$M = \left(\frac{2RT}{(1 - \bar{v}\rho)\omega^2} \right) \left(\frac{d \ln c}{dr^2} \right) \quad \text{Equation 4-7}$$

where R is the gas constant ($8.314 \times 10^7 \text{ erg K}^{-1} \text{ mol}^{-1}$), T is the absolute temperature (K) and c is the concentration of the solute (g L^{-1}). The slope of a plot of $\ln c$ against r^2 is proportional to the mass of the solute.

SE analysis using the absorbance optics of the Optima XL-A ultracentrifuge involves the direct use of the equilibrium distribution trace of the absorbing species for determination of experimental results. As a result of this the absorbance data collected for the samples must be corrected for background absorption. This is achieved by centrifugation of the sample at speeds of greater than 40,000 rpm, following attainment of equilibrium, to sediment the sample in its entirety to the base of the centrifugal cell. Any remaining absorbance is due to absorbing species other than the molecule under study. This absorbance value is

subtracted from the equilibrium trace obtained for the molecule under investigation.

4.1.1.1. Data Analysis

Data obtained from SE experiments on ES-62 were analysed to obtain the apparent whole-cell weight-average molecular mass ($M_{w, app}$) and to examine the self-interaction of ES-62 implied by the observed elevated value of $M_{w, app}$ above the known monomer molecular mass. The ASSOC4 model programmed within the ORIGIN curve fitting software supplied with the Optima XL-A was used to carry out these analyses. $M_{w, app}$ was obtained by fitting the primary data with Equation 4-8 which describes the equilibrium distribution of a single thermodynamically ideal macromolecular solute.

$$A_r = A_o \exp[H.M(r^2 - r_o^2)] + E \quad \text{Equation 4-8}$$

where A_r is the absorbance at radial position r and A_o is the absorbance at a reference point r_o (cm); H is the constant $\omega^2(1-\bar{v}\rho)/2RT$ and E is the optical baseline offset (obtained by overspeeding of the rotor).

This model is a subset of a broader model (Equation 4-9) which was used to analyse the self-interaction of ES-62. Equation 4-9 describes a self-associating system defined by up to three association constants (Ka_2 , Ka_3 , Ka_4 in units of (absorbance)⁻⁽ⁿ⁻¹⁾) for oligomers composed of n_2 , n_3 , n_4 monomers (Kim *et al.*, 1977);

$$\begin{aligned} A_r = & \exp[\ln A_o + H.M(r^2 - r_o^2)] \\ & + \exp[n_2 \ln A_o + \ln Ka_2 + n_2.H.M(r^2 - r_o^2)] \\ & + \exp[n_3 \ln A_o + \ln Ka_3 + n_3.H.M(r^2 - r_o^2)] \\ & + \exp[n_4 \ln A_o + \ln Ka_4 + n_4.H.M(r^2 - r_o^2)] + E \end{aligned} \quad \text{Equation 4-9}$$

The accuracy of the model and the presence of non-ideality or aggregation in the sample under study can be assessed by the scatter of the residuals from the fitting of a model to the experimental data. A random distribution of points about the zero value indicates a good fit. The distribution of the residuals in a tick like pattern is indicative of aggregation in the sample while the distribution of the residuals in an arch pattern is indicative of non-ideality in the sample. The plot of $M_{w, app}$ against concentration can also yield information on self-association or non-ideality present in the system. A single ideal species is present if the molecular weight remains constant with changing concentration. A decrease in molecular weight following increasing concentration is indicative of non-ideality while an increase in molecular weight following increasing concentration is indicative of self-association (McRorie & Voelker, 1993).

4.1.2. Sedimentation Velocity Experimentation

In SV experiments the solute is placed within the cell and subjected to a high angular velocity which causes the rapid sedimentation of the solute to the cell bottom resulting in a depletion of solute at the meniscus. This results in a sharp boundary forming between the depleted meniscus and the sedimenting solute. Monitoring of the movement of this boundary, in particular the rate of movement of the midpoint, r_{bnd} , leads to the determination of the sedimentation coefficient, s , which is directly dependent on the mass of the particles and inversely on the frictional coefficient. s is defined as

$$s \equiv \frac{\mu}{\omega^2 r} = \frac{dr_{bnd} / dt}{\omega^2 r} \quad \text{Equation 4-10}$$

where t is time (s).

4.1.2.1. Data Analysis

The program SEDFIT (Schuck & Demeler, 1999) was used to obtain sedimentation coefficients from the SV experimental data for ES-62. These sedimentation coefficients ($s_{t,b}$) are for ES-62 in PBS pH 7.4 at 4 °C. Sedimentation coefficients are influenced by the density and viscosity of the buffer and thus in order to allow comparison of sedimentation coefficients from samples in different buffers at different temperatures, sedimentation coefficients are always converted (using Equation 4-11) to those that would be measured in water at 20 °C.

$$s_{20,w} = s_{T,b} \frac{(1 - \bar{v}\rho)_{20,w}}{(1 - \bar{v}\rho)_{T,b}} \cdot \frac{\eta_{T,b}}{\eta_{20,w}} \quad \text{Equation 4-11}$$

The subscripts $_{20,w}$ and $_{T,b}$ refer to water at 20 °C and buffer at T °C respectively.

4.1.3. The Analytical Ultracentrifuge

A Beckman Optima XL-A AUC (Palo Alto, California) was employed for the studies described in this thesis. This centrifuge employs absorbance optics to measure the concentration distribution of the molecules within the centrifugal cell. This method of detection has increased sensitivity over other detection methods, such as schlieren and Rayleigh interference optics, and exhibits high reproducibility, the ability to scan at a wide range of wavelengths and the ability to perform baseline scans. Wavelengths from 190 to 800 nm can be employed and are emitted from a xenon flash lamp as the selected sector of the rotor passes between the light source and the detector (situated under the floor of the centrifugal chamber). A schematic diagram of this optical system is shown in Figure 4-3 while Figure 4-2 shows a typical plot of absorbance against radius obtained from the AUC. The rotor used for the AUC studies was a four hole An60Ti rotor. This rotor is capable of rotating at speeds up to 60k rpm (60,000 rpm) and is spun in a vacuum to minimise aerodynamic turbulence and frictional heating. It can accommodate three sample cells and one counterbalance reference cell required for the calibration of radial distance.

AUC cells are typically constructed of a centrepiece made of reinforced epoxy or aluminium alloy sandwiched between two thick windows of optical grade quartz or sapphire all contained within an aluminium cell housing as shown in Figure 4-4. The centrepiece consists of two or six sector shaped compartments in which the samples and reference buffers are placed. Schematic diagrams of these centrepieces can be seen in Figure 4-5. The compartments are sector shaped to avoid the convective disturbance which would result from sedimenting particles colliding with the walls of the compartments were they parallel. In SE experiments the column length, the distance from the meniscus to the cell base, is typically 1 – 3 mm, while in SV experiments the column length is typically 12 mm. The differences in column length are due to the time taken to reach equilibrium; equilibrium is reached more rapidly in shorter columns as can be seen from Equation 4-12 (van Holde & Baldwin, 1958).

$$t_{0.1} = \frac{0.7(r_b - r_m)^2}{D} \quad \text{Equation 4-12}$$

where $t_{0.1}$ is the time taken to reach equilibrium to within 0.1%, $r_b - r_m$ is the column height, the distance from the meniscus to the base of the AUC cell (cm) and the diffusion constant D (cm^2s^{-1}) is $\sim 2.7 \times 10^{-5}/(M \gamma)^{1/3}$.

In SV experiments, equilibrium is not the aim thus time is not a constraining factor. In SV experiments the sample is sedimented to the cell base and this sedimentation monitored. A longer column length allows for the monitoring of sedimentation over a longer time period and hence greater accuracy in the analysis of the experimental data.

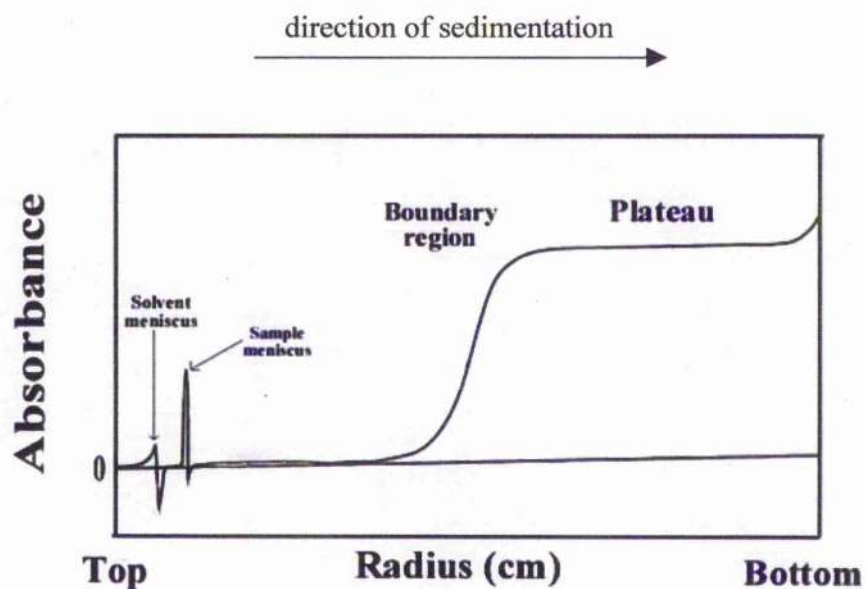


Figure 4-2: A typical plot of absorbance against radius obtained from measurement of distribution of molecules within an AUC cell (taken from Ralston, (1993)).

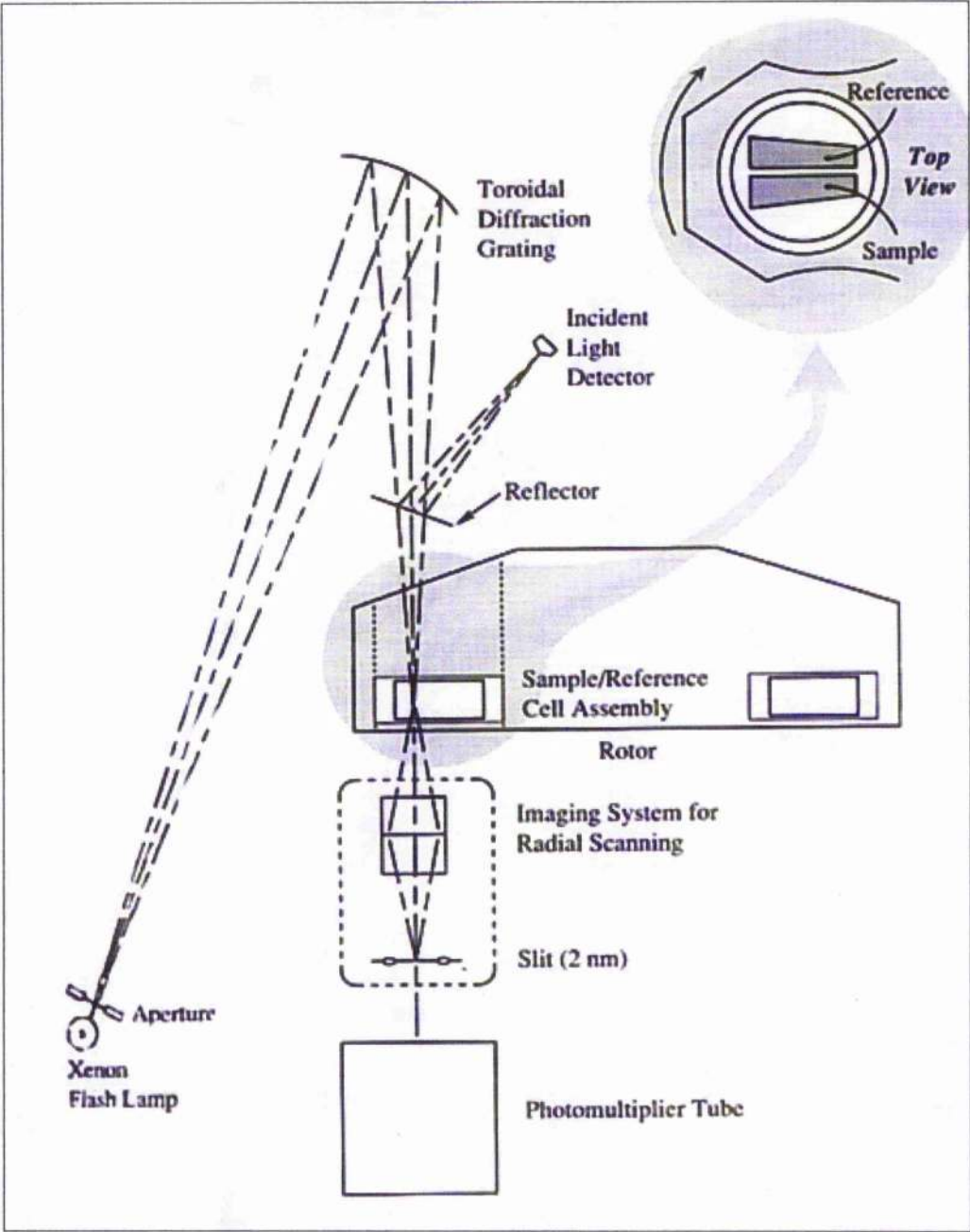


Figure 4-3: Schematic diagram of the optical system of the Beckman Optima XL-A analytical ultracentrifuge (taken from Ralston, (1993)).

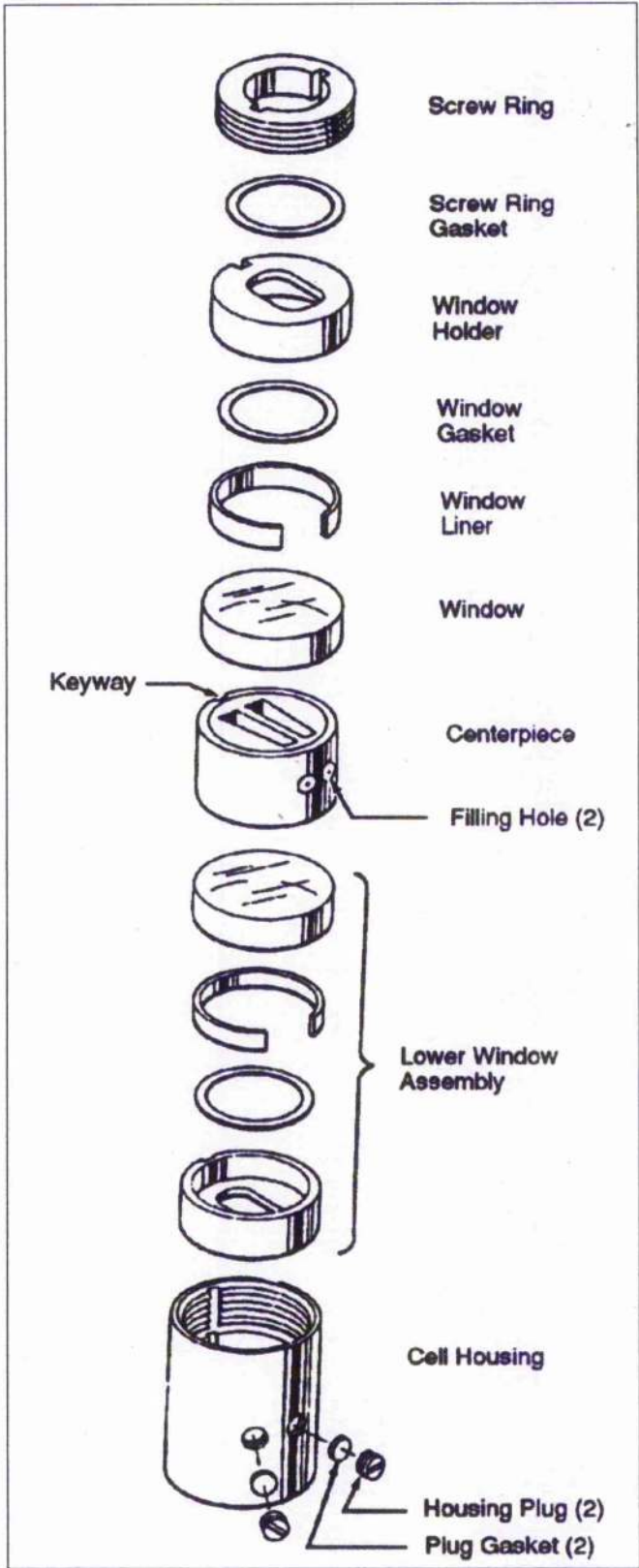


Figure 4-4: Exploded view of an analytical ultracentrifugation cell, taken from the XLA manual (Beckman Instruments, 1992).

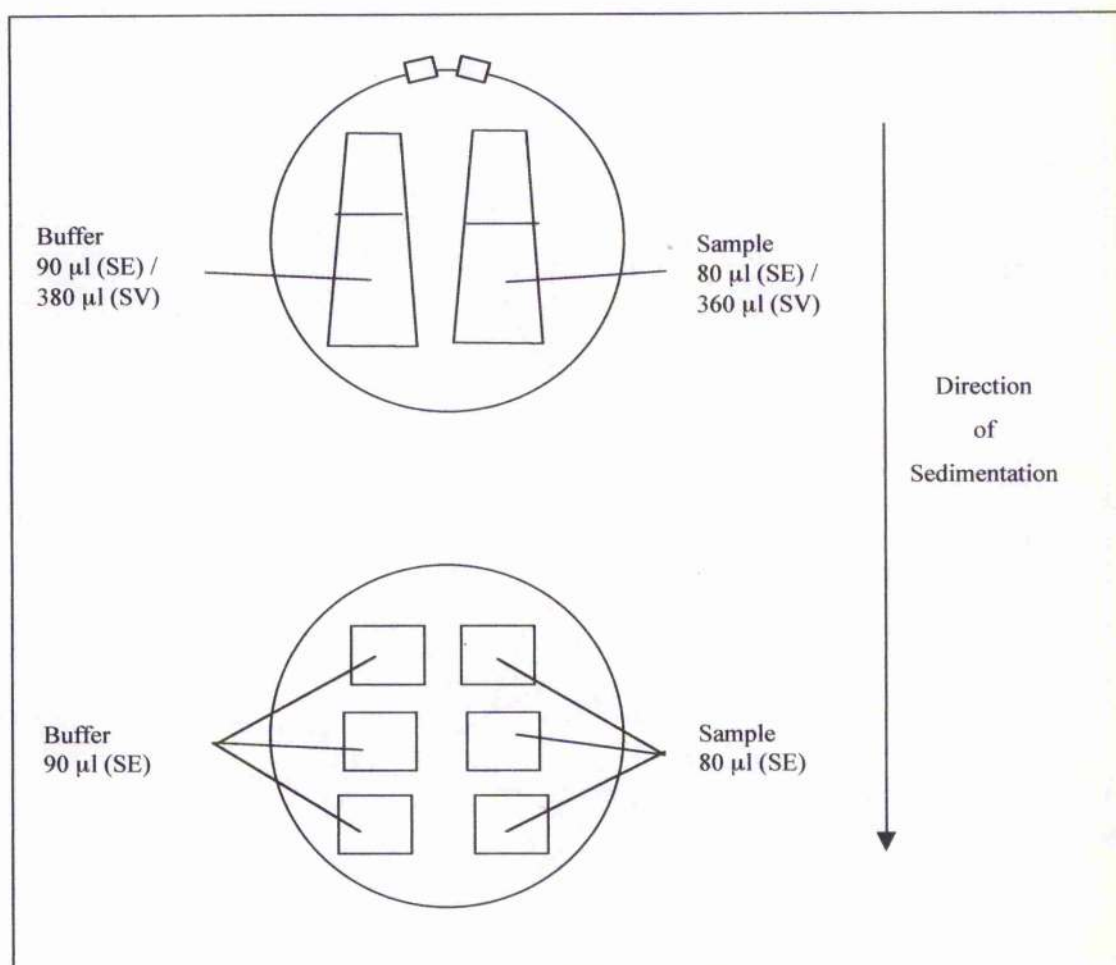


Figure 4-5: Cross-sections of two and six channel centrepieces. Two channel centrepieces can be used for SE or SV runs, the volume of the sample and buffer used varies depending on the type of run. Six channel centrepieces are generally used only for SE runs.

4.1.4. Analytical Ultracentrifugation of ES-62

For SE experiments, six channel centrepieces were employed. Cells were assembled as shown in Figure 4-4 and tightened to 120 lb inch⁻². The gaskets and screws were then inserted to fasten the lower window assembly and centrepiece into position allowing the cell to be loosened and the top window to be removed. 80 μ l of sample was then loaded into the right-hand wells and 90 μ l of buffer into the left-hand wells as shown in Figure 4-5. The top window was then replaced

and the whole cell retightened to 120 lb inch⁻². Nine samples of wild type ES-62 in PBS pH 7.4 at concentrations of between 0.9 and 5.2 μ M were loaded into six-channel Yphantis-type centrepieces (Yphantis, 1964) in this manner. The cells were then balanced to within 0.1 g and placed into the rotor. The cells were next aligned carefully to ensure that the widest part of the sample/buffer segment was furthest from the centre of the rotor and that the walls of the segment followed a radial path. The rotor was placed into the AUC and the monochromator locked into place. An initial run at a rotor speed of 3 k rpm was performed to check for leaks or cracked windows. The rotor speed was then increased to an appropriate speed for the sample being analysed and radial scans set up. The rotor speed chosen for SE experiments depends on the molecular weight of the sample. The graph shown in Figure 4-6 was used to select the speeds at which the sample should be spun. For ES-62 the estimated molecular weight is 57.8 kDa for the monomer and 231.2 kDa (4 x 57.8 kDa) for the tetramer thus the samples were spun at both 8 and 10 k rpm. The experiments were performed at 4 °C. The optics were programmed to scan from 5.8 to 7.2 cm with a step size of 0.001 cm and 10 averages. Equilibrium was seen to be established when a perfect overlay of two scans acquired three hours apart was achieved. Once equilibrium was established at the various appropriate speeds and the data collected, the rotor was oversped to 40 k rpm to sediment all the sample to the base of the cell and thus allow measurement of the optical baseline. This measurement allows any window imperfections or optical abnormalities to be taken into account during data analysis.

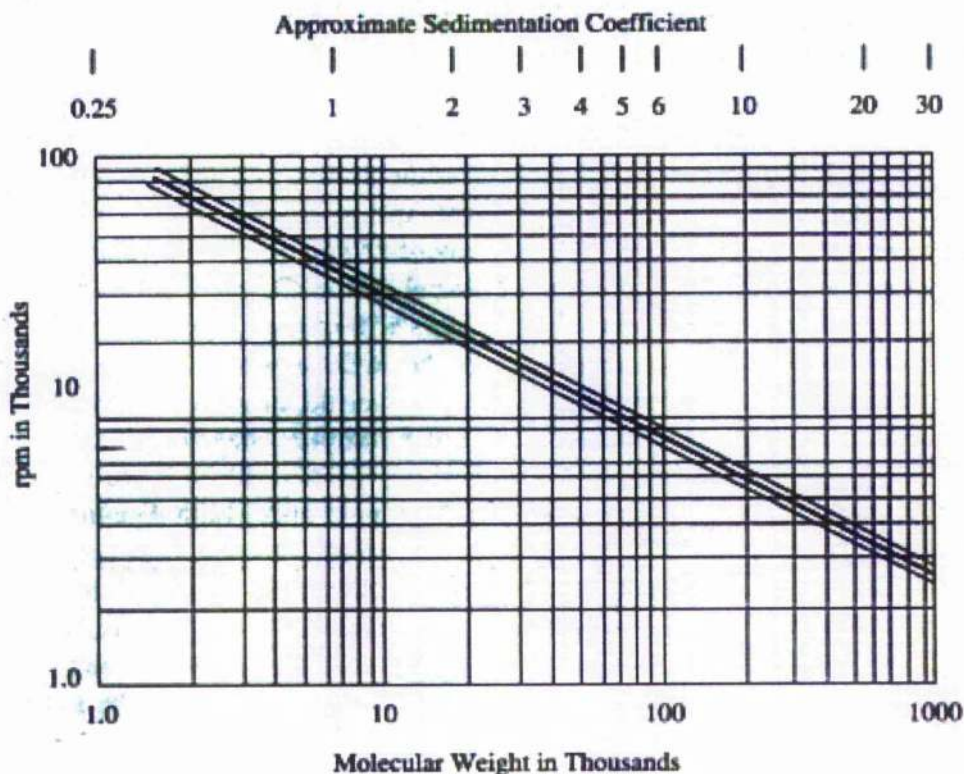


Figure 4-6: Optimum speeds for SE runs can be estimated if either the molecular weight or sedimentation coefficient is known (taken from McRorie & Voelker, (1993)).

For SV experiments double sector cells were used. It is not possible to use six channel cells for SV experiments, as the volume that they hold is too small to allow good traces to be obtained. The double sector cells were assembled as shown in Figure 4-4 and tightened to 120 lb inch^{-2} . $360 \mu\text{l}$ of sample was loaded into the right-hand chamber and $380 \mu\text{l}$ of buffer into the left-hand chamber through the two holes in the housing and centrepiece using a Hamilton (Reno, Nevada) syringe. The holes were then covered with gaskets and screws. Samples of wild type ES-62 in PBS (5.5 mM potassium chloride, 145 mM sodium chloride, 8 mM disodium hydrogen orthophosphate, 1.5 mM sodium dihydrogen orthophosphate) pH 7.4 at four concentrations between 1.7 and $6.9 \mu\text{M}$ were loaded into the double sector centrepieces. The cells were then balanced, inserted

into the rotor and the rotor and monochromator placed into the ultracentrifuge as described above. Experiments were performed at 4 °C. An initial scan was carried out at a rotor speed of 3 k rpm to check for leaks or cracked windows and then the rotor speed increased to 30 k rpm and scans programmed. Scans of the solute distribution were acquired for radial positions from 6.0 to 7.2 cm at a step size of 0.002 cm with 1 average. The scans were performed every 15 minutes until 32 scans had been collected.

The partial specific volume of ES-62 (0.73 ml g^{-1}) was calculated from the partial specific volumes of the constituent amino acids and carbohydrates (Perkins, 1986) using the program VBAR (Cohn & Edsall, 1943; Perkins, 1986) and the buffer density at 4 °C was calculated using the program SEDNTERP (Laue *et al.*, 1992).

4.1.5. Results and Discussion

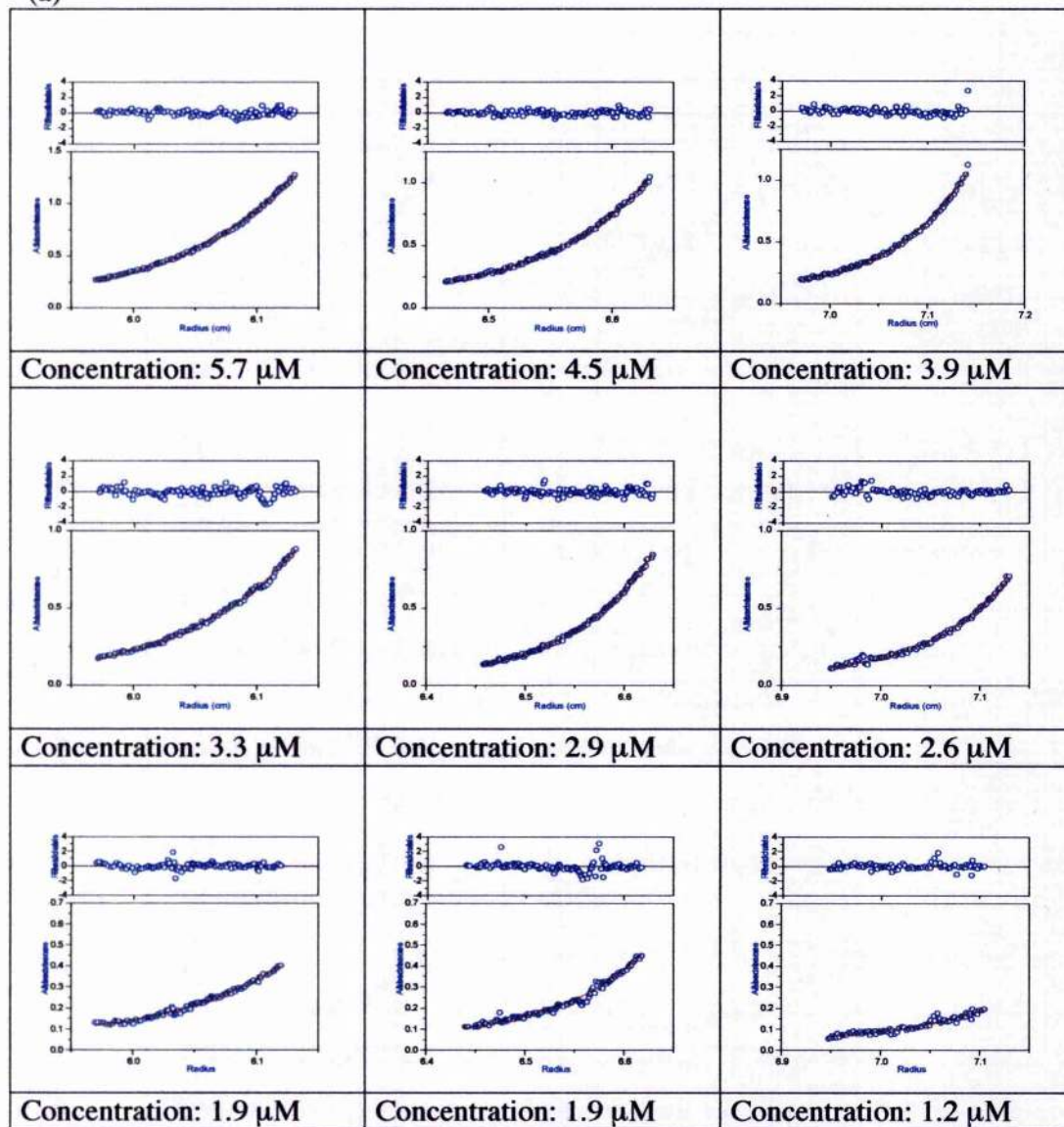
4.1.5.1. Sedimentation Equilibrium

SE data for ES-62 were analysed using the ASSOC4 model as described in section 4.1.1.1. Fitting of the primary data with Equation 4-8 gave good fits for all the samples as can be seen in Figure 4-7. The $M_{w,app}$ values obtained are plotted in Figure 4-8 as a function of concentration at both 8 and 10 k rpm.

These data show that the mass measured greatly exceeds the monomeric mass of ES-62 (57.8 kDa, calculated from the known amino acid, carbohydrate and phosphorylcholine content) and is close to the calculated tetrameric mass of ES-62 (231.2 kDa). This increased mass indicates the presence of oligomers or high molecular weight aggregates. $M_{w,app}$ does not change significantly with the change in rotor speed and in particular does not decrease at higher rotor speeds which would indicate the presence of aggregate. This indicates that the increase in mass, above that of monomer, is due to self-association.

In order to ascertain the stoichiometry and strength of this interaction, the data were fitted with Equation 4-9. Fits were attempted with two plausible models; monomer-tetramer and dimer-tetramer. In the dimer-tetramer model, the association constant, K_{a2-4} , was fitted by setting the monomeric mass at twice the actual monomer mass (i.e. dimer mass) and then fitting a monomer-dimer model to the data. The fits obtained for each data set are shown in Figure 4-9. The monomer-tetramer model and dimer-tetramer model both gave good fits to the data. This indicates that the majority of the ES-62 sample is tetrameric with only a very small proportion of monomer or dimer. As the amount of monomer or dimer is minute it is very difficult to determine in which of these two states it exists. It would perhaps be possible to determine the state of this small proportion of ES-62 by carrying out a number of SE experiments with increasingly dilute samples but as the concentration decreases the data become increasingly difficult to analyse due to the small differential between the sample absorbance and the background absorbance.

(a)



(b)

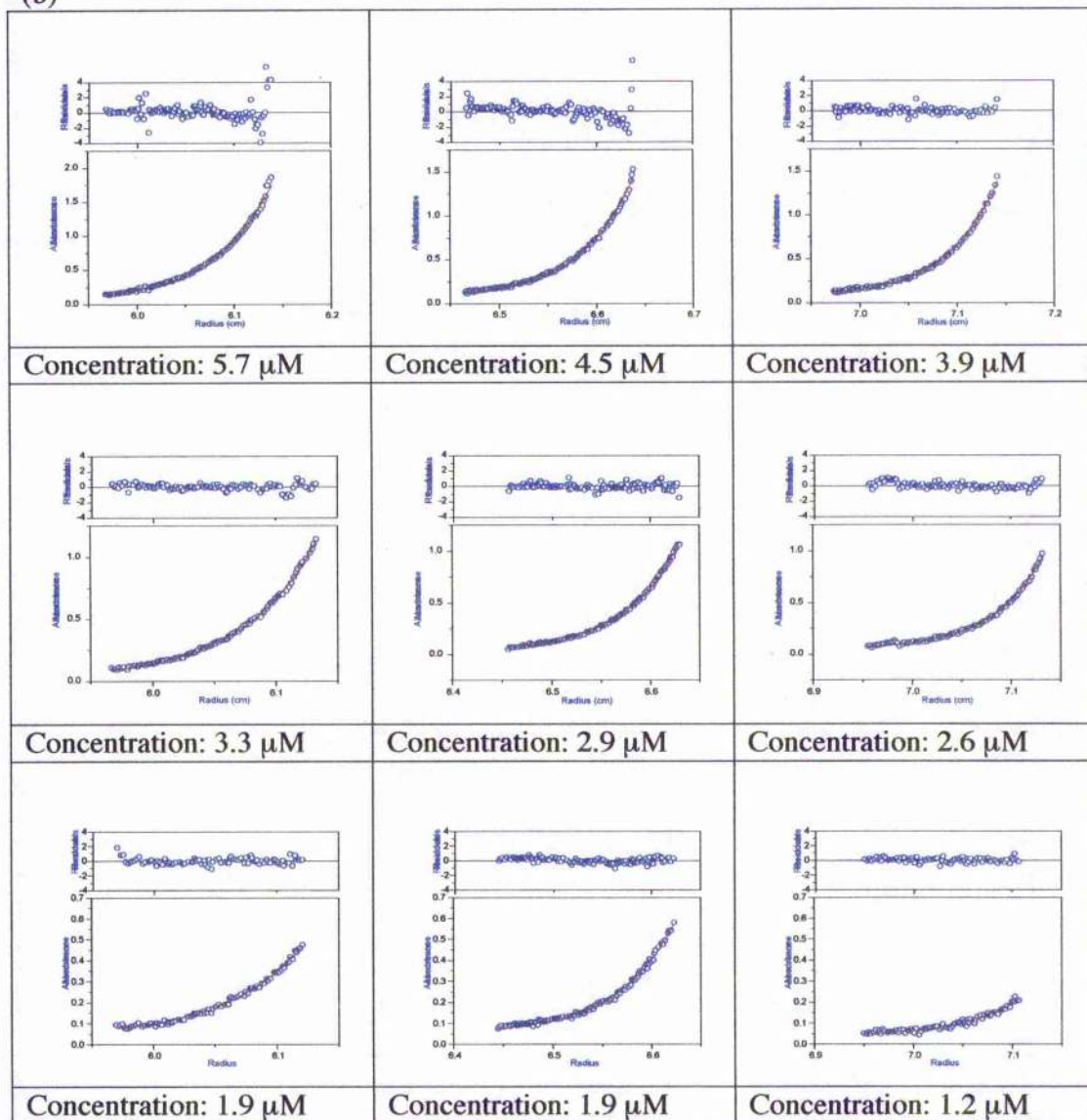


Figure 4-7: SE data for ES-62 fitted with Equation 4-7 (describing a single thermodynamically ideal species). (a) fits obtained for the 8 k rpm data; (b) fits obtained for the 10 k rpm data. The blue circles show the data points while the red line shows the model fitted. The residuals of the fit are shown above the raw fitted data.

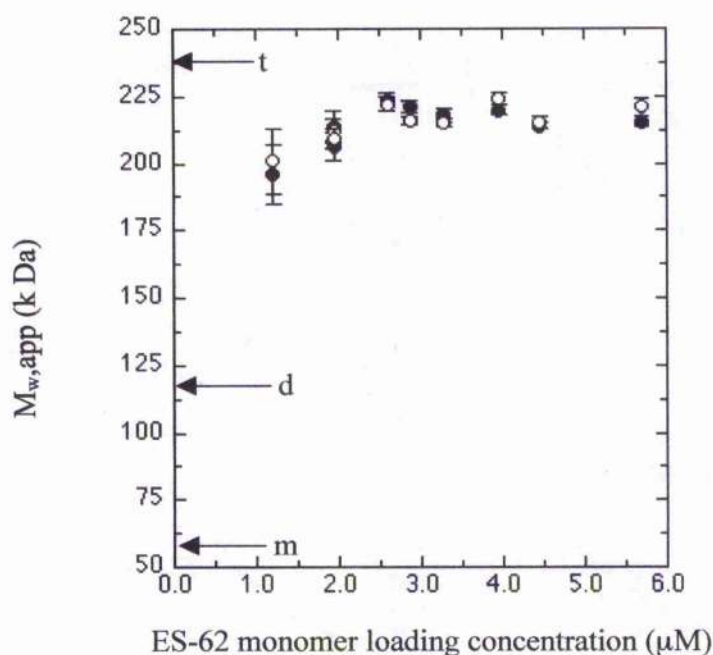
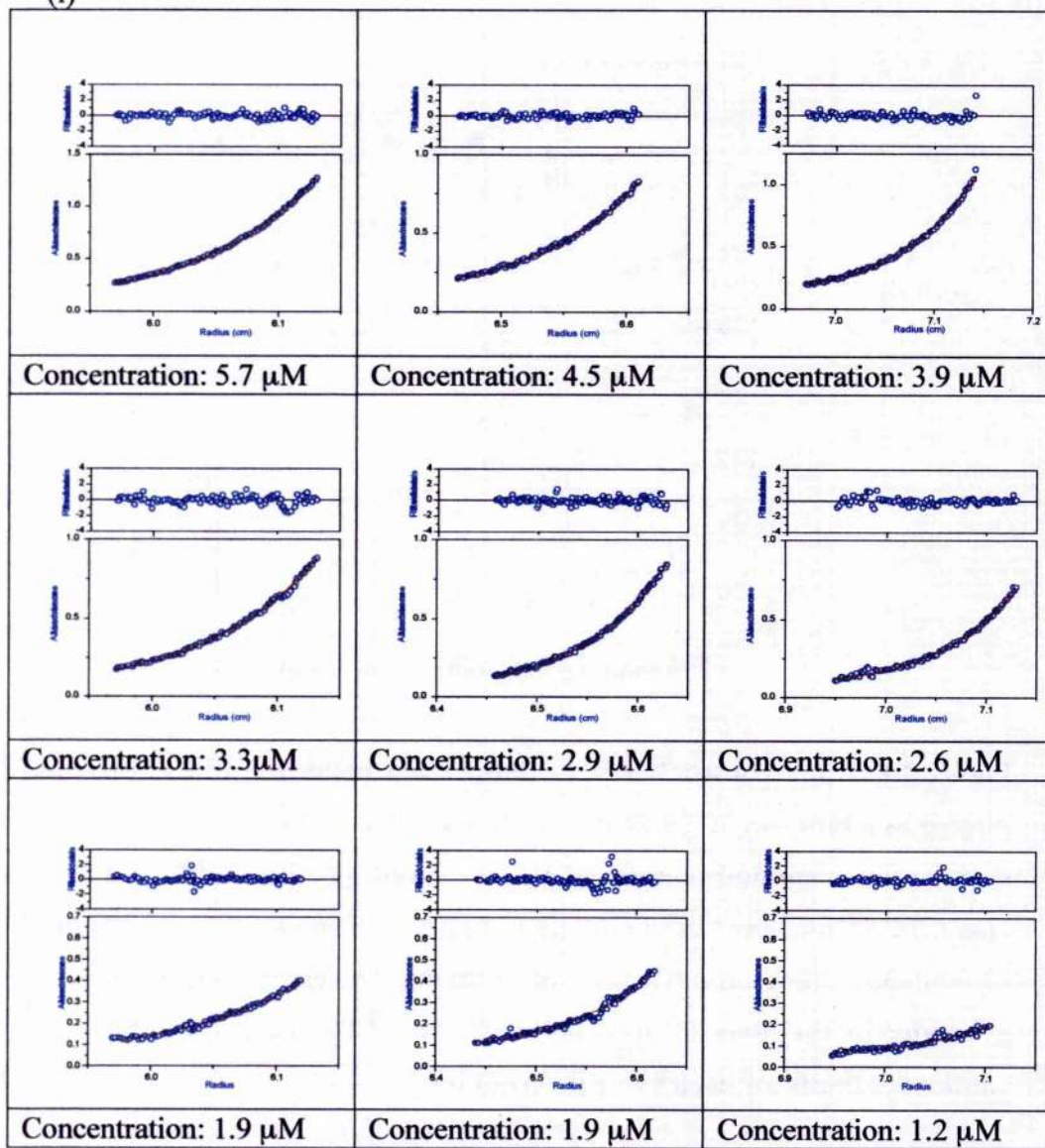


Figure 4-8: Apparent whole-cell weight-average molecular weight ($M_{w, app}$) plotted as a function of ES-62 monomer loading concentration from sedimentation equilibria obtained at rotor speeds of 8 k rpm (●) and 10 k rpm (○). Arrows annotated m; d and t indicate the molecular weights of ES-62 monomer, dimer and tetramer respectively. The errors marked are generated by the curve fitting software Origin and represent the 95 % confidence limits for each value determined.

(i)



(ii)

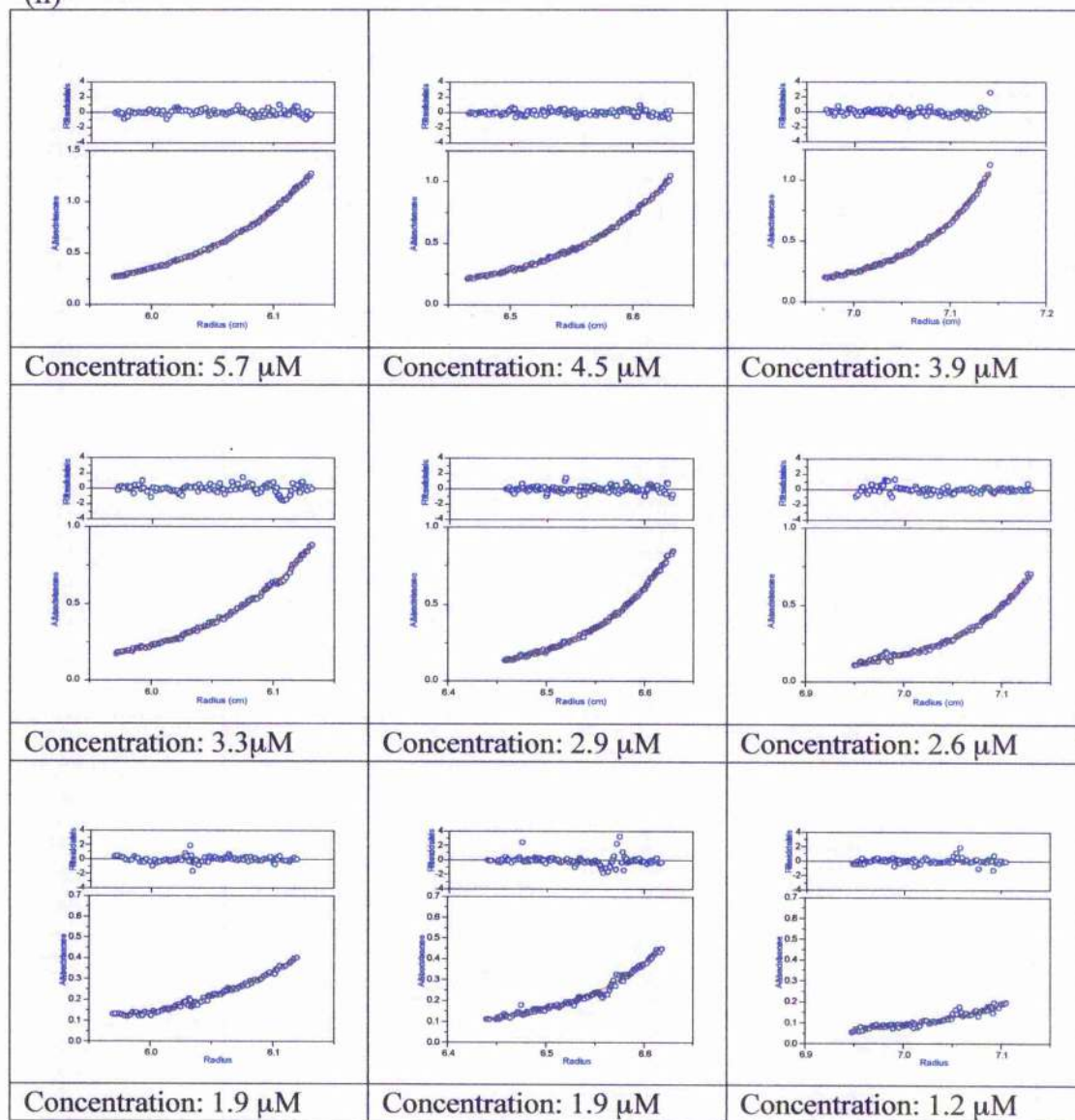
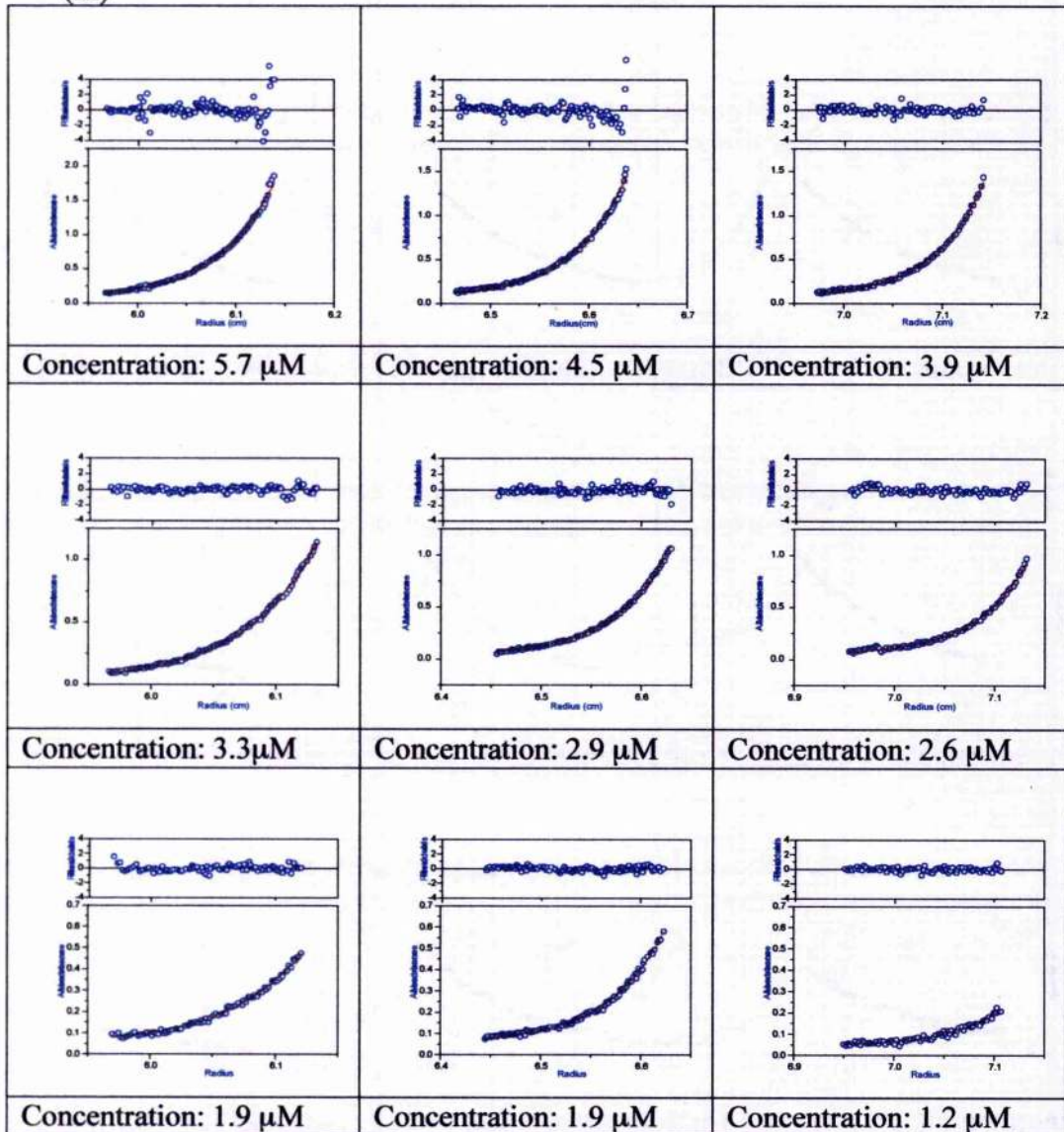


Figure 4-9 (a) Fits of the (i) dimer-tetramer and (ii) monomer-tetramer model to the 8 k rpm SE primary data. The blue circles show the data points while the red line shows the model fitted. The residuals of the fit are shown above the raw fitted data.

(iii)



(iv)

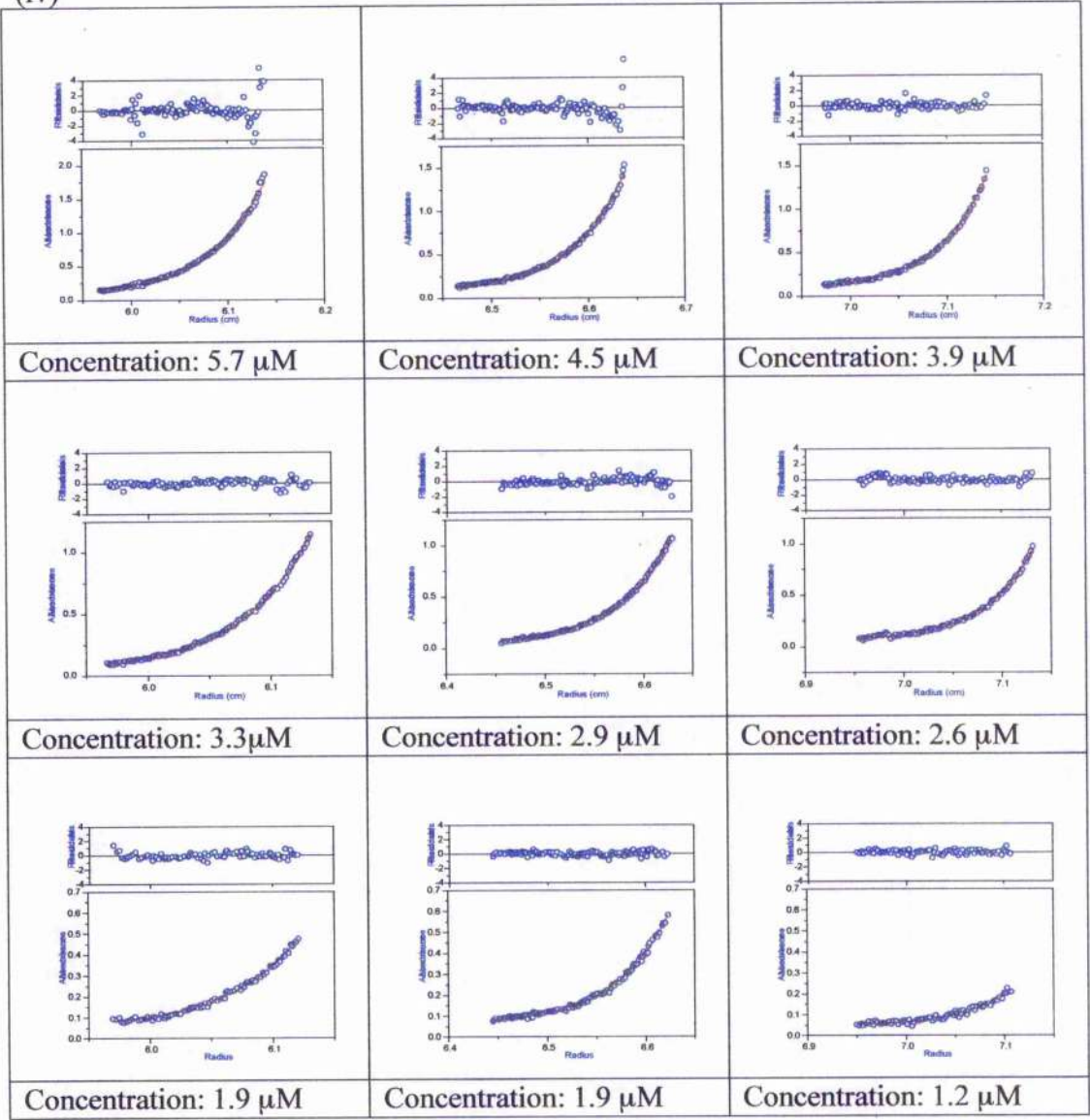


Figure 4-9 (b): Fits of the (iii) dimer-tetramer and (iv) monomer-tetramer model to the 10 krpm SE primary data. The blue circles show the data points and the red line shows the model fitted. The residuals of the fit are shown above the raw fitted data.

The K_a values obtained from the fits to each of the sedimentation equilibrium data sets were converted first to units of $M^{-(n-1)}$ and then to dissociation constant (K_d) values. The conversion to $M^{-(n-1)}$ units was achieved using Equation 4-13;

$$K_{a_{cu}} = K_{a_{au}} \frac{\epsilon l}{2} \quad \text{Equation 4-13}$$

where $K_{a_{cu}}$ is the association constant in units of $M^{-(n-1)}$, $K_{a_{au}}$ is the association constant in units of absorbance⁻¹, ϵ is the extinction coefficient ($\text{cm}^{-1} M^{-1}$) and l is the pathlength of the AUC cell centrepiece (1.2 cm).

The conversion to dissociation constants was achieved using Equation 4-14 where K_d is the dissociation constant ($M^{(n-1)}$).

$$K_d = \frac{1}{K_{a_{cu}}} \quad \text{Equation 4-14}$$

The K_d values determined at both 8 k and 10 k rpm are plotted as a function of concentration in Figure 4-10. The infinite dilution dissociation constant of 50 nM for the dimer-tetramer model and 0.04 nM³ for the monomer-tetramer model indicates a strong association between ES-62 molecules to form tetramers. Thus, at concentrations used in all biophysical studies, the majority of ES-62 is tetrameric. This result supports earlier gel filtration studies on wild type ES-62 (Harnett *et al.*, 1993) which suggested that ES-62 is tetrameric. The modelling of ES-62 as a mainly tetrameric system is of further interest as ES-62 has been shown to possess aminopeptidase activity (Harnett *et al.*, 1999a) and the biologically active forms of many aminopeptidases are dimeric or tetrameric (Acosta *et al.*, 1998; Taylor, 1993).

Figure 4-10: Dissociation constant (K_d) obtained from fitting (a) a dimer-tetramer model and (b) a monomer-tetramer model to each of the SE primary data sets plotted as a function of ES-62 monomer loading concentration and rotor speed (8 k rpm (●); 10 k rpm (○)). The errors marked are generated by the curve fitting software Origin and represent the 95 % confidence limits for each value determined.

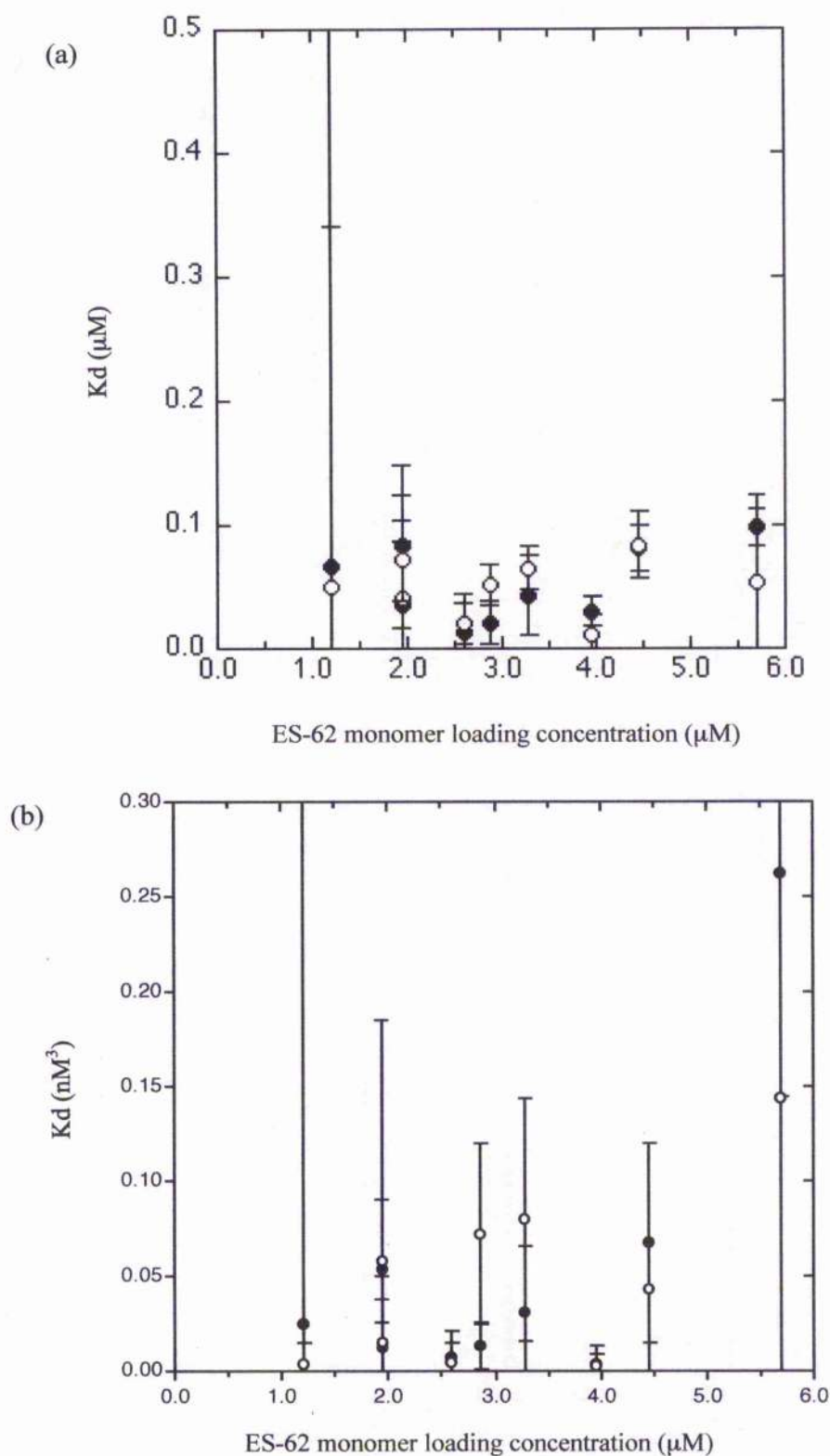


Figure 4-10: Dissociation constant (K_d) obtained from fitting (a) a dimer-tetramer model and (b) a monomer-tetramer model.

4.1.5.2. Sedimentation Velocity

SV data for ES-62 were analysed using the program SEDFIT. The sedimentation coefficients generated from the data were converted to those that would be measured in water at 20 °C as described in section 4.1.2.1. Converted sedimentation coefficients of approximately 10 S were obtained for each of the ES-62 samples. These sedimentation coefficients are plotted as a function of concentration in Figure 4-11. The infinite dilution sedimentation coefficient obtained by extrapolation of these data to zero concentration is 9.85 S.

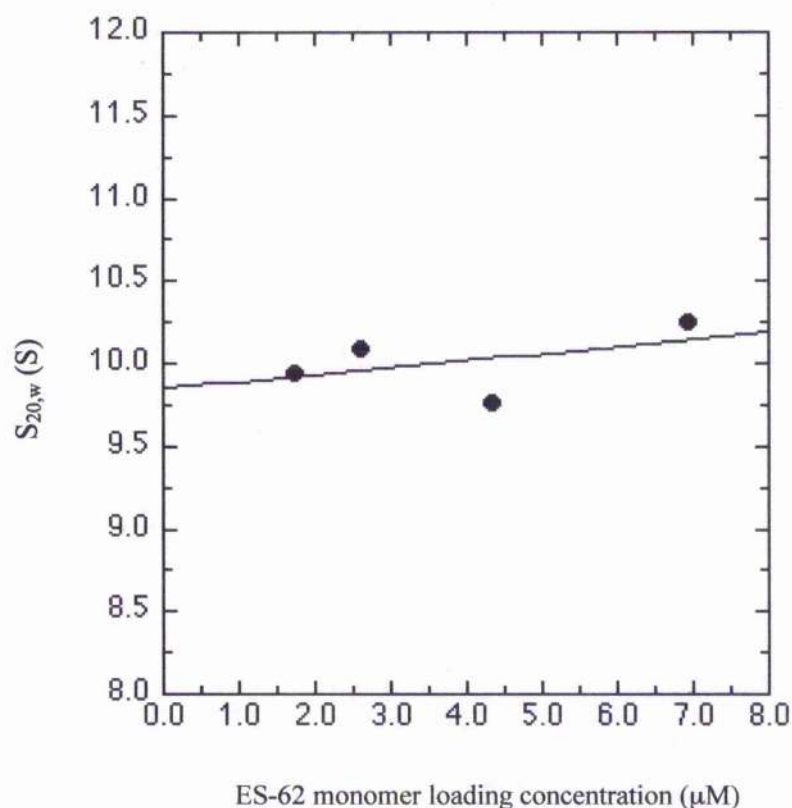


Figure 4-11: Sedimentation coefficient as a function of ES-62 monomer loading concentration.

The most compact shape for a particle is a sphere. A sphere with the same mass as monomeric ES-62, hydrated with 0.4 g water / g protein (a typical protein hydration (Squire & Himmel, 1979)) would have a sedimentation coefficient of 4.6 S, while a sphere with the same mass as tetrameric ES-62, similarly hydrated, would have a sedimentation coefficient of 11.7 S. The experimental sedimentation coefficient obtained is larger than that predicted for the spherical hydrated monomer and smaller than that calculated for the spherical hydrated tetramer. This confirms that ES-62 is likely to be a tetramer and suggests that it is either normally hydrated and slightly elongated in shape or highly hydrated and almost spherical.

4.2. *Small Angle X-Ray Scattering*

Small angle X-ray scattering (SAXS) of a protein in solution allows information about the elongation and shape of the protein to be obtained. This information can be used to generate a structural model of the protein. A more recent development, in the form of three computer programs, allows *ab initio* low resolution structure determination of the protein. This development is important as a homologous structure is no longer essential in order to obtain a structural model of the protein of interest. The information gained from these programs could also be used to solve the phase problem if X-ray crystallography was employed to generate a high resolution structure. The benefit of using SAXS, where the protein is in solution, is that the structural information obtained is for the protein in its native state rather than in a crystal. However, the resolution of the structural information is an order of magnitude less than that obtained from X-ray crystallography.

X-rays or neutrons are employed in small angle scattering. In this PhD only SAXS was carried out. X-rays are used for small angle scattering experiments as they have a wavelength of 0.15 nm which is smaller than the size of an atom. Scattering occurs in two forms; elastic and inelastic. In SAXS it is only elastic scattering that is measured. In a SAXS experiment a beam of X-rays is scattered from a protein solution. The electrons in the atoms that make up the proteins absorb the energy provided by the X-rays and then re-emit the same amount of energy in a different direction. The scattering event involves interference from waves of energy emanating from 2 separate points. Elastic scattering, where the energy is unchanged, occurs in two forms; intramolecular i.e. where interference arises due to waves of energy emanating from 2 points within the particle and intermolecular i.e. where interference arises due to waves of energy emanating from 2 points within different particles. In order to obtain structural information about a molecule it is only intramolecular scattering that is important. In intramolecular scattering interference can occur between X-rays emerging from atoms close together or far apart within the particle. The interference arising from atoms far apart in the molecule gives information about the elongation of

the molecule while that arising from atoms close together provides information about the shape of the molecule. As the protein molecules are in solution they are subject to Brownian motion and thus adopt all possible orientations, unlike the case for crystallography where all the molecules are in the same orientation. Thus the structural information obtained from SAXS is an average of all possible orientations.

The flexible carbohydrate chains on ES-62 coupled to restrictions on the amount of wild type ES-62 available meant that the determination of a high resolution structure for ES-62 by X-ray crystallography would be a difficult task. SAXS was employed as it was a method by which structural information pertaining to ES-62 could be obtained which would be physiological due to the sample being in solution rather than as a crystal. New developments have also led to *ab initio* low resolution structure determination from small angle scattering data provided the data are of sufficiently high quality. The structure determination programmes that form the basis for this new technology are continually being developed increasing the accuracy and resolution of the models obtained.

4.2.1. Scattering Theory

A number of reviews have been published describing the theory behind SAXS (Perkins, 1988a; Perkins, 1988b). This section gives only a brief overview of the theory; all equations quoted were obtained from Perkins (1988a) and Perkins (1988b) or the references cited therein.

In SAXS the intensity of the scattering curve of a molecule is measured as a function of the scattering angle or the scattering vector, Q . The information gathered at small Q values, from atoms far apart in the molecules, leads to the determination of the radius of gyration (R_g , a measure of macromolecular elongation) while that collected at large Q values, from atoms close together in the molecule, gives more detailed shape information. A typical solution scattering curve is shown in Figure 4-12.

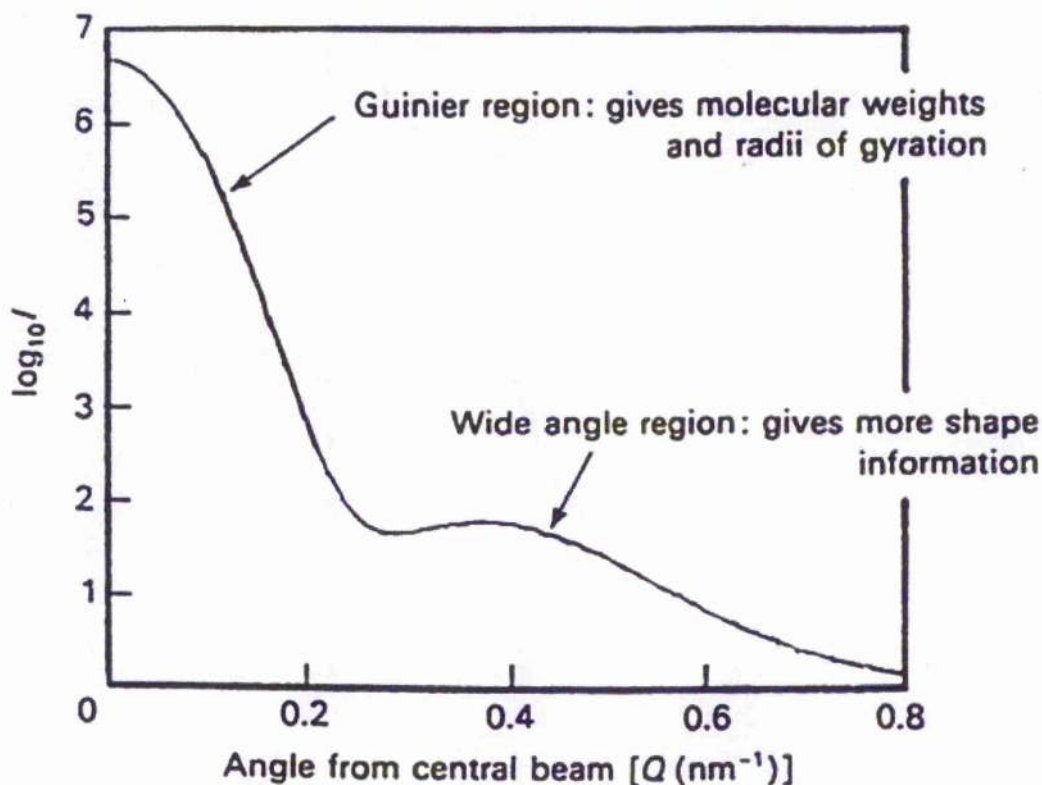


Figure 4-12: A typical solution scattering curve. The Guinier region shows data obtained from scattering arising from interference between atoms far apart in the particle while the wide angle region shows data obtained from scattering arising from interference between atoms close together in the particle. [Image taken from Perkins (1988a)].

The relationship between the wavelength of radiation (λ , nm), the separation of the scattering entities (d , nm) and the angle of diffraction (θ) is defined by Bragg's law;

$$\lambda = 2d \sin \theta$$

Equation 4-15

The scattering vector, Q , is often used in place of the scattering angle. Q is defined as

$$Q = 4\pi \sin \theta / \lambda \quad \text{Equation 4-16}$$

The resolution of the data collected is $2\pi/Q_{\max}$ where Q_{\max} is the largest scattering vector (smallest atomic distance) measured.

The two important elements of solution scattering are the scattering properties of the molecule being studied and the spatial orientation of individual elements that scatter within the molecule. When the scattering angle, 2θ (some X-ray workers replace 2θ with Q where $2\theta = Q\lambda/2\pi$ assuming $\sin 2\theta = 2\theta$) is zero the intensity is at a maximum and is a direct measure of molecular mass. When 2θ (or Q) is not equal to zero the scattering intensity is described by the Debye equation:

$$I(Q) = \sum_p \sum_q f_p f_q \frac{\sin(rQ)}{rQ} \quad \text{Equation 4-17}$$

where f_p and f_q are the scattering lengths of the electrons at points P and Q in the molecule and r corresponds to the distance between P and Q.

The scattering density, $p(r)$, is the probability that two scattering elements are separated by a distance r in the particle and is employed by the SAS data analysis program GNOM (Semenyuk & Svergun, 1991). The value for $p(r)$ is plotted as a function of r showing the probability distribution of the distances between scattering elements within a particle. This allows the determination of a value for D_{\max} , the maximum dimension within a molecule.

4.2.2. Synchrotron Radiation

Synchrotron radiation is released when high energy electrons are accelerated. The energy released by the electrons covers the whole spectral range from microwaves to hard X-rays (1-100 keV). Monochromators, which allow the selection of a particular energy range, are employed to obtain an X-ray source. A diagrammatic representation of a synchrotron source is shown in Figure 4-13. In order to alter the direction of the high energy electrons, and thus cause acceleration, strong magnets are employed that deflect the electron beam such that it maintains an orbit within the synchrotron ring.

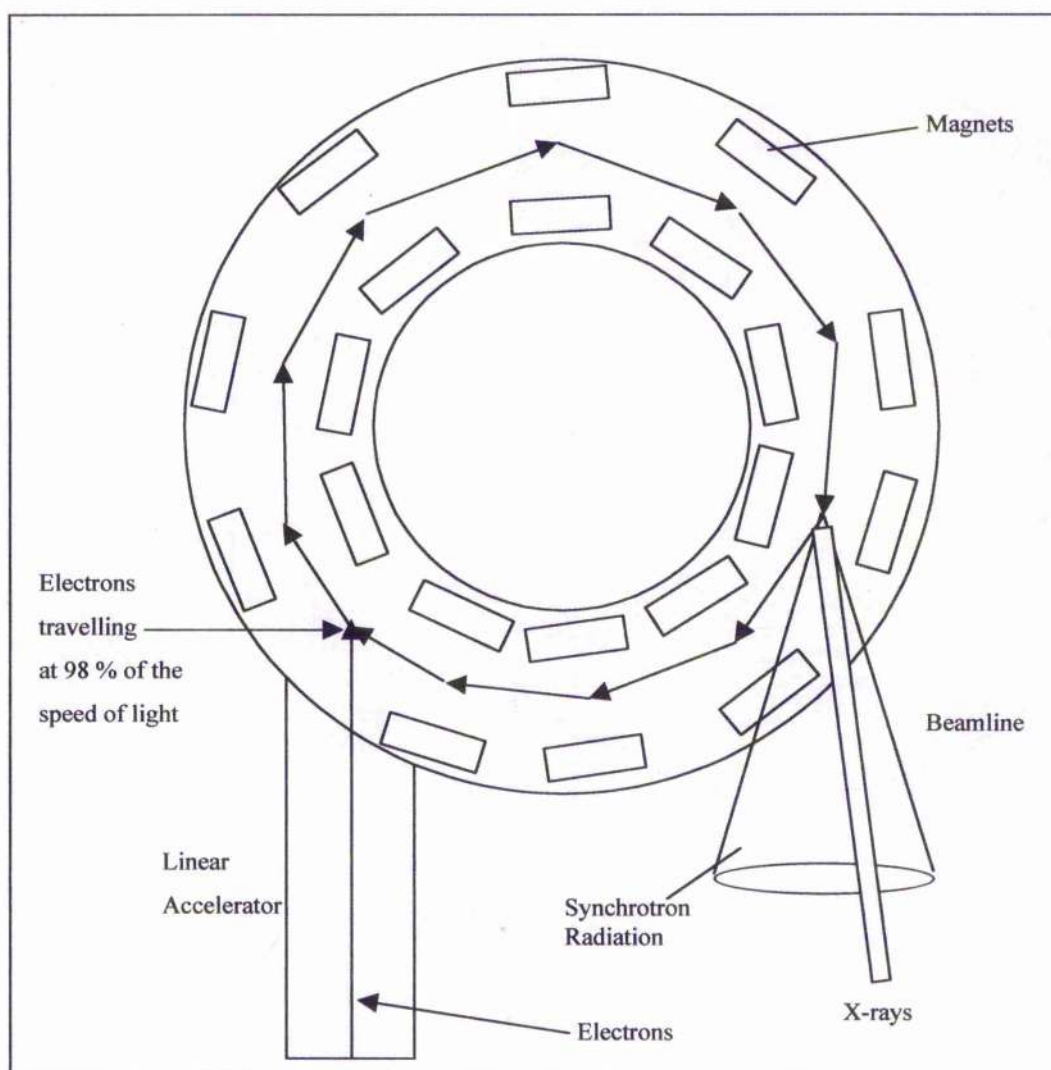


Figure 4-13: Diagrammatic representation of a synchrotron radiation source.

4.2.3. Detector and Camera

The detector used for the SAXS experiments was a quadrant multiwire proportional chamber with delay line readout. A diagrammatic representation of the camera setup is shown in Figure 4-14. Camera lengths of 3.4 and 1.9 m were used.

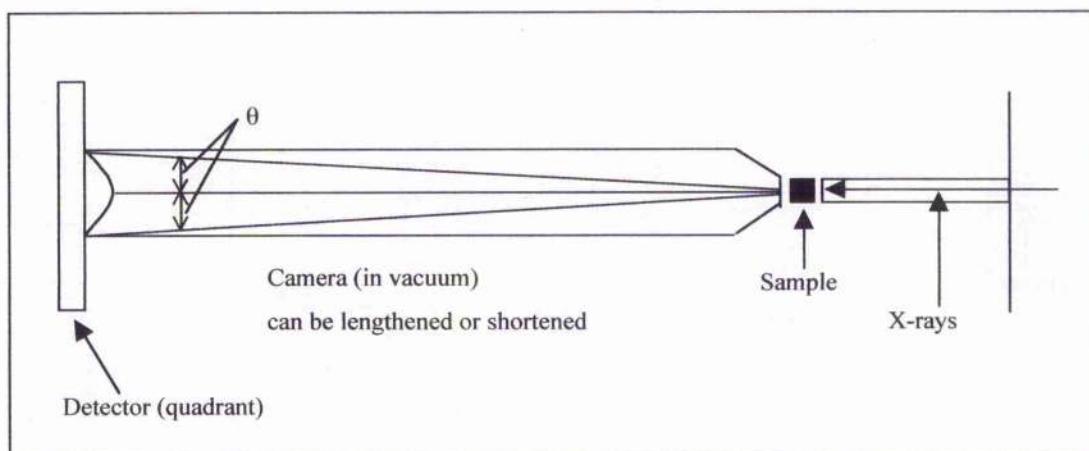


Figure 4-14: Diagrammatic representation of the camera setup for SAXS experimentation.

4.2.4. Data Analysis

SAXS data were collected at EMBL station X33 on the storage ring DORIS III of the Deutsches Elektronen Synchrotron (DESY) for samples of ES-62 in PBS (5.5 mM potassium chloride, 145 mM sodium chloride, 8 mM disodium hydrogen orthophosphate, 1.5 mM sodium dihydrogen orthophosphate) pH 7.4 at concentrations of between 8.00 and 0.25 mg ml⁻¹. The reference solvent was PBS pH 7.4. The sample-detector distances were 3.4 and 1.9 m, covering the ranges of momentum transfer of $0.13 \text{ nm}^{-1} < s < 2.0 \text{ nm}^{-1}$ and $0.5 \text{ nm}^{-1} < s < 3.7 \text{ nm}^{-1}$, respectively ($s = Q/2\pi = 1/d$).

The data were normalised to the intensity of the incident beam, corrected for the detector response, the scattering of the buffer was subtracted and the difference curves scaled for concentration. All procedures involved statistical error

propagation using the program SAPOKO (Svergun & Koch, unpublished). The data collected at the two camera lengths were merged to yield the final composite scattering curve.

The maximum dimension of the particle in solution, D_{\max} , was estimated using the orthogonal expansion program ORTOGNOM (Svergun, 1993). The forward scattering intensity at zero angle $I(0)$, distance distribution function $p(r)$ and the radius of gyration R_g were evaluated with GNOM (Semenyuk & Svergun, 1991). For the computation of the Porod (Porod, 1982) volume, V_p , a constant was subtracted from the experimental data to ensure that the intensity decayed as a function of s^{-4} following Porod's law for homogeneous particles. This procedure diminishes the scattering contribution due to the internal particle structure and yields an approximation of the "shape scattering" curve (i.e. scattering from the excluded volume of the particle filled by constant density).

4.2.5. Results and Discussion

The scattering curve obtained from merging the data from both long and short camera lengths is shown in Figure 4-15. The SAXS data were analysed as described above and the R_g of ES-62 at infinite dilution determined to be 4.25 nm. The R_g values for ES-62 are plotted as a function of concentration in Figure 4-16.

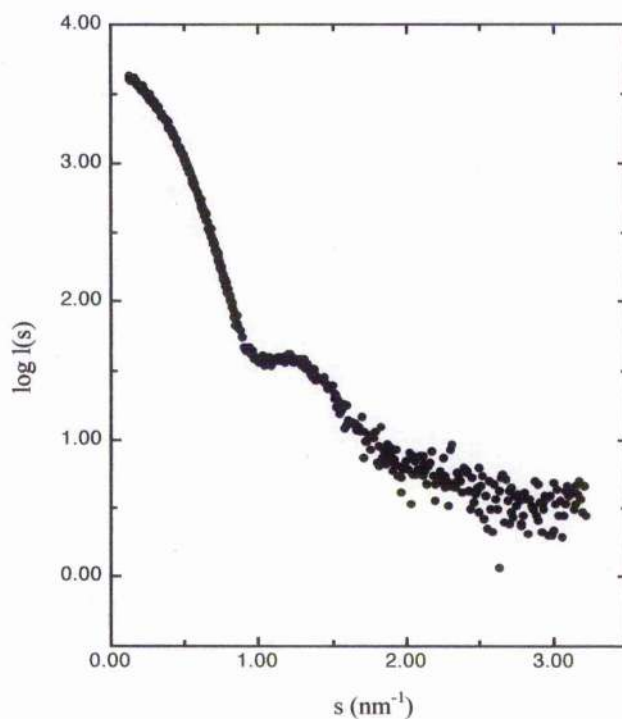


Figure 4-15: Scattering curve for the merged data collected at camera lengths of 3.4 and 1.9 m.

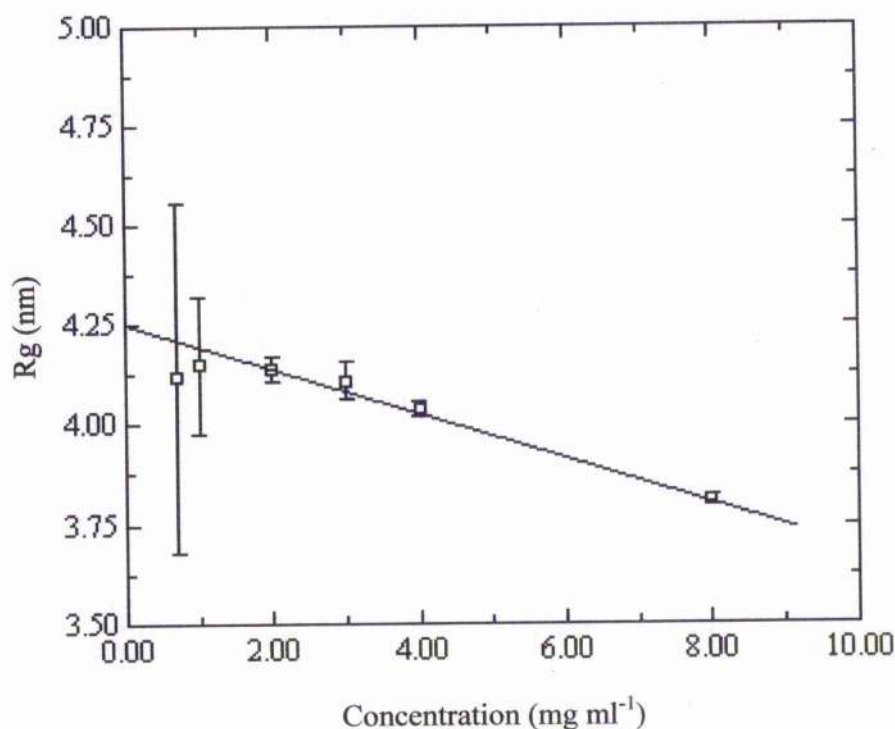


Figure 4-16: Radius of gyration (Rg) of ES-62 as a function of concentration.

Rg characterises the degree of elongation of the molecule under study. Determination of Rg at infinite dilution allows an absolute measure of the external shape of the macromolecule, free from density fluctuations, to be obtained. As discussed previously in section 4.1.5.2, the most compact shape for a particle is a sphere. The radius of gyration (Rg) of a sphere with the same molecular mass as tetrameric ES-62 was calculated to be 3.1 nm using both equations 4-18 and 4-19 from Perkins (1988b) and also Figure 12 of Perkins (1988b).

$$Rg^2 = \frac{3}{5}r^2$$

Equation 4-18

where the radius of a sphere with a molecular mass of 231.2 k Da and a partial specific volume of 0.73 ml g⁻¹ was determined to be 4.05 nm.

For a spherical protein with partial specific volume of 0.73 ml g^{-1} , the R_g at infinite dilution is related to M_r (Perkins, 1988b).

$$R_o = 0.051466 M_r^{\frac{1}{3}} \quad \text{Equation 4-19}$$

where R_o is the radius of gyration at infinite dilution.

These calculations show, by comparison with the experimentally derived R_g for ES-62 of 4.25 nm at infinite dilution, that ES-62 is elongated. This further substantiates the findings from SV studies which show that ES-62 is tetrameric and elongated in nature (section 4.1.5.2).

The SAXS data collected at both camera lengths were of sufficiently high quality to allow the *ab initio* determination of the low resolution structure of ES-62 using the programme DAMMIN (Svergun, 1999) as described in section 4.3.2.

4.3. Structural Modelling

The determination of low resolution structures of proteins from small angle scattering data is a relatively new development. Two programs, were used in this PhD project to attempt to determine the low resolution structure of ES-62. These programmes, DALAI and DAMMIN, employ different techniques in order to determine the low resolution structure. DALAI uses a genetic algorithm to generate a low resolution model with a scattering curve identical to the experimental scattering curve, while DAMMIN employs simulated annealing to achieve the same end goal.

4.3.1. DALAI

DALAI (Chacon *et al.*, 2000; Chacon *et al.*, 1998) employs a genetic algorithm to obtain a low resolution structure from solution scattering data. Figure 4-17 shows a diagrammatic overview of the methodology behind DALAI. The program works by generating an initial sphere-filled search space, based on the experimentally determined D_{\max} , which encloses the macromolecule of interest. Each sphere within the search space can be designated as either particle (1) or solvent (0). An initial random population of possible combinations of spheres designated as particle or solvent is then generated. Each of the population elements are known as chromosomes. Following generation of the initial population, the chromosomes are decoded from binary array (1 or 0) into spatial co-ordinates and the scattering curve of each calculated and compared to the target scattering curve. A fitness value is then assigned to each chromosome based on the similarity of its scattering curve to the target scattering curve. Those chromosomes assigned higher fitness values have a greater probability of reproducing through mutation and crossovers. This process of generating new chromosomes, comparing their scattering curves to the target and assigning fitness values continues until convergence is reached where the maximum fitness value no longer improves.

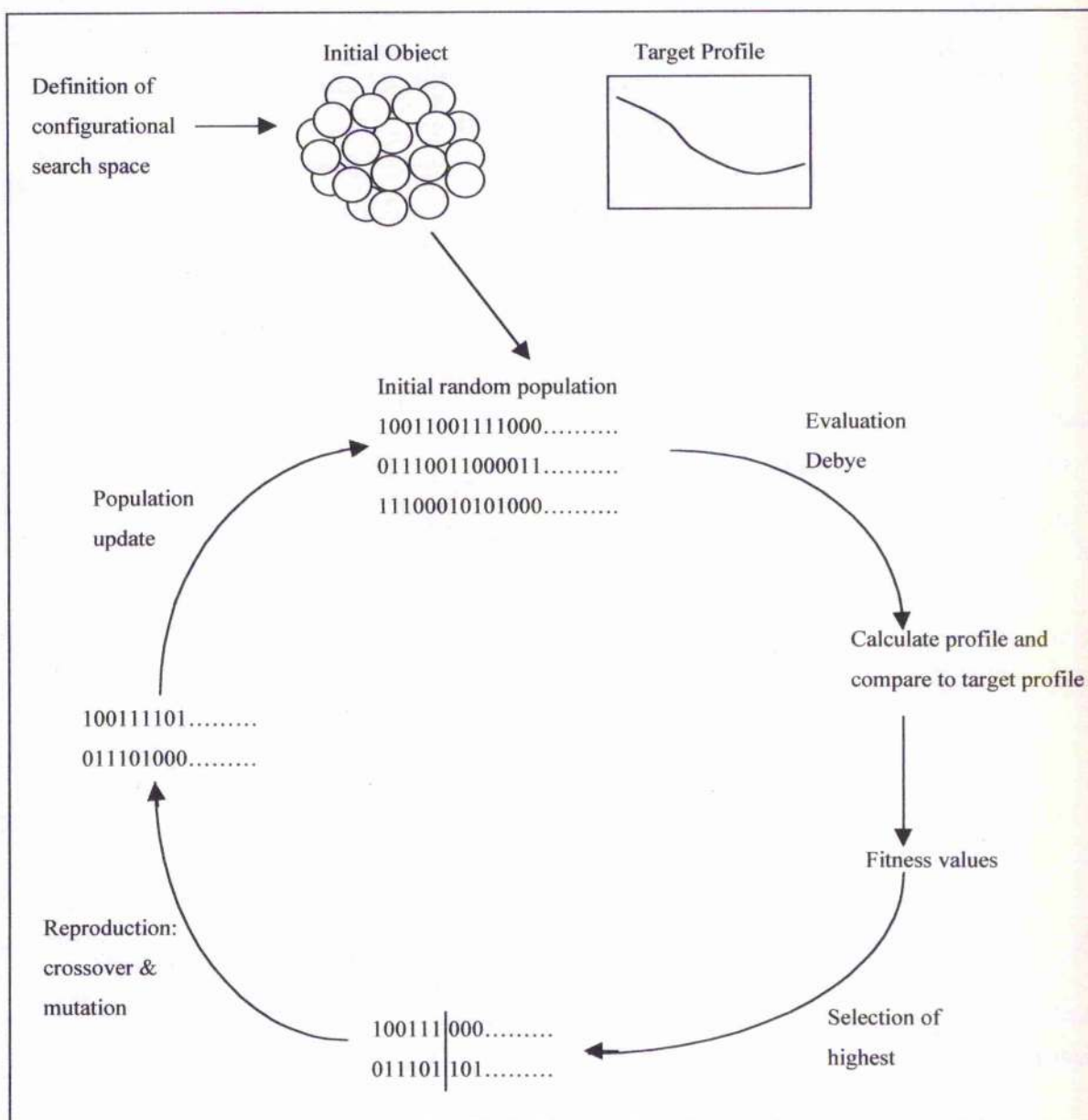


Figure 4-17: Diagrammatic overview of DALAI, reproduced from Chacon et al. (1998).

DALAI was used to restore a structure from the merged small angle scattering data collected for ES-62 at two camera lengths. Unfortunately, despite assistance from the authors of DALAI, the low resolution structure of ES-62 could not be determined using this program as the program repeatedly failed to converge despite being left to run for weeks at a time.

4.3.2. DAMMIN

DAMMIN (Svergun, 1999) employs simulated annealing to achieve *ab initio* low resolution shape restoration from solution scattering data. A volume is defined, based on D_{\max} , which encloses the particle and is filled with dummy atoms. Each dummy atom is randomly assigned as solvent or particle by the program and the scattering curve for the model calculated. The assignation of solvent or particle for one randomly chosen dummy atom is then changed and the scattering curve for this new model generated and compared to the previous scattering curve. If the energy has decreased then the dummy atom change is unconditionally accepted, however if the energy has increased then the dummy atom change is conditionally accepted with a probability rating. This process is repeated until convergence is reached and the energy level stabilises. As this method accepts both models with decreased and increased energy through use of a probability rating, it allows local minima to be overcome and thus a true global minimum can be attained.

The low resolution shape of ES-62 was determined *ab initio* from the SAXS curve using the method described by Svergun (1999). A sphere of diameter D_{\max} (determined from the small angle scattering data using GNOM) was filled with densely packed small spheres (dummy atoms) of radius $r_0 \ll D_{\max}$. Each dummy atom was then assigned as either solvent (0) or solute (1) by the program. The scattering intensity ($I(s)$) from the dummy atom model (DAM) was computed as described by Svergun (1999). As solution scattering data are of low resolution, DAMMIN searches for a configuration which minimises the function $f(X) = \chi^2 + \alpha P(X)$. χ^2 is the discrepancy and is defined as follows;

$$\chi^2 = \frac{1}{N-1} \sum_j \left[\frac{I(s_j) - I_{\exp}(s_j)}{\sigma(s_j)} \right]^2 \quad \text{Equation 4-20}$$

where N is the number of experimental points, $I(s)$ is the calculated intensity, $I_{\exp}(s)$ is the experimental shape scattering intensity and $\sigma(s)$ denotes the standard deviation.

$P(X)$ is a penalty term which, when taken with a positive weight $\alpha > 0$, ensures that the DAM has a low resolution with respect to the packing radius r_0 . The minimisation is performed starting from a random configuration using the simulated annealing method (Kirkpatrick *et al.*, 1983). DAMMIN (Svergun, 2000) allows information regarding the point symmetry of the molecule being modelled to be taken into account. This can increase the accuracy of the model and test the robustness of this modelling method by comparing models obtained when appropriate but different point symmetry conditions are imposed.

The maximum dimension (D_{\max}) and radius of gyration (R_g) for ES-62 were determined from the small angle scattering curve by GNOM to be 13.0 ± 1 nm and 4.08 ± 0.03 nm respectively while the Porod volume was calculated to be 400 ± 20 nm³. The volume of tetrameric ES-62, calculated from its mass and partial specific volume, is 280 nm³. From these values it can be calculated that the DAM contains 120 nm³ of bound water. The hydration of the model of tetrameric ES-62 can thus be estimated. The mass of each ES-62 tetramer is 3.84×10^{-19} g and the weight of the bound water is 1.20×10^{-19} g representing a hydration level of approximately 0.31 g water / g protein.

The low resolution shape of ES-62 was determined using DAMMIN under three symmetry conditions; either no symmetry (P1), 2 point (P2) symmetry or 222 point (P222) symmetry was imposed. Several restorations were performed at packing radii of $r_0 = 0.4$ to 0.5 nm for each of these three conditions and the models overlaid to confirm that reproducible results were being obtained for each of the three conditions. The fits to the experimental data when P1, P2 or P222 symmetry was imposed are shown in Figure 4-18. The calculated scattering curve neatly fits the shape scattering pattern and at high angles goes below the initial experimental data. This kind of fit is not unexpected as the outer (high angle) portion of the experimental scattering pattern contains contributions from the internal structure of the molecule which is not modelled by DAMMIN. Figure 4-19 shows typical models obtained for the low resolution structure of ES-62 when either no symmetry, P2 or P222 symmetry is imposed. The greatest amount of information regarding the structure of ES-62 can be obtained from the

model where P222 symmetry was imposed, Figure 4-19 shows that ES-62 in this model appears to consist of 2 dimers tilted by approximately 30° with respect to the long axis of the particle. Models obtained when P1 or P2 symmetry was imposed were similar in overall shape to the model obtained when P222 symmetry was imposed. Imposing P222 symmetry simply led to a much clearer visualisation of the arrangement of the dimers in the tetramer.

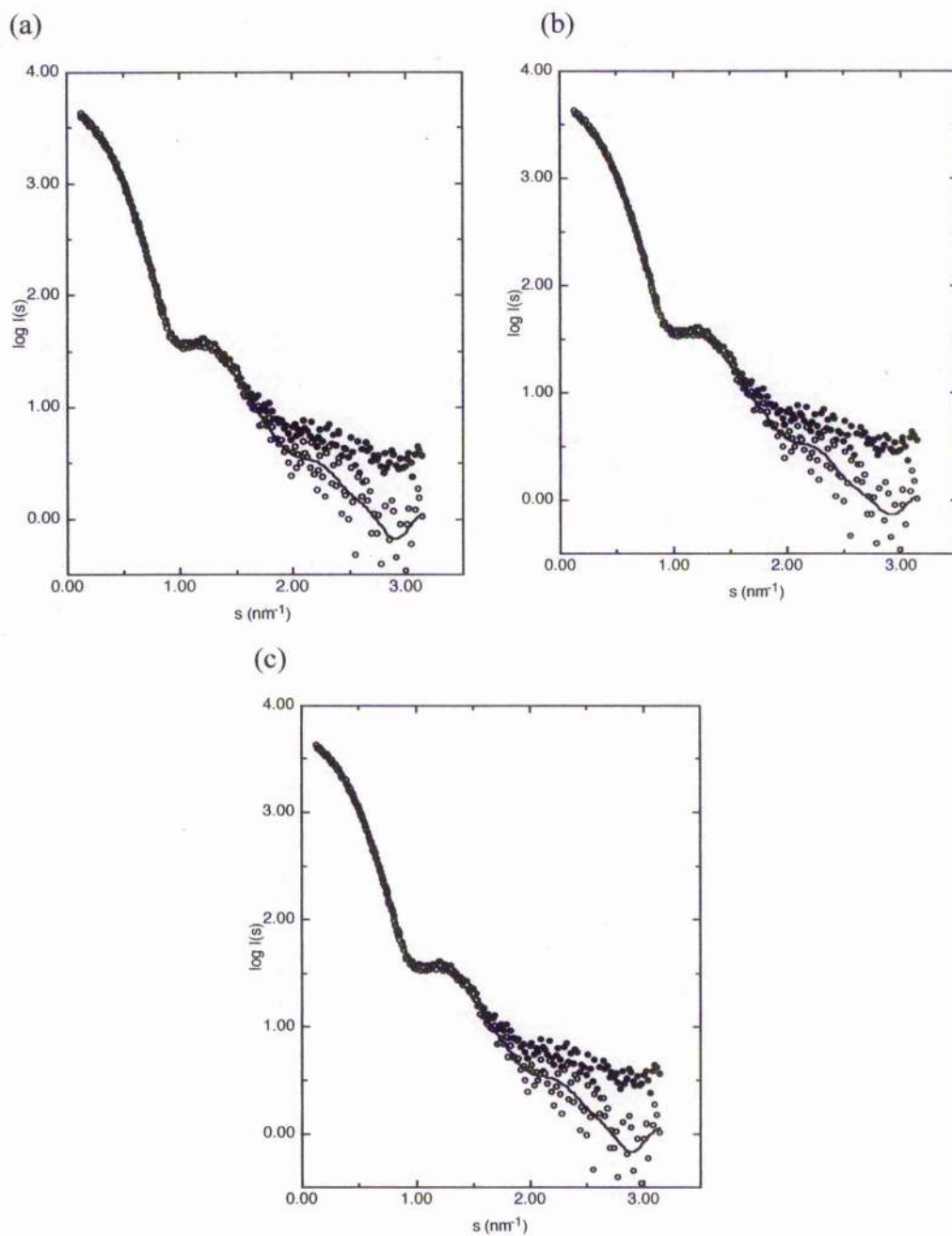


Figure 4-18: Composite scattering patterns from ES-62 (●), shape scattering curve (○) and the scattering from the *ab initio* restored model (—) imposing point symmetries of (a) P1, (b) P2 or (c) P222.

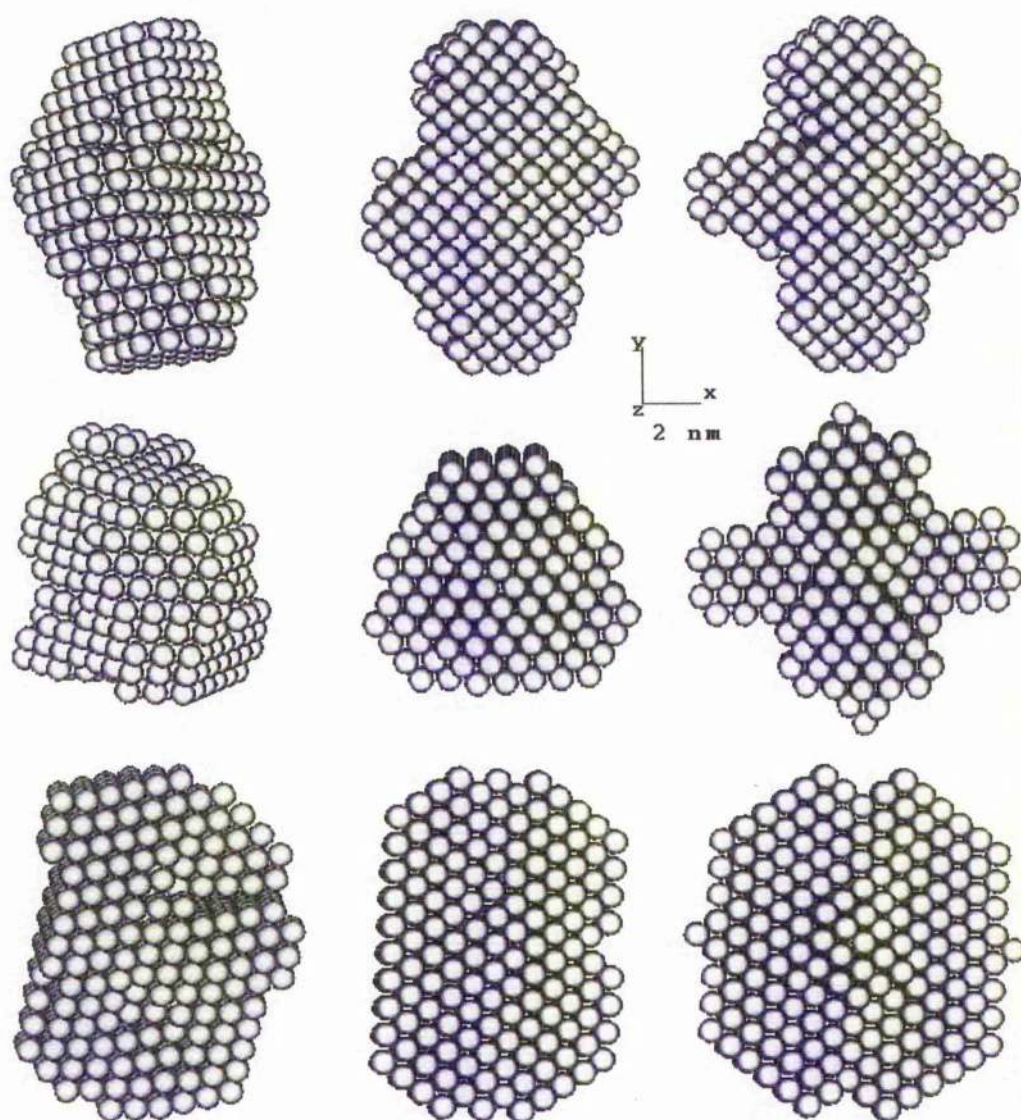


Figure 4-19: Orthogonal views (top to bottom) of the low resolution dummy atom model of ES-62 imposing point symmetries of (left to right) P1, P2 or P222. The pdb files for these 3 models are on the CD included as part of this thesis along with viewing instructions.

The models obtained for the low resolution structure of ES-62 have a resolution of 19.7 Å. This is an order of magnitude lower than the resolution of typical X-ray crystallography structures but contains much more information than the R_g , the only information obtainable from SAXS before the development of *ab initio* structural determination programs. The resolution of models generated by DAMMIN is defined by $(Q_{\max}/2\pi)^{-1}$.

The sedimentation coefficient determined from AUC studies is a valuable tool in the assessment of the model obtained for ES-62. The program HYDRO (García de la Torre *et al.*, 1994) was used to determine the sedimentation coefficients of the models shown in Figure 4-19. HYDRO requires bead models in a particular format as input thus the first step was to determine the radius of the beads in the *ab initio* models. The radius of the beads for each model was determined from the protein mass and partial specific volume and the number of beads in that model. HYDRO input files were then constructed using the calculated radius and the information in the pdb file generated by DAMMIN for each model. A sedimentation coefficient value of 10.0 S was calculated for all the models. Hydration of the model, by the amount estimated from the DAM data, 0.31 g water / g protein, results in a decrease of this value to 8.9 S, which is smaller than the value of 9.85 S obtained from AUC studies of ES-62. However, the theoretical hydrated sedimentation coefficient is obtained by uniform expansion of the structural model which often leads to "over-hydration" with a consequently exaggerated lowering of the sedimentation coefficient. Thus it would appear that this low resolution model of ES-62 is substantiated by experimental data obtained from AUC studies and is therefore highly likely to be a good model for the 3-dimensional structure of wild type ES-62.

In conclusion, the use of AUC and SAXS has lead to the discovery of some structural information about ES-62 including the *ab initio* determination of its low resolution structure. These studies demonstrate that ES-62 exists mainly in a tetrameric state, as shown by SE experiments, substantiating earlier gel filtration studies that suggested that ES-62 was tetrameric. This finding is important, especially in view of the results presented in Chapter 3 which suggest a role for ES-62 as a peptidase, as many aminopeptidases exist in a dimeric or tetrameric state. SV and SAXS studies demonstrated, through determination of the sedimentation coefficient and the Rg of ES-62, that ES-62 is likely to have a slightly elongated structure, which can be seen in the *ab initio* determined structures of ES-62 in Figure 4-19. The biological implications of these structural data will be discussed in more depth in Chapter 7.

5. Expression and Purification of Recombinant ES-62

Native ES-62 is produced and secreted by adult filarial nematodes following infection of the rodent host with *Acanthocheilonema viteae*. Studies to date on the effects induced by ES-62 have been carried out using native ES-62 isolated from the secretions of the adult filarial nematodes as described in Chapter 2. Native ES-62 has substantial heteroglycosylation (6 %) and has phosphorylcholine moieties attached to some of its carbohydrate chains. The studies of the effects induced by ES-62 utilising native ES-62 suffers from a number of disadvantages. The first is that, while ES-62 is known to be immunomodulatory, the contribution made to this role by the carbohydrate and PC components of ES-62 is unknown. The second is that native ES-62 is only produced in relatively small quantities thus limiting the experiments that can be performed.

To overcome these problems two expression systems, bacterial and baculoviral, were established for the production of recombinant ES-62 (rES-62). A bacterial expression system would allow the study of the protein component of ES-62 alone while an expression system in a higher organism, such as insect, would allow the study of the immunomodulatory effects of glycosylated ES-62 without the PC moieties. The latter of these is particularly interesting as PC is known to have immunomodulatory capabilities and there is evidence to suggest that some of the immunomodulatory effects induced by ES-62 can be attributed to its PC moieties (Harnett *et al.*, 1999a). In addition, recombinant expression systems should yield larger quantities of ES-62 thus removing the quantity limitations imposed on experiments, in particular structural studies.

The production of larger quantities of unglycosylated ES-62, i.e. that from a bacterial expression system, would enable crystallographic determination of the high resolution structure of the protein component of ES-62, which typically requires milligrams of protein. Crystallographic studies of native ES-62 are

hampered not only by the low quantities of protein available, but also by the high levels of glycosylation present on the native protein. Glycosylation introduces heterogeneity into protein samples used in crystallisation which can hamper successful crystal growth, lowering the resolution of any diffraction data.

5.1. Expression in a Bacterial System

The first choice for the production of recombinant ES-62 (rES-62) was a bacterial expression system because these systems are usually simple to establish and often yield large quantities of recombinant protein easily and cheaply. Bacteria cannot perform post-translational modification thus any rES-62 produced from a bacterial expression system would not be glycosylated and thus would lack a PC moiety. This would allow the immunomodulatory capabilities of the protein component of ES-62 to be studied without the contributory effects from the carbohydrate and PC components of native ES-62. The pET expression system from Novagen was chosen as this system had a vector available, pET 19b, that possessed all the features felt to be necessary for the expression of ES-62. One of the most important features was a cleavable histidine tag, which was attached to the N-terminus of the protein being expressed. The His tag makes purification easier, though use of a metal chromatography column, and the cleavable nature of the tag meant that rES-62 could be studied without the influence of the tag. An overview of the strategy for cloning ES-62 into the pET 19b bacterial expression system is shown in Figure 5-1.

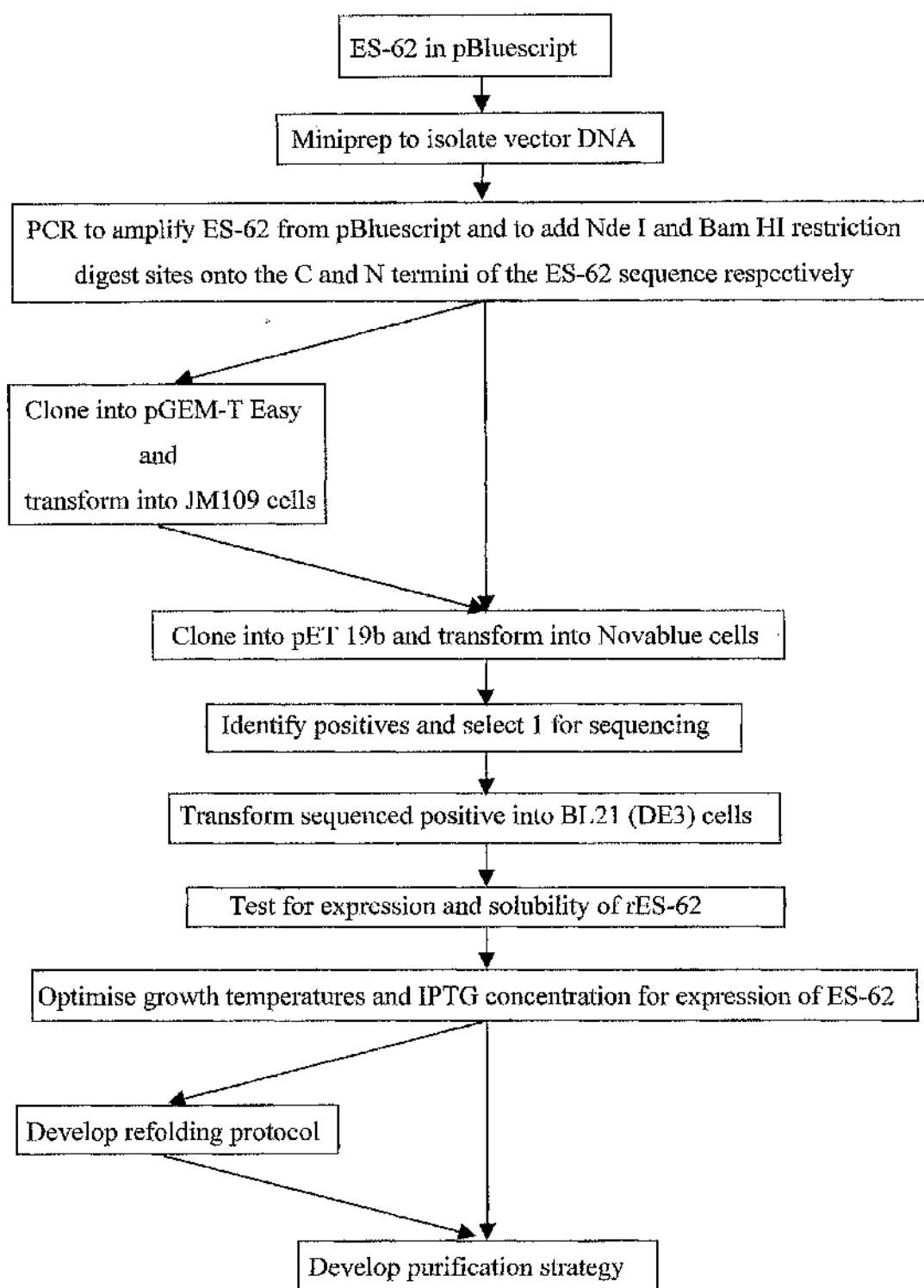


Figure 5-1: Overview of the strategy for establishing the bacterial expression of rES-62 from the Novagen pET 19b vector expression system.

5.1.1. Cloning, Ligation and Transformation

The 1.5 kb DNA sequence for ES-62 was amplified from the pBluescript construct it had been inserted into during the initial cloning experiments (Harnett *et al.*, 1999b) via PCR, as described in Chapter 2, and inserted into the pET 19b vector. Figure 5-2 shows the vector map for pBluescript. The restriction digest sites within the multiple cloning site were not suitable for cloning into pET 19b thus PCR not only isolated the sequence of ES-62 but attached Nde I and Bam HI restriction digest sites to the C and N termini of the sequence respectively. Figure 5-3 shows a 1 % agarose gel of the PCR product obtained. The markers show that the PCR product is of the correct size, 1.5 kb, as expected from the sequence.

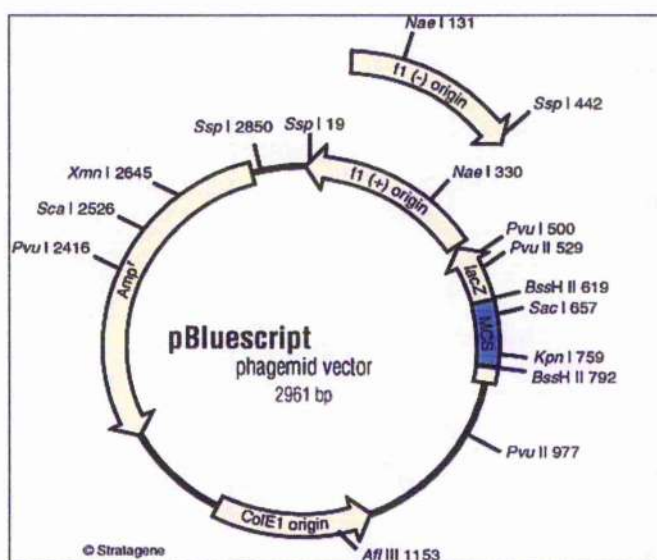


Figure 5-2: pBluescript vector map

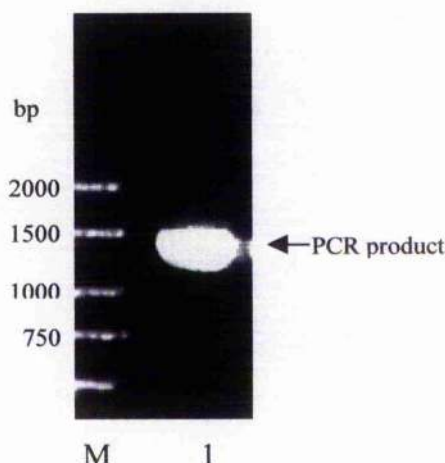


Figure 5-3: 1 % agarose gel showing 1.5 kb PCR product amplified, using ES-62 specific primers, from a construct of pBluescript containing the sequence for ES-62. The entire PCR reaction, 25 μ l, was loaded onto the gel and the PCR product isolated by gel extraction and DNA precipitation as described in Chapter 2. M is PCR markers loaded to allow determination of the size of the PCR product, 1 is the PCR reaction.

Having obtained a PCR product of ES-62 with restriction digestion sites to allow cloning into the pET 19b vector, the insert was ligated into the vector. The pET 19b vector map can be seen in Figure 5-4. This map shows the multiple cloning site including the Bam HI and Nde I restriction digest sites. The vector is 5.7 kb in size and the ES-62 insert is 1.5 kb. This gives a construct 7.2 kb in size which yields two fragments of 5.7 and 1.5 kb on digestion with Bam HI and Nde I.

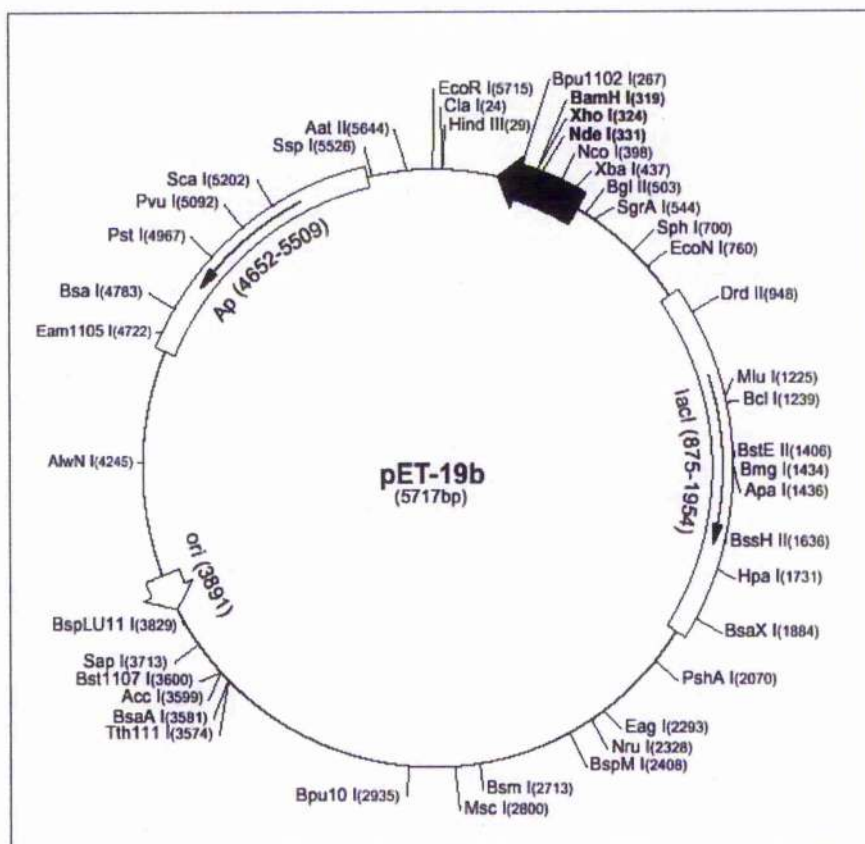


Figure 5-4: pET 19b vector map

Ligation of the digested pET 19b vector and the digested PCR product initially proved unsuccessful. This was thought to be due to incomplete digestion of both the pET 19b vector and the PCR product by Nde I, a restriction enzyme known to be less efficient at digesting DNA. The incomplete digestion may also have been exacerbated by the lack of DNA surrounding the restriction digest sites for the restriction enzymes to situate themselves on. Figure 5-4 shows that this problem arises in the pET 19b vector due to the close proximity of the two digestion sites. It is possible that when one restriction enzyme is in place for digestion, it blocks the restriction digest site of the second restriction enzyme. This problem was overcome by performing sequential digests. Bam HI was incubated alone with the vector, allowing digestion of the Bam HI sites, before addition of Nde I. Nde I was incubated with the vector DNA for longer than would normally be necessary for restriction digestion, adding extra Nde I at various timepoints as detailed in Chapter 2.

Incomplete digestion of the PCR product was thought to be due to a lack of DNA for the restriction enzymes to situate on due to the restriction digestion sites being at the ends of the PCR product. In order to circumvent this problem, the ES-62 PCR product was blunt end ligated into pGEM-T Easy, the vector map of which is shown in Figure 5-5. The ES-62 fragment was then digested whilst in the pGEM-T Easy vector, which provided sufficient DNA surrounding the restriction digest sites on which the restriction enzymes could locate in order to digest the DNA at the appropriate restriction digests sites. Sequential digests, as performed for digestion of the pET 19b vector, were performed to isolate the ES-62 fragment from pGEM-T Easy.

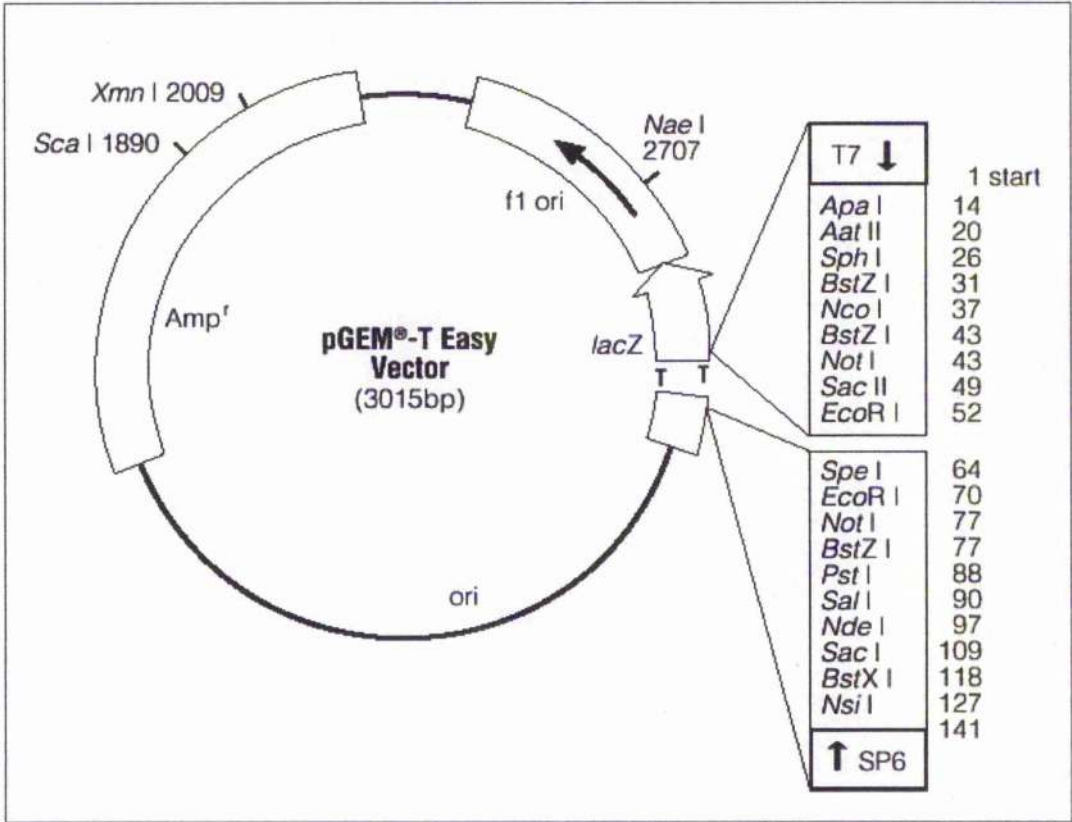


Figure 5-5: pGEM-T Easy vector map

The digested pET 19b vector and digested pGEM-T Easy vector containing ES-62, were run on a 1 % agarose gel to allow separation of linearised pET 19b vector from undigested material and the ES-62 insert from pGEM-T Easy vector DNA. The linearised pET 19b vector and the ES-62 insert were then extracted from the gel using a Qiagen gel extraction kit. This method yielded insufficient DNA for ligation, often with a low ratio between the absorbances at 260 nm and 280 nm, indicating protein contamination of the DNA. Despite many attempts to optimise this protocol, a satisfactory yield of DNA was never attained. In order to overcome this problem the digests were run on low melt agarose gels, the appropriate bands were excised and melted by heating gently and the liquidified bands, containing the digested DNA, used as the DNA sources for ligation as described in Chapter 2.

The vector constructs, following ligation and transformation into Novablue cells, were assessed for the presence of the ES-62 insert within the pET 19b vector by sequential digestion with Bam HI and Nde I. Figure 5-6 shows the success of the ligation. A 5.7 kb band, representing the linearised pET 19b vector, and a 1.5 kb band, representing ES-62, can be seen in all the colonies screened.

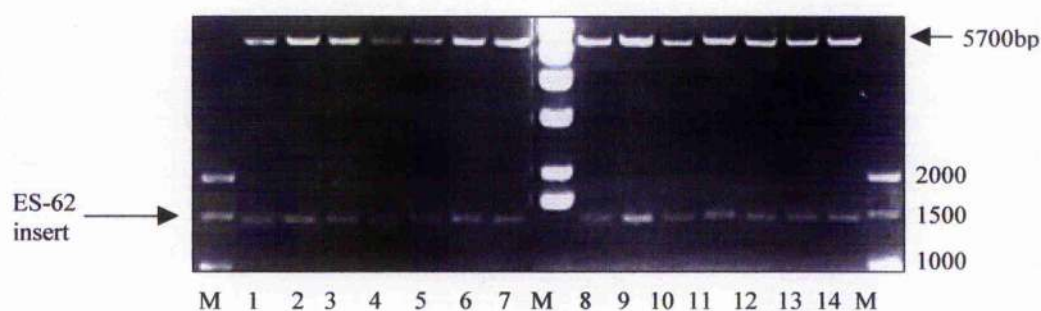


Figure 5-6: Diagnostic restriction digest of colonies obtained from the ligation of pET 19b with ES-62 and subsequent transformation into Novablue cells. M – DNA size markers, 1-14 - pET 19b vector colonies after ligation with ES-62 insert. The band seen at 5700 bp is linearised pET vector.

Novablu cells yield high levels of plasmid for identification of plasmids in which ligation has been successful, but do not contain the gene for T7 RNA polymerase and thus cannot express the gene inserted into the plasmid. DNA from six randomly selected colonies (corresponding to lanes 2, 4, 6, 10, 12 and 14) were transformed into BL21 (DE3) cells which are expression host cells. BL21 (DE3) cells possess the T7 RNA polymerase gene and can express the gene inserted into the plasmid.

5.1.2. Sequencing of the ES-62 Insert

The ES-62 insert within pET 19b was sequenced as described in Chapter 2. Analysis of the sequencing data revealed only 1 error in the sequence of the insert. The mutation was that of an amino acid change from an aspartic acid residue at position 6 of the mature ES-62 sequence (minus the signal peptide) to a glutamic acid residue. This occurred due to a single base change from a C to an A, GAC to GAA in the sequence. This construct was used despite the error as the mutation is of a conserved nature and only concerns the addition of a CH₂ group to the side chain of the amino acid as shown in Figure 5-7 below.

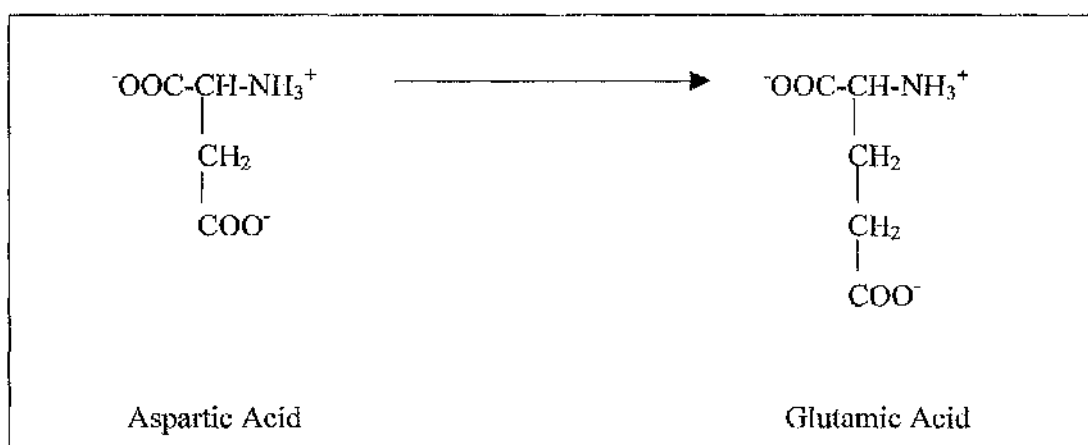


Figure 5-7: Amino acid change from aspartic acid to glutamic acid – addition of a CH₂ group to the side chain.

5.1.3. Expression

Using the BL21 (DE3) cells containing the ES-62/pET19b constructs, expression trials were performed. Six sets of L-broth (5 ml) containing ampicillin ($100\ \mu\text{g ml}^{-1}$) were inoculated with the one of six colonies transformed into BL21 (DE3) cells. These cultures were grown as detailed in Chapter 2. A sample (1 ml) of each culture was taken prior to and post induction with IPTG. The cells from these samples were pelleted, lysed and resolved on a 8 % SDS PAGE gel. The gel was then stained with Coomassie blue dye to visualise the proteins present in each sample. Figure 5-8 (a) shows a typical result for three of the six colonies. It can clearly be seen that expression of a protein following induction with IPTG occurs. As ES-62 is the only protein under the control of a promoter induced by IPTG, the expressed protein observed is rES-62. Figure 5-8 (b) shows the same samples (pre- and post- induction) after Western blotting with polyclonal rabbit anti-ES-62 (supplied by W. Harnett) at $100\ \mu\text{g ml}^{-1}$. This blot shows definitively that the IPTG induced expressed protein, observed in Figure 5-8 (a), is rES-62.

As set out in the flow chart in Figure 5-1, having established that rES-62 was being expressed, the next step was to determine if the rES-62 expressed was soluble, i.e. in the supernatant following lysis of the bacterial cell and not in the cell pellet. To determine the solubility of the expressed rES-62, a 500 ml culture was prepared as described in Chapter 2 and, following suitable incubation with an overnight inoculant culture and induction with IPTG, the cells were lysed and the cell lysate clarified by centrifugation. A sample of the pellet obtained following clarification was taken and affinity purification performed on the supernatant, again as detailed Chapter 2, with samples taken of the wash through from the column and the eluate. A sample of the cell pellet and the samples from affinity purification were resolved on an 8 % SDS PAGE gel as shown in Figure 5-9. The results of this expression trial show that the majority of rES-62 is insoluble and located in inclusion bodies (lane 1) which were pelleted by centrifugation during clarification of the cell lysate. A very small proportion of rES-62 is soluble and can be purified as seen in lane 3 of Figure 5-9.

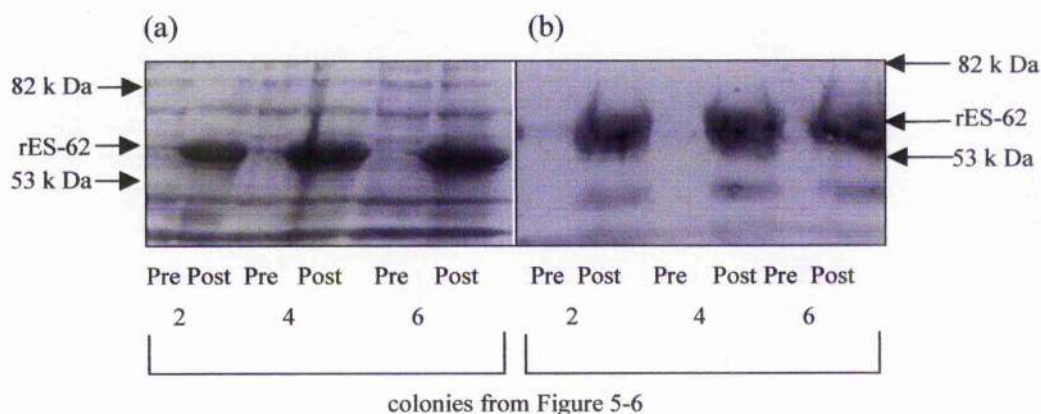


Figure 5-8: Pre- and post-induction samples of three of the six colonies selected to be transformed into BL21 (DE3) cells. Expression of ES-62 was induced by addition of 1 mM IPTG. (a) SDS PAGE gel of the 1 ml pre- and post-induction samples of each of these colonies, stained with Coomassie blue dye. (b) A Western blot of the pre- and post-induction samples seen in (a), using polyclonal rabbit anti-ES-62 at $100 \mu\text{g ml}^{-1}$.

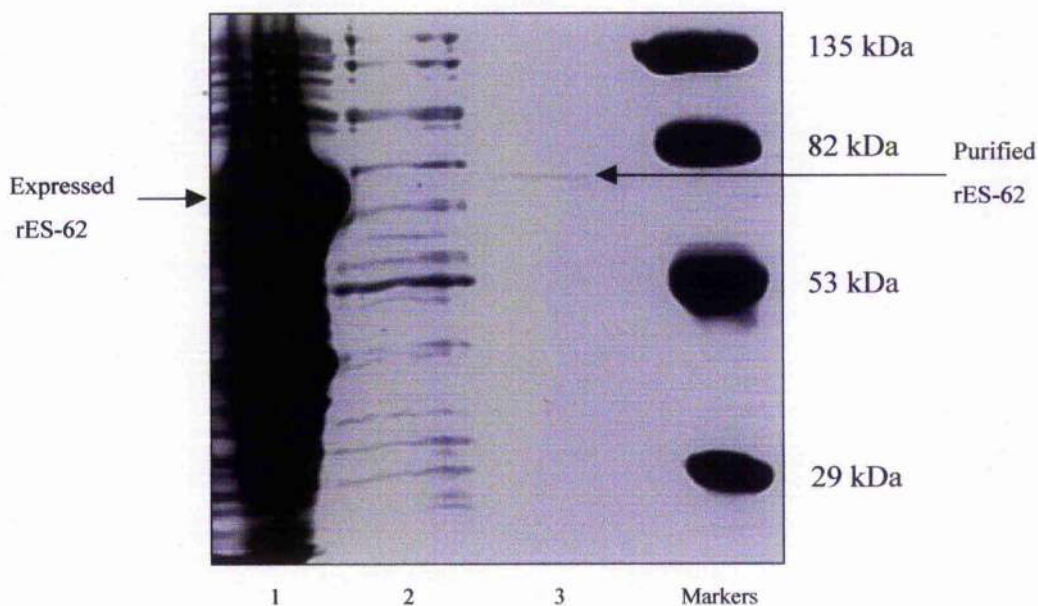


Figure 5-9: An 8 % SDS PAGE gel stained with Coomassie blue dye of (1) the pellet obtained following clarification of the cell lysate of the induced bacterial cells, (2) the wash through (20 μl) from the POROS metal chelate affinity purification and (3) the eluate (20 μl) from the POROS metal chelate affinity purification column.

To optimise the amount of soluble rES-62 expressed, a range of growth temperatures and IPTG concentrations were tested, as detailed in Table 5-1. The possibility of leaky expression, i.e. expression of rES-62 from cells grown over a long period of time without the addition of IPTG, was also tested for.

Experimental details are provided in Chapter 2. The cells obtained from these test cultures were lysed using sonication, clarified by centrifugation and samples of the supernatant and the pellet resolved by SDS PAGE.

Growth Temperature (°C)	IPTG concentration (mM)	Induction time (hours)
37	1, 0.5, 0.25, 0.1	3
30	1, 0.5, 0.25, 0.1	4
25	1, 0.5, 0.25, 0.1	5
16	1, 0.5, 0.25, 0.1	~18

Table 5-1: Growth and induction conditions for expression trials of bacterial rES-62. Cells were grown in L-broth containing $100 \mu\text{g ml}^{-1}$ ampicillin at 37°C until an optical density at 600 nm of 0.7 was reached. IPTG was then added at the appropriate concentration and the growth temperature altered accordingly.

Expression of rES-62 following incubation of the cells at 37°C and induction by addition of 1 or 0.5 mM IPTG or incubation at 25°C and induction by addition of 1 , 0.5 , 0.25 or 0.1 mM IPTG, yielded the highest levels of soluble ES-62.

These conditions were repeated in an attempt to identify one condition yielding greater amounts of soluble recombinant material than the others. These results are shown in Figure 5-10. Optimal expression of rES-62 was attained following incubation at 25°C and induction with 0.1 mM IPTG. This condition was chosen for the expression of rES-62 in bacterial cells. Although this condition yields soluble rES-62, the majority of the recombinant material is still insoluble as shown in Figure 5-10. The band observed for soluble rES-62 (in the supernatant) under these conditions, following staining with Coomassie blue dye, was very faint. As the lower level of detection when staining with Coomassie Blue dye is

approximately 0.3 - 1 μg , the level of soluble rES-62 resolved in Figure 5-10 is approximately 0.5-1 μg . Thus the yield of soluble rES-62 obtained was 2.5 mg L⁻¹. It was decided that while the soluble material would be purified, refolding of the insoluble material, isolated from the inclusion bodies, would also be attempted and any material obtained purified.

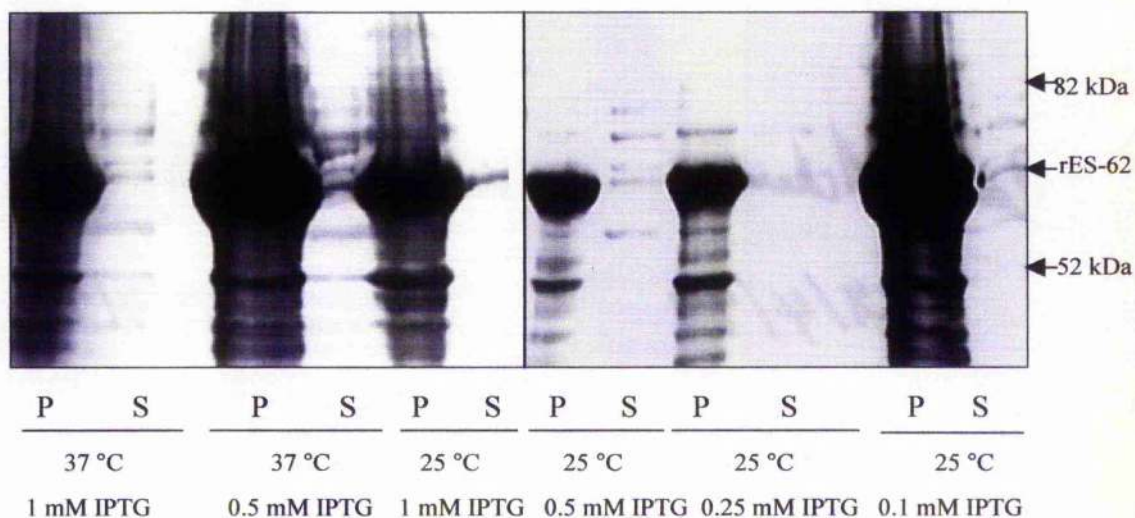


Figure 5-10: 8 % SDS PAGE gels of the pellet and supernatant of lysed bacterial cells post induction with IPTG, stained with Coomassie blue dye. P- pellet of lysed cells containing insoluble proteins, S - supernatant (20 μl) from lysed cells containing soluble proteins. The temperature at which induction took place and induction concentration of IPTG used are shown.

5.1.4. Refolding

Refolding of proteins from inclusion bodies is a complex task, made more so by the many protocols available. Proteins that are expressed and found located in inclusion bodies are insoluble due to a failure to fold correctly. Few cellular proteins are found in inclusion bodies so purifying expressed protein found in inclusion bodies, provided it can be refolded, is often a simple task due to the low level of contaminants. There are three important factors in developing a refolding protocol: pH, the presence of redox pairs and protein concentration on refolding.

pH affects the charge of amino acids within a protein and thus at the wrong pH the protein could fail to fold due to repulsion between amino acids or could aggregate due to the presence of hydrophobic patches on the outside of the protein. Studies using native ES-62 examining the stability of ES-62 at different pH indicated that ES-62 was pH sensitive. A sample (1 ml) of native ES-62 (0.57 mg ml^{-1}) in sodium phosphate buffer at pH 7.0 was dialysed against 1 L of sodium phosphate buffer (0.1 M) at pH 6 for 3 hours, the sample was then dialysed against 1 L sodium acetate buffer (0.1 M) at pH 5.5 for 3 hours, further against 1 L sodium acetate buffer (0.1M) at pH 5.0 for 3 hours and finally against 1 L sodium phosphate buffer at pH 7.0 overnight. Samples (2 μg) were taken at each pH and resolved on a non-denaturing, non-reducing gel. As shown in Figure 5-11, lower molecular weight bands were observed at pH 6.0, 5.5 and 5.0 than those observed at pH 7.0. These lower molecular weight bands were postulated to represent monomeric and dimeric forms of ES-62, while the higher molecular weight bands observed at pH 7.0 represent tetrameric ES-62. The dissociation of tetrameric ES-62 at pH values of less than 7 appears to be reversible by increasing the pH back to 7.0. However, measurement of the concentration of ES-62 prior to and following the above study indicated that a proportion (approximately 50 %) of the native ES-62 is lost, possibly by precipitation. It would appear therefore that native ES-62 is not stable at pH values below 7.0.

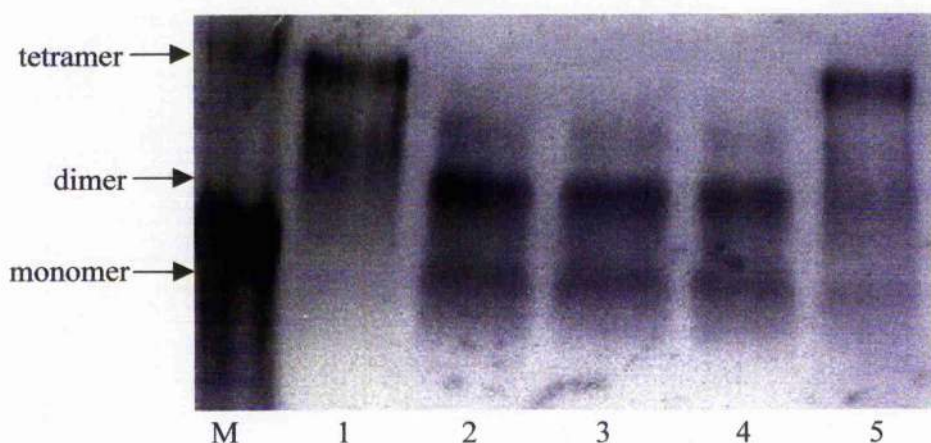


Figure 5-11: 10 % non-denaturing, non-reducing polyacrylamide gel (stained with Coomassie blue dye) of samples (2 μ g) of native ES-62 at pH values of 7.0, 6.0, 5.5, 5.0 and 7.0. M – markers; 1 - native ES-62 at pH 7.0 prior to the dialysis experiment; 2 - native ES-62 at pH 6.0; 3 - native ES-62 at pH 5.5; 4 - native ES-62 at pH 5.0; 5 - native ES-62 at pH 7.0 following the dialysis experiment.

Redox pairs such as cysteine and cystine and oxidised and reduced glutathione help the protein to refold by allowing disulphide exchange to occur. The concentration of the protein is important as at high concentrations aggregation can occur even in folded proteins. To aid refolding the protein concentration for the final refolding step should be between 10 – 500 μ g ml⁻¹ (Kuhelj *et al.*, 1995).

In the search for a refolding method that yielded soluble rES-62, two protocols were attempted with a number of modifications made to each. These are discussed below. The protocol for refolding found to be most successful is detailed in Chapter 2. The first protocol attempted used oxidised and reduced glutathione as the redox pair. This redox pair can form mixed glutathione – protein disulphides and aid the correct pairing of disulphides to allow formation of native structures. The buffer used throughout this protocol was 39 mM sodium dihydrogen orthophosphate, 61 mM disodium hydrogen orthophosphate, 50 mM sodium chloride at pH 7. Additional components were added to this buffer throughout the protocol depending on the aim of that particular part of the protocol. Isolated inclusion bodies were obtained by lysis of the bacterial cells to

remove the soluble proteins, and addition of Triton X-100 to the buffer to remove the cellular membranes and membrane proteins. The proteins in the inclusion bodies were then denatured by addition of urea to the buffer. The proteins were refolded by dialysis into buffer containing only the mixed glutathione redox pairs. Using this protocol, the majority of the proteins were found to aggregate out of solution during the final dialysis step. This aggregation may be due to the use of a redox pair to aid refolding, which is an instrumental part of this protocol. ES-62 is known to have only two cysteine residues, thus use of redox pairs may be of little use to the refolding of rES-62. Protein concentration for the final dialysis step may also have been a factor in the aggregation. It is possible that the dilution step, which forms part of this protocol, was insufficient to lower the concentration of the denatured protein to the $10 - 500 \mu\text{g ml}^{-1}$ concentration recommended.

The second protocol used for refolding of rES-62 was based on a protocol by Kuhelj *et al.* (1995) as detailed in Chapter 2. Briefly, cells were lysed by sonication and the cellular membranes and membrane proteins removed by addition of Triton X-100. The insoluble proteins, present in the pellet remaining following clarification of the cell lysate, were denatured by addition of urea. The protein concentration of the resultant denatured proteins was measured and the protein diluted to $0.01-0.5 \text{ mg ml}^{-1}$. Protein refolding was achieved by dialysis of the denatured proteins against a large volume of 100 mM sodium acetate, 50 mM sodium chloride buffer, pH 7.0. This protocol gave the best yield of refolded protein although a significant proportion of the proteins still aggregated and precipitated. Many modifications to this protocol were attempted to try to optimise the refolding procedure. These modifications fell into four categories; temperature of dialysis, buffer constituents, denaturing agents and protein concentration.

5.1.4.1. Dialysis Temperature

The final dialysis step is important as it is the point at which the denaturation agent is removed and refolding occurs. Altering the temperature at which this dialysis step occurred revealed that, while there was always some precipitation of aggregated protein, the amount of precipitation could be reduced by performing the final dialysis step at room temperature (~20 °C). If dialysis was performed at 4 °C or at temperatures higher than room temperature then the amount of precipitation increased.

5.1.4.2. Buffer Constituents

It was known that small molecules can influence the folding of proteins, in particular if these molecules, such as metal ions, are required for activity. ES-62 has been postulated to contain a metal binding site. To determine if metal ions were present in native ES-62, inductively coupled plasma atomic emission spectroscopy (ICP-AES) was performed.

ICP-AES allows analysis of the protein of interest for any elements that are constituents of the protein, for example magnesium, sulphur or tungsten. A strong magnesium signal was identified in the atomic emission spectrum obtained for native ES-62 suggesting the requirement of this divalent cation in the native protein. The analysed data obtained from ICP-AES are shown in Table 5-2. Magnesium has the highest reading at 4 µM, except for potassium and sulphur, which are contaminants from the phosphate buffer. This suggests that ES-62 has a requirement for magnesium and raises the possibility that any recombinant material would perhaps have the same requirement.

	Concentration (μM)
Potassium	458.00
Sulphur	22.60
Magnesium	4.00
Zinc	1.75
Nickel	0.60
Copper	0.41
Iron	0.12
Manganese	$<1 \times 10^{-4}$
Cobalt	$<1 \times 10^{-4}$

Table 5-2: ICP-AES results for native ES-62.

Magnesium and calcium chloride were added to the buffers described in Chapter 2 in the hope that supplementing the buffers with a divalent cation would aid refolding. Sucrose was added to help mask any hydrophobic patches on the protein that may be causing aggregation to occur. Addition of sucrose to the dialysis buffer actually resulted in an increase in precipitation of the protein while addition of the magnesium and calcium chloride had no noticeable effect on the refolding of the rES-62. In view of these results, the sodium acetate buffers described in Chapter 2 were used with no additional constituents.

5.1.4.3. Denaturing Agents

Use of guanidine hydrochloride (GuHCl) at 2 and 6 M in place of urea at 2 and 8 M concentrations had no noticeable effect on the amount of precipitation that occurred, but no refolded protein could be detected following purification. The protein may have refolded but in an incorrect manner such that the His tag was inaccessible for purification. As a result of these findings, GuHCl was discarded in favour of the original use of urea.

5.1.4.4. Protein Concentration

Adjusting the protein concentration prior to the final dialysis revealed that at lower protein concentrations, 0.1 mg ml^{-1} compared to 0.3 or 0.5 mg ml^{-1} , less precipitation of aggregated protein was observed. As a result all refolding steps were performed at 0.1 mg ml^{-1} if possible.

Despite optimisation of the refolding protocol, refolding of insoluble rES-62 was of limited success. Although refolded protein that could subsequently be purified was obtained, refolding was complex and time consuming especially considering the small yields of rES-62 obtained (see section 5.1.5).

5.1.5. Purification using Affinity Chromatography

Purification of recombinant protein aims to remove all contaminants and yield a pure, concentrated sample of recombinant protein. The development of a purification system is dependent on how the recombinant protein is expressed and any unique or unusual characteristics that it may possess. Very little is known about any ES-62 substrates that could be exploited for purification purposes thus the bacterial expression system chosen was selected with purification in mind.

The bacterial expression system involved the use of a vector that attaches a cleavable 6 x His affinity tag to the N terminus of the protein. This 6 x His tag exploits the high affinity of histidine for divalent metals, especially nickel, to aid purification of the protein. The purification of the bacterially expressed ES-62 was achieved using a POROS nickel charged affinity column and the perfusion chromatography purification system (PerSeptive Biosystems). Perfusion chromatography uses POROS particles as the chromatography media. Unlike conventional chromatography particles, POROS particles have large through-pores that allow for faster transport of the sample molecules into the particles and allow contact with internal binding sites of the particles. As a result chromatography separations can be carried out more quickly with perfusion chromatography than with traditional methods and with little or no loss of

resolution. The sample was loaded onto the POROS nickel charged affinity column and elution achieved by addition of an imidazole solution that competes with histidine for binding to the immobilised metal ions.

Due to problems with precipitation during the refolding experiments and with the hypothesis that the lack of glycosylation of the rES-62 may be leading to exposure of hydrophobic patches on the outside of the protein, lysis, purification and storage of the purified protein was performed at high salt concentrations and in the presence of glycerol.

While the presence of 20 % glycerol in the lysis buffer promoted increased yields of soluble rES-62 obtained, addition of 10 % glycerol to the purification buffers appeared to reduce the amount of rES-62 which could be successfully purified. Dialysis of purified rES-62 into PBS containing high salt (sodium chloride 150 mM to 300 mM) and 20 % glycerol prevented precipitation of the purified protein. Further, trials were performed in which glycerol was replaced with concentrations of 0.01, 0.05 and 0.1 % of the detergent LDAO. No noticeable difference in the yields of purified protein was obtained using LDAO.

The best yields of soluble bacterial rES-62 were obtained by lysing the bacterial cells in the presence of 20 % glycerol, purifying the soluble protein obtained in the absence of glycerol and then dialysing the pure protein into a high salt buffer containing 10 % glycerol. Figure 5-12 shows a typical trace from the purification of soluble expressed protein when glycerol is present in the resuspension (lysis) buffer. Typically, the cell pellet from 6 L of bacterial cell culture was resuspended in 150 ml resuspension buffer containing glycerol and then lysed. The clarified supernatant was then purified using a POROS nickel charged affinity column, the fractions containing rES-62 collected, pooled and dialysed into a high salt phosphate buffer containing 10 % glycerol. Figure 5-13 shows an 8 % SDS PAGE gel stained with Coomassie blue dye showing the samples, from one purification run, of the wash through, eluate and tail highlighted in Figure 5-11. Purification using the above protocol typically yielded approximately 8-10 mg ($1.3\text{--}1.6\text{ mg L}^{-1}$) of soluble rES-62. Unfortunately further work, including

small angle X-ray scattering, analytical ultracentrifugation and dynamic light scattering studies, using this recombinant material revealed that the rES-62 was highly aggregated and unsuitable for biophysical studies or *in vivo* experimentation.

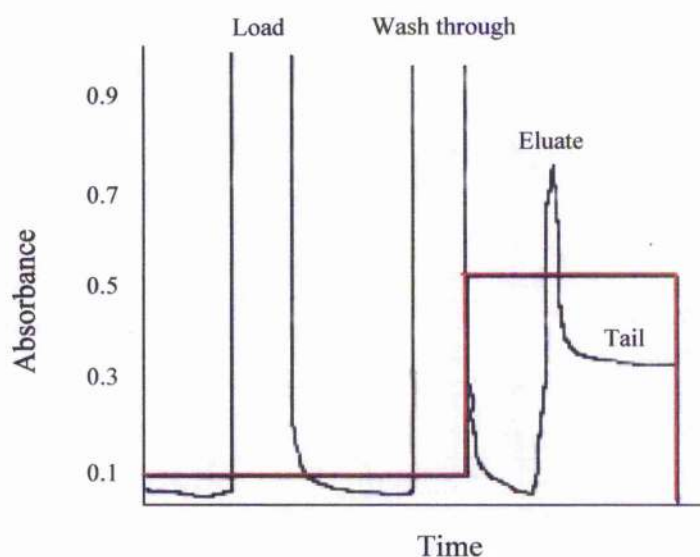


Figure 5-12: A typical purification trace from the purification of soluble rES-62 using a POROS metal chelate column. Imidazole gradient is shown in red.

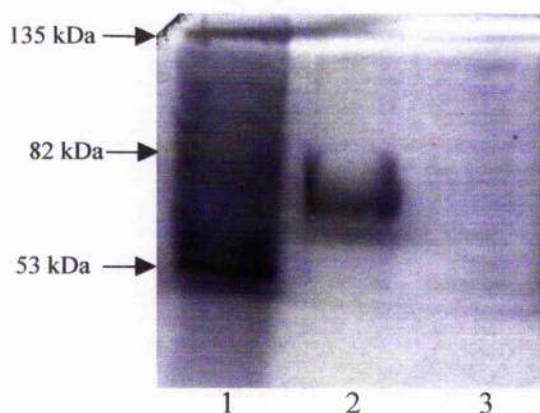


Figure 5-13: 8 % SDS PAGE gel stained with Coomassie blue dye showing the samples, from one purification run. 1 is a sample (15 μ l) of the wash through, 2 is a sample (15 μ l) of the eluate and 3 is a sample (15 μ l) of the tail.

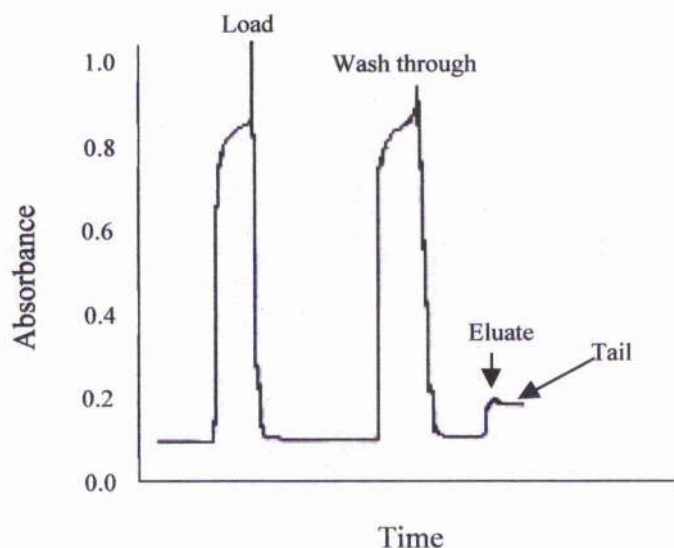


Figure 5-14: A typical purification trace from the purification of refolded rES-62 using a POROS metal chelate column.

Purification of refolded rES-62 was carried out using the same strategy as outlined above. Figure 5-14 shows a typical example of the absorbance trace obtained from purification of refolded rES-62. Typically 500 ml of bacterial cell culture was lysed and the inclusion bodies isolated. The insoluble proteins present in the inclusion bodies were then refolded and purified as described in Chapter 2. Despite the higher levels of insoluble rES-62 expressed, the purification of refolded rES-62 typically yielded only 66 μg of soluble rES-62 (0.132 mg ml^{-1}).

5.2. Expression in a Baculovirus System

The ability of expression systems to glycosylate expressed protein was an important consideration in the selection of a eukaryotic expression system, as it would allow expression of a glycosylated form of rES-62 which lacked the phosphorylcholine moieties found on native ES-62 (although glycosylation would differ from that in the native). The baculovirus expression system from PharMingen was chosen as it is a powerful and versatile eukaryotic expression system that allows for expression of the protein of interest in insect cells. The expression of rES-62 in insect cells was favoured over that of expression in yeast cells as insects are the natural vector of filarial parasites thus it was hoped that this system would be closer to the natural lifecycle of the filarial parasites and hence the natural environment for production of native ES-62.

The PharMingen baculovirus expression system is easier to use than earlier baculovirus expression systems as the baculovirus DNA has been modified such that homologous recombination with the vector is essential for viral particle production. As a result 99 % of successful homologous recombination yields virus particles containing the inserted gene. The vector chosen for expression of rES-62, pAcGP67-B, contains a secretion signal sequence which is attached to the N-terminus of ES-62 and results in the secretion of the rES-62 into the cell media. This aids purification as the insect cells can be grown in protein-free media and thus the major protein present in the harvested media following infection should be rES-62. In addition, the secretion of rES-62 from the insect cells mimics the production of native ES-62, which is secreted by the adult filarial worms into the bloodstream of the parasitised host and thus the protein is not retained in a cellular environment.

An overview of the strategy for cloning ES-62 into the baculovirus expression system is shown in Figure 5-15.

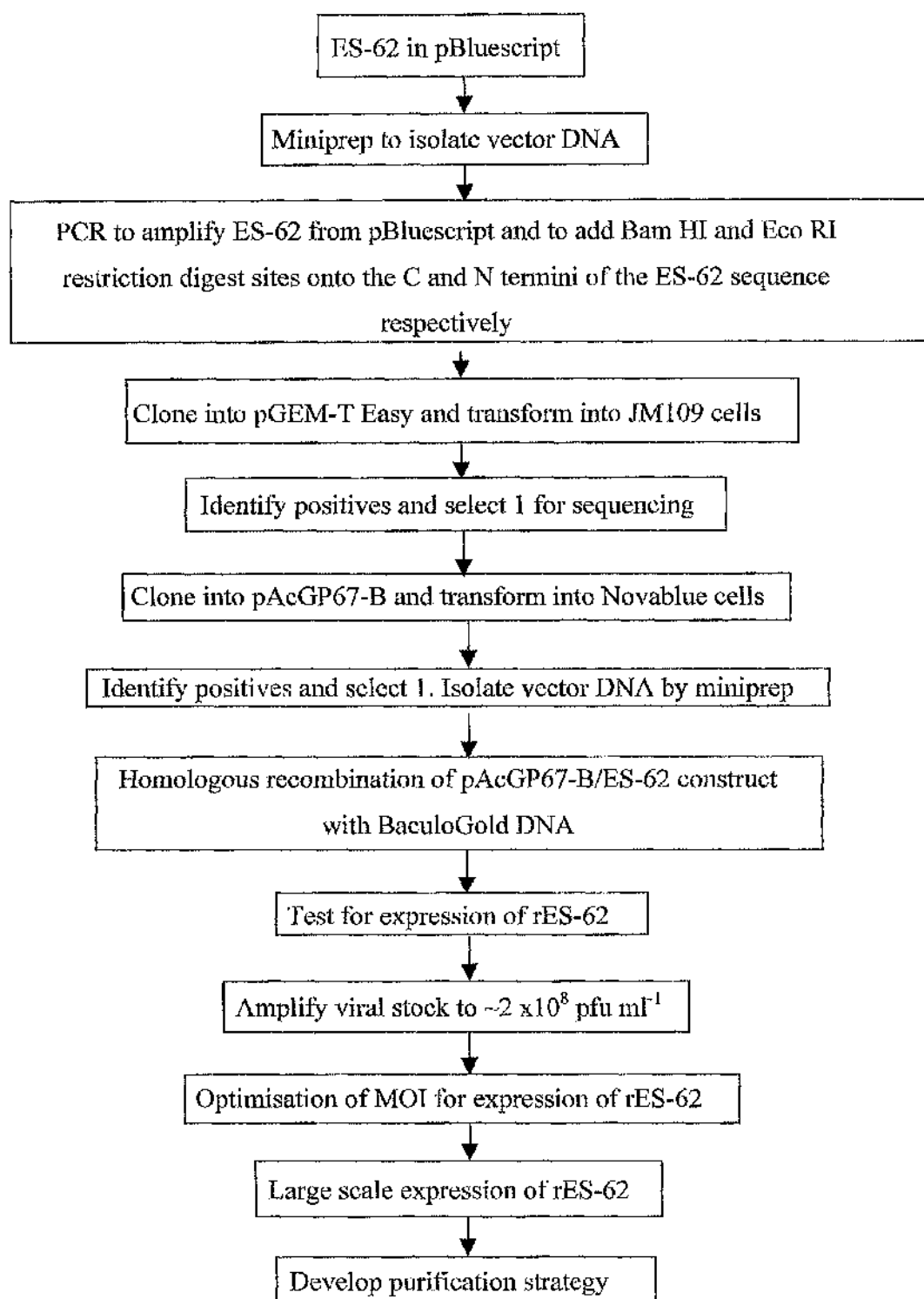


Figure 5-15: Strategy for the expression of ES-62 in a baculovirus expression system.

5.2.1. Cloning, Ligation and Transformation

The 1.5 kb DNA sequence for ES-62 was amplified, from the pBluescript construct (as shown in Figure 5-2) it had been inserted into during the initial cloning experiments (Harnett *et al.*, 1999b) via PCR. Restriction digest sites within the multiple cloning site of the pBluescript vector were not suitable for cloning into pAcGP67-B thus PCR not only isolated the sequence of ES-62 but attached Bam HI and Eco RI restriction digest sites to the C and N termini of the sequence respectively. The vector map for pAcGP67-B is shown in Figure 5-17. The PCR product was first inserted into a pGEM-T Easy vector to overcome problems of incomplete restriction digestion of the PCR fragment as discussed in section 5.1.1. The digested fragment was then cloned into the pAcGP67-B vector of the PharMingen baculovirus expression system as described in Chapter 2.

Diagnostic restriction digests with Bam HI and Eco RI, which released the insert from the vector, were used to identify positive clones. The diagnostic restriction digest of the pAcGP67-B clones can be seen in Figure 5-16. The ten colonies selected were digested with Bam HI and Eco RI and resolved on a 0.7 % agarose gel. Seven of the ten colonies show the presence of the ES-62 insert in the pAcGP67-B vector as shown by the 1.5 kb band in lanes 1, 2, 4, 5, 6, 7 & 8.

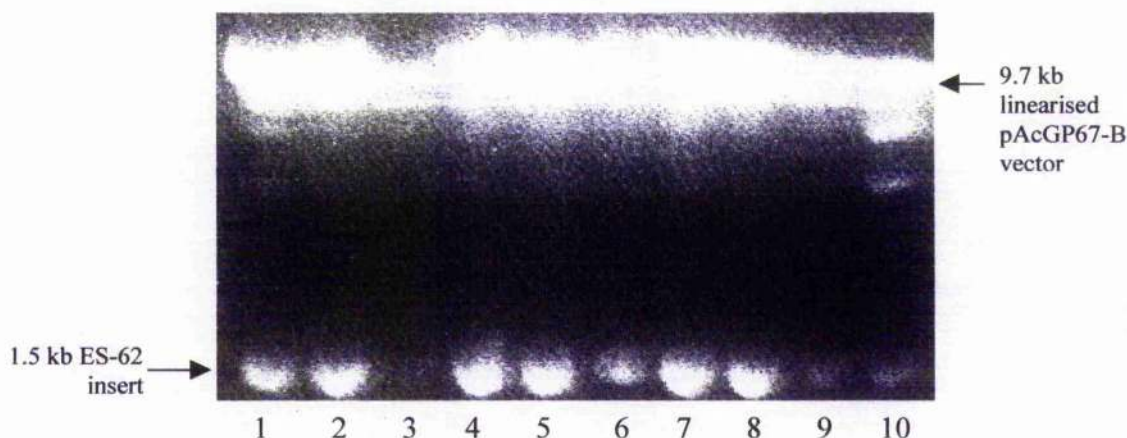
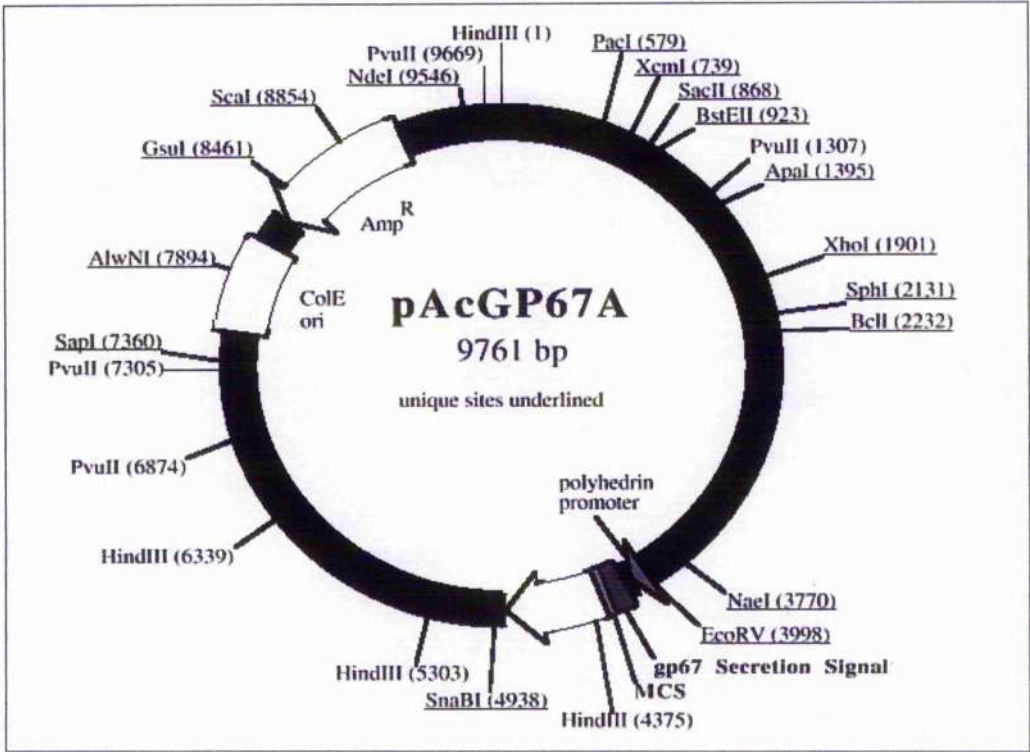


Figure 5-16: Diagnostic restriction digests of pAcGP67-B/ES-62 constructs using Bam HI and Eco RI. 10 µl of the restriction digests were run on a 0.7 % agarose gel containing ethidium bromide. To visualise the 1.5 kb insert bands the contrast was adjusted resulting in overexposure of the 9.7 kb vector band.



4135 SpeI(4140)

ATG CTA CTA GTA AAT CAG TCA CAC CAA GGC TTC AAT AAG GAA CAC ACA AGC AAG ATG
Met Leu Leu Val Asn Gln Ser His Gln Gly Phe Asn Lys Glu His Thr Ser Lys Met
gp67 secretion signal sequence (underlined)

signal peptide cleavage site

GTA AGC GCT ATT GTT TTA TAT GTG CTT TTG GCG GCG GCG GCG CAT TCT GCC TTT GCG
Val Ser Ala Ile Val Leu Tyr Val Leu Leu Ala Ala Ala His Ser Ala Phe Ala
gp67 secretion signal sequence (underlined)

Xma I(4255) PstI(4291)
Sma I(4255) NotI(4284)
NcoI(4268) BglII(4295)
BamHI(4258) EcoRI(4274) EagI(4285)

GCG GAT CTT GGA TCC CGG GCC ATG GGA ATT CCG GAG CGG CCG CTG CAG ATC TGA
Ala Asp Leu Gly Ser Arg Ala Met Gly Ile Pro Glu Arg Pro Leu Gln Ile Stop

Figure 5-17: pAcGP67-B vector map

5.2.2. Sequencing of the ES-62 Insert

The ES-62 insert within pGEM-T Easy was sequenced as described in Chapter 2. Analysis of the sequencing data revealed the same single error that was observed in the sequence of the insert for the bacterial expression system. Again this construct was used, despite the error, as the mutation is of a conserved nature as shown in Figure 5-7. The sequence of native ES-62 against which both sequencing data sets were compared had been previously determined by both DNA sequencing and N-terminal amino acid sequencing (Harnett *et al.*, 1999), thus it was most likely that these identical mutations arose through PCR and are coincidental.

5.2.3. Optimisation of Infection

Following confirmation of the presence of the ES-62 insert within the pAcGP67-B vector by diagnostic restriction digests, the vector construct was incorporated into the baculoviral DNA by homologous recombination as described in Chapter 2. The virus then underwent several rounds of amplification until a high viral titre, in the region of 2×10^8 pfu ml⁻¹, as assessed by plaque assay, was obtained. This high viral titre stock was used to infect SF9 insect cells for the purpose of expression. In order to optimise expression of the rES-62, SF9 insect cells were infected with high titre viral stock at multiplicities of infection (MOIs) of 3, 7 and 10. Figure 5-18 shows samples of the supernatants of cells infected at each of these MOIs, Western blotted with rabbit polyclonal anti-ES-62 (100 µg ml⁻¹). These blots show that the expressed protein is rES-62, as it reacts positively with the anti-ES-62 antibody, and that there is little difference in the level of expressed protein at each of these three MOIs. A slight increase in the level of expression at a MOI of 10 was observed and thus SF9 insect cells were infected at a MOI of 10 for expression of rES-62.

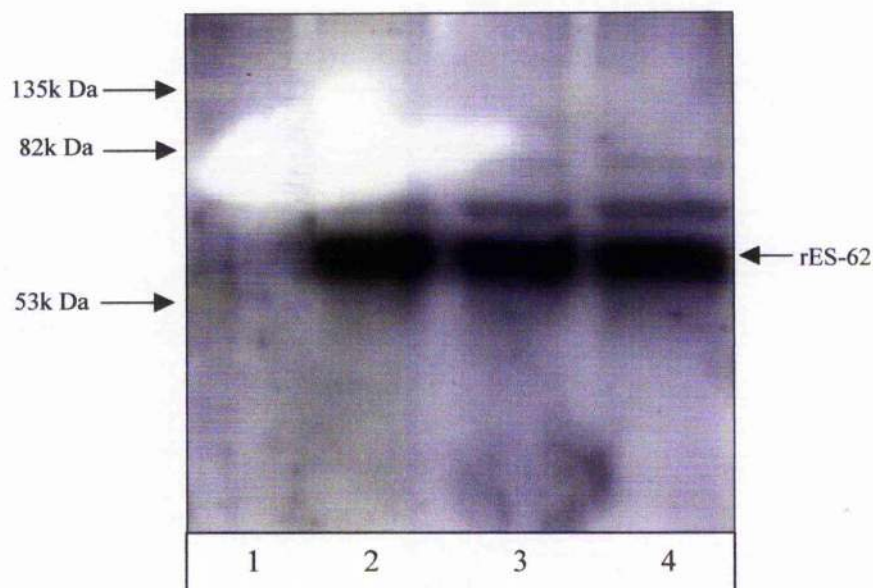


Figure 5-18: Infection of SF9 insect cells with a high titre virus stock of recombinant virus at MOIs of 3, 7 and 10. Samples of the cell supernatant of the cells, 3 days post-infection, were resolved on a 10 % SDS PAGE gel, transferred to nitrocellulose and Western blotted using rabbit polyclonal anti-ES-62 ($100 \mu\text{g mL}^{-1}$) and Amersham anti-rabbit IgG-HRP (1:3000). 1 - control lane: uninfected cells; 2 - cells infected with recombinant baculovirus at a MOI of 3; 3 - cells infected with recombinant baculovirus at a MOI of 7; 4 - cells infected with recombinant baculovirus at a MOI of 10.

5.2.4. Purification

Unlike the bacterial rES-62, the baculovirus rES-62 has no tag to aid purification. However, the recombinant protein is secreted into the protein-free media, containing only amino acids, sugars and lipids. Secretion into the media greatly reduces the number of contaminants, as there are few cellular proteins present in the media. The only other contaminants present at high levels in the supernatant should be recombinant virus particles. These should not affect purification, (PharMingen., 1999) but were removed by centrifugation for 1 hour at 50,000 x g. Three different methods of purification were used to purify baculovirus rES-62; ion exchange, gel filtration and filtration using size cut-off membranes, as used in the purification of the native protein.

5.2.4.1. Ion Exchange

Ion exchange chromatography separates proteins on the basis of their charge. As binding and elution conditions of ion exchange chromatography are typically mild and this method enables relatively good separation of different proteins, it is a popular purification method. Ion exchange chromatography media can be split into two groups; cation exchange in which the chromatography media consists of functional groups with a negative charge and anion exchange in which the chromatography media consists of functional groups with a positive charge. Elution of proteins from ion exchange columns can be achieved by altering the pH of the buffer solution, which in turn alters the charge of the sample molecules bound to the column. Elution can also be achieved by increasing the salt concentration of the buffer solution, which results in the displacement of the bound sample molecules by salt molecules in the buffer solution.

The pI of ES-62 was determined via IEF to be 5.6 (Chapter 2). Figure 5-19 shows that the resolved bands of both the ES-62 and rES-62 lie between the 5.2 and 5.85 markers indicating a pI of ~ 5.6. The native ES-62 band is more disperse, especially when compared to the tight rES-62 bands. This is thought to be due to the heteroglycosylation of the native protein. The pI of 5.6 of ES-62

means it is negatively charged at pH 7 thus anion exchange chromatography using a POROS 20HQ column was used to purify the baculovirus expressed rES-62, as discussed in Chapter 2.

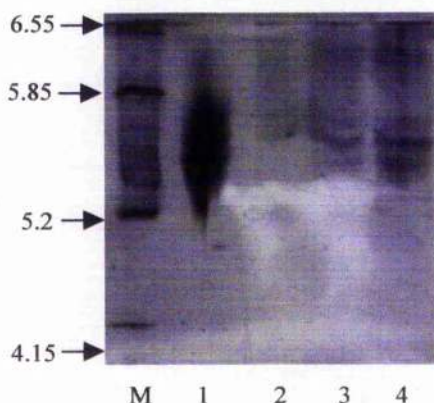


Figure 5-19: An IEF gel of native ES-62 and rES-62. Bands were resolved by silver staining. M – Markers; 1 – native ES-62 (a diffuse band is observed due to the heteroglycosylation of native ES-62); 2-4 – baculoviral rES-62.

Figure 5-20 (a) shows a silver stained 10 % SDS PAGE gel of the fractions collected from a typical anion exchange purification following a wash step of 0.045 M sodium chloride over 10 column volumes, and gradient elution of 0.045 M sodium chloride to 0.3 M over 30 column volumes. A salt concentration of 0.045 M was required during the wash step to remove contaminant proteins. Unfortunately, this concentration also caused elution of a proportion of the rES-62. Reduction of the salt concentration during the wash step was attempted, but this did not sufficiently remove contaminants from the sample. Figure 5-20 (b) is a Western blot of the samples shown in Figure 5-20 (a) probed with rabbit polyclonal anti-ES-62 ($100 \mu\text{g ml}^{-1}$) and Amersham anti-rabbit IgG-HRP (1:3000). These gels confirm that the protein purified was rES-62 and that two forms of rES-62 were produced. The relative levels of these two forms appeared to vary across the fractions collected suggesting that each form might have a slightly different pI value. The difference in pI value might be due to heteroglycosylation of the protein within the insect cells.

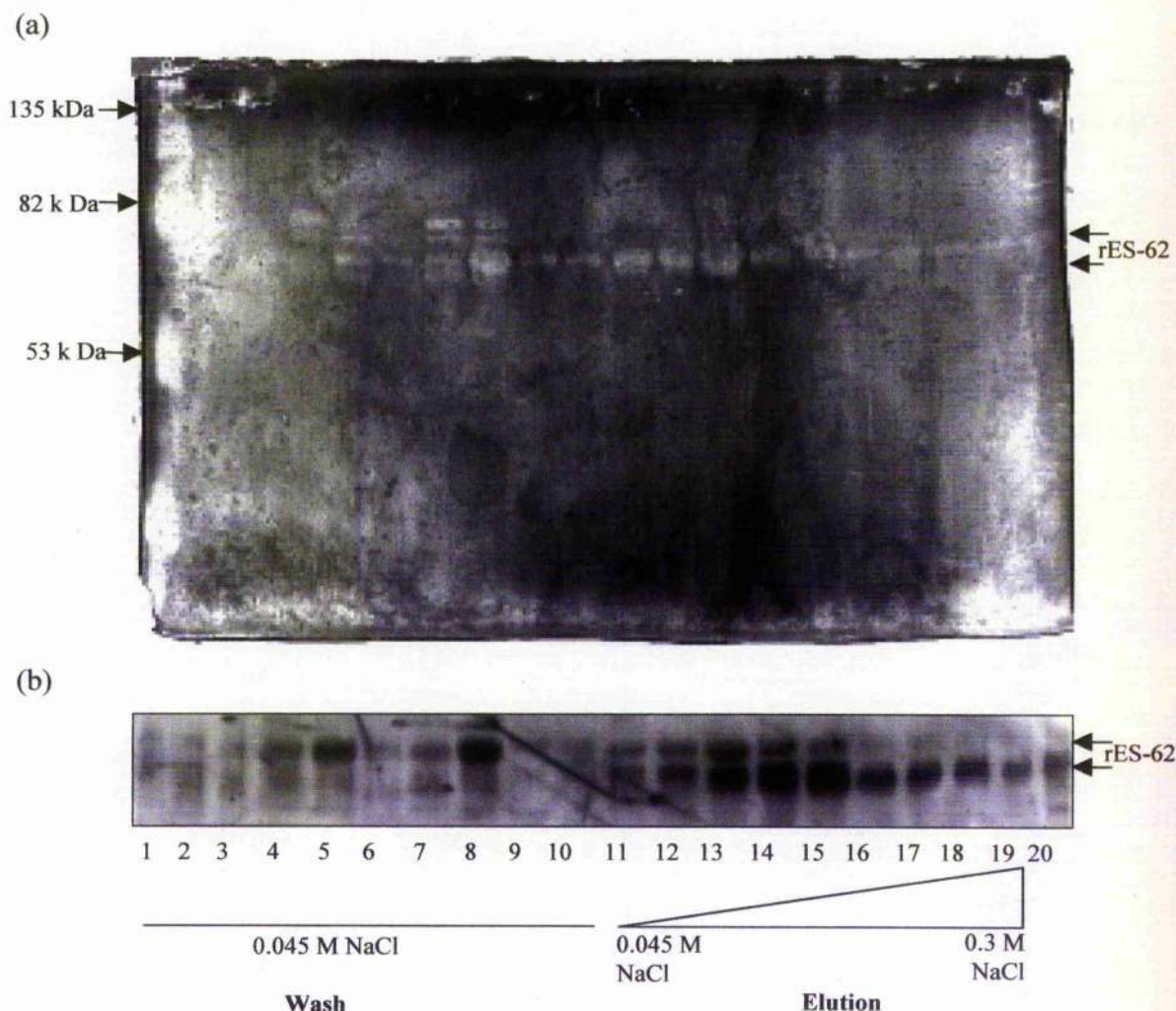


Figure 5-20: Fractions from a typical anion exchange purification. (a) Silver stained gel of the fractions, (b) Western blot of the fractions probed with rabbit polyclonal anti-ES-62 ($100 \mu\text{g ml}^{-1}$) and Amersham anti-rabbit IgG-HRP (1:3000). 1 – marker; 2-10 - wash through fractions following 3 loading steps; 11-19 - elution fractions; 20 is the clean step (1.5 M NaCl).

5.2.4.2. Gel Filtration

Gel filtration or size exclusion chromatography separates molecules on the basis of size. This is achieved due to the special nature of the beads used as chromatographic media, which contain pores of specific sizes. Small molecules can fit through the pores and enter the beads, larger molecules are completely excluded from entering the beads and those molecules between these two extremes can enter the pores to a certain extent. This causes large molecules to pass quickly through the column, while smaller molecules take longer as they pass through the beads and are retarded on their way through the column. To achieve high resolution, a slow flow rate must be employed and the sample load should ideally be 1 % of the column volume. Due to these constraints gel filtration is often used as the final step in purification when the majority of contaminants have been removed and the sample volume is low.

Gel filtration chromatography was tested as a method of purification both on the eluate collected following anion exchange described above and as a first purification step of the protein-free media, into which the recombinant baculovirus expressed protein had been secreted. The use of gel filtration following anion exchange will be described first.

The purified protein obtained from anion exchange was of relatively high purity, however, the anion exchange eluate resolved on a non-denaturing, non-reducing gel (Figure 5-21) contained high and low molecular weight bands possibly relating to monomeric and tetrameric rES-62. To remove contaminants remaining after anion exchange and to separate monomeric and tetrameric rES-62, fractions eluted from anion exchange (identified as containing rES-62) were pooled, concentrated and gel filtration using a Superose 12 (HR 10/30) column was performed as described in Chapter 2.

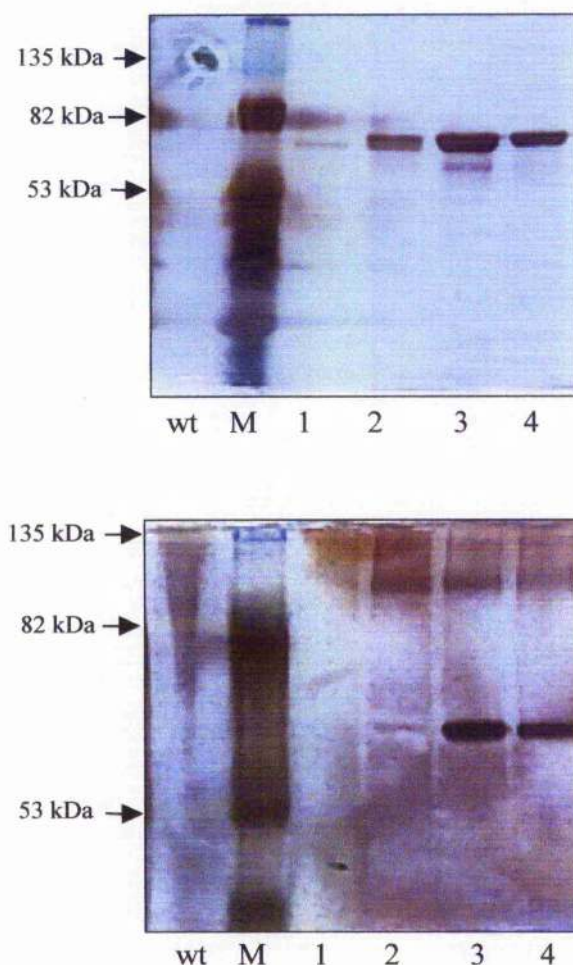


Figure 5-21: (a) Silver stained 10 % SDS PAGE gel of native ES-62 and fractions eluted from anion exchange purification of baculovirally produced rES-62. (b) Silver stained 10 % non-denaturing, non-reducing polyacrylamide gel of native ES-62 and fractions eluted from anion exchange purification of baculovirally produced rES-62. M – marker, WT – native ES-62; 1-4 show fractions eluted following anion exchange.

Gel filtration fractions were initially identified as containing rES-62 by probing dot blots of all fractions eluted with rabbit polyclonal anti-ES-62. Figure 5-22 shows the fractions from gel filtration identified as containing rES-62. Figure 5-22 (a) shows silver stained gels while Figure 5-22 (b) shows Western blots of these fractions probed with rabbit polyclonal anti-ES-62 ($100 \mu\text{g ml}^{-1}$) and Amersham anti-rabbit IgG-HRP (1:3000). Many of the fractions, shown to

contain rES-62, comprise only 1 band (rES-62) indicating that the protein is pure, while others possess a few additional contaminating bands.

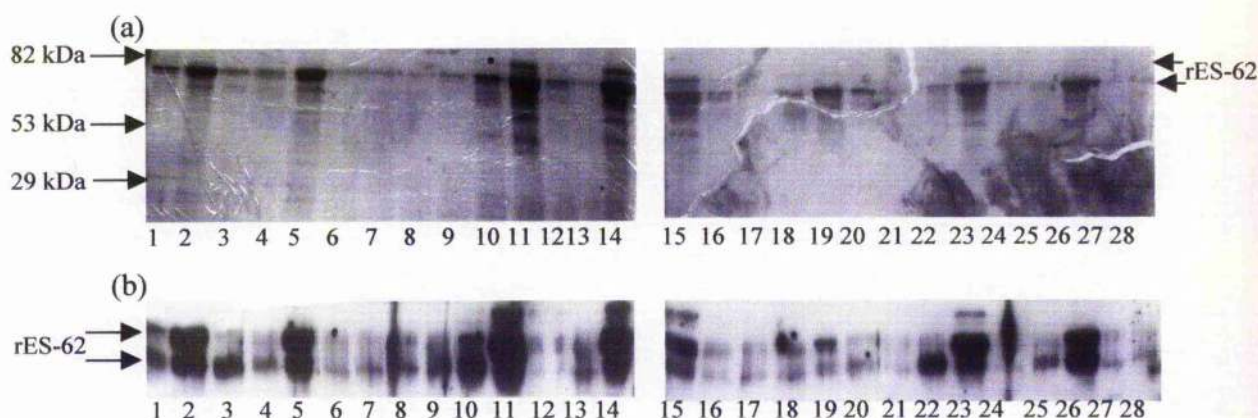


Figure 5-22: Fractions obtained from gel filtration of anion exchange purified rES-62 (lanes 1-28) and of crude supernatant from infected cells (lanes 29-34). (a) Silver stained gels of the fractions, (b) Western blots of the fractions using rabbit polyclonal anti-ES-62 ($100 \mu\text{g ml}^{-1}$) and Amersham anti-rabbit IgG -HRP (1:3000). Arrows mark the rES-62 bands.

Silver staining of proteins in a gel can give rise to artefacts, which make pure samples appear contaminated. To ensure the contaminant bands seen in Figure 5-22 above were not artefacts the fractions were assessed by staining with Coomassie blue dye. Fractions were pooled into two groups; A and B. Pool A contained the fractions that appeared pure from the silver stained gels (fractions corresponding to lanes 1, 3, 4, 6, 7, 8, 9, 12, 13, 16, 17, 18, 19, 20, 21, 22, 24, 25 and 26 in Figure 5-22). Pool B contained the two fractions that appeared to contain only a few contaminating proteins (fractions corresponding to lanes 2 and 5 in Figure 5-22). Samples of pools A and B were resolved on a 10 % SDS PAGE gel and stained with Coomassie blue dye. As shown in Figure 5-23, samples from pools A and B run at the same molecular weight as native ES-62. Pools A and B appear pure, with no evidence of any of the contaminating proteins observed in Figure 5-22. This suggests that the contaminant bands previously observed in those fractions of pool B were either artefacts or

contaminating proteins of concentration less than 0.3-1 μg , the lower level of detection when staining with Coomassie blue dye.

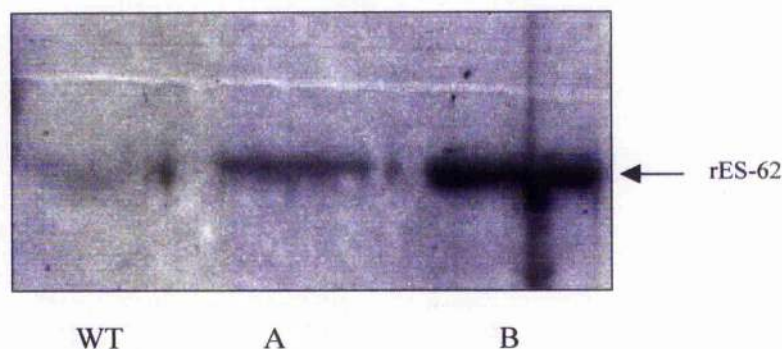


Figure 5-23: 10 % SDS PAGE gels of rES-62 purified by anion exchange and gel filtration (lanes A and B) and stained with Coomassie blue dye. Native ES-62 was run as a control in the lane marked WT.

Typical yields of rES-62 following anion exchange and gel filtration, determined by a BCA protein assay, were approximately 500 μg from 4 flasks of infected SF9 cells, each flask contained 2×10^7 cells in 30 ml protein-free medium ($4 \mu\text{g ml}^{-1}$). To determine the extinction coefficient of rES-62, its absorbance at 280 nm was measured. However, a wavelength scan of the absorbance of rES-62 identified that maximal absorbance occurred at 260 nm rather than 280 nm as would be expected for proteins. This was postulated to be due to the presence of DNA contaminants. Two strategies were employed to remove this contamination. The first was centrifugation of the sample, in a Beckman ultracentrifuge, at 50000 x g for 1 hour. This removes baculovirus particles from the sample. The second was treatment of the samples with DNase to remove DNA contaminants by digestion. Unfortunately, neither of these strategies resulted in a shift in the maximal absorbance from 260 to 280 nm. This suggests that either rES-62 can bind DNA present in the supernatant from the infected cells, thus preventing its removal or that the absorbance peak at 260 nm is attributable to another, unidentified source. This made the rES-62 unacceptable for experimentation and necessitated another appraisal of the purification strategy.

As an alternative purification method, gel filtration was also performed on crude protein-free media, into which rES-62 had been secreted. Figure 5-24 (a) shows the fractions eluted and resolved on a 10 % SDS PAGE gel subsequently silver stained. Figure 5-24 (b) shows these fractions Western blotted with rabbit polyclonal anti-ES-62 ($100 \mu\text{g ml}^{-1}$) and Amersham anti-rabbit IgG-HRP (1:3000). Fractions obtained from gel filtration of crude material show surprisingly few contaminants, in some cases appearing purer than those obtained from anion exchange and gel filtration together. However, there was no appreciable difference in the yield of rES-62 obtained by gel filtration alone compared to that obtained by anion exchange and gel filtration. Similarly to the results observed from anion exchange purification (Figure 5-20), there appear to be two forms of rES-62 expressed and purified from the baculovirus expression system. The two forms of rES-62 may represent heteroglycosylated forms of the protein. In order to investigate possible heteroglycosylation of rES-62 by insect cells, further work including separation of the two forms of rES-62 and examination by mass spectroscopy to compare their carbohydrate content would be necessary.

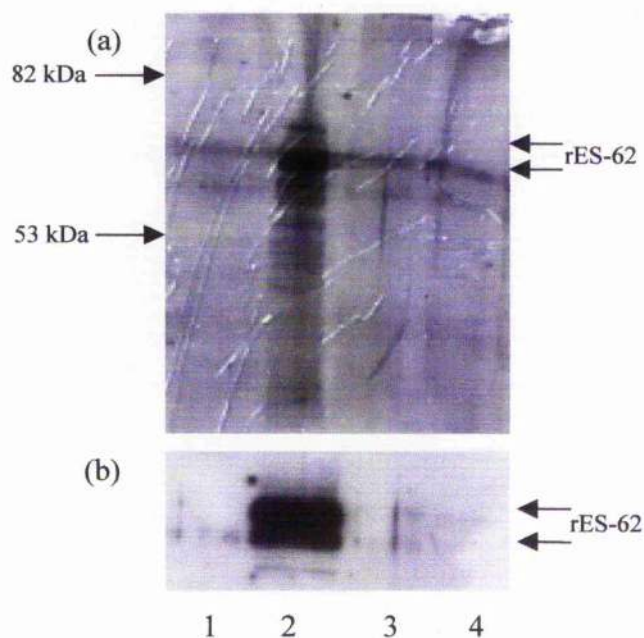


Figure 5-24: Fractions obtained from gel filtration of the protein-free media from infected cells (lanes 1-4). (a) Silver stained gel of the fractions, (b) Western blot of the fractions using rabbit polyclonal anti-ES-62 ($100 \mu\text{g ml}^{-1}$)

¹) and Amersham anti-rabbit IgG -HRP (1:3000). Arrows mark the rES-62 bands.

Gel filtration appears to improve the purity of the sample obtained both when used in conjunction with anion exchange and when used alone. Due to the bed volume of the gel filtration column (200 ml), only 200 μ l of sample could be loaded thus this purification step, when used on crude material rather than that obtained following anion exchange, was very time consuming and not practical for the purification of large amounts of rES-62. However, in both cases possible DNA contaminants, as discussed above, appear to be present thus the rES-62 is not acceptable for either biological or biophysical experimentation.

5.2.4.3. Filtration

Native ES-62 is purified using a series of molecular weight cut-off membranes in an ultrafiltration stirred cell. A similar strategy was used to remove some of the contaminants and separate monomeric and tetrameric rES-62. This was an alternative purification method and allowed enrichment and concentration of either the crude protein-free media from infected insect cells or the eluate from anion exchange.

Two molecular weight cut-off membranes were used, one with a cut-off of 100 k Da (YM 100), which should retain only tetrameric rES-62, and a second with a cut-off of 30 k Da (YM 30), which should retain anything with a mass above 30 k Da, as described in Chapter 2. Figure 5-25 shows a SDS PAGE gel stained with Coomassie blue dye and a Western blot of the samples of proteins retained by the YM 100 and YM 30 filters. The YM 100 filter retains the majority of the recombinant material, indicating that it is above 100 k Da in size and not monomeric. The recombinant material retained by the YM 30 filter appears purer than that retained by the YM 100 filter. This difference in purity may be due to the existence of degradation products, as some of the bands of the YM 100 fraction observed on the gel stained with Coomassie blue dye react positively with the anti-ES-62 antibody. Filtration appears to successfully separate

recombinant monomeric and tetrameric ES-62. However, the presence of contaminants indicates that filtration alone is insufficient for purification of rES-62. An optimal purification strategy would be a combination of filtration and anion exchange.

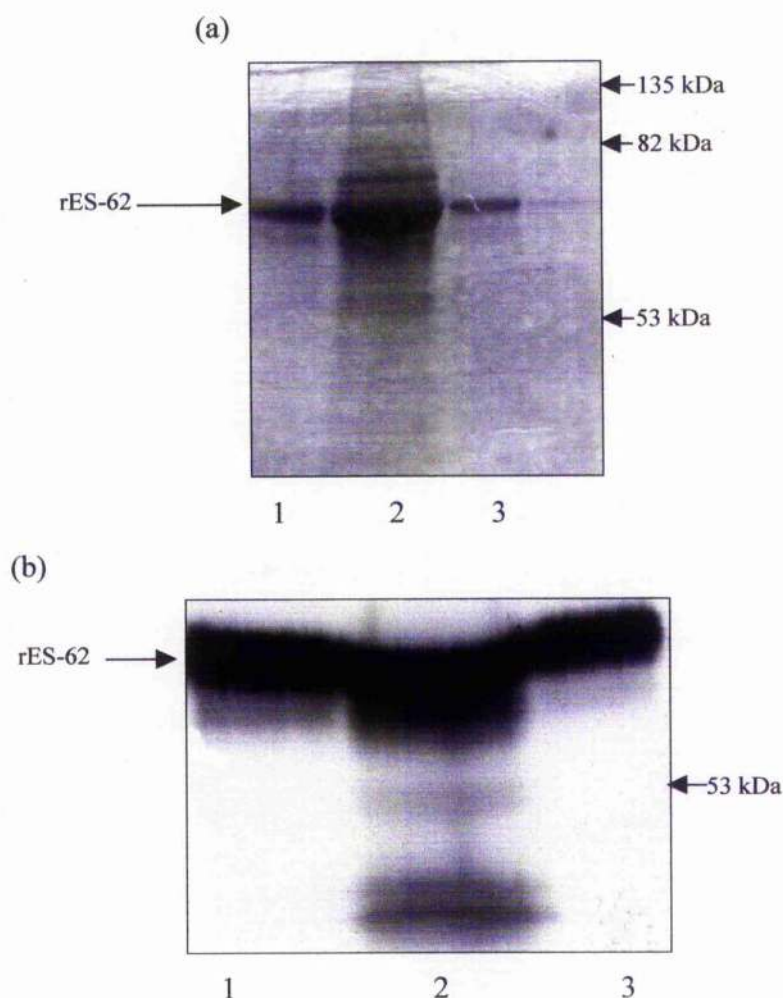


Figure 5-25: Purification of baculovirus rES-62 from infected cell supernatants using YM 30 and YM 100 filters in an ultrafiltration stirred cell. (a) SDS PAGE gel stained with Coomassie blue dye, (b) Western blot using rabbit polyclonal anti-ES-62 ($100 \mu\text{g ml}^{-1}$) and anti-rabbit IgG-HRP (1:3000). Lane 1 – crude media from infected cells; lane 2 – proteins from the infected cell supernatant retained by the YM 100 membrane and dialysed into PBS; lane 3 – proteins from the infected cell supernatant retained by the YM 30 membrane and dialysed into PBS.

Purification of rES-62 using molecular weight cut off membranes appeared to be a hopeful first step however, during the optimisation of the purification strategy for rES-62 the yields of rES-62 being expressed by the baculovirus system were found to decrease. To overcome this problem, fresh SF9 cells were brought up from storage in liquid nitrogen, fresh TMN-FH and protein-free media were used and new infective stock prepared. However, the yields of rES-62 expressed by the baculovirus system failed to improve. As a result a number of different conditions were then employed both for expression and purification of rES-62.

Infections of SF9 cells were previously carried out at a MOI of 10 following optimisation of infection. In order to test if the decrease in yield of rES-62 was due to excessively high levels of expression overloading the cellular post-translational modification machinery, infection at a MOI of 1 was compared with that at a MOI of 10. It was also proposed that the pH of the SF9 cell medium (pH 6.2) might be promoting the poor yields of rES-62. ES-62 is known to be stable at pH 7 and monomerises at pHs below 7 (section 5.1.4). SF9 cells were thus infected at both MOIs in normal medium and in medium adjusted to pH 7. In addition, the method employed to clarify the protein free media containing the secreted rES-62 was also examined. In all the expression trials, i.e. at MOIs of 10 and 1 and at pH 6.2 and 7, half the sample was spun at 50,000 x g for 1 hour and the other half treated with DNase to remove any virus particle or DNA contamination respectively. An illustration of the conditions tested is shown in Figure 5-25.

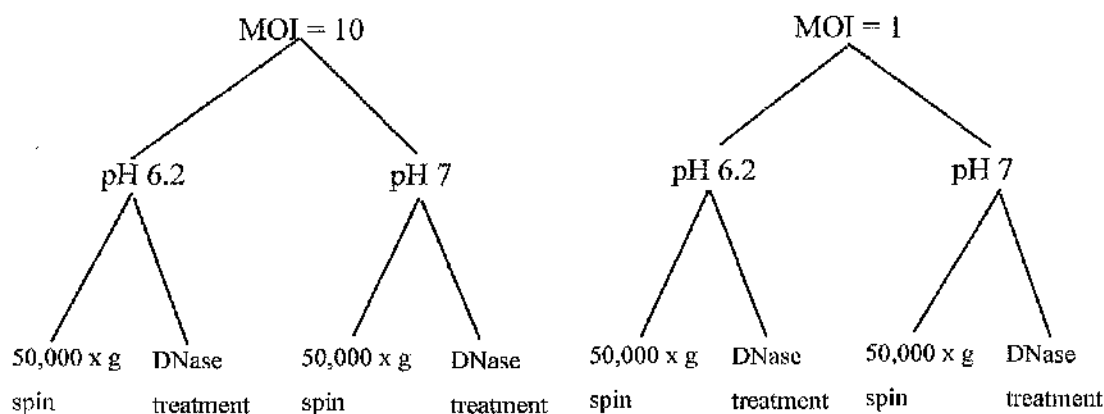


Figure 5-26: Conditions tested for baculovirus expression of rES-62.

The rES-62 obtained from each condition tested was then purified using filtration as discussed above (section 5.2.4.3 & Chapter 2). The samples obtained from these purifications were then resolved on a series of SDS PAGE and non-denaturing, non-reducing polyacrylamide gels as shown in Figures 5-27 and 5-28. No rES-62 was present in the SF9 cellular pellets however, small amounts were present in the pellet obtained following the 50,000 x g ultracentrifuge spin, perhaps suggesting that rES-62 can bind viral DNA.

As shown in Figures 5-27 (a) and 5-28 (a), levels of rES-62 obtained following purification were again higher following infection of SF9 cells at a MOI of 10 than at a MOI of 1. This substantiates the earlier optimisation studies, which demonstrated that infection of SF9 cells at a MOI of 10 yielded the highest levels of rES-62 expression. Adjusting the pH of the SF9 cellular medium from pH 6.2 to 7, not only affected the growth of the SF9 cells which were less adherent and no longer round in appearance, but also led to reduced levels of rES-62 obtained following purification. As the protein-free SF9 media has presumably been optimised for growth of SF9 cells and given the changes in the SF9 cells when grown in pH 7 media this finding is perhaps not surprising. The final condition tested, the method of clarification of the medium harvested from infected SF9 cells, appeared to have no effect on the levels of rES-62 obtained following purification. Wavelength scans of samples of the purified protein, clarified by either the 50,000 x g ultracentrifuge spin or by DNase treatment also revealed that the maximum absorbance of the samples had not been shifted and remained at 260 nm. This indicated that the DNA contamination was still present. Figures 5-27 (a) and 5-28 (a) show that rES-26 was present, as a very faint band, and that it appears to have been resolved at a corresponding position on the gel as the native protein. The heavily stained band of Figures 5-27 (b) and 5-28 (b) does not appear to be rES-62 as it does not run at the same molecular weight as native ES-62. The faint staining observed for rES-62 indicates that the levels of rES-62 resolved on the gels were at the lower limit of detection when staining with Coomassie blue dye (0.3-1 μ g). The yield of rES-62 obtained from baculovirus expression was less than 100 μ g per flask of 2×10^7 SF9 cells in 30 ml medium (3 mg L⁻¹)

Figure 5-27: Medium harvested from SF9 cells infected with recombinant baculovirus particles at MOIs of 1 and 10 in cell culture media at pH 6.2 and 7. The medium harvested from SF9 cells infected at different MOIs (10 or 1) and at different pHs (6.2 or 7.0) was clarified by either ultracentrifugation or DNase treatment and then purified by filtration through molecular weight cut off membranes as described in Chapter 2. M – markers, wt - wild type ES-62, 1 indicates sample was spun at 50000 x g for 1 hour, 2 indicates sample was treated with DNase. 100 k or 30 k filter shows samples retained by the 100 k Da or 30 k Da filter respectively. (a) Samples resolved by SDS-PAGE, transferred to nitrocellulose and Western blotted with anti-ES-62 antibody. (b) Samples resolved by SDS-PAGE and stained with Coomassie blue dye.

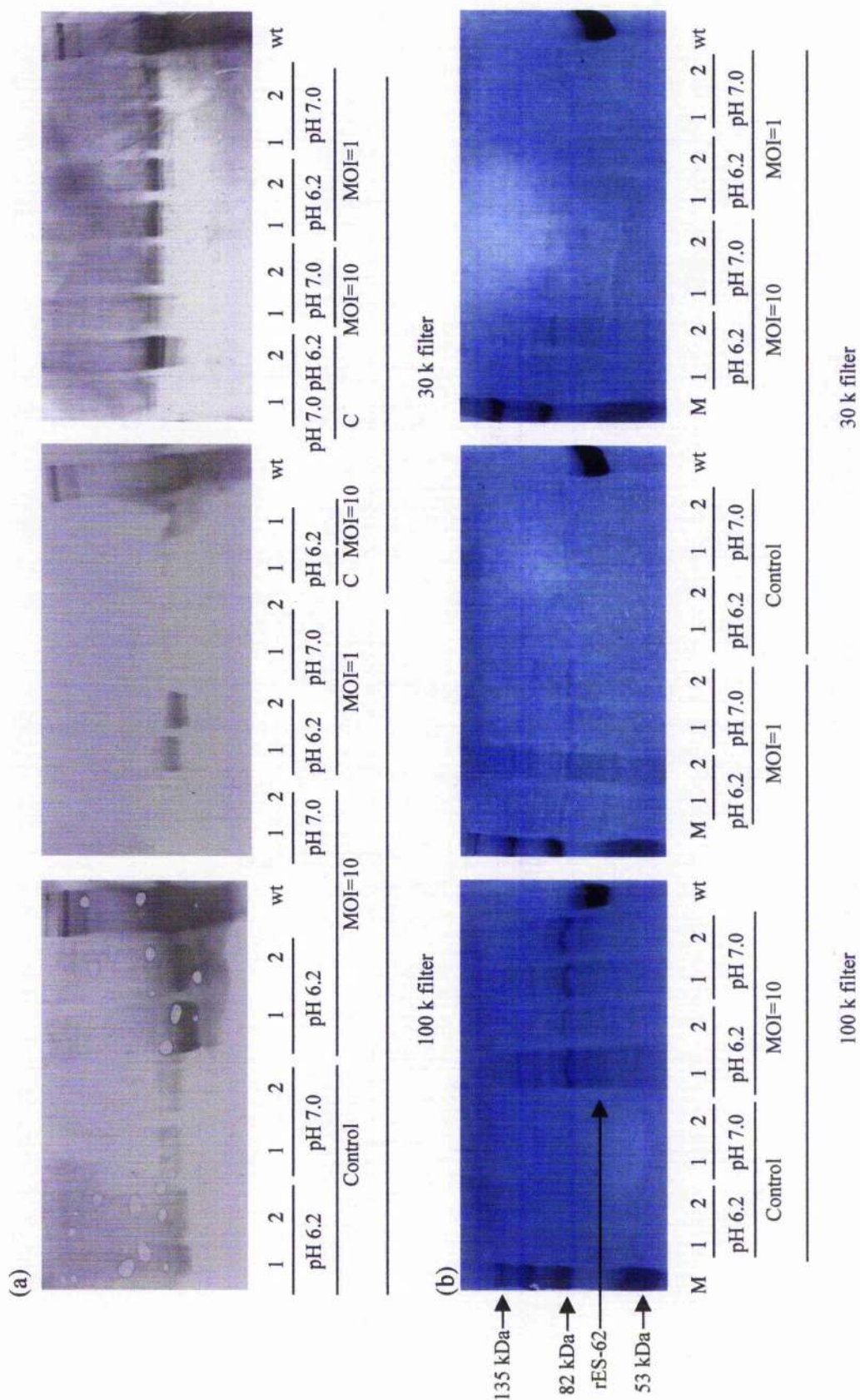
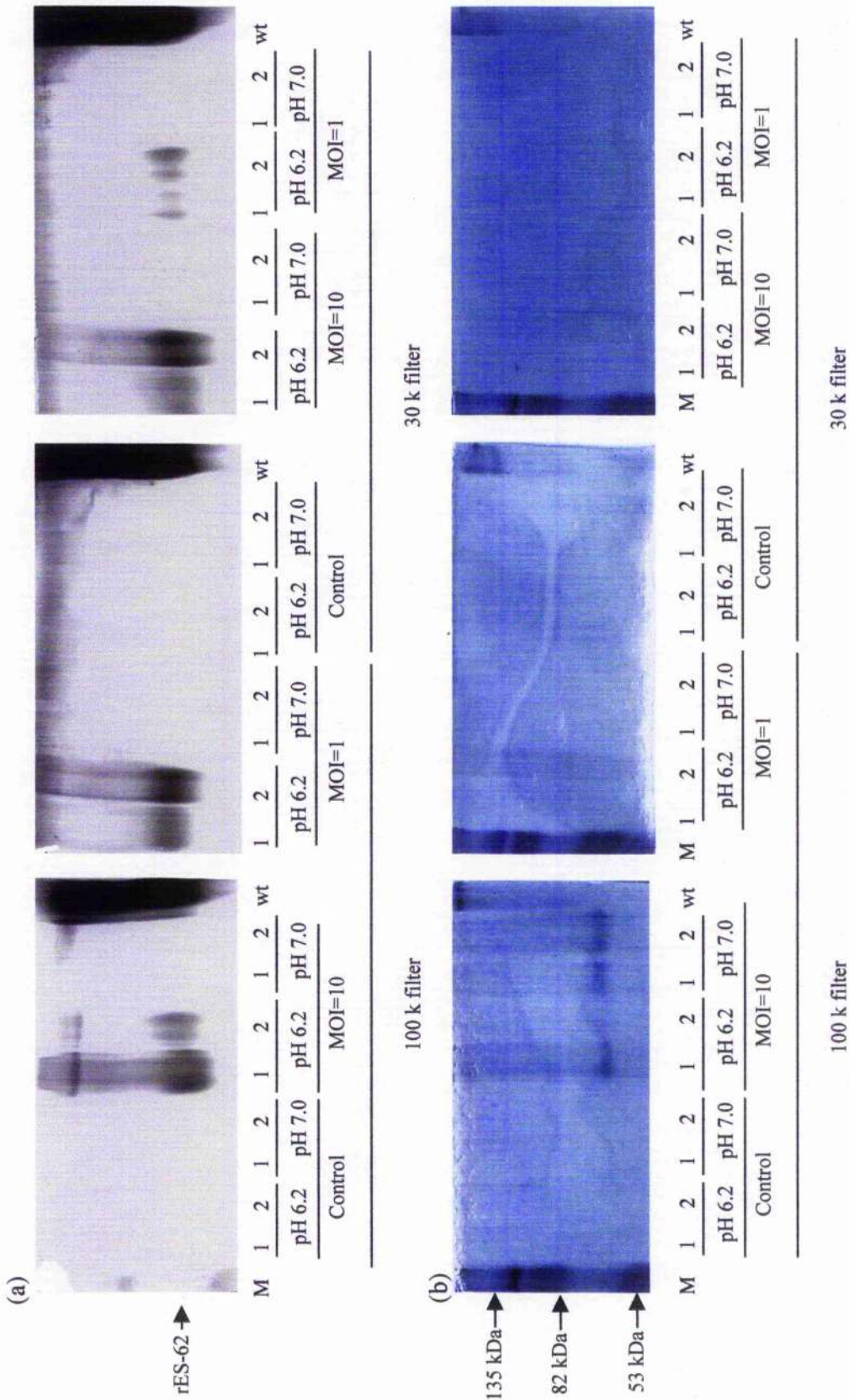


Figure 5-28: Medium harvested from SF9 cells infected with recombinant baculovirus particles at MOIs of 1 and 10 in cell culture media at pH 6.2 and 7. The medium harvested from SF9 cells infected at different MOIs (10 or 1) and at different pHs (6.2 or 7.0) was clarified by either ultracentrifugation or DNase treatment and then purified by filtration through molecular weight cut off membranes as described in Chapter 2. M – markers, wt - wild type ES-62, 1 indicates sample was spun at 50000 x g for 1 hour, 2 indicates sample was treated with DNase. 100 k or 30 k filter shows samples retained by the 100 k or 30 k filter respectively. (a) samples resolved on non-denaturing, non-reducing polyacrylamide gels, transferred to nitrocellulose and Western blotted with anti-ES-62 antibody. (b) samples resolved on non-denaturing, non-reducing polyacrylamide gels and stained with Coomassie blue dye.



DNA contamination of the rES-62 was not removed using either of the two methods described above. Thus the rES-62 obtained was unacceptable for use in biological and biophysical experiments. The DNA contamination would have to be overcome before further development of the purification strategy for rES-62 and biological experimentation utilising rES-62 would be possible.

5.2.5. Testing Recombinant ES-62

Utilising the baculovirus expression and purification strategy described above, further characterisation of the rES-62 was performed. As discussed, with reference to Figures 5-18, 5-20 and 5-22, Western blot analysis of gels of purified rES-62 show that the expressed protein is recognised by the polyclonal anti-ES-62 antibody. To determine if the rES-62 was correctly folded, slot blot analysis was performed utilising a monoclonal antibody, raised in mouse, known to recognise a conformational epitope of native ES-62. Figure 5-29 compares recognition of native and rES-62 by the monoclonal antibody. rES-62 is recognised by the monoclonal antibody suggesting that at least some of the recombinant protein is folded, or at least folded in the region of the conformational epitope.

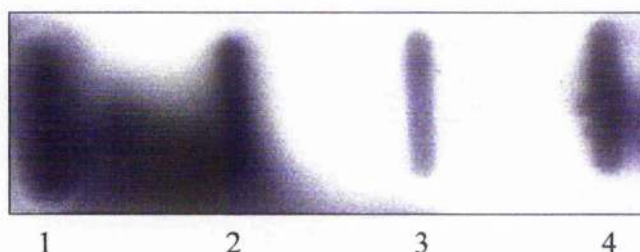


Figure 5-29: Recognition of baculovirus rES-62 by monoclonal anti-ES-62. Baculovirus rES-62 samples (200 μ l) were dotted onto nitrocellulose using a slot blotter. The nitrocellulose was blocked with 1 % BSA in TBS for 1 hour and then probed with mouse monoclonal anti-ES-62 serum (1:500) and Amersham anti-mouse-HRP (1:3000). 1 is native ES-62 control, 2 is pool A of rES-62, 3 is pool B of rES-62 and 4 is the pool of rES-62 purified from crude protein-free media from infected SF9 cells by gel filtration alone. Pools A and B are the pooled rES-62 samples discussed earlier and shown in Figure 5-23.

In addition, Western blotting of rES-62 was performed with TEPC-15 (anti-PC) antibody. Following treatment of the transferred nitrocellulose membrane as discussed in Chapter 2, no bands were visualised. This indicates that, as anticipated, the recombinant material being produced by the baculovirus expression system does not appear to have PC moieties attached to its carbohydrate chains.

5.3. *Conclusions*

Expression of rES-62 was achieved in the Novagen pET 19b bacterial expression system. However, the majority of rES-62 produced was insoluble and present in inclusion bodies within the bacterial cells. Refolding of the insoluble rES-62 was performed, but only a small proportion was successfully refolded. Optimisation of expression, lysis and purification of the soluble rES-62 obtained was carried out and both the soluble rES-62 and the refolded rES-62 purified using metal chelate chromatography. Purification of the soluble rES-62 yielded a significant amount of recombinant material - approximately 10 mg from 6 L of bacterial culture. Unfortunately small angle x-ray scattering and analytical ultracentrifugation studies revealed that the rES-62 was highly aggregated and unsuitable for biophysical studies or *in vivo* experimentation.

Native ES-62 is a tetramer of approximately 230 k Da, 6 % of which is carbohydrate. Native ES-62 also possesses phosphorylcholine moieties attached to some of its carbohydrate chains. The quaternary structure of native ES-62 and the post-translational modification that occurs could explain the inability of a bacterial expression system to produce soluble, non-aggregated rES-62. Bacterial expression systems are incapable of post-translational modification thus the rES-62 produced will not be glycosylated and hence will also not possess phosphorylcholine moieties. Although this was precisely the reason for selecting a bacterial expression system, to allow study of the protein component of ES-62 alone, it may also be a factor in the inability of this expression system to produce suitable rES-62. A number of hypotheses exist as to why the bacterial expression system did not appear to yield suitable protein. These include: (1) glycosylation

in native ES-62 may mask hydrophobic regions and thus the lack of glycosylation in rES-62 may result in aggregation of the protein produced. (2) Glycosylation may be essential for the correct folding of ES-62. Native ES-62 cannot be deglycosylated without being denatured thus it is possible that the carbohydrate chains form an integral part of the structure of ES-62 and that without them the protein cannot fold correctly and thus aggregates. (3) Native ES-62 is tetrameric. It is possible that tetramerisation is dependent on glycosylation of the monomeric units. The rES-62, which is not glycosylated, may not be able to correctly form tetrameric units and the deglycosylated monomer units may instead aggregate randomly, causing the observed insoluble nature of the recombinant protein.

The aggregated nature of the bacterially produced rES-62 prevented study of the protein component of ES-62 alone. However, it provided a valuable insight into the vital structural role that the carbohydrate chains may play in the folding of native ES-62 and substantiated the suggestion from attempts to deglycosylate the native protein that the carbohydrate chains of ES-62 are an integral part of the structure of native ES-62.

Expression of rES-62 in the PharMingen baculovirus expression was successful and rES-62 was produced and purified. However, DNA contamination of the recombinant protein precluded characterisation of rES-62 via biophysical or biochemical studies. Optimisation of the purification strategy for rES-62 produced by baculovirus determined that molecular weight cut-off membranes were able to separate monomeric and tetrameric forms of rES-62, but were not sufficient to remove other contaminants present in the medium to yield pure rES-62. The use of anion exchange and gel filtration yielded rES-62 purer than that obtained from the use of molecular weight cut-off membranes, however, anion exchange was unable to separate monomeric and tetrameric forms of rES-62 and gel filtration suffered from restrictions on the sample size which could be loaded and successfully resolved. Concentration of the sample to be loaded onto the gel filtration column resulted in a loss of rES-62, which was thought to be due to rES-62 sticking to the membrane of the concentration device. A combination of

anion exchange and filtration is considered to be the optimal purification strategy. Analysis, by absorbance measurement, of purified rES-62 obtained using either anion exchange or filtration indicated that the protein obtained was contaminated, possibly by DNA. This contamination would need to be overcome before the purification strategy could be developed further.

DNA contamination was shown to remain following either DNase treatment of the samples or ultracentrifugation at 50,000 x g to pellet the viral particles. Studies performed with native ES-62, as discussed in Chapter 6, indicated that native ES-62 localises to the nucleus of cells, thus it is conceivable that ES-62 might bind directly to DNA. Although initial experiments involving the incubation of native ES-62 with digested genomic DNA from macrophages and WEHI-231 B cells were inconclusive, binding of ES-62 to DNA might protect DNA from DNase, preventing digestion of contaminating DNA. The hypothesis that ES-62 binds to DNA is supported by additional work discussed in section 6.3.4 which indicated that ES-62 is translocated to the nucleus. In addition, as discussed in chapter 3, ES-62 possesses a leucine rich region (Harnett *et al.*, 1999b). Leucine rich zipper motifs are known to mediate DNA binding. Alternatively maximal absorbance at 260 nm may be indicative of the protein being incorrectly folded giving rise to anomalous absorbance.

Further work on this expression system would allow the study of the influence of the phosphorylcholine moieties on the immunomodulatory capabilities of native ES-62. The role of the PC moieties has been studied by comparing the signalling occurring in cells following incubation with PC or PC conjugated to BSA, with the signalling that occurs following incubation with ES-62 (Harnett *et al.*, 1999a). These studies show that PC can induce many, but not all of the effects induced by ES-62, indicating an important role for the PC moieties of ES-62. rES-62 lacking PC moieties would allow the effects induced by the protein component of ES-62 to be studied in more depth perhaps identifying a distinction between those effects induced by PC and those induced by the protein component of ES-62. One hypothesis proposed is that the PC moieties induce immunomodulatory effects which allow ES-62 to gain access to the cells where,

once internalised, ES-62 can induce further longer term immunomodulatory effects which mask the presence of the parasite and the microfilariae from the infected hosts' immune system.

6. Mammalian Cell Response to ES-62

The effects of ES-62 on cells of the immune system, in particular the effects on B lymphocytes, have been studied in depth (Deehan *et al.*, 1998a; Deehan *et al.*, 1998b; Goodridge *et al.*, 2001; Harnett & Harnett, 1999a; Harnett *et al.*, 1999; Harnett & Harnett, 1993; Harnett *et al.*, 1989). These studies have shown that ES-62 polyclonally activates certain protein tyrosine kinases (PTKs) and MAP kinase signal transduction elements and modulates PKC activity and expression leading to desensitisation of both B and T lymphocytes to subsequent antigen receptor mediated activity. In addition, effects of ES-62 on antibody production and cytokine release lead to a biasing of the immune response to a Th2 type phenotype which appears to be beneficial to the filarial nematode, allowing it to survive for long periods within the host. Some of the effects described can be mimicked by treatment of cells with PC alone (Harnett & Harnett, 1993) suggesting an important role for the PC moieties of ES-62. Although the effects induced by ES-62 have been studied, the receptor to which it binds is unknown, as is whether ES-62 requires to be internalised to induce its effects.

Previous work examining the binding of ES-62 to the membranes of monocytes, B lymphocytes and T lymphocytes and whether this binding was PC dependent had been performed using BiaCore technology (M. M and W. Harnett; Unpublished). BiaCore technology allows the identification of biomolecules and the monitoring of the kinetics of interaction between two biomolecules without the use of labels. It is based on surface plasmon resonance. As shown in Figure 6-1, light is directed at and reflected from the side of the surface of the BiaCore chip opposite to that which biomolecules can bind. Surface plasmon resonance causes reductions in reflected light intensity at particular wavelengths and angles. The binding of a biomolecule to the surface of the chip alters the refractive index and results in an alteration in the surface plasmon resonance (SPR) signal obtained.

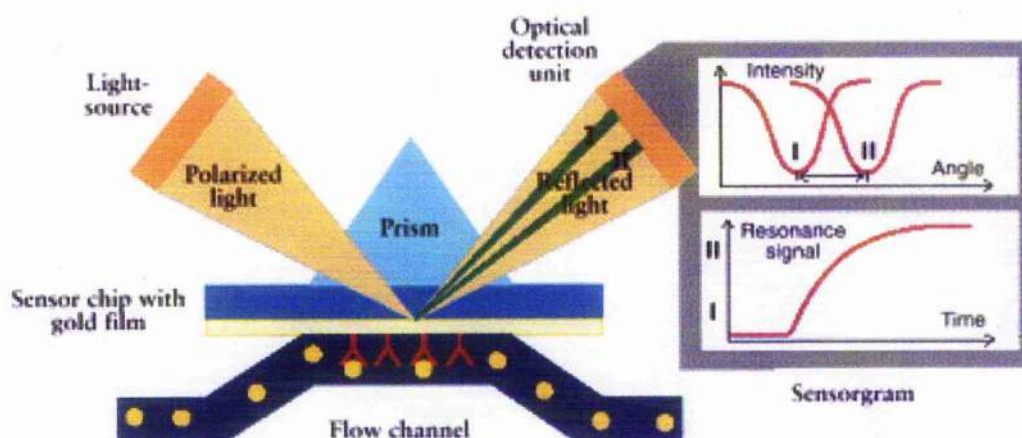


Figure 6-1: BiaCore technology (taken from the BiaCore web site

<http://www.biacore.com/biomol/biomol.shtml>) Polarised light is reflected off the back surface of the sensor chip to which specific molecules can bind. The intensity of the reflected light (also known as the SPR signal) is measured by the optical detection unit. In the diagram shown, antibody molecules, which can recognise and bind a specific molecule (antigen), are attached to the surface of the sensor chip. Sample is injected into the flow channel and passes across the sensor chip. Binding of the antigen to the immobilised antibody results in a change in the refractive index of the chip, leading to a change in the SPR signal obtained. This alteration in SPR signal is detected by the optical detection unit and provides information on the kinetics of the binding of the antigen to the antibody.

Cell membranes from splenic B cells, U937 cells (monocytic cell line) and Jurkat cells (T cell line) were injected across a BiaCore chip surface to which ES-62 had been covalently attached and the kinetics of binding recorded. Figure 6-2 shows the graphs obtained for the binding of ES-62 to the membranes of these three immune system cell types.

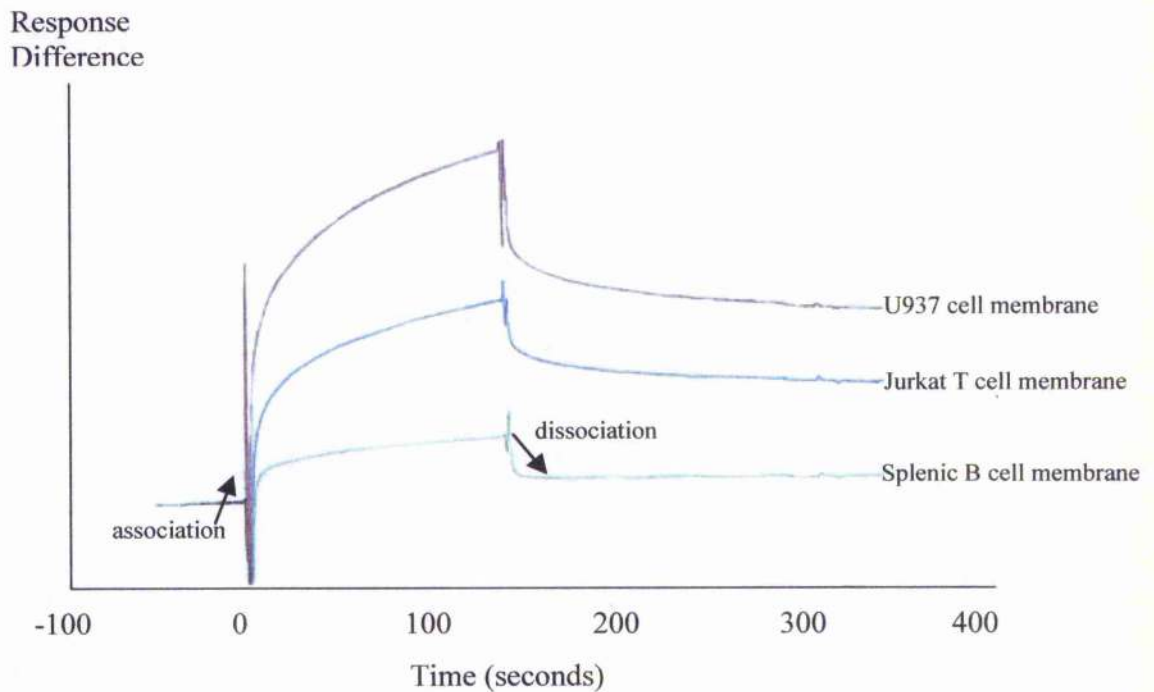


Figure 6-2: BiaCore analysis of the binding of membranes of U937 (monocytic) cells, B cells and Jurkat T cells to ES-62. – Monocytic membranes, – Jurkat (T cell line) cell membranes and – Splenic B cell membranes binding to ES-62. ES-62 was covalently attached to the sensor chip and the chip inserted into the BiaCore machine. The membrane under investigation was then injected into the BiaCore machine and washed over the sensor chip. On binding to ES-62 an increase in the SPR signal was seen. The rate of the increase in the SPR signal gives a measure of the kinetics of binding. Following injection of the sample under investigation, the sensor chip was washed in buffer and a decrease in the SPR signal was observed which corresponds to the dissociation of the cellular membrane from the chip bound ES-62. The rate of this decrease in SPR signal corresponds to the kinetics of dissociation. Progress of the different stages of interaction (association and dissociation) for splenic B cell membrane is shown.

As shown in Figure 6-2, binding of ES-62 to the membranes of splenic B cells, U937 monocytic cells and Jurkat T cells was observed to occur with different kinetics. ES-62 bound to splenic B cell membranes with rapid association and dissociation kinetics. Binding to U937 cell membranes occurs with much slower association and dissociation kinetics to those observed for binding to both splenic B and Jurkat T cell membranes. The differences in the kinetics of binding of ES-62 to splenic B, Jurkat T and U937 cell membranes implies that each of these cell types possess one or more molecules on their surface that ES-62 can exploit to elicit its effects and thus different molecules may be exploited as receptors for ES-62 on different cell types. Further studies in which TEPC-15 (anti-PC antibody) was passed across the BiaCore chips to which ES-62 was attached prior to injection of the cell membranes of splenic B cells, U937 monocytic cells or Jurkat T cells into the flow cell found that binding of ES-62 to its receptors on these cell types was inhibited. This inhibition of binding of ES-62 to membranes following blockage of its phosphorylcholine moiety suggests that binding of ES-62 to receptors on the cell types is PC dependent.

It is known that PC is present on a number of different pathogens and is often involved in the entry of these pathogens into the host cells. This, in conjunction with the PC dependency of the binding of cellular membranes to ES-62, raised the possibility that the PC moiety of ES-62 could be responsible for receptor recruitment. A number of receptors, known to be expressed on B, T and monocytic cells, are known to recognise PC or act as pattern recognition receptors. The receptor for platelet activating factor (PAF) is known to interact with PC-containing bacteria (Cundell *et al.*, 1995) and the toll-like receptor (TLR) family are pattern recognition receptors. Both TLRs and the PAF receptor demonstrate downstream signalling events similar to those induced in response to ES-62.

6.1. Platelet Activating Factor Receptor

Platelet activating factor (PAF) is a unique phospholipid mediator which possesses potent proinflammatory, smooth muscle contractile and hypertensive activities. It is crucial in the pathogenesis of bronchial asthma and in the lethality of endotoxin and anaphylactic shock (Honda *et al.*, 1991; Seyfried *et al.*, 1992). The platelet activating factor receptor (PAF-R), which recognises PAF and through which PAF induces its effects, is encoded by a single gene on human chromosome 1 (Honda *et al.*, 1991). It is a seven transmembrane G protein coupled receptor (GPCR) of 39 kDa as shown in Figure 6-3 below.

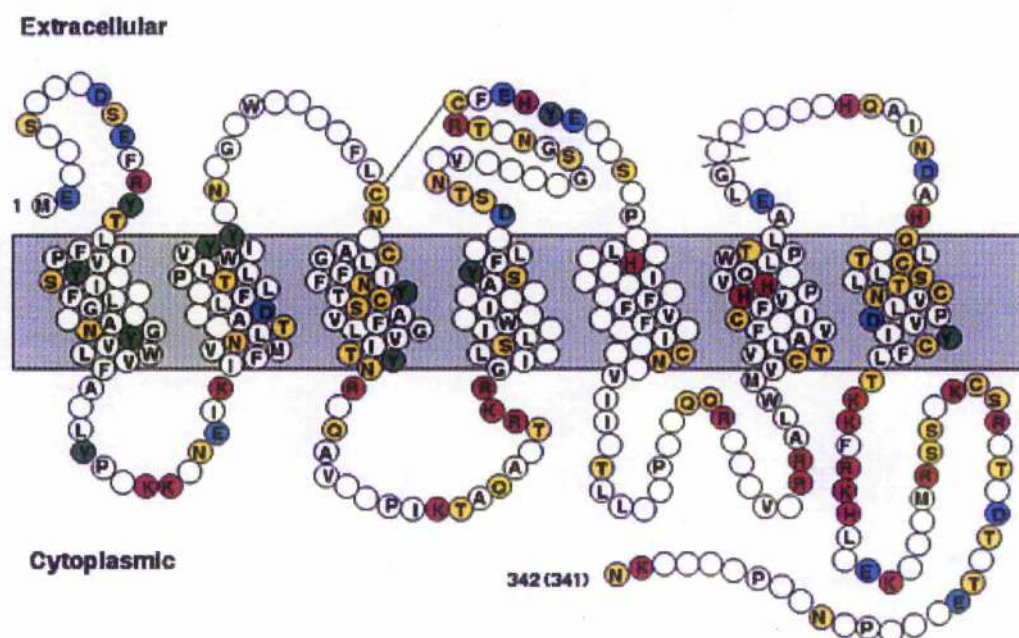


Figure 6-3: PAF-R structure. Amino acids in coloured characters are conserved among guinea-pig, human and rat PAF-R. Images taken from <http://www.biochem2.m.u-tokyo.ac.jp/web/contents/PAFR.html>

GPCRs form a large family of proteins with a diverse range of functions, which can be separated into distinct sub families on the basis of amino acid sequence. PAF-R belongs to the rhodopsin like family of GPCRs and is known to participate in the trafficking of leucocytes, generation of broncospasms and inflammation in asthma (Cundell *et al.*, 1995).

Following interaction with ligand, the PAF-R modulates certain B cell activation responses in a similar fashion to the B cell suppression induced by ES-62, for example Erk and p38 forms of mitogen activated kinase are activated but jun is not (Marques *et al.*, 2002). In addition, PAF-R rapidly internalises following ligand binding (Gerard & Gerard, 1994). The PAF-R is known to be expressed on B, T and monocytic cells and has been shown to act as the receptor for *Streptococcus pneumoniae* which expresses PC on its surface (Cundell *et al.*, 1995) allowing *S. pneumoniae* to gain access to host cells through the internalisation of the PAF-R. These factors raised the possibility of PAF-R acting as the receptor for ES-62, binding via the PC moieties (Harnett & Harnett, 1999a; Harnett & Harnett, 1999b). The use of PAF-R by ES-62 could allow ES-62 to gain entry into the host cells to elicit its immunomodulatory effects or alternatively, ES-62 may desensitise cells to subsequent activation by abortive signalling via the PAF-R (Harnett & Harnett, 1999a).

6.2. *Toll-like Receptors*

Toll-like receptors (TLRs) are human homologues of Toll receptors, pattern recognition receptors, first identified in *Drosophila*. Pattern recognition receptors recognise evolutionarily conserved motifs expressed by pathogens and act to modulate the host immune system. They have been proposed to initiate and link the innate and adaptive immune responses by recognition of conserved motifs such as certain groupings of carbohydrate moieties. TLRs play an important role in the innate immune system and have been proposed to play a crucial role in linking innate and adaptive immunity. TLRs, expressed on the cells of the innate immune system, can recognise pathogen associated structures, such as certain groupings of carbohydrate or phosphorylcholine moieties. This leads to activation of the TLRs, which can regulate the production of cytokines in order to polarise the phenotype of the adaptive immune response to either a Th1 cell mediated, or a Th2 humoral, response. TLRs belong to the IL-1R/TLR receptor superfamily which can be split broadly into two sub-families, those with three Ig domains as their extracellular portion and those with a leucine rich extracellular portion. TLRs belong to the second of these two subfamilies. The cytoplasmic domain of the TLRs contains a region, known as the TIR domain, which is homologous to the IL-1R1 cytoplasmic domain.

Investigation into the ligands for the TLR receptors have shown that TLR4 acts as the receptor for LPS from Gram negative bacteria as well as for a plant product, Taxol, heat shock protein 60 and a respiratory syncytial virus coat protein F. TLR2 can act as the receptor for lipopolysaccharide (LPS) from bacteria other than Gram negative bacteria and for bacterial lipoproteins, glycolipids and peptidoglycan. TLR1 and TLR6 have been shown to act in association with TLR2 and hence respond to some of the same ligands as TLR2. Both TLR2 and 6 are required for macrophage TNF α production in response to yeast and Gram positive bacteria (Heldwein *et al.*, 2001; Krutzik *et al.*, 2001).

As discussed, TLRs can polarise the phenotype of the adaptive immune response. This is observed by recognition of LPS by CD14 and its co-receptor TLR4 (Liu *et al.*, 2001; Systems, 2000), which promotes polarisation of the adaptive immune response to a Th1 response. The recognition of LPS by CD14 and TLR4 induces an inflammatory response with the release of IL-1, IL-6, IL-8 and TNF as a result of activation of NF- κ B and AP-1 transcription factors. Activation of TLR2 on dendritic cells (DCs) by bacterial products triggers induction of IL-12 and it is believed to trigger maturation of DCs. This provides an innate mechanism by which microbial pathogens can preferentially activate a cell mediated (Th1) immune response (Hertz *et al.*, 2001; Thoma-Uszyaski *et al.*, 2000). This ability to bias the immune system is of particular interest in the search for the receptor of ES-62, as ES-62 is known to induce the biasing of the immune response to a Th2 type response.

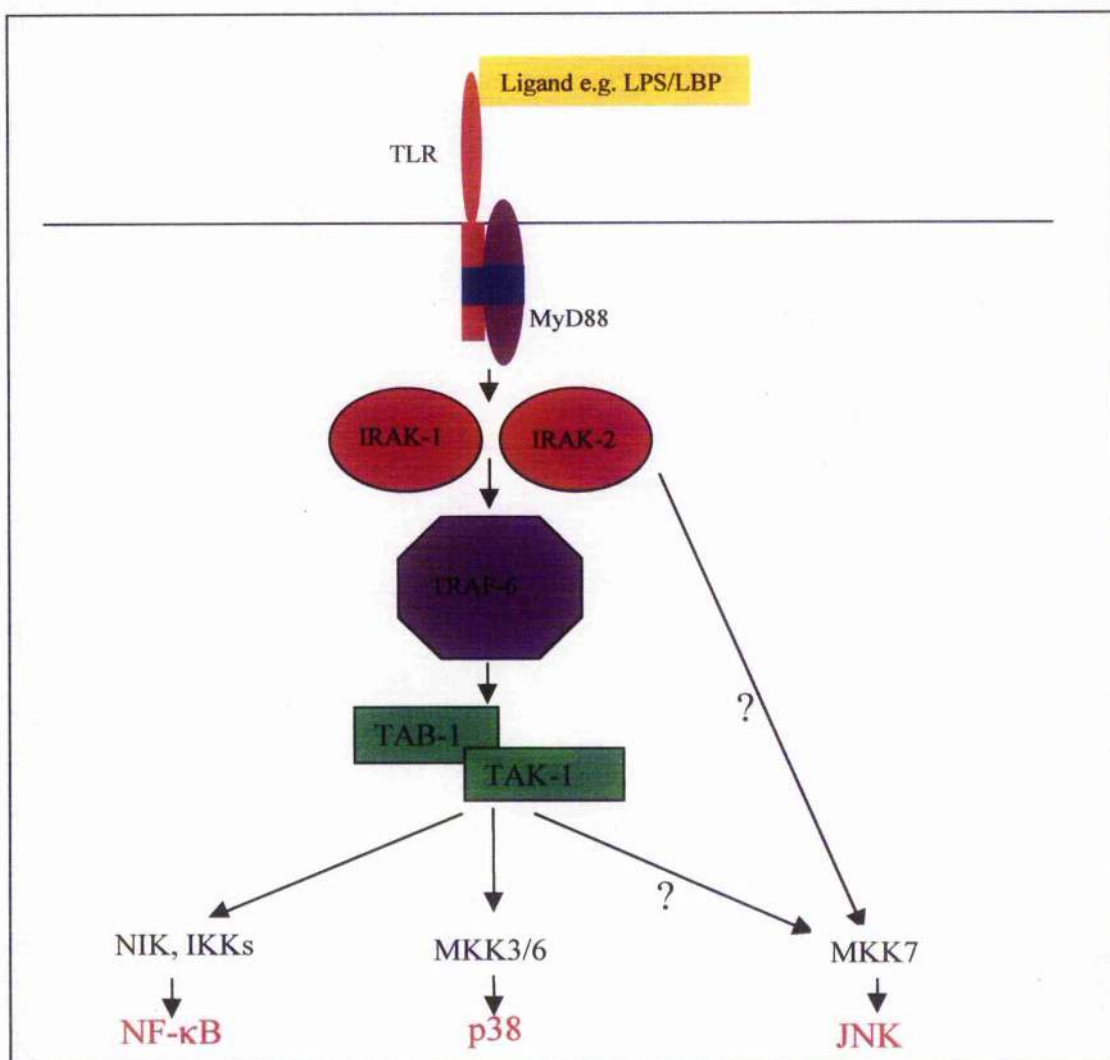


Figure 6-4: Signalling cascade of TLRs [adapted from (O'Neill & Dinarello, 2000). MyD88, which has the TIR domain characteristic of TLRs but no extracellular domain, is located in the cytosol. It is believed to play a role in connecting TLRs with downstream signalling proteins (Means *et al.*, 1999; O'Neill & Dinarello, 2000) by forming a protein-protein interaction with the TLRs via their TIR domains (Xu *et al.*, 2000). MyD88 recruits IRAK-1 and 2 which recruit TRAF-6. TRAF-6 can then activate two kinases, TAB-1 and TAK-1. TAB-1 and TAK-1 are known to phosphorylate and activate NIK and IKK which leads to NF- κ B activation. They are also believed to play a role in the activation of p38 and JNK possibly via phosphorylation and activation of MAPKK 3, 6 and 7.

Based on the results of previous BioCore studies that had determined that at least one receptor for ES-62 was present in the membranes of splenic B, U937 (monocytic) and Jurkat T cells, the aim was to identify and further characterise the receptor employed by ES-62. In addition, the aim was also to determine if the effects induced in response to ES-62 were due to receptor binding alone or whether ES-62 was internalised following receptor binding.

A number of different techniques were employed in the search for the receptor and in the localisation studies. In particular Far Western blot analysis and immunoprecipitations of a number of different B cell lines, Jurkat T cells and U937 monocytic cells using biotin or FITC labelled ES-62 were employed to identify the receptor for ES-62. FACS, microscopy, radiolabelling and cellular fractionation were employed in an attempt to identify whether ES-62 is internalised following binding to immune system cells and, if internalised, its location within the cell.

In addition, Western blot analysis using a variety of antibodies against components of the core signalling pathways of B cells was employed to examine the effects induced on B cell signalling by ES-62 alone. Previous studies had examined the activation of signalling molecules in B and T cells following pre-incubation with ES-62 (4 hours) and stimulation with anti-immunoglobulin (anti-Ig). To examine the differences in activation of signalling molecules downstream of the BcR following stimulation with ES-62 or anti-Ig (which activates the B cell receptor), cells were incubated with either ES-62 or anti-Ig alone for various timepoints. These studies enabled the comparison of the signalling profile generated in response to ES-62 treatment of cells with the known signalling profiles generated by ligation and activation of putative receptors such as the PAF receptor and the TLRs.

6.3. Results

6.3.1. Receptor Binding

As mentioned above, work carried out using *BiaCore* technology revealed that membranes from U937 cells (a human monocytic cell line), murine splenic B cells and Jurkat cells (a human T cell line) bind to ES-62 with receptor like affinity. In an attempt to identify the proteins acting as receptors for ES-62, Far Western blot analysis of ES-62 binding to whole cell lysates of a number of different cell types was performed. As described in Chapter 2, the whole cell lysates were resolved by SDS PAGE and transferred to nitrocellulose. ES-62 binding was visualised by probing the nitrocellulose using ES-62 labelled by biotinylation. Exposure of the Far Western blots to anti-biotin-HRP allowed visualisation of the ES-62 biotin conjugate. Biotinylated ES-62 should bind to any proteins in the whole cell lysate that ES-62 would bind to in a physiological setting. This allows identification of proteins acting as the receptor for ES-62 along with any cytosolic or nuclear proteins to which ES-62 can bind. As shown in Figure 6-5 (a) two bands were identified as binding ES-62 from splenic B cell whole cell lysates resolved by SDS PAGE. These bands were of approximately 135 kDa and 82 kDa. In Jurkat whole cell lysates, resolved by SDS PAGE, six bands were identified. These bands were of 135 kDa, a doublet of 82 kDa, 53 kDa and two bands of lower molecular weights (approximately 48 and 40 kDa). In U937 whole cell lysates, resolved by SDS PAGE, two bands of 82 kDa and approximately 60 kDa were observed. The band of 82 kDa identified in all three cell types may or may not relate to the same 82 kDa protein. The identification of different banding patterns for the different cell types substantiates the hypothesis that different cell types employ different proteins as receptors for ES-62, first suggested by the different binding kinetics identified for different cell types using *BiaCore* technology.

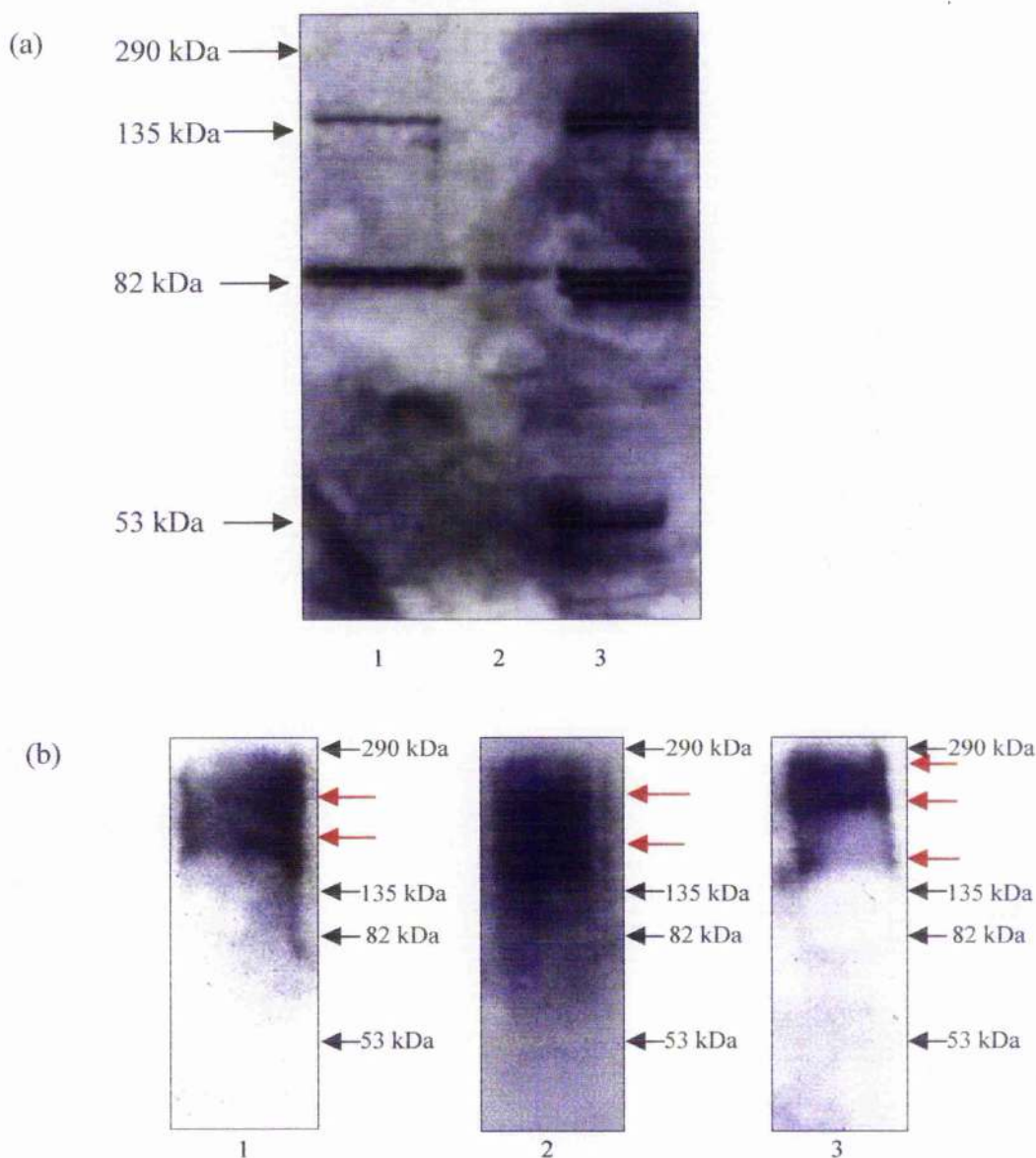


Figure 6-5: Binding of ES-62 to proteins from splenic B cells, U937 cells and Jurkat cells. (a) Splenic B cell whole cell lysates (lanes 1), U937 cell whole cell lysates (lane 2) and Jurkat cell whole cell lysates (lane 3) resolved on a 10 % SDS PAGE gel. (b) Splenic B cell whole cell lysates (lanes 1), U937 cell whole cell lysates (lane 2) and Jurkat cell whole cell lysates (lane 3) resolved on a 10 % non-denaturing, non-reducing gel. In (b) red arrows denoted bands visualised by binding of biotinylated ES-62.

As shown in Figure 6-5 (b) the band pattern observed alters when whole cell lysates are resolved under non-denaturing, non-reducing conditions. Under non-denaturing, non-reducing conditions a similar banding pattern is observed for splenic B, U937 and Jurkat T cells, the bands observed are of a greater mass than those observed under denaturing, reducing conditions. Resolution of splenic B cell and U937 cell whole cell lysates yields bands of approximately 200 and 150 kDa. Resolution of Jurkat T cell whole cell lysates yields three bands of approximately 290, 200 and 150 kDa. These bands could correspond to oligomerisation of proteins to form receptor complexes. Homo-dimerisation of the protein of 135 kDa, observed under denaturing, reducing conditions in splenic B and Jurkat T cells, would give a complex of ~290 kDa, as observed under non-denaturing, non-reducing conditions for Jurkat T cells. Homo-dimerisation of the protein of 82 kDa, observed under denaturing, reducing conditions in splenic B, U937 and Jurkat T cells would give a complex of ~150 kDa, as observed under non-denaturing, non-reducing conditions for splenic B, U937 and Jurkat T cells. Whereas hetero-oligomerisation of the 82 and 135 kDa proteins, observed under denaturing, reducing conditions in splenic B and Jurkat T cells or two 82 kDa proteins and the 60 kDa protein, observed under denaturing, reducing conditions in U937 cells would yield a complex of ~200 kDa, observed under non-denaturing, non-reducing conditions for splenic B, U937 and Jurkat T cells. Many proteins homo or heterodimerise in order to function as a receptor, for example the IL-2 receptor is a hetero-oligomer, as is the TNF- α receptor.

To identify whether homo and hetero dimerisation was occurring crosslinking studies were performed. WEHI-231 B cells were surface biotinylated, as described in Chapter 2, and incubated with an ES-62-FITC conjugate. A cross-linking agent (AFDP, Pierce) was then added, the cells lysed and immunoprecipitation performed using an anti-FITC antibody. A sample of the immunoprecipitation was resolved on a 10% SDS PAGE gel under reducing and non-reducing conditions. The addition of β -mercaptoethanol, to resolve the sample under reducing conditions, resulted in the dissociation of the crosslinking bonds and thus allowed visualisation of the

proteins which constitute the receptor complex for ES-62. Comparison of the stained gels obtained under reducing and non-reducing conditions did not indicate any differences in the banding patterns obtained. This indicates that no crosslinking occurred following ES-62 incubation, which may be attributable to the crosslinking reagent employed. Time constraints prevented optimisation of crosslinking agents, which may allow this issue to be resolved.

As discussed, previous BiaCore experimentation had shown binding of membranes from splenic B, U937 and Jurkat T cells to ES-62 to be PC-dependent. To determine if binding of ES-62 to those proteins identified by Far Western blotting (Figure 6-5) was occurring in a PC-dependent manner, whole cells lysates from splenic B, U937 and Jurkat T cells, resolved by SDS PAGE and transferred to nitrocellulose, were pre-incubated with PC prior to Far Western blot analysis with an ES-62-biotin conjugate. No bands were visualised following Far Western blot analysis of the pre-incubated blots indicating that binding of ES-62 to the proteins identified by Far Western blotting (Figure 6-5) was PC dependent, substantiating previous BiaCore studies.

Due to the observed differences in the proteins binding to ES-62 in murine splenic B, human U937 (monocytic) and human Jurkat T cells, the proteins identified as binding ES-62 from cells of different levels of maturity were examined to determine whether ES-62 exploits different proteins as receptors at different stages of immune cell development. The cell lines chosen for study were from the B cell lineage as previous studies ((Deehan et al., 1998a; Deehan et al., 1998b; Goodridge et al., 2001; Harnett & Harnett, 1999a; Harnett et al., 1999; Harnett & Harnett, 1993; Harnett et al., 1989)) examining the effects of ES-62 on the signalling pathways of B cells have been performed. Eight different cell types were chosen for investigation; REH cells, Nalm6 cells, 697 cells, 207 cells, WEHI-231 cells, Daudi cells, Ramos cells and splenic B cells. REH, Nalm6, 697 and 207 cell lines are human pre-B cell lines of increasing maturity with the REH cell line being the most immature and the 207 cell line being the most mature of these pre-B cells. The WEHI-231 cell line is

an immature murine B cell line. The Ramos cell line is a mature human B cell line which is germinal centre like in character and the Daudi cell line is a mature human follicular/germinal centre like B cell line. Splenic B cells are murine naive primary B cells and as such are the only cells studied that are not activated or from a cell line. The developmental pathway of B cells can be seen in Figure 6-7.

Far Western blot analysis was carried out on whole cell lysates from REH cells, Nalm6 cells, 207 cells, 697 cells, WEHI-231 cells, Daudi cells, Ramos cells and splenic B cells resolved on a 10 % SDS PAGE gel and transferred to nitrocellulose.

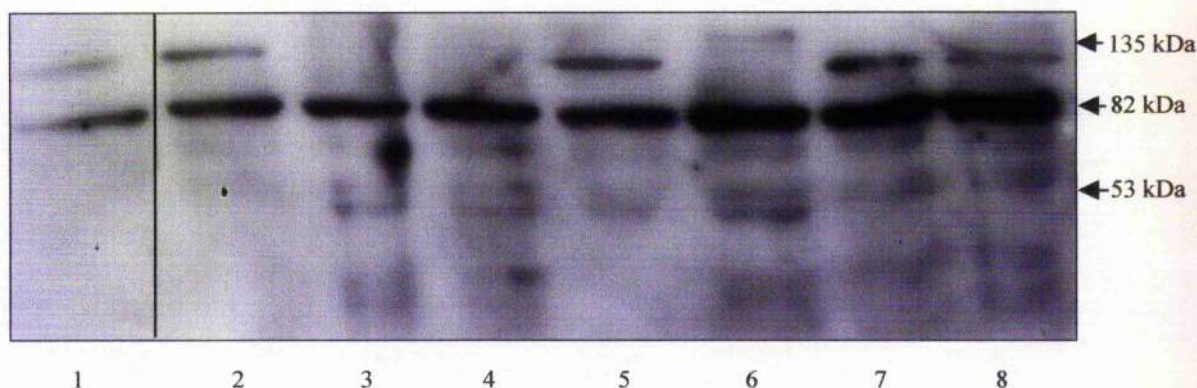


Figure 6-6: Binding of ES-62 to proteins from whole cell lysates of splenic B cells (lane 1), WEHI cells, (lane 2), Daudi cells, (lane 3), Ramos cells (lane 4), Nalm 6 cell (lane 5), 207 cell (lane 6), 697 cell (lane 7) and REH cell (lane 8), all B cells of different stages of maturation. 20 μ g of whole cell lysates from these cells were resolved on a 10 % SDS PAGE gel and transferred to nitrocellulose. Far Western blot analysis was then performed using ES-62-biotin and anti-biotin-HRP as described in Chapter 2.

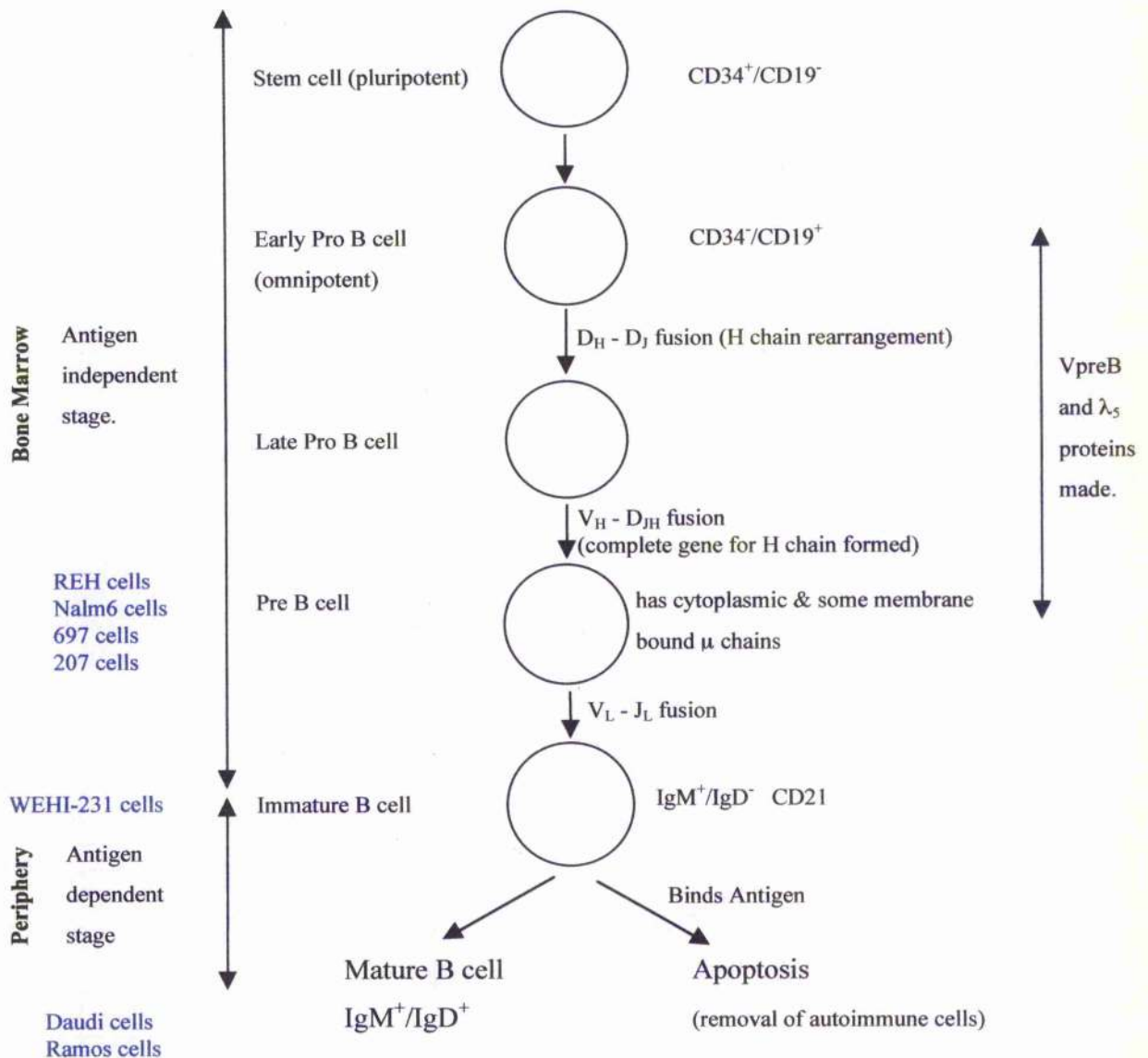


Figure 6-7: The developmental pathway of B cells. REH, Nalm6, 697 and 207 cell lines are human pre-B cell lines of increasing maturity with the REH cell line being the most immature and the 207 cell line being the most mature of these pre-B cells. The WEHI-231 cell line is an immature murine B cell line. The Ramos cell line is a mature human B cell line which is germinal centre like in character and the Daudi cell line is a mature human follicular/germinal centre like B cell line.

As shown in Figure 6-6, a band of 82 kDa was identified as binding ES-62 in all the B cell types analysed. However, the band of 135 kDa identified in splenic B cells and Jurkat T cells as binding ES-62 (Figure 6-4) is only present in splenic B cells and WEHI-231 B cells. In whole cell lysates from Nalm6, 697 and REH cell lines a band of approximately 125 kDa was identified, in addition to the 82 kDa band identified. In 207 cells a band of approximately 145 kDa band was identified in addition to the 82 kDa band. In Daudi and Ramos B cell lines, in addition to the 82 kDa band, some lower molecular weight bands were also identified.

The differences in banding patterns between the different cell types suggests that a protein of 82 kDa, which binds ES-62 and is present in all cell types, perhaps forms the core component of the receptor for ES-62. The other proteins present in the receptor complex appear to vary depending on cell type (Figure 6-4) and on the level of maturity of the cell (Figure 6-5). The three earliest precursor B cell lines, REH, 697 and Nalm-6, all show similar banding patterns, different from those observed for more developmentally mature cell lines, sharing only the band of 82 kDa. The 207 cell line which is more mature than the REH, 697 and Nalm6 cell lines, but is still classified a pre-B cell line due to cell surface marker expression, again shares the 82 kDa band but the higher molecular weight protein identified is different from both that identified in the more developmental immature and more developmentally mature cell lines.

All the analyses described above were carried out on whole cell lysates of cells, thus intracellular proteins as well as membranes proteins that bind ES-62 could be identified. Although the non-denaturing, non-reducing gels (Figure 6-4 (b)) indicate that the bands identified oligomerise, it is possible that some of the bands identified and shown in Figure 6-4 (a) and Figure 6-6 may not form part of the receptor complex for ES-62 but instead be intracellular proteins. To confirm which of these bands represent cell surface receptor chains for ES-62, ES-62 bound proteins from the surface biotinylated membrane fraction of U937 monocytic cells and WEHI-231 immature B cells were immunoprecipitated as described in Chapter 2, resolved by

SDS PAGE, transferred to nitrocellulose and visualised using an anti-biotin-HRP conjugate as shown in Figure 6-8.

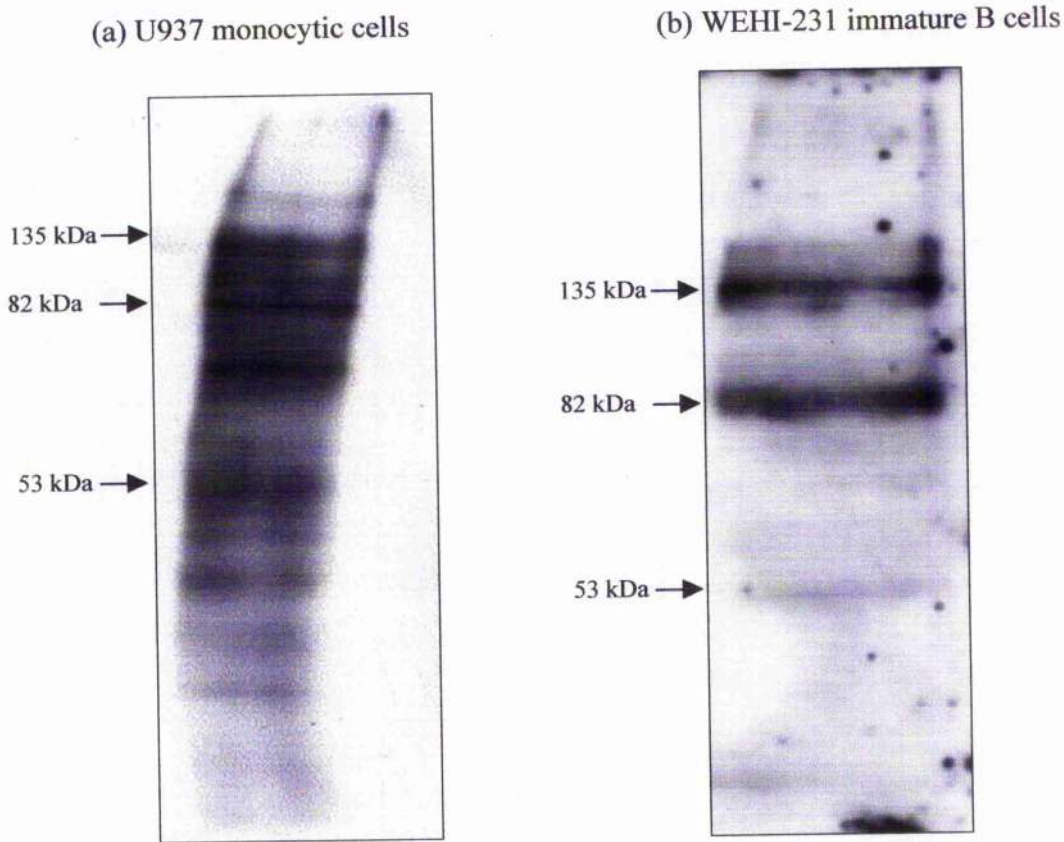


Figure 6-8: Immunoprecipitation of surface biotinylated membrane proteins that bind ES-62 from (a) U937 monocytic cells and (b) WEHI-231 immature B cell membranes fractions. U927 monocytic cells and WEHI-231 immature B cells were biotinylated, membrane fractions made and probed for ES-62 binding using an ES-62-FITC conjugate. Immunoprecipitation was then performed using anti-FITC antibodies and protein G-sepharose. This immunoprecipitation allowed the isolation of the membrane proteins bound to ES-62.

As shown in Figure 6-7, the immunoprecipitation experiment from WEHI-231 B cell membranes identified bands capable of binding ES-62 of 135 and 82 kDa. These bands are the same size as those observed following Far Western blot analyses (Figure 6-5). The immunoprecipitation experiment from U937 cell membranes identified a greater number of proteins that are capable of binding ES-62 than the Far Western analyses of U937 cell whole cell lysates. The bands identified as binding ES-62 were of 135, 100, 90, 82 and ~65 kDa (Figure 6-7). Far Western blot analysis only identified bands at 82 kDa and ~65 kDa (Figure 6-4). The 53 kDa band identified from WEHI-231 cell membranes and the 135, 100 and 90 kDa bands identified from U937 cell membranes as binding ES-62 (Figure 6-7) suggest the presence of a greater number of membrane proteins capable of binding ES-62 than were identified from the Far Western blots. The identification of these bands following immunoprecipitation, but not following Far Western blot analysis is postulated to be due to protein concentration. Only the cellular membrane proteins are analysed in the immunoprecipitation experiments whereas all cellular proteins are present in the whole cell lysates studied by Far Western blot analysis. As a result, the immunoprecipitations were carried out on an enriched membrane protein source and thus, it is postulated, the immunoprecipitations allow visualisation of proteins capable of binding ES-62, not present in sufficiently high quantities in the Far Western blot analyses.

The molecular weights of the bands identified as binding ES-62, approximately 82 and 135 kDa, could not lead to direct identification of specific proteins, as there are many proteins with molecular weights in the range of 80 to 140 kDa. However, the molecular weights of the bands identified as capable of binding ES-62 does exclude the PAF receptor, which has a molecular weight of 39 kDa. The data from the Far Western blot analyses and the ES-62 immunoprecipitation experiments demonstrated that the two major proteins to which ES-62 binds are of approximately 82 and 135 kDa in size. Further, these experiments demonstrated that binding to ES-62 is PC dependent. As a result of these studies, two protein families, the integrin

and toll-like receptor families, were investigated as an initial step in the identification of the receptor for ES-62.

6.3.1.1. Integrins

Integrins are the principal receptors on mammalian cells for binding most extracellular matrix proteins including collagen, fibronectin and laminin. Unlike typical cell surface receptors for soluble cell signalling molecules, integrins bind their ligand with relatively low affinity ($K_a = 10^6 - 10^9$ litres mol^{-1}). In addition integrins are typically present at the cell surface at concentrations 10 – 100 times greater than other receptors (Alberts *et al.*, 1994). Integrins are also involved in the immune response. They play roles in leukocyte, neutrophil and dendritic cell recruitment and can influence signalling pathways by transducing signals or by interfering with the signalling of other receptors. For example, a defect in the synthesis of the common integrin $\beta 2$ chain results in a susceptibility to infection with extracellular bacteria (Janeway & Travers, 1996). In addition, integrins are also known to induce intracellular signalling in response to stimuli (Alberts *et al.*, 1994). In macrophages, the leukocyte integrin CD11b/CD18 (as known as CR3) is capable of recognising LPS, lipophosphoglycan of *Leishmania* and structures on yeast such as *Candida* (Janeway & Travers, 1996).

Integrins are heterodimers consisting of an α and a β subunit, both of which contribute to the binding of matrix proteins. Each $\alpha\beta$ heterodimer is specific for a particular ligand and has a distinct ligand binding specificity. Further, identical integrin molecules in different cells types have been determined as having different ligand binding specificities. This has been postulated to be due to cell type specific factors able to modulate ligand binding. There are 25 known integrins, which consist of various combinations of at least 17 α and 9 β subunits. The α and β subunits vary greatly in size, the α subunits ranging between approximately 120 to 210 kDa, the β subunits ranging between approximately 95 to 220 kDa. These size ranges are generally similar to the molecular weights of the proteins identified as capable of

binding ES-62. This, in conjunction with the involvement of integrins in signalling and general immune system modulation, led to the investigation of integrins as receptors for ES-62.

Binding of ligands to integrins can be blocked by the presence of molecules such as fucose which bind to the integrins and block binding of extracellular matrix proteins, intracellular adhesion molecules and complement components. In addition, at least 8 of the 25 known integrins are known to recognise a sequence motif of Arg-Gly-Asp (RGD) (Assa-Munt *et al.*, 2001). Integrin binding via the RGD (or related) motifs has been shown to be blocked by the use of RGD peptides (Kijimoto-Ochiai & Noguchi, 2000; Rahman *et al.*, 2000).

The use of the RGD motif by pathogens to gain entry into the host cells via integrins has been shown for *Bordetella pertussis* (Hagen & Klager, 2001). Integrin-like RGD-dependent cell adhesion has also been shown to be involved in the removal of *Onchocerca microfilariae* within a specific species of the vector for human and bovine onchocerciasis, the blackfly, *S. damnosum* (Ishibashi *et al.*, 2001). Research into the integrin-like receptors of the blackfly haematocytes has shown that the presence of the peptide sequence RGDS, as a blocking agent, significantly increases the survival of *Onchocerca microfilariae*. This finding raises the possibility that integrins, and in particular those recognising the RGD motif, could play a role in filarial disease. In addition, the identification of several DDX (Asp-Asp-any amino acid) motifs, the complementary motifs of the RGD motifs, within the amino acid sequence of ES-62 strengthens the hypothesis that integrins could be acting as the receptor for ES-62. To examine the possibility that integrins act as receptors for ES-62, WEHI-231 B cells were biotinylated and membrane fractions prepared. The biotinylated membrane fractions were pre-incubated with media alone or media containing 1 mM fucose, 1 mM PC, 1 mM RGDS (Arg-Gly-Asp-Ser) peptide or 1 mM RGES (Arg-Gly-Glu-Ser) peptide prior to incubation with an ES-62-FITC conjugate and subsequent immunoprecipitation using anti-FITC and protein G - sepharose. The membrane proteins capable of binding ES-62-FITC were resolved by

SDS PAGE, transferred to nitrocellulose and visualised by probing with an anti-biotin-HRP conjugate. Fucose was used to test for the involvement of integrins while RGDS and RGES peptides were used to identify if the integrins involved interacted via RGD motifs. Pre-incubation with an RGDS peptide would block any binding that was occurring, the RGES peptide was employed as an irrelevant peptide control.

As can be seen from Figure 6-9, pre-incubation with fucose or either of the peptides had no effect on binding suggesting that integrins are not involved in the receptor complex for ES-62. As a positive control, and for further corroboration, the PC dependent nature of ES-62 binding was examined with regard to the membrane proteins that ES-62 bound in these assays. Figure 6-9 shows that pre-incubation of biotinylated WEHI-231 B cell membranes with PC substantially blocks the binding of ES-62 to the membrane proteins of WEHI-231 B cells. This substantiates earlier findings from BiaCore and Far Western analyses that ES-62 receptor binding is PC dependent.

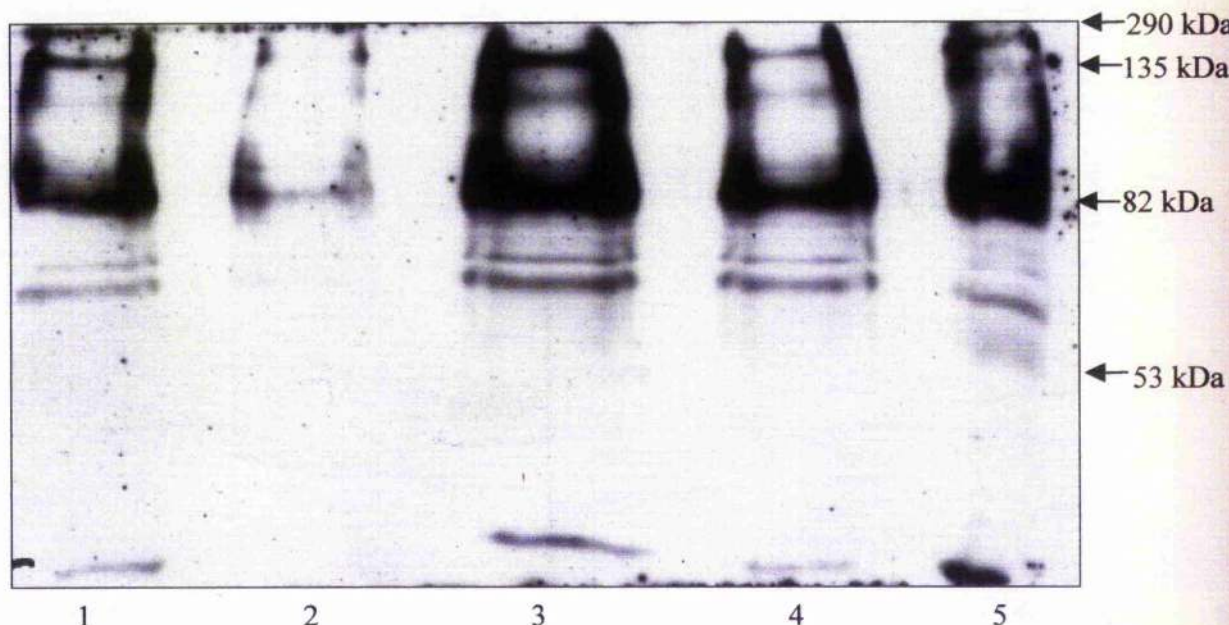


Figure 6-9: Effects of phosphorylcholine, fucose, RGDS and RGES peptides on binding of ES-62 to membrane proteins from WEHI-231 B cells. WEHI-231 B cells were biotinylated and the membrane fraction of these cells then extracted. The biotinylated WEHI-231 B cell membranes were then pre-incubated with either media alone or media containing 1 mM PC, 1 mM fucose, 1 mM RGDS peptide or 1 mM RGES peptide prior to immunoprecipitation with ES-62-FITC, anti-FITC antibodies and protein G-sepharose. Lane 1 contains WEHI-231 B cell membranes pre-incubated with media alone and then immunoprecipitated with ES-62-FITC. Lanes 2 - 5 contain WEHI-231 B cell membranes pre-incubated with media containing 1 mM PC (lane 2), 1 mM fucose (lane 3), 1 mM RGDS peptide (lane 4) or 1 mM RDES peptide (lane 5) and then immunoprecipitated with ES-62-FITC.

6.3.1.2. *Toll-Like Receptors*

Following exclusion of the role of the PAF receptor and integrins as receptors for ES-62, studies were carried out to ascertain whether any of the TLRs act as a receptor for the filarial ES product, ES-62. TLRs, as discussed previously, are pattern recognition receptors and as such recognise features such as specific carbohydrate motifs and phosphorylcholine moieties on proteins. TLRs play an important role in both the innate and adaptive immune response and are known to act as part of the receptor for LPS. Stimulation of the TLRs results in the activation of NF κ B and MAPK activity which, as discussed in section 6.3.2, are also induced by ES-62. These factors, in conjunction with the mass of the TLRs, which ranges between 70-90 kDa, make the TLR family a strong candidate for the role of ES-62 receptor.

Interestingly, TLR4 is believed to be involved in the induction of inflammatory responses by *Brugia malayi*. These responses are mediated by LPS-like activity from the endosymbiotic *Wolbachia* bacteria which, it is believed, exploits TLR-4 as its receptor (Taylor *et al.*, 2000). *Wolbachia* bacterial LPS may be one of the major mediators of inflammatory pathogenesis in filarial nematode disease. However, it should be noted that *Wolbachia* bacteria are not found on *A. viteae*, which is the filarial parasite from which ES-62 is obtained (Kennedy & Harnett.W., 2001; Werren, 1997).

To investigate if TLR2 or TLR4 were acting as the receptor for ES-62, the blot shown in Figure 6-6 above was stripped of antibody, tested for the presence of any residual ES-62-biotin and then reprobed with anti-TLR2 and anti-TLR4 antibodies in turn (the efficient stripping of each of these antibodies was tested). Probing of this blot with the TLR2- and TLR4-specific antibodies in turn produced the banding patterns shown in Figure 6-10. This experiment was also repeated with fresh whole cell lysate samples resolved as described previously and probed with anti-TLR2 and anti-TLR4 antibodies from a different source. The results obtained were very similar

to those reproduced in Figure 6-10 (results not shown). The results shown in Figure 6-10 suggest that the 82 kDa protein identified as binding ES-62 in all cells except U937 cells, Jurkat cells and Nalm6 cells is a TLR. Unfortunately both the anti-TLR2 and 4 antibodies show identical banding patterns. This could be the result of cross-reactivity which is widely known to occur between TLR antibodies of common sequence specificity. However, as a result it was not possible to identify which of these two TLRs binds ES-62 or whether both are capable of binding ES-62. The differences in the level of TLR 2 and TLR 4 detected for each cell type may be due to differential recognition of the TLR present by these two antibodies.

Alternatively, the differences in levels of TLR 2 and 4 identified in the different cell types may be due to cell type differences, resulting in different levels of TLR proteins being expressed at the cell surface. Many of the cell types studied are B cells of different levels of maturity; REH cells as the most developmentally immature of the pre B cells through 207 cells, more developmentally mature pre B cells, to WEHI-231 immature B cells and finally Daudi and Ramos follicular B cells. Consideration of the levels of TLR 2 and 4 detected in relation to the development of the various B cell types indicates that the levels of TLR 2 and 4 identified increases as B cells develop. TLRs are involved in the innate and adaptive immune response thus an increase in expression of TLRs as the B cells develop could be expected, as only fully developed cells play an active role in the host immune response and thus have a requirement for TLR cell surface expression.

The identification of only one of the two proteins that bind ES-62 as a TLR suggests that either the TLR involved is recruiting a TLR which is not recognised by either the TLR2 and 4 antibodies or that the second protein involved in the recognition of ES-62 is not a TLR but is recruited and can form a heterodimer with these proteins as is the case with the receptor for LPS.

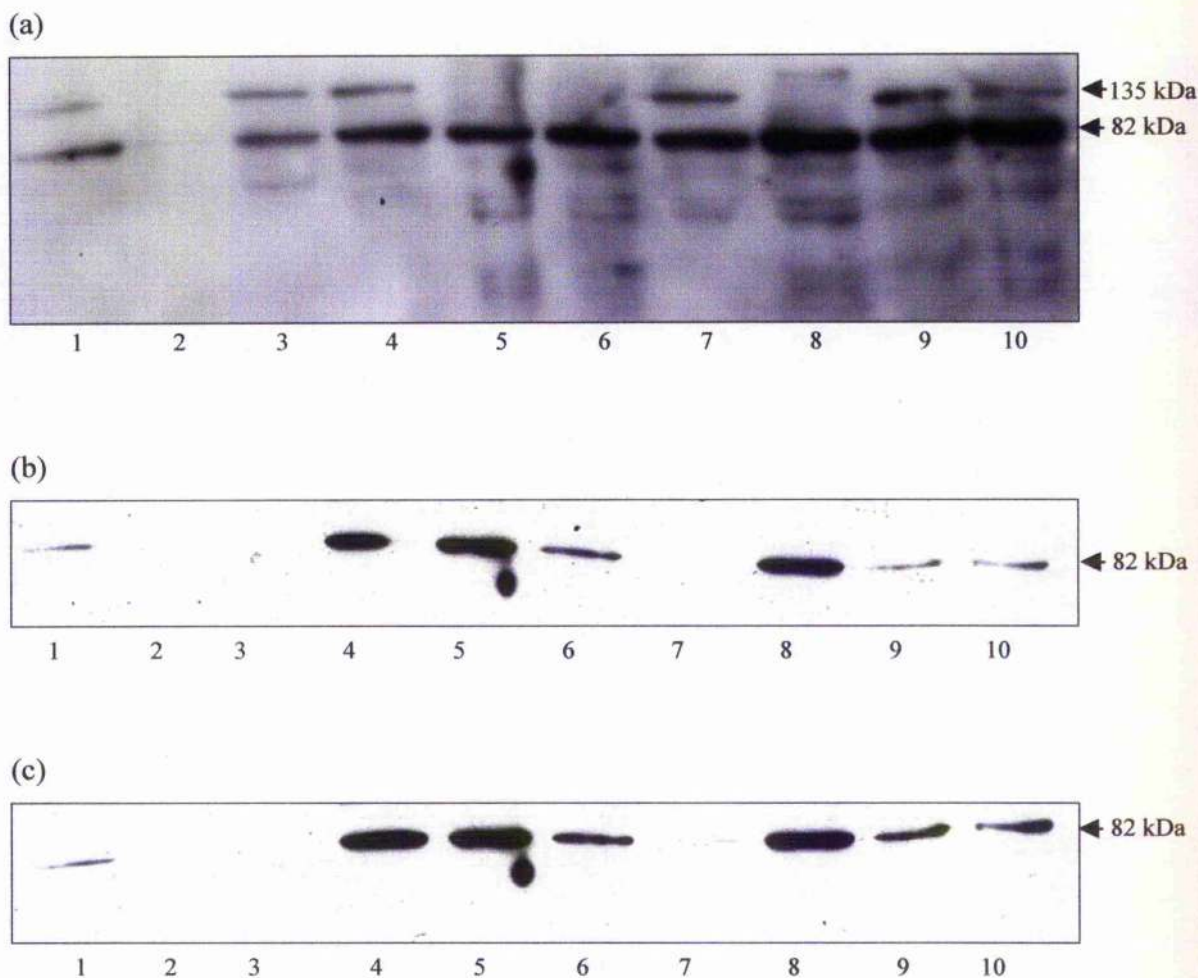


Figure 6-10: Potential identification of the p82 protein of B cells that binds ES-62 as one or more Toll-like receptors. Whole cell lysates of splenic B cells (lane 1), U937 cells (lane 2), Jurkat cells, (lane 3), WEHI cells, (lane 4), Daudi cells, (lane 5), Ramos cells (lane 6), Nalm 6 cell (lane 7), 207 cell (lane 8), 697 cell (lane 9) and REH cell (lane 10) were resolved on a 10 % SDS PAGE gel, transferred to nitrocellulose and (a) Far Western blotted using ES-62-biotin and anti-biotin-HRP as described in Chapter 2, (b) Western blotted with anti-TLR2 antibody and (c) Western blotted with anti-TLR4.

6.3.2. ES-62 Effects on Erk, JNK and p38

TLR receptors couple to NF κ B and Erk, Jnk and p38 MAPK signalling. Previous work in this laboratory has shown that ES-62 stimulates Erk, MAPK (B cells, T cells and macrophages) and NF κ B (macrophages) (Deehan et al., 1998a; Goodridge et al., 2001). These findings could lend support to the putative identification of TLR involvement in ES-62 signalling. To further explore this, the effects of ES-62 on MAPK and NF κ B signalling was examined in B cells. Splenic B cells were stimulated with either ES-62 or anti-Ig for 1, 5, 10, 30, 60, 120 and 240 minutes. Whole cell lysates of the stimulated cells were prepared and resolved by SDS PAGE, transferred to nitrocellulose and Western blotted with anti-phospho Erk, anti-phospho JNK and anti-phospho p38.

As shown in Figure 6-11, following treatment of splenic B cells with anti-Ig, phosphorylated Erk was detected after 30 minutes and was still present (at slightly higher levels) after 240 minutes. Treatment of splenic B cells with ES-62 resulted in detection of phosphorylated Erk after 5 minutes. Activation of Erk was maximal following stimulation of splenic B cells for 30-60 minutes with ES-62. The level of phosphorylated Erk detected then decreased with time up to 240 minutes.

Following stimulation of splenic B cells with anti-Ig, phosphorylated Jnk was detected after 1 minute. Stimulation of splenic B cells with ES-62 also resulted in an increase in the level of activation of Jnk. Similar to the results obtained following stimulation with anti-Ig, activation of Jnk following ES-62 stimulation was observed after one minute. However, splenic B cells stimulated with ES-62 did not exhibit the same prominent initial activation and deactivation kinetics as observed in cells stimulated with anti-Ig. Following stimulation with ES-62, activated Jnk could still be detected after 240 minutes whereas activated Jnk could no longer be detected after 60 minutes following stimulation with anti-Ig, indicating that the activation induced by ES-62 is less transient than that induced by anti-Ig.

Phospho p38 was not detected in either the ES-62 or anti-Ig treated cells. The absence of detectable phospho p38 may be due to a lack of sensitivity and specificity of the phospho p38 antibody rather than a lack of phospho p38 within the cells.

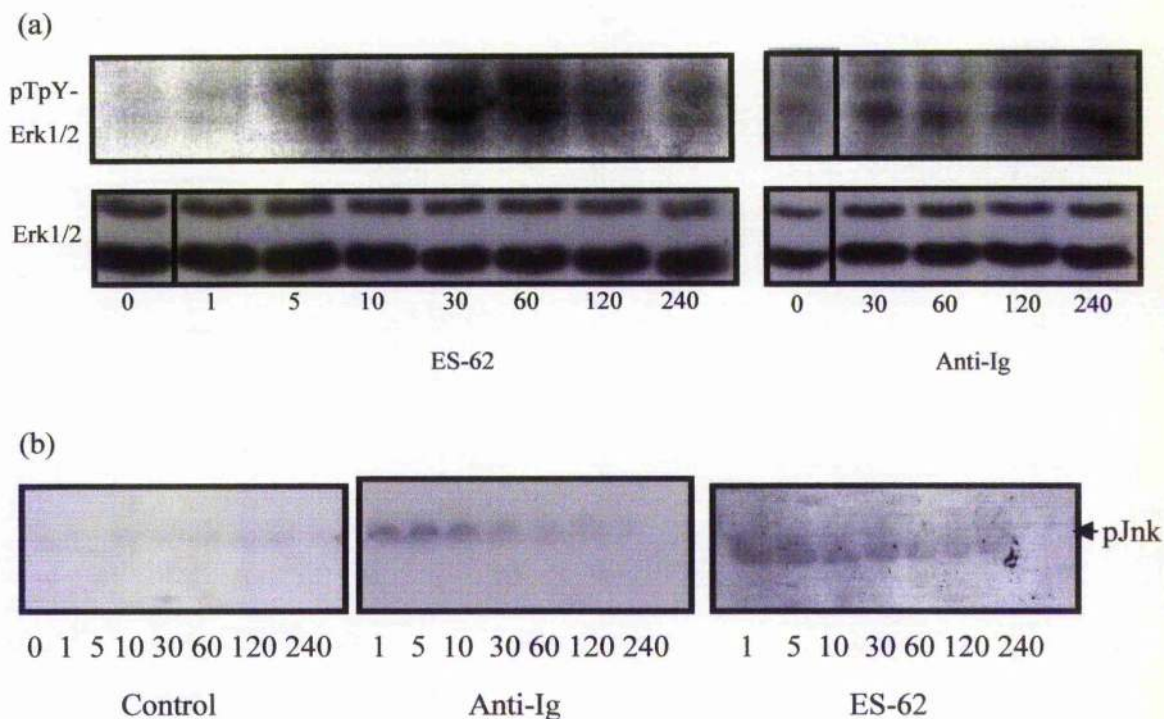


Figure 6-11: ES-62 causes an initial activation of Erk and Jnk followed by a rapid deactivation. 6.4×10^6 control splenic B cells or splenic B cells treated with medium containing either ES-62 ($2 \mu\text{g ml}^{-1}$) or anti-Ig ($50 \mu\text{g ml}^{-1}$) for 0, 1, 5, 10, 30, 60, 120 or 240 minutes were lysed and resolved on 7.5 % SDS PAGE gels, transferred to nitrocellulose and probed with (a) anti phospho Erk or (b) anti phospho Jnk antibodies. Probing of the blots in (a) was also carried out with anti-Erk, which detects both phosphorylated and non-phosphorylated forms of Erk, as a loading control. The bands were visualised through use of HRP conjugated secondary antibodies and Amersham ECL technology.

Earlier work (Deehan et al., 1998a) indicated that stimulation of splenic B cells with anti-Ig following pre-incubation with ES-62 did not lead to activation of Erk. The

results above show that stimulation of splenic B cells with ES-62 alone induces an initial activation of Erk however, this activation is rapidly switched off. ES-62 treatment thus appears to desensitise the cells to further activation. It is postulated that ES-62 treatment causes the activation, and thus dual phosphorylation, of Erk, and that it also recruits a phosphatase which rapidly dephosphorylates the dual phosphorylation sites of Erk (Deehan *et al.*, 2001).

6.3.3. ES-62 Modulates Transcription Factor Activity

NF κ B transcription factors are a family of eukaryotic transcription factors that are involved in the normal cellular processes including immune and inflammatory responses. The NF κ B proteins are all related through a highly conserved DNA-binding domain known as the Rel homology (RH) domain which contains DNA-binding and protein dimerisation motifs and a nuclear localisation signal. However, they can be divided into two classes; the first class contains Rel A (p65), RelB and c-rel which possess transactivation domains and as such can induce gene transcription. The second class, p50 and p52, do not possess this domain and cannot directly induce gene transcription. NF κ B proteins exist as homo or heterodimers and members of the second class can only induce gene transcription when they form a heterodimer with a member of the first class. NF κ B homo and heterodimers exist in an inactive state in the cytoplasm of cells bound to an inhibitory I κ B protein. Following cellular activation, I κ B may be phosphorylated and dissociate from the NF κ B dimer allowing its translocation to the nucleus and subsequent gene transcription as shown in Figure 6-11.

Electromobility shift assays (EMSAs) were performed on nuclear fractions of WEHI-231 B cells treated with media alone (control) or ES-62 for a range of times from 5 minutes to 48 hours. As shown in Figure 6-13, following ES-62 stimulation of WEHI-231 B cells, an initial increase in both E2F and NF κ B activity was observed at early timepoints. This was followed by a downregulation at later time points. This correlates with the work discussed in section 6.3.2 and earlier work

(Deehan et al., 1998a) that showed that ES-62 causes an initial partial activation of the signalling pathway downstream of the B cell receptor. This partial activation is insufficient to induce a full response however, it results in desensitisation of the cells to further exposure to ES-62 and the down-regulation of the PI3K and Ras-MAPK signalling pathways. As shown in Figure 6-14, Western blot analysis of the nuclear and cytosolic fractions of WEHI-231 B cells stimulated with ES-62 was carried out to examine the effects of ES-62 on the localisation and expression of the p65 and p50 subunits of NF κ B.

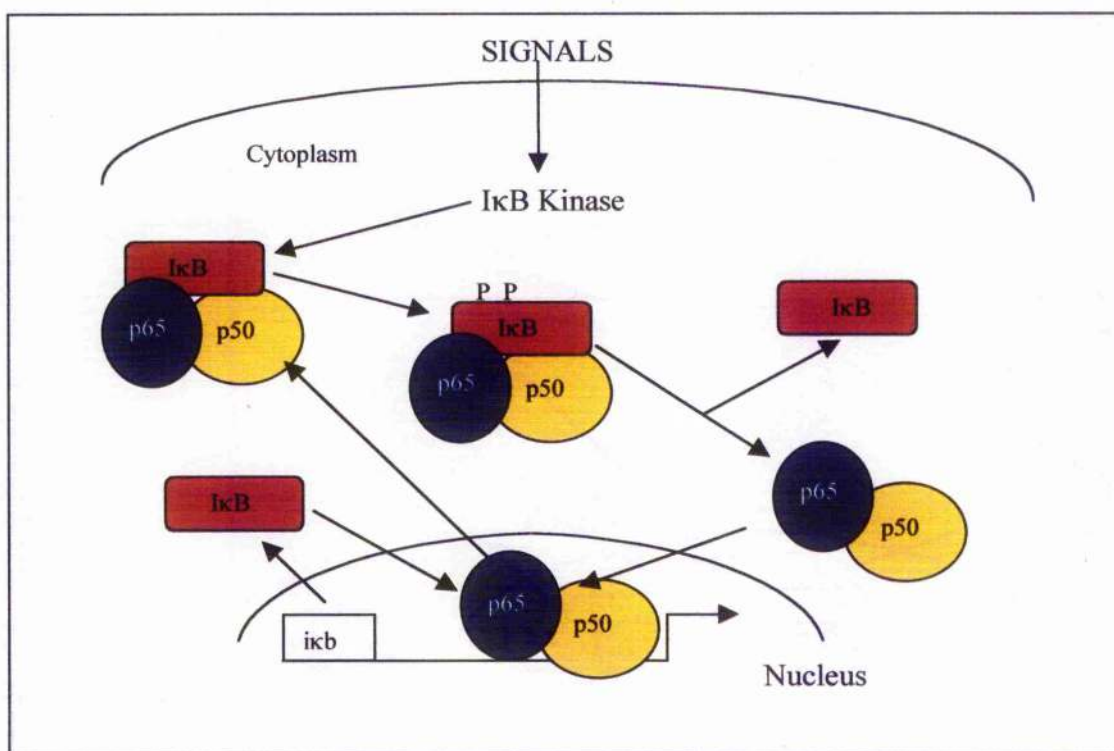


Figure 6-12: Activation of NF κ B and its subsequent translocation to the nucleus to induce gene transcription.

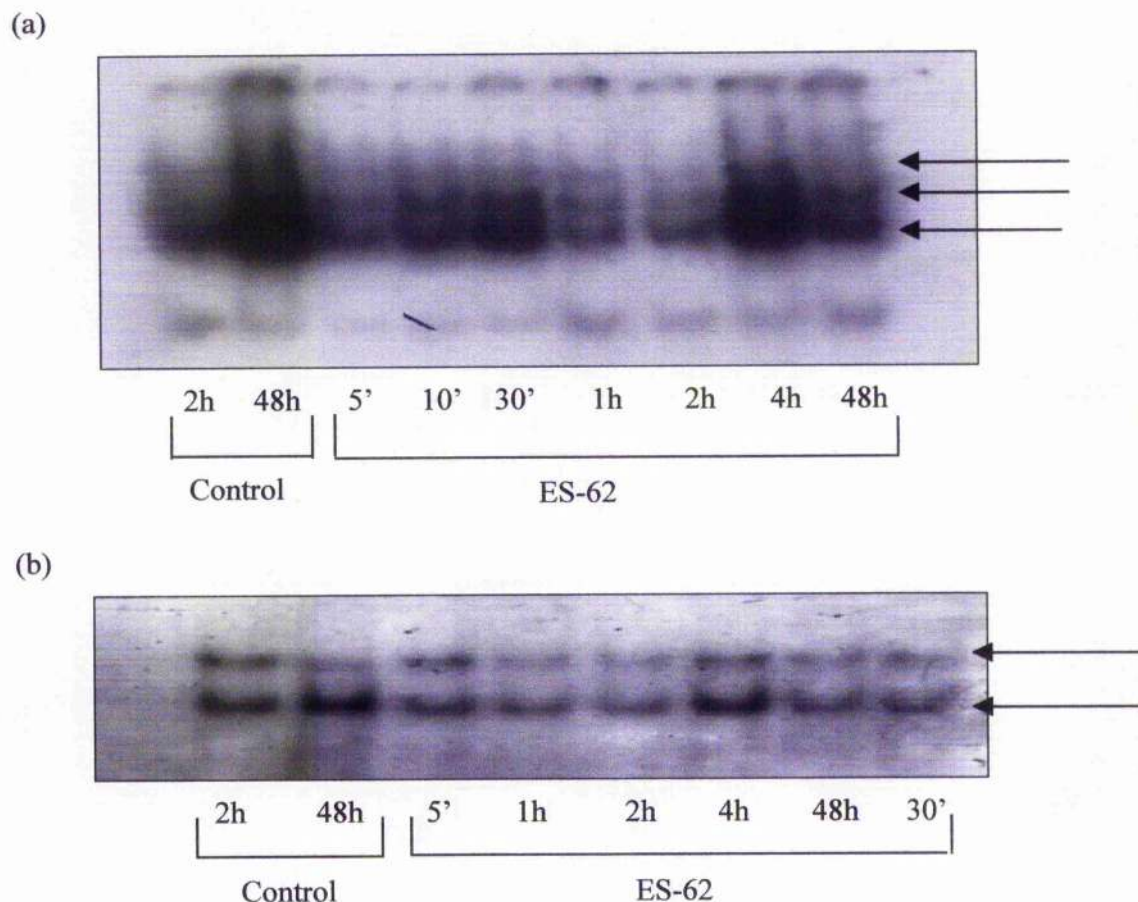


Figure 6-13: EMSA, using ^{32}P labelled probes for (a) NFκB and (b) E2F.

Following incubation of WEHI-231 B cells with media alone (control) or media containing ES-62 ($2\ \mu\text{g ml}^{-1}$) for 5, 10, 30, 60, 120, 240 minutes or 48 hours, nuclear fractions were prepared, incubated with radiolabelled probe and resolved on a 6 % polyacrylamide gel. The gel was then fixed (2 methanol : 1 acetic acid : 1 glycerol : 6 water (v/v)) for 20 minutes, dried in a gel drier for 1-2 hours at $80\ ^\circ\text{C}$ and developed using autoradiography.

a) NFκB p50 subunit

Control cells cytosolic fractions



5' 10' 30' 1h 2h 4h 24h

ES-62 treated cells cytosolic fractions



5' 10' 30' 1h 2h 4h 24h

Control cells nuclear fractions



5' 10' 30' 1h 2h 4h 24h

ES-62 treated cells nuclear fractions



5' 10' 30' 1h 2h 4h 24h

(b) NFκB p65 subunit

Control cells cytosolic fractions



5' 10' 30' 1h 2h 4h 24h

ES-62 treated cells cytosolic fractions



5' 10' 30' 1h 2h 4h 24h

Control cells nuclear fractions



5' 10' 30' 1h 2h 4h 24h

ES-62 treated cells nuclear fractions



5' 10' 30' 1h 2h 4h 24h

Figure 6-14: ES-62 stimulation of WEHI-231 B cells alters the levels of the p65 and p50 subunits of NFκB. WEHI-231 B cells were incubated with ES-62 ($2 \mu\text{g ml}^{-1}$) for 5, 10, 30, 60, 120, 240 minutes or 24 hours. Cytosolic and nuclear fractions were made of each sample and 30 μg of each of the cytosolic fractions and 15 μg of each of the nuclear fractions resolved on a 10 % SDS PAGE gel, transferred to nitrocellulose and Western blotted with anti p65 and anti p50 antibodies. Western blotting with NFκB p50 subunit antibody is shown in (a) while Western blotting with NFκB p65 subunit antibody is shown in (b).

As shown in Figure 6-14, ES-62 stimulation of WEHI-231 B cells results in an overall decrease in the level of the p50 subunit of NF κ B in the cytosolic fraction, compared to the levels of p50 in the cytoplasmic fraction of the control cells. The decrease in the p50 subunit is especially noticeable at the 30 minute and 1 hour timepoints where only a very low level of p50 was detected. The p50 subunit of NF κ B was not detected in the control cell nuclear fraction. However, the p50 subunit of NF κ B was detectable in the nuclear fractions from ES-62 treated cells especially at the 30 minute timepoint. This correlates with the decrease in the levels of the p50 subunit observed in the cytosolic fractions at 30 minutes and could indicate translocation of the p50 subunit of NF κ B to the nucleus.

A decrease in the level of the p65 subunit of NF κ B is also observed in the cytosolic fractions of WEHI-231 B cells stimulated with ES-62. This decrease is especially noticeable at 30 minutes. In contrast, the level of the p65 subunit in the nuclear fractions of WEHI-231 B cells stimulated with ES-62 at 30 minutes is increased compared with control cells. Similarly to the results observed for the p50 subunit of NF κ B, this indicates that translocation of the p65 subunit to the nucleus is occurring. Translocation of both the p50 and p65 subunits to the nucleus in response to ES-62 stimulation of WEHI-231 B cells suggests that ES-62 induces upregulation of NF κ B. This correlates with the data obtained from the EMSA experiment, shown in Figure 6-10 (a), which indicate that upregulation of NF κ B occurred following ES-62 stimulation of WEHI-231 B cells for 30 minutes.

As it appears that ES-62 induces changes in the levels of the two transcription factors, NF κ B and E2F, it is postulated that this transcription factor modulation occurs in order to induce some of the immunomodulatory effects which have been attributed to ES-62. The induction of changes in the levels of transcription factors in ES-62 treated cells and, in particular the change in levels of NF κ B, lends support to the proposition that TLRs could be involved as receptors for ES-62. The modulation of E2F by ES-62 could explain the decrease in B cell proliferation observed

following ES-62 stimulation of B cells as E2F is involved in the regulation of the cell cycle and thus in the division of cells.

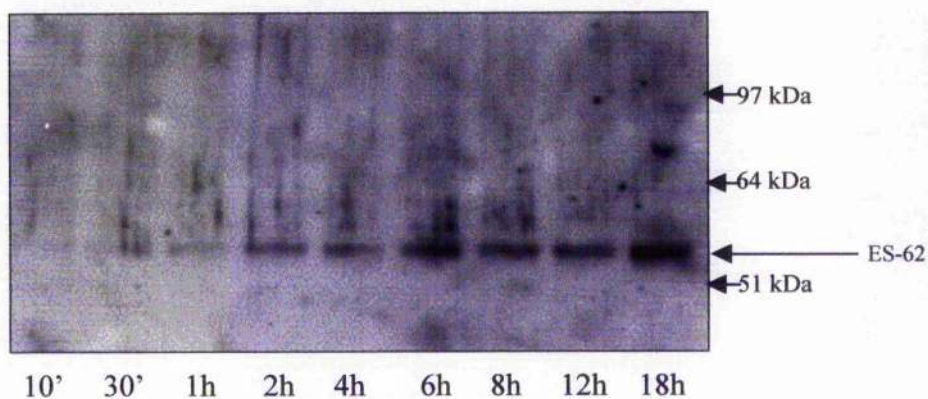
6.3.4. Subcellular localisation

In addition to identifying the receptors of ES-62, the fate of ES-62 following receptor binding was also examined to determine whether ES-62 is internalised following receptor binding. Should ES-62 be internalised, ES-62 may bind intracellular proteins to induce immunomodulatory effects on immune system cells. The concept that ES-62 may be internalised following receptor binding was postulated in view of studies (O.Halaas, Keystone Symposium, 2001) which demonstrated that at least TLR2 translocates to the nucleus following stimulation. As an initial experiment to investigate whether ES-62 was internalised following receptor binding, nuclear and cytosolic fractions of macrophages stimulated with ES-62 ($2 \mu\text{g ml}^{-1}$) for 10, 30 minutes, 1, 2, 4, 6, 8, 12 or 18 hours were obtained from Dr. H. Goodridge, resolved by SDS PAGE, transferred to nitrocellulose and Western blotted with anti-ES-62 antibody. As shown in Figure 6-15, ES-62 was detected in both the cytosolic and nuclear fractions of macrophages stimulated with ES-62.

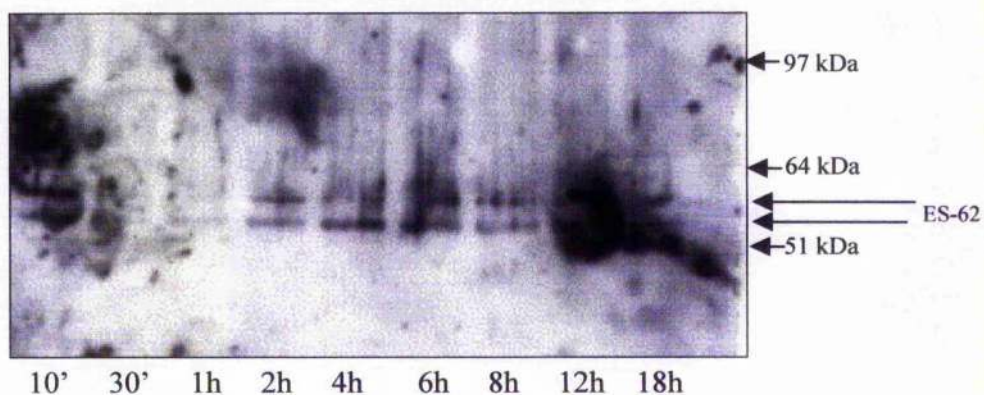
As shown in Figure 6-15, with time ES-62 is located in both the cytoplasm and nucleus of macrophages incubated with ES-62. ES-62 appears to be present as a doublet of approximately p55 and 60 kDa in the nuclear fraction and as a single band of approximately 55 kDa in the cytoplasmic fraction. This suggests that ES-62 is undergoing modification following internalisation. ES-62 has been shown to possess aminopeptidase activity as mentioned previously. It is possible that ES-62 may undergo self digestion, utilising the aminopeptidase activity that it possesses to yield a modified form of the protein, which is capable of inducing further immunomodulatory effects.

Figure 6-15: ES-62 is internalised by macrophages following receptor binding and is located in both the nucleus and cytosol of these cells. (a) Cytoplasmic fractions of macrophages incubated with ES-62 ($2 \mu\text{g ml}^{-1}$) for 10, 30 minutes, 1, 2, 4, 6, 8, 12 or 18 hours and Western blotted using anti-ES-62 as described in Chapter 2. (b) Nuclear fractions of macrophages incubated with ES-62 ($2 \mu\text{g ml}^{-1}$) for 10, 30 minutes, 1, 2, 4, 6, 8, 12 or 18 hours and Western blotted using anti-ES-62 antibody as described in Chapter 2. (c) Blot (b) described above stripped following Western blotting with anti-ES-62 antibody, and Western blotted with TEPC-15 (anti-PC) antibody. Cytoplasmic and nuclear fractions of macrophages incubated with ES-62 were obtained from Dr. H. Goodridge as were the scans shown in (a) and (b) above.

(a) Cytosolic fractions Western blotted with anti-ES-62 antibody.



(b) Nuclear fractions Western blotted with anti-ES-62 antibody.



(c) Nuclear fractions Western blotted with TEPC-15 (anti-PC) antibody.

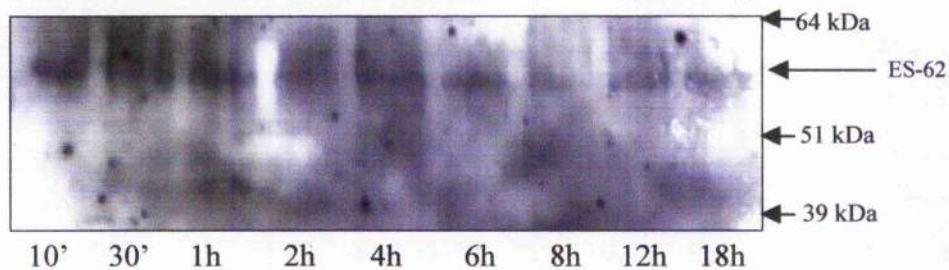


Figure 6-15: ES-62 is internalised by macrophages following receptor binding and is located in both the nucleus and cytosol of these cells.

Western blotting of the resolved nuclear and cytosolic fractions of macrophages stimulated with ES-62 with TEPC-15 (anti-PC) revealed that only one of the two bands in the nuclear fractions demonstrated to be PC-containing ES-62 and that the ES-62 present in the cytoplasm did not contain PC (not shown). This suggested that 2 forms of ES-62 were present in the nucleus of ES-62 treated macrophages; wild type ES-62 i.e. that containing PC, and a PC lacking form of ES-62. The PC lacking form of ES-62 is the form present in the cytoplasm of ES-62 treated macrophages. The identification of bands by TEPC-15 (anti-PC) similar to those identified by anti-ES-62 corroborates the finding that ES-62 is internalised following receptor binding.

One hypothesis is that ES-62 is internalised by macrophages following receptor binding and is delivered, by an as yet unknown method, to the nucleus of the cells. Once in the nucleus it is modified in such a way that the PC moieties are removed and the PC lacking form of ES-62 then locates to the cytoplasm. PC is known to act as a second messenger and to possess immunomodulatory properties (Cuadrado *et al.*, 1993). Therefore it is possible that ES-62 is modified to release the PC moieties so that the PC moieties can induce various signalling effects within the cell, including some of the observed immunomodulatory effects. The PC lacking form of ES-62 may translocate to different regions of the cell and induce further immunomodulatory effects.

Following the discovery that ES-62 was internalised by macrophages and was located in both the nucleus and cytoplasm of these cells, the fate of ES-62 following receptor binding in B cells was examined using the murine immature B cell line, WEHI-231. As a result of the identification of different forms of ES-62 in the nucleus and cytoplasm of ES-62 stimulated macrophages, radiolabelled forms of ES-62 were employed to allow the quantitative measurement of the different forms of ES-62 present. Two radiolabelled forms of ES-62 were made and supplied by Professor W. Harnett, Strathclyde. The two forms utilised were [^3H]-choline labelled ES-62, and [^{35}S] labelled ES-62. The [^3H]-choline labelled ES-62 allowed the location of the PC-containing ES-62 to be determined while the [^{35}S] labelled ES-62

allowed the location of the protein component of ES-62 to be determined regardless of the presence or absence of PC moieties. WEHI-231 B cells were incubated with either [^3H]-choline labelled ES-62 or [^{35}S] labelled ES-62 over a range of timepoints and cytosolic and nuclear fractions prepared for each timepoint. The levels of radiolabelled ES-62 present in each sample was then measured using a scintillation counter as described in Chapter 2. The data obtained is shown in Figure 6-16, presented in a graphical format with the background counts subtracted. As shown in Figure 6-16, [^3H] choline labelled ES-62 was detected rapidly within the nucleus, with two peaks, one at 30 minutes and the other at 4 hours. [^3H] choline labelled ES-62 was also detected in the cytosol of the cells, but at very low levels. Following 24 hour incubation of [^3H] choline labelled ES-62 with WEHI-231 B cells, PC-ES-62 was not detected in the nucleus and was only present in very small quantities in the cytoplasm. This suggests that PC-ES-62 was degraded in a relatively short time period either by proteases within the cell or by self-degradation. *In vivo*, ES-62 is secreted by the parasite continually giving rise to a constant level of ES-62 present in the host bloodstream. The degradation of PC-ES-62 could be the result of a host immune response mounted against ES-62 or it could be a method by which the parasite limits the level of immunomodulation induced.

[^{35}S] labelled ES-62 was detected in both the nucleus and the cytosol of WEHI-231 B cells. Peak levels of [^{35}S] labelled ES-62 were detected between 1 and 4 hours. Similarly to [^3H] choline labelled ES-62, the levels of [^{35}S] labelled ES-62 were undetectable following 24 hours incubation. The levels of [^{35}S] labelled ES-62 detected were greater in the cytosol than in the nucleus. These results demonstrate that while the protein component of ES-62 can be shown to reside in both the cytosol and nucleus of cells, the majority resides in the cytosol. In contrast, the majority of the PC-ES-62 is located in the nucleus. These findings suggest that, like macrophages, WEHI-231 B cells internalise ES-62 following receptor binding and that two forms of ES-62 are present in the nucleus – a PC containing and a PC lacking form of ES-62, while in the cytosol only the PC lacking form of ES-62 exists. Macrophages are known to internalise many proteins by receptor mediated

endocytosis and thus this may be the process by which ES-62 is internalised by macrophages. Whether WEHI-231 cells also employ endocytosis to internalise ES-62 is unknown. As discussed, TLRs, the putative receptors for ES-62, are known to internalise following ligand binding perhaps providing further substantiating evidence for the utilisation of TLRs as receptors for ES-62.

To corroborate the location of internalised ES-62 within the cells, murine splenic mononuclear cells were incubated with ES-62-FITC for various timepoints, stained for either mIg (B cells) or CD3 (T cells), fixed and microscopy analysis performed. Visualisation of the stained cells allowed identification of the splenic B cell preparation as positive for mIg, however, no ES-62-FITC signal was observed. As the location of the ES-62-FITC could not be detected using microscopy, FACS analysis, capable of detecting a much weaker signal than microscopy but which does not provide intracellular localisation information, was employed. For FACS analysis, murine splenic B cells were stained with ES-62-FITC alone or in conjunction with mIg or CD3 stains. FACS analysis allowed detection of B cells within the purified splenic B cell samples, but again ES-62-FITC could not be detected. It was postulated that this inability to detect ES-62 bound to or internalised by splenic B cells may be due to low receptor numbers on splenic B cells leading to a low signal that was undetectable.

The ability of ES-62 to bind DNA was investigated following Western blotting analysis of nuclear and cytosolic fractions of macrophages and WEHI-231 B cells incubated with ES-62 (Figure 6-14), which showed that ES-62 translocates to the nucleus following receptor binding. In addition, earlier EMSA studies had demonstrated that ES-62 modulates transcription factor activity (Figure 6-12 and Figure 6-13). Genomic DNA from WEHI-231 B cells and macrophages was digested with Eco RI or Bam HI and then incubated with [³⁵S] labelled ES-62 for 30 minutes. The samples were then resolved on a 6 % polyacrylamide gel, fixed, incubated in Amplify (amplifies radioactive signal to aid detection), dried and exposed to X-ray film. Visualisation of the radiolabelled ES-62 showed no

discernible differences between the control sample to which no digested DNA had been added and the samples to which digested DNA had been added. In addition, to investigate whether ES-62 was capable of binding directly to the NF κ B or E2F DNA motif, ES-62 was incubated with radiolabelled NF κ B or E2F DNA motifs. The results from this experiment showed that ES-62 did not bind directly to either the NF κ B or E2F DNA motif. Thus ES-62 must be inducing its effects on NF κ B and E2F through activation and suppression of the relevant NF κ B or E2F subunits as suggested in Figure 6-11.

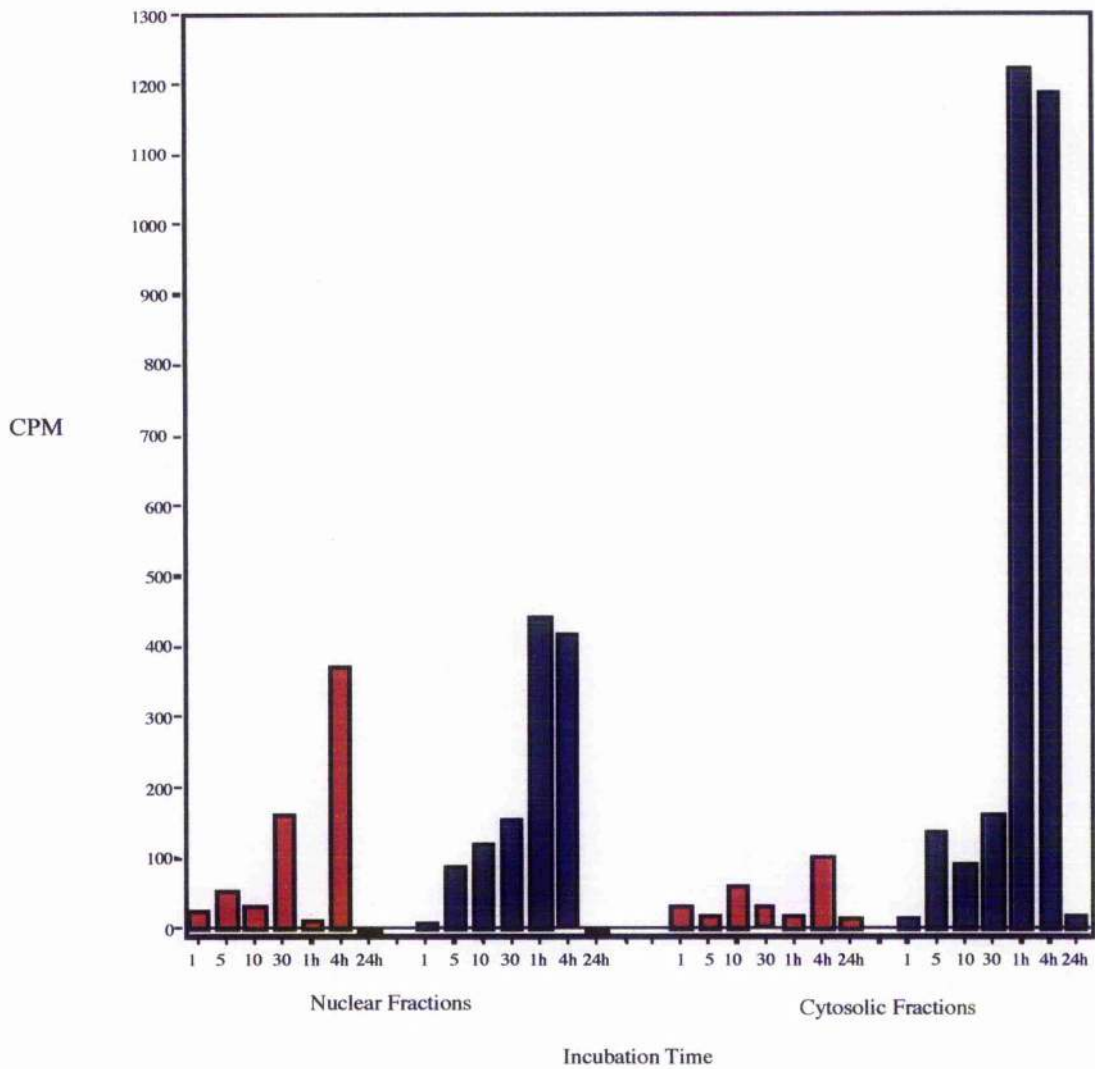


Figure 6-16: Localisation of ES-62 in WEHI-231 B cells following receptor binding. WEHI-231 B cells were incubated separately with either [^3H]-choline labelled or [^{35}S] labelled ES-62 for specific time periods. Nuclear and cytosolic fractions were prepared as discussed in Chapter 2. Scintillant was then added to the nuclear and cytosolic fractions to allow determination of the level of radioactive protein in each fraction. Red bars represent samples incubated with [^3H]-choline labelled ES-62. Blue bars represent samples incubated with [^{35}S] labelled ES-62. CPM values are corrected for background readings.

6.4. Discussion

These studies have identified a number of cellular proteins of varying molecular weights, which bind ES-62. Examination of both whole cell lysates and membrane fractions, resolved by SDS PAGE, identified two cellular surface proteins that appeared to bind ES-62. One or more proteins of approximately 82 kDa are present in all the cell types tested (splenic B cells, U937 monocytic cells, Jurkat T cells, REH cells, Nalm6 cells, 207 cells, 697 cells, WEHI-231 B cells, Daudi follicular B cells and Ramos follicular B cells). A higher molecular weight protein, approximately 135 kDa, was detected in splenic B cells, Jurkat T cells, REH cells, Nalm6 cells, 207 cells, 697 cells and WEHI-231 B cells. As the higher molecular weight protein is not present in all of the cell lines and can vary in size, it would appear that different proteins are forming a receptor complex capable of binding ES-62 depending on the cell type under consideration.

Western blotting and immunoprecipitation techniques demonstrated that ES-62 bound to the proteins identified in a PC dependent manner indicating an important role for the PC moieties of ES-62 in receptor binding. These findings are substantiated by data from BiaCore experiments (*W and M Harnett*, unpublished) which demonstrated that membranes from splenic B cells, U937 monocytic cells and Jurkat T cells bound ES-62 in a PC-dependent manner and with receptor like affinity but with different binding kinetics depending on the cell type. It is postulated that the different binding kinetics are due to the recruitment of different proteins to form an ES-62 receptor complex in different cell types.

Studies carried out to identify the proteins detected as binding to ES-62 revealed that the 82 kDa protein identified in splenic B cells, U937 monocytic cells, Jurkat T cells, REH cells, Nalm6 cells, 207 cells, 697 cells, WEHI-231 B cells, Daudi follicular B cells and Ramos follicular B cells showed reactivity with anti-TLR antibodies, reacting positively with both TLR2 and TLR4 antibodies. The 82 kDa protein identified in U937 monocytic cells, Jurkat T cells and Nalm6 cells did not react positively with either the TLR2 or 4 antibody. As U937 monocytic cells have

been reported not to express TLR2 on their cell surface (Cario *et al.*, 2000) this finding is not unexpected. However, it is possible that this 82 kDa protein is one of the other TLR proteins. The proposal that one of the proteins that constitutes the receptor for ES-62 is a TLR is supported by the finding that ES-62 and TLRs induce similar downstream signalling events, such as induction of NF κ B and modulation of the Ras MAPK pathway. Preliminary data from ongoing research carried out with Dr. H. Goodridge, using TLR knockout mice suggests that ES-62 may at least in part utilise one of the TLRs as a receptor. The higher molecular weight protein identified as binding ES-62 has not been characterised as yet and appears to vary depending on cell type. Integrins were investigated as one of the possibilities for the 135 kDa receptor chain, however, experiments involving the pre-incubation of biotinylated membranes with fucose or RGDS/RDES peptides showed no effect on ES-62 binding. These results appeared to exclude at least some of the integrins as a possible receptor for ES-62.

N-terminal sequencing of the proteins identified as binding ES-62 would be the definitive method of identifying the proteins. However, preliminary experiments, involving the isolation of the proteins identified to bind ES-62 from SDS PAGE gels, revealed obtaining sufficient suitable material to be difficult. Alternatively the use of mass spectrometry to analyse small quantities of protein within a polyacrylamide gel might enable further characterisation of the identified proteins. These two techniques would be worthwhile future experiments to carry out in the search to definitively identify the proteins that act as a receptor for ES-62.

Studies carried out as part of this PhD project have shown that ES-62 stimulation of cells causes an initial activation of the signalling pathways downstream of the B cell receptor leading to an early activation of Erk. Erk is then rapidly deactivated in such a way that further activation in response to stimulation of the B cell receptor does not occur. This data corroborated earlier work (Deehan *et al.*, 1998a) that showed pre-incubation of splenic B cells with ES-62 prior to stimulation with anti-Ig resulted in abortive activation of B cell signalling. This abortive activation is thought

to occur by a mechanism in which ES-62 promotes dual phosphorylation of Erk and simultaneously primes recruitment of phosphatase. This phosphatase then dephosphorylates one of the two phosphorylated sites of Erk. The remaining phosphorylated site then blocks rephosphorylation of the second site and hence activation of Erk.

ES-62 was also shown to induce effects on the two transcription factors, NF κ B and E2F, through the use of EMSAs and Western blotting of cytosolic and nuclear fractions of cells stimulated with ES-62. The induction of NF κ B and the modulation of MAP kinase family members in response to ES-62 treatment further supports the proposal that TLRs form part of the receptor for ES-62 as TLR stimulation also leads to activation of NF κ B via recruitment of MAP kinase family members.

The discovery that ES-62 influences transcription factors raises the question as to how these effects are induced, i.e. solely through the receptor or through internalisation of ES-62 and direct interaction of ES-62 with cytosolic or nuclear proteins. As ES-62 is found within both the cytosol and nucleus of stimulated cells it is likely that ES-62 induces at least some of its effects through direct binding with cytosolic, nuclear proteins or perhaps even DNA. A bacterial aminopeptidase, Pep A, is known to be a sequence specific DNA binding protein capable of regulating expression of bacterial genes (Charlier *et al.*, 1995). This raises the possibility that ES-62, also known to possess aminopeptidase activity, could regulate gene expression by binding directly to DNA motifs that control gene expression. As discussed in section 6.3.4, ES-62 does not bind to the NF κ B or E2F motifs and preliminary studies into the DNA binding capabilities of ES-62, involving the incubation of radiolabelled ES-62 with digested genomic DNA, were inconclusive. Further work including a DNase protection assay (Charlier *et al.*, 1995), could be performed to identify the DNA binding capabilities of ES-62. To carry out this assay ES-62 would be incubated separately with radioactively end-labelled DNA from a variety of cells. DNase would then added to digest any unprotected DNA. The sample would then be resolved polyacrylamide gel. If ES-62 did not bind to DNA

then a DNA ladder would be observed. However, if ES-62 did bind to DNA then in contrast to digested radioactively end labelled DNA to which no protein had been added a gap would be observed in the DNA ladder .

Further studies to examine the methods by which ES-62 induces its immunomodulatory effects upon cells could include examination of whether ES-62 affects any other transcription factors and whether it is capable of binding to DNA itself. It would also be interesting to attempt to identify whether internalised ES-62 is capable of binding to cytosolic or nuclear proteins. Identification of these proteins would enable elucidation of the signalling pathways employed by ES-62 to elicit its immunomodulatory effects.

7. Conclusions

The aim of this PhD was to obtain structural information about the filarial parasite excretory-secretory product ES-62 and to identify the host cellular proteins exploited as receptors for this immunomodulatory protein. Three methodologies were used to obtain structural information pertaining to ES-62; bioinformatics techniques, analytical ultracentrifugation studies and small angle X-ray scattering studies. In addition, a range of techniques including far Western blotting, Western blotting, immunoprecipitation and localisation studies were employed to determine the identity of the receptor for ES-62 and to examine the fate of ES-62 following receptor binding. Further, two expression systems for the production of recombinant ES-62 lacking either the PC component or the PC and carbohydrate components of wild type ES-62 were established, to allow both structural and biochemical studies of the effects of the carbohydrate and PC moieties on ES-62.

Filariasis affects approximately 150 million people world-wide and currently there are few effective treatments available. Filariasis has been classified by the W.H.O. as potentially eradicable (W.H.O., 1999a; W.I.L.O., 1999b). Many studies are ongoing to determine more effective chemotherapy targets and potential vaccines to treat filariasis. ES-62 was chosen as the target for study in this PhD as it is the excretory-secretory glycoprotein of the rodent filarial parasite *A. viteae* which is widely employed as a model system for the study of human filariasis. It was believed that structural studies and further characterisation of ES-62 would lead to a better understanding of the mechanism of action of ES-62 and ES proteins in general. In addition, it was hoped that identification of proteins homologous to ES-62 would further aid elucidation of the immunomodulatory function of ES-62 and the methods it exploits.

On the basis of the information gained from the various methodologies employed during this PhD, this chapter presents a putative method of action of ES-62. Earlier work (Deehan *et al.*, 1998a; Deehan *et al.*, 1998b; Goodridge *et al.*, 2001; Harnett & Harnett, 1999a; Harnett *et al.*, 1999a; Harnett & Harnett, 1993; Harnett & Harnett, 2001; Harnett *et al.*, 1989) has shown that ES-62 binds, via a unknown receptor, to immune system cells, polyclonally activates certain protein tyrosine kinases (PTKs) and MAP kinase signal transduction elements and modulates PKC activity and expression leading to desensitisation of both B and T lymphocytes to subsequent BcR mediated activity. ES-62 signalling promotes BcR activation of SHP-1 tyrosine phosphatase. SHP-1 prevents BcR signalling by maintaining the ITAM motifs of Ig α and Ig β in a resting dephosphorylated state. This prevents recruitment of the Shc-Grb2-Sos complexes to the BcR and thus Ras cannot be activated. ES-62 signalling also promotes BcR-driven association of the nuclear MAP kinase dual (tyr/thr) phosphatase, PAC-1, with Erk to terminate any persisting Erk signals. This dual pronged mechanism results in a rapid and profound desensitisation of BcR coupling to the Ras/Erk MAP kinases cascade.

7.1. A Proposed Mechanism of Action of ES-62

7.1.1. Tetrameric Nature of ES-62

Structural characterisation that revealed the quaternary structure and the overall shape of ES-62, was performed using AUC and SAXS. Sedimentation equilibrium and sedimentation velocity AUC studies confirmed earlier gel filtration experiments that showed that ES-62 exists as a tetramer. SAXS further substantiated the finding that the majority of ES-62 exists in a tetrameric state and enabled the generation of a low resolution, 19Å, three dimensional model of ES-62.

The three models generated for ES-62, using different point symmetries, were found to be similar, indicating that the models generated were robust and likely to be correct. As SAXS relies on contrast between the solute under study and the solvent,

and given that the contrast between carbohydrate and solvent is very small, the carbohydrate component of proteins is not always fully visualised. This has implications for the SAXS determined structure of ES-62, as ES-62 is glycosylated and the DAMMIN structure may not fully represent the full carbohydrate component of ES-62. However, the sedimentation coefficients determined for the modelled structures show good correlation with the experimentally derived (AUC) sedimentation coefficient supporting the DAMMIN models as the structure of ES-62. The low resolution structure of ES-62 also provides phase information, which may be of importance in the future if crystals of ES-62 are obtained for X-ray crystallography studies.

The tetrameric nature of ES-62, determined by the AUC and SAXS, is hypothesised to be essential for steric purposes such that the PC moieties of ES-62, essential for receptor binding, adopt the correct conformation for recruitment and binding to the cellular membrane proteins.

7.1.2. Identification of the Receptor of ES-62

As shown in Figure 7-1, it is proposed that the tetrameric form of ES-62 binds to a cell surface receptor to elicit its immunomodulatory effects. Far Western and Western blot analyses and immunoprecipitation experiments of a number of different cell types and at different levels of maturity, suggest that one of the proteins acting as part of the receptor for ES-62 could be one or more Toll like receptors (TLRs). This finding was further substantiated by previous studies on the signalling induced in response to TLR stimulation (O'Neill & Dinarello, 2000) which revealed strong similarities of TLR signalling to the signalling induced in response to ES-62.

The second, higher molecular weight protein identified as acting in conjunction with the TLR as a receptor for ES-62, appeared to vary with cell type. Studies to date indicate that the second protein is not TLR2 or TLR4. Initial studies, examining

whether Arg-Gly-Asp (RGD) peptides could block binding of ES-62 to the higher molecular weight protein acting as a receptor for ES-62, suggested that the second protein was not a member of the integrin family of proteins, which typically recognise the RGD motif. However, as not all integrins bind via these RGD motifs (Assa-Munt *et al.*, 2001), further studies including Western blotting or immunoprecipitation using specific integrin antibodies, would be required before integrins could be entirely ruled out as plausible receptors of ES-62.

ES-62 receptor binding was shown to be PC dependent through far Western blotting, immunoprecipitation experimentation and BiaCore analysis. As discussed, the existence of ES-62 in a tetrameric state was postulated to provide the correct steric arrangement of the PC moieties such that the two receptor chains which bind ES-62 can be recruited. Future studies involving the stimulation of cells with a monomeric form of ES-62 would allow this hypothesis to be tested. ES-62 can be induced to monomerise by lowering the pH to below 6. However, initial attempts to obtain monomeric ES-62 were hampered by low yields of soluble protein. Further investigation suggested that a gradual lowering of the pH may increase yields allowing these experiments to be carried out, but time constraints inhibited further study.

7.1.3. The Fate of ES-62 following Receptor Binding

Studies examining the fate of ES-62 following receptor binding show that ES-62 is internalised following receptor binding and is located in both the cytoplasm and nucleus of cells as shown in Figure 7-1. Two forms of ES-62 can be identified within the nucleus; PC-containing and PC-free forms of ES-62. Within the cytoplasm only the PC-free form of ES-62 is present. These findings led to the hypothesis that ES-62 is internalised to the nucleus following receptor binding where it is modified such that the PC moieties are removed. The putative mechanisms by which ES-62 is internalised and the PC moieties are removed are

suggested by the results obtained through AUC studies, bioinformatics and experimental work.

Sedimentation equilibrium AUC experiments showed the presence of a lower molecular weight form of ES-62, present in such minute quantities that it was not possible to determine whether it was monomer or dimer that was present. Sedimentation equilibrium experiments performed at increasingly dilute concentrations could possibly allow this to be resolved. However, as the protein concentration decreases the difference between sample signal and background noise also decreases making analysis of data increasingly more difficult.

As ES-62 exists in both a lower molecular weight form (either monomeric or dimeric) and a tetrameric state, the question exists as to whether ES-62 is secreted by the parasite in a monomeric or dimeric state and then tetramerises or whether it is secreted in the tetrameric form and then becomes monomeric or dimeric. As AUC studies indicated the majority of ES-62 to be tetrameric, it is possible that ES-62 has to be tetrameric to fulfil steric requirements in order to gain entry into host cells. Once internalised, it may monomerise or dimerise via endocytosis internalisation which would expose ES-62 to lower pH levels. ES-62 has been shown to dissociate to monomeric and dimeric forms when the pH is dropped below 6. As shown in Figure 7-1, internalisation of ES-62 may occur via receptor mediated endocytosis, which due to the reduction of pH within the endosome, could allow dissociation of the ES-62 tetramer to occur prior to its delivery to the cell nucleus. Once within the nucleus ES-62 may undergo modification to create a PC-free form. This may be the result of self-digestion.

Earlier experimental work (Harnett *et al.*, 1999b) has shown ES-62 to possess aminopeptidase activity. Bioinformatic techniques (Chapter 3) identified six proteins of 37-39 % identity to ES-62, two of which are classified as aminopeptidases and three of which possess carboxypeptidase activity. All six proteins identified were shown to possess a peptidase motif. These findings indicate a role for peptidase

activity in the induction of immunomodulatory effects by ES-62. It is possible that ES-62 utilises this aminopeptidase activity for self digestion which could lead to an active form of ES-62 capable of inducing immunomodulatory effects. Self-digestion may also enable release of the PC moieties of ES-62 resulting in a PC-free form of ES-62, which is found in the cytoplasm of host cells. To investigate this further, it would be necessary to determine if ES-62 possesses aminopeptidase target motifs near to glycosylation sites which, if digested, could lead to the removal of the PC components of ES-62. The released PC moieties (free PC, PC-glycan or PC-glycan-peptide) may induce immunomodulatory effects within the cell, as indicated by earlier work (Harnett & Harnett, 1993), which demonstrated that PC alone could induce many of the effects on signalling cascades which occur following incubation of cells with ES-62.

Alternatively the aminopeptidase activity may allow ES-62 to digest cellular proteins either to prevent removal of ES-62 by the host immune response or to induce some form of immunomodulation. Further studies including identification of target sequences for ES-62 aminopeptidase activity, optimal conditions for digestion and the effects of peptidase inhibitors on ES-62 induced effects would be essential in order to determine the role of the aminopeptidase activity of ES-62. It would also be interesting to incubate ES-62 under optimal conditions for aminopeptidase activity, but in the absence of any substrate to determine if self-digestion is feasible.

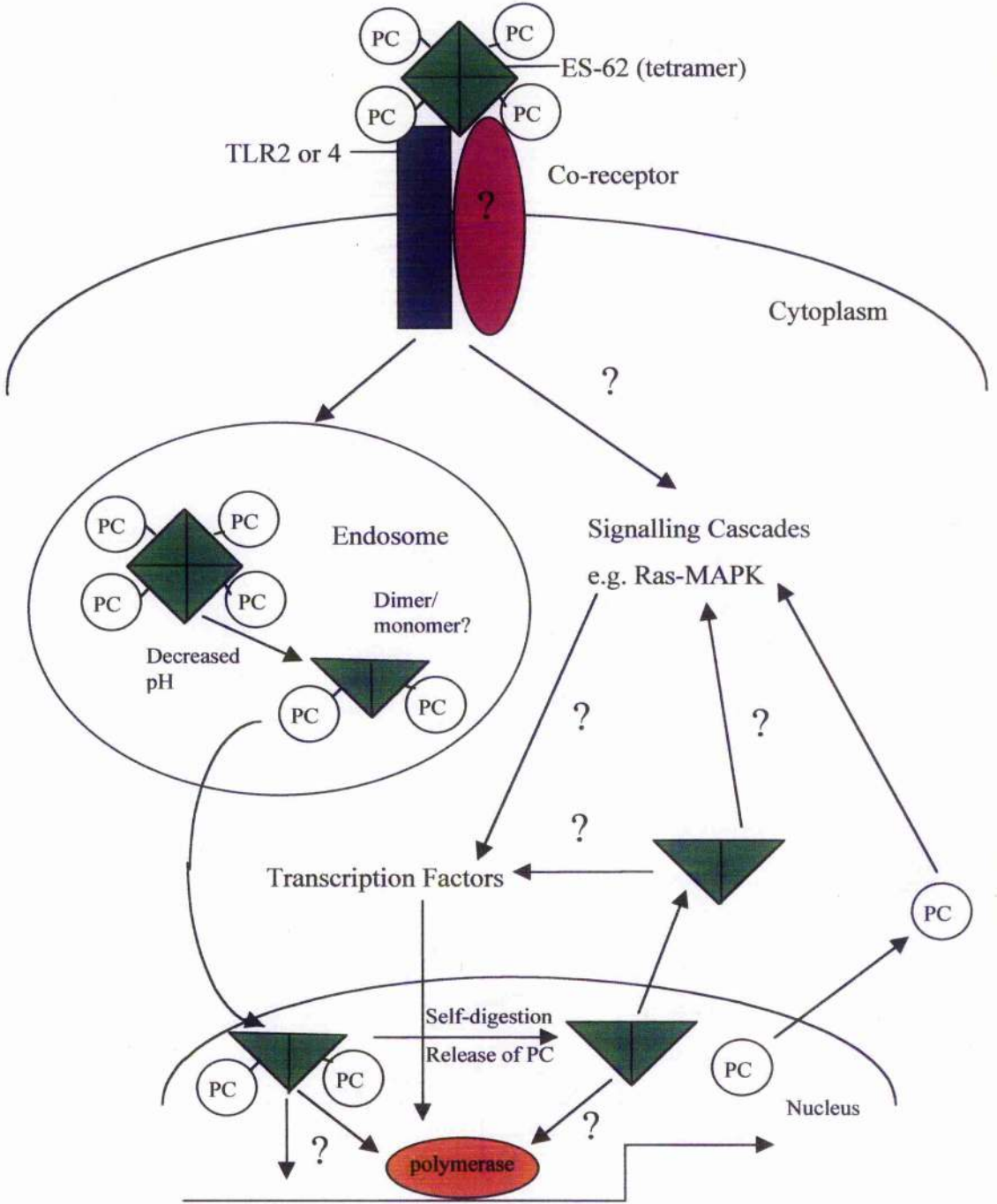
The PC-free form of ES-62 in the nucleus is postulated to translocate to the cytoplasm as shown by internalisation studies discussed in section 6.3.4. This hypothesis suggests that induction of a signalling cascade following receptor binding is not the sole mechanism by which ES-62 modulates the host immune system. The location of ES-62 in both the nucleus and cytoplasm and its existence in different forms in these two locations suggest that ES-62 is multifunctional.

It is possible that in the nucleus ES-62 binds directly to DNA motifs to regulate gene expression. This hypothesis is supported by the possible presence of DNA bound to

the recombinant form of ES-62 produced using the baculovirus expression system. It is also plausible that if ES-62 is not binding directly to DNA to modify gene expression that it is binding, perhaps via its leucine rich regions, to transcription factors and inducing its effects in this manner. The discovery of the modulatory effects of ES-62 on NF κ B and E2F further support this hypothesis.

The PC-free form of ES-62 present in the cytoplasm is postulated to induce distinct modulatory effects, perhaps acting on signalling cascades such as the Ras-MAPK pathway which are known to be affected by ES-62 (Harnett & Harnett, 1999a; Harnett et al., 1999a). In addition, the PC-free form of ES-62 present in the cytoplasm may induce the activation or translocation of transcription factors, such as NF κ B, to the nucleus as described in section 6.3.3.

Figure 7-1: Proposed mechanism of action of ES-62. ES-62 is recognised and internalised by a receptor complex of TLR 2 or 4 and an unidentified co-receptor. Low pH in the endosome may result in ES-62 dissociation to dimers (or monomers) which are delivered to the nucleus. ES-62 may then undergo self-digestion to form a PC-free form which translocates to the cytoplasm to induce immunomodulatory effects. The free PC moieties also translocate out of the nucleus to induce modulatory effects. The ES-62 remaining in the nucleus may modulate gene expression either by binding directly to DNA or to transcription factors.



7.2. *Future Work*

The structural studies of ES-62 carried out as part of this PhD were successful and led to the identification of a number of proteins homologous to ES-62, the characterisation of ES-62 as a tetramer and the generation of a three dimensional model of ES-62. However, there are still many avenues to investigate, not least the aminopeptidase activity of ES-62 and its ability to dissociate into monomers or dimers. Continuation of these structural studies would ideally address these questions as well as encompassing new strategies to further the structural characterisation of ES-62. Structural studies, including CD, AUC and SAXS, on a monomeric form of ES-62, ideally monomeric ES-62 obtained through the lowering of the solvent pH in a solution of wild type ES-62, would allow the determination of any differences in the secondary structure of monomeric and tetrameric ES-62 and whether monomeric ES-62 can exist without aggregation occurring. This would provide information as to whether it is plausible that ES-62 can form monomeric or dimeric units following internalisation to induce immunomodulatory effects. Structural studies of recombinant ES-62, lacking PC and perhaps possessing less carbohydrate moieties could lead to a greater understanding of the effects these two moieties elicit on the structure of ES-62

Utilisation of new strategies to obtain structural information regarding ES-62 could include the use of genetic techniques to selectively knock-out residues conserved between ES-62 and the identified homologous proteins to determine if these conserved residues play a structural role in these proteins. Similarly it would be interesting to further investigate the similarity between ES-62 and C-reactive protein, particularly in the PC binding region of C-reactive protein, which has been shown to demonstrate similarities to a small region of ES-62 (Harnett et al., 1999a).

Studies to further characterise both the receptors for ES-62 could include isolating these proteins for N-terminal sequencing possibly by performing an immunoprecipitation, using anti-ES-62 antibodies or anti-FITC antibodies, of cellular membranes pre-incubated with either ES-62 or an ES-62 – FITC conjugate.

Ongoing work by H. Goodridge examining the effects of ES-62 on TLR knockout mice will hopefully aid characterisation of the receptors of ES-62 and its mechanism of action.

Clearly ES-62 elicits its range of immunomodulatory activities by a variety of mechanisms, with the PC and the protein components of ES-62 playing particular roles. Further investigation, including detailed structural characterisation of this intriguing molecule is essential to understand the signalling mechanisms promoted by this molecule and to allow the development of novel agents for the treatment of filarial infections.

8. References

- Acosta, D., Goni, F. & Carmona, C. (1998). Characterisation and partial purification of a leucine aminopeptidase from *Fasciola hepatica*. *Journal of Parasitology* **84**, 1-7.
- Alberts, B., Bray, D., Lewis, J., Raff, M., Roberts, K. & Watson, J. D. (1994). *Molecular Biology of the Cell*. Third edition (Robertson, M., Ed.), Garland Publishing Inc., New York.
- Allen, J. E. & MacDonald, A. S. (1998). Profound suppression of cellular proliferation mediated by the secretions of nematodes. *Parasite Immunology* **20**, 241-247.
- Altschul, S. F. & Koonin, E. V. (1998). Iterated profile searches with PSI-BLAST - a tool for discovery in protein databases. *Trends in Biological Sciences* **23**, 444-447.
- Altschul, S. F., Madden, T. L., Schaffer, A. A., Zhang, J. H., Zhang, Z. & Miller, W. (1997). Gapped BLAST and PSI-BLAST: a new generation of protein database. *Nucleic Acids Research* **25**(17), 3389-3402.
- Assa-Munt, N., Jia, X., Laakkonen, P. & Ruoslahti, E. (2001). Solution structures and integrin binding activities of an RGD peptide with two isomers. *Biochemistry* **40**, 2373-2378.
- Aszodi, A. & Taylor, W. R. (1994a). Folding polypeptide α -carbon backbones by distance geometry methods. *Biopolymers* **34**, 489-505.
- Aszodi, A. & Taylor, W. R. (1994b). Secondary structure formation in model polypeptide chains. *Protein Engineering* **7**(5), 613-644.

Babu, S., Porte, P., Klei, T.R., Shultz, L.D., Rajan, T.V. (1998) Host NK Cells are Required for the Growth of the Human Filarial Parasite *Brugia malayi* in Mice. *Journal of Immunology* **161**, 1428-1432

Bach, M. A., Kohler, H. & Levitt, D. (1983). Binding of phosphorlycholine by non-immunoglobulin molecules on mouse B cells. *Journal of Immunology* **131**(1), 365-369.

Bairoch, A., Bucher, P. & Hofmann, K. (1997). The PROSITE database, its status in 1997. *Nucleic Acids Research* **25**, 217-221.

Barton, G. J. (1994). *Unpublished*.

Barton, G. J. (1996). Protein sequence alignment and database scanning. In *Protein Structure Prediction: A Practical Approach* (Sternberg, M. J. E., ed.), pp. 31-64. IRL Press at Oxford University Press, Oxford.

Baschong, W. (1985). Changes in the surface of *Dipetalonema viteae* (*Filarioidea*) during its development as shown by comparative peptide mapping. *Parasitology* **90**, 351-356.

Beckman Instruments. (1992). *Beckman Model XL-A Analytical Ultracentrifuge Training Guide.*, Beckman Instruments Inc., Palo Alto, CA.

Bleasby, A. J., Akrigg, D. & Attwood, T. K. (1994). OWL - a non-redundant composite protein sequence database. *Nucleic Acids Research* **22**(17), 3574-3577.

Boussinesq, M., Prodhon, J. & Chippaux, J. P. (1997). *Onchocerca volvulus*: striking decreases in transmission in the Vina valley (Cameroon) after eight large scale ivermectin treatments. *Transactions of the Royal Society of Tropical Medicine and Hygiene* **91**, 82-86.

- Bruschi, F., Carulli, G., Azzara, A., Marini, A., Ruocco, L. & Ambrogi, F. (1989). Modulating effects by *Trichella spiralis* "sensu stricto" excretory secretory antigens of human neutrophil functions. *Wiadomosci Parazytologiczne* **35**, 391-400.
- Bustelo, X. R., Ledbetter, J. A. & Barbacid, M. (1992). Product of vav proto-oncogene defines a new class of tyrosine protein kinase substrates. *Nature* **356**, 68-71.
- Caberra, Z., Parkhouse, R. M. E., Forsyth, K., Gomez-Priego, A., Pabon, R. & Yarzabal, L. (1989). Specific detection of human antibodies to *Onchocerca volvulus*. *Tropical Medicine and Parasitology* **40**, 454-459.
- Cambier, J. C., Pleiman, C. M. & Clark, M. R. (1994). Signal-transduction by the B-cell antigen receptor and its coreceptors. *Annual Review of Immunology* **12**, 457-486.
- Cario E, Rosenberg IM, Brandwein SI, Beck PL, Reinecker HC, Podolsky DK. (2000) Lipopolysaccharide activates distinct signaling pathways in intestinal epithelial cell lines expressing Toll-like receptors. *Journal of Immunology* **164** (2), 966-72.
- Chacón, P., Díaz, J. F., Moran, F. & Andreu, J. M. (2000). Reconstruction of protein form with X-ray solution scattering and a genetic algorithm. *Journal of Molecular Biology* **299**(5), 1289-1302.
- Chacón, P., Moran, F., Díaz, J. F., Pantos, E. & Andreu, J. M. (1998). Low-resolution structures of proteins in solution retrieved from X-ray scattering with a genetic algorithm. *Biophysical Journal* **74**(6), 2760-2775.
- Chandrashekar, R., Van Swinderen, B., Taylor, H. R. & Weil, G. J. (1995). Effect of ivermectin prophylaxis on antibody responses to *Onchocerca volvulus*

- recombinant antigens in experimentally infected chimpanzees. *International Journal for Parasitology* **25**(8), 983-988.
- Charlier, D., Hassanzadeh G., G., Kholti, A., Gigot, D., Pierard, A. & Glansdorff, N. (1995). carP, involved in pyrimidine regulation of the *Escherichia coli* carbamoylphosphate synthetase operon, encodes a sequence-specific DNA-binding protein identical to XerB and PepA, also required for resolution of ColEI multimers. *Journal of Molecular Biology* **250**(4), 392-406.
- Chen, Y. & Talmage (1998), Institute of Human Nutrition. Direct submission.
- Cheong, W. C. & Yap, H. H. (1985). Bioassays of *Bacillus sphaericus* (strain 1593) against mosquitoes of public health importance in Malaysia. *South East Asian Journal of Tropical Medicine and Public Health* **16**(1), 54-58.
- Chevrier, B., D'Orchymont, H., Schalk, C., Tarnus, C. & Moras, D. (1996). The structure of the *Aeromonas proteolytica* aminopeptidase complexed with a hydroxamate inhibitor. Involvement in catalysis of Glu151 and two zinc ions of the co-catalytic unit. *European Journal of Biochemistry* **237**(2), 393-398.
- Chevrier, B., Schalk, C., D'Orchymont, H., Rondeau, J. M., Moras, D. & Tarnus, C. (1994). Crystal structure of *Aeromonas proteolytica* aminopeptidase: A prototypical member of the co-catalytic zinc enzyme family. *Structure* **2**, 283-291.
- Cohn, E. J. & Edsall, J. T. (1943). *Proteins, Amino Acids and Peptides as Ions and Dipolar Ions*. American Chemical Society Monograph Series, Reinhold Publishing Corp., New York.
- Corpet, F. (1998). Multiple sequence alignment with hierarchical clustering. *Nucleic Acids Research* **16**(22), 10881-10890.

- Corpet, F., Gouzy, J. & Kahn, D. (1998). The ProDom database of protein domain families. *Nucleic Acids Research* **26**(1), 323-326.
- Cuadrado, A., Camero, A., Dolfi, F., Jimenez, B. & Lacal, J. C. (1993). Phosphorylcholine - a novel 2nd messenger essential for mitogenic activity of growth-factors. *Oncogene* **8**(11), 2959-2968.
- Cuff, J. A. & Barton, G. J. (1999). Evaluation and improvement of multiple sequence methods for protein secondary structure prediction. *Proteins: Structure, Function and Genetics* **34**, 508-519.
- Cuff, J. A., Clamp, M. E., Siddiqui, A. S., Finlay, M. & Barton, G. J. (1998a). Jpred: a consensus secondary structure prediction server. *CCP11 Newsletter* **2**, 4 (6).
- Cuff, J. A., Clamp, M. E., Siddiqui, A. S., Finlay, M. & Barton, G. J. (1998b). Jpred: a consensus secondary structure prediction server. *Bioinformatics* **14**(10), 892-893.
- Cundell, D. R., Gerard, N. P., Gerard, C., Idanpaan-Heikkila, I. & Tuomanen, E. I. (1995). *Streptococcus pneumoniae* anchor to activated human cells by the receptor for platelet-activating factor. *Nature* **377**(6548), 435-438.
- Cushley, W. & Harnett, M. M. (1993). Cellular signalling mechanisms in B lymphocytes. *Biochemical Journal* **292**(2), 313-332.
- Deehan, M. R., Frame, M. J., Parkhouse, R. M., Seatter, S. D., Reid, S. D., Harnett, M. M. & Harnett, W. (1998a). A phosphorylcholine-containing filarial nematode-secreted product disrupts B lymphocyte activation by targeting key proliferative signaling pathways. *Journal of Immunology* **160**(6), 2692-2699.

- Deehan, M. R., Harnett, M. M. & Harnett, W. (1998b). A filarial nematode secreted product differentially modulates expression and activation of protein kinase C isoforms in B lymphocytes. *Journal of Immunology* **159**(12), 6105-6111.
- Deehan, M.R., Harnett, W., Harnett, M.M. (2001) A filarial nematode-secreted phosphorylcholine-containing glycoprotein uncouples the B cell antigen receptor from extracellular signal-regulated kinase-mitogen-activated protein kinase by promoting the surface Ig-mediated recruitment of Src homology 2 domain-containing tyrosine phosphatase-1 and Pac-1 mitogen-activated kinase-phosphatase. *Journal of Immunology* **166** (12), 7462-8.
- Dikshit, M., Misra, S. & Chatterjee, R. K. (1995). Cell-mediated immune response and immunoprophylactic potential of adult *Acanthocheilonema viteae* fractionated molecules. *Journal of Parasitic Diseases* **19**, 35-40.
- Dissanayake, S., Forsyth, K. P., Ismail, M. M. & Mitchell, G. F. (1984). Detection of circulating antigen in Bancroftian filariasis by using a monoclonal antibody. *American Journal of Tropical Medicine and Hygiene* **33**, 1130-1140.
- Dreyer, G., Addiss, D., Santos, A., Figueredo-Silva, J. & Noroes, J. (1998). Direct assessment *in vivo* of the efficacy of combined single-dose ivermectin and diethylcarbamazine against adult *Wuchereria bancrofti*. *Transactions of the Royal Society of Tropical Medicine and Hygiene*. **92**, 219-222.
- Egwang, T. G., Dupont, A., Akue, J. P. & Pinder, M. (1988). Biochemical and immunochemical characterisation of surface and excretory-secretory antigens of *Loa loa* microfilariae. *Molecular and Biochemical Parasitology* **31**, 251-262.
- Elkhalifa, M. Y., Ghalib, H. W., Dafaalla, T. & Williams, J. F. (1991). Suppression of human lymphocyte-responses to specific and nonspecific stimuli in human onchocerciasis. *Clinical Experimental Immunology* **86**(3), 433-439.

Evered, D., Clark, S. & Foundation, C. (1987). Filariasis. Ciba Foundation Symposium; 127, Wiley, Chicester.

Faubert, G. M. (1976). Depression of the plaque forming cells to sheep red blood cells by the new-born larvae of *Trichinella spiralis*. *Immunology* **30**, 485-489.

Feig, L. A. (1993). The many roads that lead to ras. *Science* **260**, 767-768.

Forsyth, K. P., Copeman, D. B. & Mitchell, G. F. (1984a). Differences in the surface radioiodinated proteins of skin and uterine microfilariae of *Onchocerca gibsoni*. *Molecular and Biochemical Parasitology* **10**, 217-229.

Forsyth, K. P., Copeman, D. B. & Mitchell, G. F. (1984b). *Onchocerca gibsoni*: increase of circulating egg antigen with chemotherapy in bovines. *Experimental Parasitology* **58**, 41-55.

Frishman, D. & Argos, P. (1996). Incorporation of non-local interactions in protein secondary structure prediction from the amino acid sequence. *Protein Engineering* **9**(2), 133-142.

Frishman, D. & Argos, P. (1997). Seventy-five percent accuracy in protein secondary structure prediction. *Proteins: Structure, Function and Genetics* **27**, 329-335.

García de la Torre, J., Navarro, J. S., López Martínez, M. C., Díaz, F. G. & López Cascales, J. J. (1994). HYDRO: a computer software for the prediction of hydrodynamic properties of macromolecules. *Biophysical Journal* **67**, 530-531.

Garnier, J., Osguthorpe, D. J. & Robson, B. (1978). Analysis of the accuracy and implications of simple methods for predicting the secondary structure of globular proteins. *Journal of Molecular Biology* **120**, 97-120.

Gerard, N. & Gerard, C. (1994). Receptor-dependent internalisation of platelet activating factor. *Journal of Immunology* **152**, 793-800.

Gilbert, D., Westhead, D., Nagano, N. & Thornton, J. (1999). Motif-based searching in TOPS protein topology databases. *Bioinformatics* **15**(4), 317-326.

Gingras, R., Richard, C., El-Alfy, M., Morales, C. R., Potier, M. & Pshezhetsky, A. V. (1999). Purification, cDNA cloning and expression of a new human blood plasma glutamate carboxypeptidase homologous to N-acetyl-aspartyl-a-glutamate carboxypeptidase/prostate-specific membrane antigen. *Journal of Biological Chemistry* **274**(17), 11742-11750.

Goebel, U., Sander, C., Schneider, R. & Valencia, A. (1994). Correlated mutations and residue contacts in proteins. *Proteins* **18**, 309-317

Gold, M. R., Crowley, M. T., Martin, G. A., McCormick, F. & DeFranco, A. L. (1992). Targets of the B lymphocyte antigen receptor signal transduction include the p21ras GTPase-activating protein (GAP) and two GAP-associated proteins. *Journal of Immunology* **150**, 377-386.

Goodridge, H. S., Wilson, E. H., Harnett, W., Campbell, C. C., Harnett, M. M. & Liew, F. Y. (2001). Modulation of macrophage cytokine production by ES-62, a secreted product of the filarial nematode *Acanthocheilium viteae*. *Journal of Immunology* **167**, 940

Gulbins, E., Coggeshall, K. M., Baier, G., Katzav, S., Burn, P. & Altman, A. (1993). Tyrosine kinase stimulated guanine nucleotide exchange activity of VAV in T-cell activation. *Science* **260**, 822-825.

Hagen, H. E. & Klager, S. L. (2001). Integrin-like RGD-dependent cell adhesion mechanism is involved in the rapid killing of *Onchocerca microfilariae* during early infection of *Simulium damnosum s.l.* *Parasitology* **122**, 433-438.

Harlow, E. & Lane, D. (1988). *Antibodies: A Laboratory Manual.*, Cold Spring Harbor Laboratory Press, New York.

Harnett, M. M. & Harnett, W. (1999a). Subversion of immune signalling by a phosphorylcholine-containing secreted filarial nematode glycoprotein. *Recent Research Developments in Immunology* **1**, 9-20.

Harnett, W. & Harnett, M. M. (1999b). Phosphorylcholine: friend or foe of the immune system? *Immunology Today* **20**(3), 125-129.

Harnett, M. M., Deehan, M. R., Williams, D. M. & Harnett, W. (1998). Induction of signalling anergy via the T-cell receptor in cultured Jurkat T cells by pre-exposure to a filarial nematode product. *Parasite Immunology* **20**(11), 551-563.

Harnett, W. & Harnett, M. M. (1993). Inhibition of murine B cell proliferation and down-regulation of protein kinase C levels by a phosphorylcholine-containing filarial excretory-secretory product. *Journal of Immunology* **151**(9), 4829-4837.

Harnett, W. & Harnett, M. M. (2001). Modulation of the host immune system by phosphorylcholine-containing glycoproteins secreted by parasitic filarial nematodes. *Biochimica et Biophysica Acta* **1539**, 7-15.

Harnett, W. & Parkhouse, R. M. E. (1995). Nature and function of parasitic nematode surface and excretory-secretory antigens. In *Perspectives in Nematode Physiology and Biochemistry* (Sood, M. L. & Kapur, J., eds.), pp. 207-242. Narendra Publishing House

Harnett, W., Deehan, M. R., Houston, K. M. & Harnett, M. M. (1999a). Immunomodulatory properties of a phosphorylcholine-containing secreted filarial glycoprotein. *Parasite Immunology* **21**(12), 601-608.

- Harnett, W., Deehan, M., Frame, M. J. & Harnett, M. M. (1995). Effect of phosphorylcholine-containing filarial excretory-secretory products on B-lymphocyte signaling pathways. *Journal of Cellular Biochemistry*(S21A), 167.
- Harnett, W., Frame, M. J., Nor, Z. M., MacDonald, M. & Houston, K. M. (1994). Some preliminary data on the nature/structure of the PC-glycan of the major excretory-secretory product of *Acanthocheilonema viteae* (ES-62). *Parasite* **1**(2), 179-181.
- Harnett, W., Houston, K. M., Amess, R. & Worms, M. J. (1993). *Acanthocheilonema viteae*: phosphorylcholine is attached to the major excretory-secretory product via an N-linked glycan. *Experimental Parasitology* **77**(4), 498-502.
- Harnett, W., Houston, K. M., Tate, R., Garate, T., Apfel, H., Adam, R., Haslam, S. M., Panico, M., Paxton, T., Dell, A., Morris, H. & Brzeski, H. (1999b). Molecular cloning and demonstration of an aminopeptidase activity in a filarial nematode glycoprotein. *Molecular and Biochemical Parasitology* **104**, 11-23.
- Harnett, W., Meghji, M., Worms, M. J. & Parkhouse, R. M. E. (1986). Quantitative and qualitative changes in production of excretions secretions by *litomosoides-carinii* during development in the Jird (*Meriones-Unguiculatus*). *Parasitology* **93**(2), 317-331.
- Harnett, W., Worms, M. J., Grainger, M., Pyke, S. D. & Parkhouse, R. M. (1990). Association between circulating antigen and parasite load in a model filarial system, *Acanthocheilonema viteae* in jirds. *Parasitology* **101**(3), 435-444.
- Harnett, W., Worms, M. J., Kapil, A., Grainger, M. & Parkhouse, R. M. (1989). Origin, kinetics of circulation and fate *in vivo* of the major excretory-secretory product of *Acanthocheilonema viteae*. *Parasitology* **99**(2), 229-239.

- Harwood, A. E. & Cambier, J. C. (1993). B cell antigen receptor crosslinking triggers rapid PKC independent activation of p21ras. *Journal of Immunology* **151**(9), 4513-4522.
- Haslam, S. M., Houston, K. M., Harnett, W., Reason, A. J., Morris, H. R. & Dell, A. (1999). Structural studies of N-glycans of filarial parasites. *Journal of Biological Chemistry* **274**(30), 20953-20960.
- Haslam, S. M., Khoo, K. H., Houston, K. M., Harnett, W., Morris, H. R. & Dell, A. (1997). Characterisation of the phosphorylcholine-containing N-linked oligosaccharides in the excretory-secretory 62 kDa glycoprotein of *Acanthocheilonema viteae*. *Molecular and Biochemical Parasitology* **85**(1), 53-66.
- Heldwein, K. A., Golenbock, D. T. & Fenton, M. J. (2001). Recent advances in the biology of Toll-like receptors. *Modern Aspects of Immunobiology* **1**(6), 249-252.
- Helmy, H., Weil, G. J., Faris, R., Gad, A. D., Chandrashekar, R., Ashour, A. & Ramzy, R. M. R. (2000). Human antibody responses to *Wuchereria bancrofti* infective larvae. *Parasite Immunology* **22**, 89-96.
- Heringa, J. (2000). Predicting secondary structure from protein sequence. In *Bioinformatics: Sequence, Structure and Databanks. A Practical Approach*. (Higgins, D. & Taylor, W., eds.), pp. 113-142. Oxford University Press, Oxford.
- Hertz, C. J., Kiertcher, S. M., Godowski, P. J., Bouis, D. A., Norgard, M. V., Roth, M. D. & Modlin, R. L. (2001). Microbial lipopeptides stimulate dendritic cell maturation via Toll-like receptor 2. *Journal of Immunology* **166**, 2444-2450.
- Hinsk, L. W. & Ivey, M. H. (1976). Proteinase activity in *Ascaris suum* eggs, hatching fluid and excretions secretions. *Journal of Parasitology* **62**, 771-774.

Hofmann, K., Bucher, P., Falquet, L. & Bairoch, A. (1999). The PROSITE database, its status in 1999. *Nucleic Acids Research* **27**, 215-219.

Honda, Z., Nakamura, M., Miki, I., Watanabe, T., Seyama, Y., Okado, H., Toh, H., Ito, K. & Miyamoto, T. (1991). Cloning by functional expression of platelet activation factor receptor from guinea pig lung. *Nature* **349**(342-346).

Hougard, J. M., Mbentengam, R., Lochouart, L., Escaffre, H., Darriet, F., Barbazan, P. & Quillévéré, D. (1993). Fight against *Culex quinquefasciatus* by *Bacillus sphaericus* results of a pilot campaign in a great urban centre of equatorial Africa. *Bulletin of the World Health Organisation*. **71**(3-4), 367-375.

Houston, K. M. & Harnett, W. (1996). Prevention of attachment of phosphorylcholine to a major excretory-secretory product of *Acanthocheilonema viteae* using tunicamycin. *Journal of Parasitology* **82**(2), 320-324.

Houston, K. M. & Harnett, W. (1999a). Attachment of phosphorylcholine to a nematode glycoprotein. *Trends in Glycoscience and Glycotechnology* **11**(58), 43-52.

Houston, K. M. & Harnett, W. (1999b). Mechanisms underlying the transfer of phosphorylcholine to filarial nematode glycoproteins - a possible role for choline kinase. *Parasitology* **118**, 311-318.

Houston, K. M., Cushley, W. & Harnett, W. (1997). Studies on the site and mechanism of attachment of phosphorylcholine to a filarial nematode secreted glycoprotein. *Journal of Biological Chemistry* **272**(3), 1527-1533.

Ishibashi, Y., Relman, D. A. & Nishikawa, A. (2001). Invasion of human respiratory epithelial cells by *Bordetella pertussis*: Possible role for a filamentous hemagglutinin Arg-Gly-Asp sequence and $\alpha 5 \beta 1$ integrin. *Microbial Pathogenesis* **30**, 279-288.

- Ismail, M. M., Jayakody, R. I., Weil, G. J., Nirmalan, N., Jayasinghe, K. S. A., Abeyewickrema, W., Rezvi Sheriff, M. H., Rajaratnam, H. N., Amarasekera, N., de Silva, D. C., Michalski, M. L. & Dissanaika, A. S. (1998). Efficacy of single dose combinations of albendazole, ivermectin and diethylcarbamazine for the treatment of bancroftian filariasis. *Transactions of the Royal Society of Tropical Medicine and Hygiene*. **92**, 94-97.
- Jancway, C. A. & Travers, P. (1996). *Immunobiology*. second edition (Robertson, M. & Lawrence, E., Eds.), Current Biology Ltd and Garland Publishing Inc., London.
- Kaushal, N. A., Hussain, R., Nash, T. E. & Ottensen, E. A. (1982). Identification and characterisation of excretory-secretory products of *Brugia malayi*, adult filarial parasites. *Journal of Immunology* **129**, 338-343.
- Kazura, J. W., Nutman, T. B. & Greene, B. M. (1993). Filariasis. In *Immunology and Molecular Biology of Parasitic Infections* (Warren, K. S., ed.), pp. 473-495. Blackwell Scientific Publications, Oxford.
- Kelly, S. M. & Price, N. C. (1997). Applications of circular dichroism to studies of protein folding and unfolding. *Biochimica et Biophysica Acta* **1338**, 161-185.
- Kennedy, M. W. & Harnett, W. (2001). *Parasitic Nematodes; Molecular Biology, Biochemistry and Immunology*, CABI Publishing, Oxon.
- Kijimoto-Ochiai, S. & Noguchi, A. (2000). Two peptides from CD23, including the inverse RGD sequence and its related peptide, interact with MHC Class II molecule. *Biochemical and Biophysical Research Communications* **267**(3), 686-691.
- Kim, H., Deonier, R. C. & Williams, J. W. (1977). The investigation of self-association reactions by equilibrium ultracentrifugation. *Chemical Reviews* **77**(5), 659-690.

King, R. D. & Sternberg, M. J. E. (1996). Identification and application of the concepts important for accurate and reliable protein secondary structure prediction. *Protein Science* **5**, 2298-2310.

King, R. D. (1996). Prediction of secondary structure. In *Protein Structure Prediction: A Practical Approach* (Sternberg, M. J. E., ed.), pp. 79-100. IRL Press at Oxford University Press, Oxford.

Kirkpatrick, S., Gelatt Jr, C. D. & Vecchi, M. P. (1983). Optimisation by simulated annealing. *Science* **220**, 671-680.

Knox, D. P. & Kennedy, M. W. (1988). Proteinases released by the parasite larval stages of *Ascaris suum*, and their inhibition by antibody. *Molecular and Biochemical Parasitology* **28**, 207-216.

Krutzik, S. R., Sieling, P. A. & Modlin, R. L. (2001). The role of Toll-like receptors in host defense against microbial infection. *Current Opinion in Immunobiology* **13**, 104-108.

Kuhelj, R., Dolinar, M., Pungercar, J. & Turk, V. (1995). The preparation of catalytically active human cathepsin B from its precursor expressed in *Escherichia coli* in the form of inclusion bodies. *European Journal of Biochemistry* **229**, 533-539.

Kurniawan-Atmadja, A., Sartono, E., Parono, F., Yazdanbakhsh, M. & Maizels, R. (1998). Specificity of predominant IgG4 antibodies to adult and microfilarial stages of *Brugia malayi*. *Parasite Immunology* **20**, 155-162.

Kwan-Lim, G. E., Gregory, W. F., Selkirk, M. E., Partono, F. & Maizels, R. M. (1989). Secreted antigens of filarial nematodes: a survey and characterisation of in vitro excreted/secreted products of adult *Brugia malayi*. *Parasite Immunology* **11**, 629-654.

- Laemmli, U. K. (1970). Cleavage of the structural proteins during the assembly of the head of bacteriophage T4. *Nature* **227**, 680-685.
- Lal, R. B., Kumaraswami, V., Steel, C. & Nutman, T. B. (1990). Phosphorylcholine-containing antigens of *Brugia malayi* nonspecifically suppress lymphocyte function. *American Journal of Tropical Medicine Hygiene* **42**(1), 56-64.
- Lattemann, C. T., Yan, Z.-X., Matzen, A., Meyer, T. F. & Apfel, H. (1999). Immunogenicity of the extracellular copper/zinc superoxide dismutase of the filarial parasite *Acanthocheilonema viteae* delivered by a two-phase vaccine strain of *Salmonella typhimurium*. *Parasite Immunology* **21**, 219-224.
- Laue, T. M., Shah, B. D., Ridgeway, T. M. & Pelletier, S. L. (1992). Computer-aided interpretation of analytical sedimentation data for proteins. In *Analytical Ultracentrifugation in Biochemistry and Polymer Science* (Harding, S. E., Rowe, A. J. & Horton, J. C., eds.), Chapter 7., 90-123. Royal Society of Chemistry, Cambridge.
- Lim, V. I. (1974). Algorithm for prediction of alpha-helical and beta-structural regions in globular proteins. *Journal of Molecular Biology* **88**, 857-872.
- Liu, C. H., Lin, B. Y. & Chang, L. Y. Cloning of the human aminopeptidase gene. *Unpublished*.
- Liu, Y., Wang, Y., Yamakuchi, M., Isowaki, S., Nagata, E., Kanmura, Y., Kitajima, I. & Maruyama, I. (2001). Upregulation of Toll-like receptor 2 gene expression in macrophage response to peptidoglycan and high concentration of lipopolysaccharide is involved in NF- κ B activation. *Infection and Immunity* **69**(5), 2788-2796.

Lucius, R. & Textor, G. (1995). *Acanthocheilonema viteae*: Rational design of the life cycle to increase production of parasite material with less experimental animals. *Applied Parasitology* **36**(1), 22-33.

Lucius, R., Kapuan, A. & Diesfeld, H. J. (1987). *Dipetalonema viteae* infection in three species of rodents: species specific patterns of the antibody response. *Parasite Immunology* **9**, 67-80.

Lucius, R., Textor, G., Kern, A. & Kirsten, C. (1991). *Acanthocheilonema viteae*: vaccination of jirds with irradiation-attenuated stage-3 larvae and with exported larval antigens. *Experimental Parasitology* **73**, 184-196.

Mahanty, S. & Nutman, T. B. (1995). Immunoregulation in human lymphatic filariasis - the role of interleukin-10. *Parasite Immunology* **17**(8), 385-392.

Maizels, R. M. & Lawrence, R. A. (1991). Immunological-tolerance - the key feature in human filariasis. *Parasitology Today* **7**(10), 271-276.

Maizels, R. M., Burke, J. & Denham, D. A. (1987). Phosphorylcholine-bearing antigens in filarial nematode parasites: analysis of somatic extracts and *in vitro* secretions of *Brugia malayi* and *B. pahangi*. *Parasite Immunology* **9**, 46-66.

Maizels, R. M., Denham, D. A. & Sutanto, I. (1985a). Secreted and circulating antigens of the filarial parasite *Brugia pahangi*: analysis of *in vitro* released components and detection of parasite products *in vivo*. *Molecular and Biochemical Parasitology* **17**, 277-288.

Maizels, R. M., Meghji, M. & Ogilvie, B. M. (1983). Restricted sets of parasite antigens from the surface of different stages and sexes of the nematode *Nippostrongylus brasiliensis*. *Immunology* **48**, 107-121.

Maizels, R. M., Sutanto, I., Gomez-Priego, A., Lilywhite, J. & Denham, D. A. (1985b). Specificity of surface molecules of adult *Brugia* parasites: cross-

reactivity with antibody from *Wuchereria*, *Onchocerca* and other human filarial infections. *Tropical Medicine and Parasitology* **36**, 233-237.

Marley, S. E., Lammie, P. J., Eberhard, M. L. & Hightower, A. W. (1995). Reduced antifilarial IgG4 responsiveness in a subpopulation of microfilaremic persons. *Journal of Infectious Diseases* **172**, 1630-1633.

Marques, S. A., Dy, L. C., Southall, M. D., Yi, Q., Smietana, E., Kapur, R., Marques, M., Travers, J. B. & Spandau, D. F. (2002). The platelet-activating factor receptor activates the extracellular signal-regulated kinase mitogen-activated protein kinase and induces proliferation of epidermal cells through an epidermal growth factor-receptor-dependent pathway. *Journal of Pharmacological Experimental Therapy* **300**(3), 1026-1035.

Matthews, B. E. (1982). Skin penetration by *Necator americanus* larvae. *Zeitschrift für Parasitenkunde* **68**, 81-86.

McRorie, D. K. & Voelker, P. J. (1993). *Self-associating systems in the analytical ultracentrifuge*. Analytical Ultracentrifugation, Beckman Instruments, Inc, California.

Means, T. K., Wang, S., Lien, H., Yoshimura, A., Golenbock, D. T. & Fenton, M. J. (1999). Human Toll-like receptors mediate cellular activation by *Mycobacterium tuberculosis*. *Journal of Immunology* **163**, 3920-3927.

Meghji, M. & Maizels, R. M. (1986). Biochemical properties of larval excretory-secretory glycoproteins of the parasitic nematode *Toxocara canis*. *Molecular and Biochemical Parasitology* **18**, 155-170.

Ngu, J. L., Ndume, P. M., Titanji, V. & Leke, R. (1981). A diagnostic test for *Onchocerca volvulus* infection. *Tropenmedizin und Parasitologie* **32**, 165-170.

Nicolas, L., Langy, S., Plichart, C. & Deparis, X. (1999). Filarial antibody responses in *Wuchereria bancrofti* transmission area are related to parasitological but not clinical status. *Parasite Immunology* **21**, 73-80.

Nicolas, L., Plichart, C., Nguyen, L. N. & Moulia-Pelat, J. (1997). Reduction of *Wuchereria bancrofti* adult worm circulating antigen after annual treatments of diethylcarbazine combined with ivermectin in French Polynesia. *Journal of Infectious Diseases* **175**, 489-493.

Nogami, S., Hayashi, Y., Tanaka, M., Korenaka, M., Tada, I. & Tanaka, H. (1986). Antigenic similarity of *Onchocerca volvulus* to other helminths examined by monoclonal antibodies against *O. volvulus*. *Japanese Journal of Experimental Medicine* **56**, 177-183.

Noroës, J., Dreyer, G., Santos, A., Mendes, V. G., Medeiros, Z. & Addiss, D. (1997). Assessment of the efficacy of diethylcarbamazine on adult *Wuchereria bancrofti* in vivo. *Transactions of the Royal Society of Tropical Medicine and Hygiene*. **91**, 78-81.

Nutman, T. B., Kumaraswami, V. & Ottesen, E. A. (1987a). Parasite-specific anergy in human filariasis - insights after analysis of parasite antigen-driven lymphokine production. *Journal of Clinical Investigation* **79**(5), 1516-1523.
Nutman, T. B., Kumaraswami, V., Pao, L., Narayanan, P. R. & Ottesen, E. A. (1987b). An analysis of *in vitro* B-cell immune responsiveness in human lymphatic filariasis. *Journal of Immunology* **138**(11), 3954-3959.

O'Neill, L. A. J. & Dinarello, C. A. (2000). The IL-1 receptor/toll-like receptor superfamily: crucial receptors for inflammation and host defence. *Immunology Today* **21**(5), 206-209.

Ortega-Pierres, G., Clark, N. W. T. & Parkhouse, R. M. E. (1986). Regional specialisation of the surface of a parasitic nematode. *Parasite Immunology* **8**, 613-617.

- Ottesen, E. A. (1984). Immunological aspects in lymphatic filariasis and onchocerciasis in man. *Transactions of the Royal Society of Tropical Medicine and Hygiene Supplement*, Supplement., 9-18.
- Ottesen, E. A., Duke, B. O. L., Karam, M. & Behbehani, K. (1997). Strategies and tools for the control/elimination of lymphatic filariasis. *Bulletin of the World Health Organisation* **75**(6), 491-503.
- Parkhouse, R. M. E. & Clark, N. W. T. (1983). Stage specific secreted and somatic antigens of *Trichinella spiralis* infective larvae. *Molecular and Biochemical Parasitology*, **9**(4), 319-327.
- Pastrana, D. V., Raghavan, N., Fitzgerald, P., Eisinger, S. W., Metz, C., Bucala, R., Schleimer, R. P., Bickel, C. & Scott, A. L. (1998). Filarial nematode parasites secrete a homologue of the human cytokine macrophage migration inhibitory factor. *Infection and Immunity* **66**(12), 5955-5963.
- Peitsch, M. C. (1996). ProMod and Swiss-Model: internet based tools for automated comparative modelling. *Biochemistry Society Transactions* **24**, 274-279.
- Perkins, S. J. (1986). Protein volumes and hydration effects - the calculations of partial specific volumes, neutron-scattering matchpoints and 280 nm absorption coefficients for proteins and glycoproteins from amino acid sequences. *European Journal of Biochemistry* **157**(1), 169-180.
- Perkins, S. J. (1988a). Structural studies of proteins by high-flux X-ray and neutron solution scattering. *Biochemical Journal* **254**(2), 313-327.
- Perkins, S. J. (1988b). X-ray and neutron solution scattering. In *Modern Physical Methods in Biochemistry; part B* (Neuberger, A. & Van Deenen, L. L. M., eds.), Vol. IIB, pp. Chapter 6. Elsevier Science Publishers B.V. (Biomedical Division).

Petralanda, I., Yarzabal, L. & Piessens, W. F. (1986). Studies on a filarial antigen with collagenase activity. *Molecular and Biochemical Parasitology* **19**, 51-59.

PharMingen. (1999). *Baculovirus Expression Vector System Manual*. Sixth edition, Becton Dickinson Company.

Phillipp, M., Gomez-Priego, A., Parkhouse, R. M. E., Davies, M. W., Clark, N. W., Ogilvie, B. M. & Beltran-Hernandez, F. (1984). Identification of an antigen *Onchocerca volvulus* of possible diagnostic use. *Parasitology* **89**, 295-309.

Phillipp, M., Parkhouse, R. M. E. & Ogilvie, B. M. (1980). Changing proteins on the surface of a parasitic nematode. *Nature* **287**, 538-540.

Porod, G. (1982). General theory. In *Small-Angle X-ray Scattering*. (Glatter, O. & Kratky, O., eds.). Academic Press, London.

Price, N. C. (1995). Protein analysis by circular dichroism. In *The Encyclopedia of Molecular Biology and Molecular Medicine* (Meyers, R. A., ed.), Vol. 1, pp. 384-396. VCH Press, Weinheim.

Rahman, S., Flynn, G., Aitken, A., Patel, Y., Hussain, F., Lu, X., Loftus, J. C., French, D., Wijelath, E., Strand, K. & Savidge, G. F. (2000). Differential recognition of snake venom proteins expressing specific Arg-Gly-Asp (RGD) sequence motifs by wild-type and variant integrin $\alpha_{11b}\beta_3$: further evidence for distinct sites of RGD ligand recognition exhibiting negative allostery. *Biochemical Journal* **345**, 701-709.

Ralston, G. (1993). Introduction to Analytical Ultracentrifugation. *Analytical Ultracentrifugation*, Beckman Instruments, Inc., California.

Rang, H. P., Dale, M. M. & Ritter, J. M. (1998). *Pharmacology*. Third edition (Simmons, B., Ed.), Churchill Livingstone, U.S.A.

Rhoads, M. L. (1983). *Trichella spiralis*: identification and purification of superoxide dismutase. *Experimental Parasitology* **56**, 41-54.

Rost, B. & Sander, C. (1993). Prediction of protein secondary structure at better than 70 % accuracy. *Journal of Molecular Biology* **232**, 584-599.

Rost, B. & Sander, C. (1994a). Combining evolutionary information and neural networks to predict protein secondary structure. *Proteins: Structure, Function and Genetics* **19**, 55-72.

Rost, B. & Sander, C. (1994b). Conservation and prediction of solvent accessibility in protein families. *Proteins: Structure, Function and Genetics* **20**, 216-226.

Rost, B. & Sander, C. (1998). Prediction of secondary structure. In *Predicting Protein Structure* (Webster, D. M., ed.). Human Press.

Rost, B. & Valencia, A. (1996). Pitfalls of protein sequence analysis. *Current Opinion in Biotechnology* **7**, 457-461.

Rost, B. (1996). PHD: predicting 1D protein structure by profile based neural networks. *Methods in Enzymology* **266**, 525-539.

Rost, B. (1998). Protein structure prediction in 1D, 2D and 3D. In *Encyclopedia of Computational Chemistry* (von Rague-Schleyer, P., Allinger, N. L., Clark, T. C., Gasteiger, J., Kollman, P. A. & Schaefer, H. F., eds.), pp. 2242-2255. John Wiley, Sussex.

Rost, B., Casadio, C., Fariselli, P. & Sander, C. (1995). Transmembrane helices predicted at 95 % accuracy. *Protein Science* **4**, 521-533.

Rost, B., Sander, C. & Schneider, R. (1994). Redefining the goals of protein secondary structure prediction. *Journal of Molecular Biology* **235**, 13-26.

- Saiki, R. K., Scharf, S. J., Faloona, F., Mullis, K. B. & Horn, G. T. (1985). Enzymatic amplification of beta globulin genomic sequences and restriction site analysis for diagnosis of sickle cell anemia. *Science* **230**, 1350.
- Salamov, A. A. & Solovyev, V. V. (1995). Prediction of protein secondary structure by combining nearest-neighbor algorithms and multiple sequence alignments. *Journal of Molecular Biology* **247**(1), 11-15.
- Sambrook, J., Fritsch, E. F. & Maniatis, T. (1989). *Molecular Cloning: A Laboratory Manual*. 2nd edition (Nolan, C., Ed.), Cold Spring Harbor Laboratory Press, New York.
- Sayle, R. A. & Milner-White, E. J. (1995). RASMOL: biomolecular graphics for all. *Trends in Biochemical Sciences* **20**(9), 374-376.
- Schalk, C., Remy, J. M., Chevrier, B., Moras, D. & Tarnus, C. (1992). Rapid purification of the *Aeromonas proteolytica* aminopeptidase: crystallization and preliminary X-ray data. *Archives of Biochemical Biophysics* **294**(1), 91-97.
- SchrempfEppstein, B., Kern, A., Textor, G. & Lucius, R. (1997). *Acanthocheilonema viteae*: Vaccination with irradiated L3 induces resistance in three species of rodents (*Meriones unguiculatus*, *Mastomys coucha*, *Mesocricetus auratus*). *Tropical Medicine International Health* **2**(1), 104-110.
- Schuck, P. & Demeler, B. (1999). Direct sedimentation analysis of interference optical data in analytical ultracentrifugation. *Biophysical Journal* **76**, 2288-2296.
- Selkirk, M. E., Gregory, W. F., Yazdanbakhs, M., Jenkins, R. E. & Maizels, R. M. (1990). Cuticular localisation and turnover of the major surface glycoprotein (gp29) of adult *Brugia malayi*. *Molecular and Biochemical Parasitology* **42**, 31-44.

- Semenyuk, A. V. & Svergun, D. I. (1991). GNOM - a program package for small-angle scattering data processing. *Journal of Applied Crystallography* **24**, 537-540.
- Servillo, G., Della Faziz, M. A., Piobbico, D., Castelli, M., Brancorsini, S. & Viola Magni, M. (*Unpublished*) LAL, a novel gene involved during liver regeneration. .
- Seyfried, C. E., Schweickart, V. I., Godiska, R. & Gray, P. W. (1992). The human platelet activating factor receptor gene (PTAFR) contains no introns and maps to chromosome one. *Genomics* **13**, 832-834.
- Shan, Q., Haddrill, J. L. & Lynch, J. W. (2001). Ivermectin, an unconventional agonist of the glycine receptor chloride channel. *Journal of Biological Chemistry* **276**(16), 12556-12564.
- Soboslay, P. T., Dreweck, C. M., Taylor, H. R., Brotman, B., Wenk, P. & Greene, B. M. (1991). Experimental onchocerciasis in chimpanzees; cell-mediated immune responses, and production and effects of IL-1 and IL-2 with *Onchocerca volvulus* infection. *Journal of Immunology* **147**(1), 346-353.
- Soboslay, P. T., Iuder, C. G. K., Riesch, S., Geiger, S. M., Banla, M., Batchassi, E., Stadler, A. & Schulz-key, H. (1999). Regulatory effects of Th1-type (IFN- γ , IL-12) and Th2-type cytokines (IL-10, IL-13) on parasite specific cellular responsiveness in *Onchocerca volvulus*-infected humans and exposed endemic controls. *Immunology* **97**, 219-225.
- Squire, P. G. & Himmel, M. E. (1979). Hydrodynamics and Protein Hydration. *Archives of Biochemistry and Biophysics* **196**(1), 165-177.
- Staniunas, R. J. & Hammerberg, B. (1982). Diethylcarbamazine-enhanced activation of complement by intact microfilariae of *Dirofilaria immitis* and their *in vitro* products. *Journal of Parasitology* **68**, 809-816.

- Stewart, G. R., Boussinesq, Coulson, T., Elson, L., Nutman, T. & Bradley, J. E. (1999). Onchocerciasis modulates the immune response to mycobacterial antigens. *Clinical and Experimental Immunology* **117**, 517-523.
- Stromberg, B. E. (1979). The isolation and partial characterisation of a protective antigen from developing larvae of *Ascaris suum*. *International Journal for Parasitology* **9**, 307-311.
- Sturrock, S. S. & Dryden, D. T. F. (1997). A prediction of the amino acids and structures involved in DNA recognition by type I DNA restriction and modification enzymes. *Nucleic Acids Research* **25**(17), 3408-3414.
- Svergun, D. I. (1993). A direct indirect method of small-angle scattering data treatment. *Journal of Applied Crystallography* **26**, 258-267.
- Svergun, D. I. (1999). Restoring low resolution structure of biological macromolecules from solution scattering using simulated annealing. *Biophysical Journal* **76**, 2879-2886.
- Svergun, D. I. (2000). Advanced solution scattering data analysis methods and their applications. *Journal of Applied Crystallography*. **33**, 530-534
- Svergun, D. I., Barberato, C. & Koch, M. H. J. (1995). CRY SOL - a program to evaluate X-ray solution scattering of biological macromolecules from atomic coordinates. *Journal of Applied Crystallography* **28**, 768-773.
- Systems, R. D. (2000). Innate immunity and the Toll-like receptor family. *Cytokine Bulletin, R & D Systems*, 3.
- Tamashiro, W. K., Ehrenberg, J. P., Levy, D. A. & Scott, A. L. (1986). Peptides on the surface of *Dirofilaria immitis* microfilariae. *Molecular and Biochemical Parasitology* **18**, 369-376.

Tanner, M. & Weiss, N. (1981). *Dipetalonema viteae* (filarioidea): development of the infective larvae in micropore chambers implanted into normal, infected and immunised jirds. *Transactions of the Royal Society of Tropical Medicine and Hygiene* **75**, 173-174.

Taylor, A. (1993). Aminopeptidases: towards a mechanism of action. *Trends in Biological Science* **18**, 167-172.

Taylor, M. J., Cross, H. F. & Bilo, K. (2000). Inflammatory responses induced by the filarial nematode *Brugia malayi* are mediated by lipopolysaccharide-like activity from endosymbiotic *Wolbachia* bacteria. *Journal of Experimental Medicine* **191**(8), 1429-1436.

Taylor, P. R., Botto, M., Seixas, E., Packwood, L., Langhorne, J. & Walport, M. J. (1998). Impaired clearance of malarial parasites by C1q-deficient mice is associated with an augmented IFN-gamma response. *Molecular Immunology - Meeting Abstract* **35**(6-7 SISI), 57.

Taylor, W. R. & Aszodi, A. (1994). Building protein folds using distance geometry: towards a general modelling and prediction methods. In *The Protein Folding Problem and Tertiary Structure Prediction*. (Merz, J., K. & LeGrand, S., eds.), pp. 165-192. Birkhauser, Boston.

Thoma-Uszyaski, S., Kiertscher, S. M., Ochoa, M. T., Bouis, D. A., Norgard, M. V., Miyake, K., Godowski, P. J., Roth, M. D. & Modlin, R. L. (2000). Activation of Toll-like receptor 2 on human dendritic cells triggers induction of IL-12, but not IL-10. *Journal of Immunology* **165**(7), 3804-3810.

UNDP - Special programme for research and training in tropical diseases.(1997) Prospects for elimination (for some TDR diseases): chagas' disease, leprosy, lymphatic filariasis, onchocerciasis., TDR/Gen 197.1.

van Holde, K. E. & Baldwin, R. L. (1958). Rapid attainment of sedimentation equilibrium. *Journal of Physical Chemistry* **62**, 734-743.

Vanamail, P., Ramaiah, K. D., Pani, S. P., Das, P. K. & Grenfell, B. T. (1996). Estimation of the fecund life-span of *Wuchereria bancrofti* in an endemic area. *Transactions of the Royal Society of Tropical Medicine and Hygiene* **90**, 119.

W.H.O. (1995a). Onchocerciasis. *W.H.O. fact sheet* 95.

W.H.O. (1996). Lymphatic filariasis. *W.H.O. Fact Sheet* 102.

W.H.O. (1997). Causes of death. <http://www.who.org/whr/1998/fig6e.jpg>.

W.H.O. (1998). Lymphatic filariasis. *W.H.O. fact sheet* 189.

W.H.O. (1999a). Eliminating lymphatic filariasis. <http://www.filariasis.org.html>.

W.H.O. (1999b). Tropical diseases. <http://www.who.int/ctd/html/aboutctd.html>.

W.H.O. (1995b). Tropical Disease Research Highlights 1993-1994. W.H.O.

W.H.O. (1997). Prospects for elimination (for some TDR diseases): chagas' disease, leprosy, lymphatic filariasis, onchocerciasis.

W.H.O./C.T.D. (1998). *Annual Report*. W.H.O.

Walter, R. D., Arias, A. E., Rathaur, S. & Dickmann, E. F. (1987). Secretory proteins from *Onchocerca volvulus* during *in vitro* maintenance. *Tropical Medical Parasitology* **28**, 339-350.

Weil, G. J., Steel, C., Liftis, F., Li, B.-W., Mearns, G., Lobos, E. & Nutman, T. B. (2000). A rapid-format antibody card test for diagnosis of onchocerciasis. *Journal of Infectious Diseases* **182**(6), 1796-1799.

- Weiss, N. & Tanner, M. (1981). Experimental filariasis in the Syrian hamster: Immunological aspects of complex host-parasite-interactions. *Hamster Immune Response in Infectious and Oncologic Diseases* pp. 253-265. Plenum Publishing Corporation, New York.
- Wenger, J. D., Forsyth, K. P. & Kuzura, J. W. (1988). Identification of phosphorylcholine epitope containing antigens in *Brugia malayi* and relation of serum epitope levels to infection status of jirds with Brugian filariasis. *American Journal of Tropical Medicine and Hygiene* **38**, 133-141.
- Werren, J. H. (1997). Biology of Wolbachia. *Annual Review of Entomology* **42**, 587-609.
- Westhead, D. R., Slidel, T. W. F., Flores, T. P. J. & Thornton, J. M. (1999). Protein structural topology: automated analysis and diagrammatic representation. *Protein Science* **8**, 897-904.
- Whelan, M., Harnett, M. M., Houston, K. M., Patel, V., Harnett, W. & Rigley, K. P. (2000). A filarial nematode-secreted product signals dendritic cells to acquire a phenotype that drives development of Th2 cells. *Journal of Immunology* **164**, 6453-6460.
- Wilson, M. L. (1993). Avermectins in arthropod vector management - prospects and pitfalls. *Parasitology Today* **9**(3), 83-87.
- Wilson, E.H., Dechan, M.R., Katz, E., Goodridge, H.S., Brown, K.S., Houston, K.M., Watson, K., Harnett, M.M., Harnett, W. (2002). Secreted Filarial Nematode Phosphorylcholine Containing Glycoprotein ES-62 Anergise B2 Lymphocytes, Activates B1 Lymphocytes and Polarises T Lymphocyte Responses *in vivo*. *Infection and Immunity*, Submitted.
- Winkler, S., Menyawi, I. E., Linnau, K. F. & Graninger, W. (1998). Short Report: Total serum levels of the nitric oxide derivatives nitrite/nitrate during

microfilarial clearance in human filarial disease. *American Journal of Tropical Medicine and Hygiene* **59**(4), 523-525.

Xu, Y., Tao, X., Shen, B., Horng, T., Medzhitov, R., Manley, J. L. & Tong, L. (2000). Structural basis for signal transduction by the Toll/interleukin-1 receptor domain. *Nature* **408**, 111-115.

Yphantis, D. A. (1964). Equilibrium ultracentrifugation in dilute solutions. *Biochemistry* **3**, 297-317.

Zahner, H. & Schares, G. (1993). Experimental chemotherapy of filariasis: Comparative evaluation of the efficacy of filaricidal compounds in *Mastomys coucha* infected with *Litomosoides carinii*, *Acanthocheilonema viteae*, *Brugia malayi* and *B. pahangi*. *Acta Tropica* **52**, 221-266.

Zvelebil, M. J., Barton G.J., Taylor W.R. & Sternberg, M.J., (1987). Prediction of protein secondary structure and active sites using the alignment of homologous sequences. *Journal of Molecular Biology* **195**(4), 957-961.

Appendix 1: Bioinformatics CD

This appendix explains how to use the CD enclosed in this thesis as a supplement to Chapter 3 and Chapter 4. The CD contains 2 folders; Web Page and Structures.

The Web Page folder contains a web page consisting of links to the programs discussed in Chapter 3. This web page can be viewed by opening through an internet browser such as Netscape Navigator.

The structures folder contains a number of pdb and script files as well as the program RasMol (Sayle & Milner-White, 1995) (an Apple Macintosh Version) which can be used to view the pdb files. The script files are for use with RasMol. Table 1 gives a list of the pdb files supplied, details of the structure and the accompanying script file. To view any of the structures open RasMol and then select the open command in the file menu and select the pdb file to view. Next open the accompanying script file in a text viewing program such as Microsoft Word and copy and paste the contents into the command window within RasMol. This will result in the structure being displayed as described in Chapter 3 or 4 with the relevant sections highlighted. The structure can then be moved using either a mouse or the scroll bars on the window. The pdb files generated by DAMMIN; DAMMIN_P1.pdb, DAMMIN_P2.pdb and DAMMIN_P222.pdb, when viewed in RasMol, do not appear as shown in Figure 4-20. This is due to an inability of RasMol to increase the size of the beads such that they overlap. Use of Assa, a modelling program downloadable using anonymous FTP from <ftp.embl-hamburg.de>, directory /sax, to view these files overcomes this problem as bead size can be increased so that the beads overlap.

pdb file	Structure	Script file
lamph.pdb	Residues 74-168 of the leucyl aminopeptidase from <i>Aeromonas proteolytica</i> (homologous to residues 252-343 of ES-62).	lamph.script
DAMMIN_P1.pdb	Structure obtained from DAMMIN when P1 symmetry was imposed.	DAMMIN.script
DAMMIN_P2.pdb	Structure obtained from DAMMIN when P2 symmetry was imposed.	DAMMIN.script
DAMMIN_P222.pdb	Structure obtained from DAMMIN when P222 symmetry was imposed.	DAMMIN.script
Dragon_all.pdb	All the structures obtained for ES-62 in its entirety from the different iterations of DRAGON.	Dragon_all.script
ES62h.pdb	The structure of the region of ES-62 (residues 252-343) homologous to residues 74-168 of the leucyl aminopeptidase from <i>Aeromonas proteolytica</i> , generated by DRAGON.	ES62h.script
ES62_best.pdb	The highest ranked structure of ES-62 generated by DRAGON.	ES62_best.script

Table 1: pdb and script files.

Appendix 2: Input Files for DRAGON

This section outlines the text of the DRAGON input files for the modelling of residues 252-343 of ES-62, homologous to residues 74-168 of the leucyl aminopeptidase from *Aeromonas proteolytica* (Chevrier *et al.*, 1996; Chevrier *et al.*, 1994; Schalk *et al.*, 1992). Strictness values where mentioned are between 0.0 (totally unreliable) and 1.0 (absolute certainty). Lines in input files which start with # are comment lines not read by DRAGON. Text on the right hand side of the page provides an explanation as to the content of the files.

Alnfm file: Multiple alignment file

```
MSF of: mul.aln from: 1 to: 100
mul.aln MSF: 100 Type: P 13-Jan-99 11:45:4 Check: 0 ..
Name: es62h Len: 100 Check: 8786 Weight: 1.55
Name: hematopoietic Len: 100 Check: 4681 Weight: 1.55
Name: Bacterial Len: 100 Check: 3967 Weight: 0.63
Name: LAMP Len: 100 Check: 3967 Weight: 0.63
Name: leucine Len: 100 Check: 3967 Weight: 0.63
//
es62h NSSNLIFEIT GSERPSEVVL LSAHVDSW.. .....DVGQGalDDGAGCA
hemato DSFNTVAEIT GSKYPEEVVL VSGHLD SW.. .....DVGQGalDDGGGAF
Bacterial NQKSVMTIT GSEAPDEWIV IGGHLDSTIG SHTNEQSVAPGADDDASGIA
LAMP NQKSVMTIT GSEAPDEWIV IGGHLDSTIG SHTNEQSVAPGADDDASGIA
leucine NQKSVMTIT GSEAPDEWIV IGGHLDSTIG SHTNEQSVAPGADDDASGIA

es62h VVWSALHSLK KLAERNPKFK PKRTIRGIFW TSEEQGYGGAkHYIITHKND
hemato ISWEALSLVK DLGLR..... PKRTLRLVLW TAEEQGGVGASQYYELHK..
Bacterial AVTEVIRVLS ENNFQ..... PKRSIAFMAY AAEEVGLRGSQDLANQYKSE
LAMP AVTEVIRVLS ENNFQ..... PKRSIAFMAY AAEEVGLRGSQDLANQYKSE
leucine AVTEVIRVLS ENNFQ..... PKRSIAFMAY AAEEVGLRGSQDLANQYKSE
```

Accfm file: Residue accessibility file

b 8 22 43 84	Residues 8, 22, 43 and 84 are probably buried (b)
s 1 3 14 15 16 17 18 19 31	Residues 1, 3, 14-19, 31, 38-39, 41, 48, 54-55, 57-
s 38 39 41 48 54 55 57 58	62, 64, 66-67, 77, 80, 82, 85-86, 89, 90 and 92
s 59 60 61 62 64 66 67 77	probably lie on the surface of ES-62 (s).
s 80 82 85 86 89 90 92	

Restrfnm file: Distance restraints file

```
# dist.restr
# 13-Jan-1999.
4 72 4.50 4.70 1.0 CA CA
4 80 9.90 10.1 1.0 CA CA
9 65 8.50 8.70 1.0 CA CA
14 65 4.80 5.00 1.0 CA CA
24 38 7.90 8.10 1.0 CA CA
24 72 4.15 4.35 1.0 CA CA
```

Lines with # symbols are comment lines and are not read by DRAGON.

The distance between the C α atoms of residues 4 and 72 is between 4.5 and 4.7 Å and the strictness value is 1, meaning absolute certainty. The rest of the file delineates distance restraints between other atoms laid out in the same way as described for the first line.

Sstrfnn file: Secondary structure file

```
#es62h
#es62 homologous to lamp
SHEET 0.7
STRAND 4 9
STRAND 65 72 ANTI 65 9
14 24 PAR 14 65
END
ALPHA 38 56
ALPHA 80 91
```

Lines with # symbols are comment lines and are not read by DRAGON.

Sheet with strictness value of 0.7

First strand of sheet, residues 4-9

2nd strand (65-72) anti parallel to 1st strand residues

65 & 9 hydrogen bonded, 3rd strand (14-24) parallel to 2nd, residues 14 & 65 hydrogen bonded.

α -helix comprising residues 38-56

α -helix comprising residues 80-91

This section outlines the text of the DRAGON input files for the modelling of ES-62 in its entirety.

Alnfrm file:

```
MSF of: mul.aln from: 1 to: 555
mul.aln MSF: 555 Type: P 22-Mar-009 11:45:4 Check: 0 ..
Name: ES62 Len: 555 Check: 3315 Weight: 2.67
Name: plasma Len: 555 Check: 8097 Weight: 0.71
Name: amino Len: 555 Check: 3633 Weight: 0.71
Name: switch Len: 555 Check: 4113 Weight: 0.34
Name: liver Len: 555 Check: 4237 Weight: 0.34
Name: mouse Len: 555 Check: 4560 Weight: 0.79
Name: hemato Len: 555 Check: 4992 Weight: 1.43
//
ES62 MLLNSSTFFF LVTLTVVLGA AVLPDKTVAP KNY..IQETF GK..EVAE.L
plasma MKFLIFAFFG GVHLLSLCSG KAICKNGISK RTFEEIKEEI ASCGDVAKAI
amino MKFLIFAFFG GVHLLSLCSG KAICKNGISK RTFEEIKEEI ASCGDVAKAI
switch MRFLFFLFVA VVHLFSLGSG KAIYKSGVSQ RTFQEIKEEI ANYEDVAKAI
liver MRFLFFLFVA VVHLFSLGSG KAIYKSGVSQ RTFQEIKEEI ANYEDVAKAI
mouse MRSLEFLFI .VHLLALGSG KAVFKNGVSQ RTFREIKEEI ANYEDVAKAI
hemato MRSLEFLFI .VHLLALGSG KAVFKNGVSQ RTFREIKEEI ANYEDVAKAI

ES62 IQYITKGEEV GLAYQWLSKL VDGFGHRMVG SDSLEKSIAF LEESLKNDNF
plasma INLAVYGKAQ NRSYERLALL VDTVGPRLSG SKNLEKAIQI MYQNLQQDGL
amino INLAVYGKAQ NRSYERLALL VDTVGPRLSG SKNLEKAIQI MYQNLQQDGL
switch INLAVYGKYQ NRSYERLGLL VDTVGPRLSG SKNLEKAIQI MYQNLQQDGL
liver INLAVYGKYQ NRSYERLGLL VDTVGPRLSG SKNLEKAIQI MYQNLQQDGL
mouse INLAVYGKYQ NRSYERLGLL VDTVGPRLSG SKNLEKAIQI MYQNLQQDGL
hemato INLAVYGKYQ NRSYERLGLL VDTVGPRLSG SKNLEKAIQI MYQNLQQDGL

ES62 DKVHTEEVPN LPHWVRGNDV VEMIEPRNQR LNVLAIG... GSEPASATGE
plasma EKVHLEPV.R IPHWERGEES AVMLEPRIHK IAILGLGSSI GTPPEGITAE
amino EKVHLEPV.R IPHWERGEES AVMLEPRIHK IAILGLGSSI GTPPEGITAE
switch ENVHLEQV.R IPHWERGEES AVMVVPRIHK LAILGLGSSI GTPPEGITAE
liver ENVHLEQV.R IPHWERGEES AVMVVPRIHK LAILGLGSSI GTPPEGITAE
mouse ENVHLEQV.R IPHWERGEES AVMLEPRIHK MAILGLGSSI GTPPGGITAE
hemato ENVHLEQV.R IPHWERGEES AVMLEPRIHK MAILGLGSSI GTPPGGITAE

ES62 VTVIYDLDV ..KPDDVRGK IVVTAQTFAG YPLTLKYR.R SVKLFEQLGA
plasma VLVVTSFDEL QRRASEARGK IVVYNQPYIN YSRTVQYRTQ GAVEAAKVGA
amino VLVVTSFDEL QRRASEARGK IVVYNQPYIN YSRTVQYRTQ GAVEAAKVGA
switch VLVVASFVEL QRRASEARGK IVVYNQPYTD YGKTVQYRER GAVEAAKVGA
liver VLVVASFVEL QRRASEARGK IVVYNQPYTD YGKTVQYRER GAVEAAKVGA
mouse VLVVASFDEL QRRASEARGK IIVYNQPYTG YEKTVQYRVQ GAVEAAKVGA
hemato VLVVASFDEL QRRASEARGK IIVYNQPYTG YEKTVQYRVQ GAVEAAKVGA

ES62 IGVLVKSITS FSINSPHTGT GAENT...TI PAACLTIEEA EMLERLYRSG
plasma LASLIRSVAS FSIYSPHTGT QEYQDGVPKI PTACITVEDA EMMSRMASHG
amino LASLIRSVAS FSIYSPHTGT QEYQDGVPKI PTACITVEDA EMMSRMASHG
switch VASLIRSVAS FSIYSPHTGH QGYQDGVPKI PTACITIEDA EMMSRMASRG
liver VASLIRSVAS FSIYSPHTGH QGYQDGVPKI PTACITIEDA EMMSRTASRG
mouse VASLIQSVAS FSIYSPHTGT QKYQDGVPKI PTACITVEDA EMMSRMASRG
hemato VASLIQSVAS FSIYSPHTGT QKYQDGVPKI PTACITVEDA EMMSRMASRG
```

ES62	KKIVIRMDMK	SHYEETINSS	NLIFEITGSE	RPSEVVLLSA	HVDSWDVGQG
plasma	IKIVIQLKMG	AKTYPDTDSF	NTVAEITGSK	YPEQVVLVSG	HLDSWDVGQG
amino	IKIVIQLKMG	AKTYPDTDSF	NTVAEITGSK	YPEQVVLVSG	HLDSWDVGQG
switch	DKIVIHLMKG	AKTYPDTDSF	NTVAEITGSK	YPEEVVLVSG	HLDSWDVGQG
liver	DKIVIHLMKG	AKTYPDTDSF	NTVAEITGSK	YPEEVVLVSG	HLDSWDVGQG
mouse	NKIVIHLEMG	AKTYPDTDSF	NTVAEITGSM	YPEEVVLVSG	HLDSWDVGQG
hemato	NKIVIHLEMG	AKTYPDTDSF	NTVAEITGSM	YPE.....DVGQG
ES62	ALDDGGGCAV	VWSALHSLKK	LAERNPKFKP	KRTIRGIPWT	SEEQGYGGAK
plasma	AMDDGGGAFI	SWEALSLIKD	LGLR.....P	KRTLRLVLWT	AEEQGGVGAF
amino	AMDDGGGAFI	SWEALSLIKD	LGLR.....P	KRTLRLVLWT	AEEQGGVGAF
switch	ALDDGGGAFI	SWEALSLVKD	LGLR.....P	KRTLRLVLWT	AEEQGGVGAS
liver	ALDDGGGAFI	SWEALSLVKD	LGLR.....P	KRTLRLVLWT	AEEQGGVGAS
mouse	ALDDGGGAFI	SWEALSLVKD	LGLR.....P	KRTLRLVLWT	AEEQGGIGAS
hemato	ALDDGGGAFI	SWEALSLVKD	LGLR.....P	KRTLRLVLWT	AEEQGGIGAS
ES62	HYIITHKNDS	PEKFYFVSET	DTGTFKSTNW	LAHLSFSGDK	KSMRLRLKEIT
plasma	QYYQLHKVNI	.SNYSLVME	DAGTFLPTG.	...LQFTGSE	KARAIMEEVM
amino	QYYQLHKVNI	.SNYSLVME	DAGTFLPTG.	...LQFTGSE	KARAIMEEVM
switch	QYYELHKANI	.SKYSLVMEA	DSGTFLPTG.	...LQFTGSD	KARAIMKEVM
liver	QYYELHKANI	.SKYSLVMEA	DSGTFLPTG.	...LQFTGSD	KARAIMKEVM
mouse	QYYELHKANI	.SKYSLVMEA	DSGTFLPTG.	...LQFTGSD	KARAIMKEVM
hemato	QYYELHKANI	.SKYSLVMEA	DSGTFLPTG.	...LQFTGSD	KARAIMKEVM
ES62	RLLSRNGIAL	GLINSSVQGD	VTFWAKDGIP	SVNYIPDKAV	DYYFYFHETA
plasma	SLLQPLNITQ	.VLSHGEGTD	INFWIQAGVP	GASLLDD..L	YKYFFFHESH
amino	SLLQPLNITQ	.VLSHGEGTD	INFWIQAGVP	GASLLDD..L	YKYFFFHESH
switch	SLLQPLNITK	.VFNDABGTD	INFWIQAGVP	GASLRDD..L	YKYFFFHESH
liver	SLLQPLNITK	.VFNDABGTD	INFWIQAGVP	GASLRDD..L	YKYFFFHESH
mouse	NLLQPLNVTK	.VFSNGEGTD	INFWIQAGVP	GASLRDD..L	YKYFFFHESH
hemato	NLLQPLNVTK	.VFSNGEGTD	INFWIQAGVP	GASLRDD..L	YKYFFFHESH
ES62	GDYMTVLKDG	DLEYTTSIFA	TLGHVIANMD	DWGSDPNQPQ	QLNSKQSTTE
plasma	GDTMTVMDBS	RWMLLLLFGL	LFLMLLQTWK	KCCLGPRNSK	KETTFSCFWPG
amino	GDTMTVMDBK	QMNVAADVWA	VVSYYVADME	EML..PRS..
switch	GDTMTAMDBK	QMNVAADVWA	VVAYVVADME	EML..PRS..
liver	GDTMTAMDBK	QMNVAADVWA	VVAYVVADME	EML..PRS..
mouse	GDTMTVMDBK	QMNVAADVWA	VVAYVVADMD	EML..PRS..
hemato	GDTMTSWIQS	R.....
ES62	KSDRKKL...
plasma	ILGLQLWKTP	LHITISSNSS	SKENSISCFL	LLSFLILSKF	SDSRKRNHSP
amino
switch
liver
mouse
hemato
ES62
plasma	LPPTT
amino
switch
liver
mouse
hemato

Accfnum file:

b 10 62 82 129 130 161 162 219
 b. 239 241 259 273 294 335 353

s 19 21 25 26 27 28 29 30 31 32
 s 35 36 37 39 40 41 44 47 51 53
 s 54 55 56 60 61 64 67 71 77 78
 s 80 81 84 87 88 89 91 92 93 94
 s 96 97 100 101 102 104 105 108
 s 110 111 112 112 114 117 120 122
 s 124 125 133 135 136 137 138 148
 s 150 151 153 154 155 156 157 158
 s 167 169 170 172 173 176 180 181
 s 183 186 187 203 209 210 211 212
 s 213 214 215 218 224 225 227 230
 s 231 234 235 237 238 242 244 246
 s 248 249 250 251 252 254 265 266
 s 267 268 269 270 282 289 290 292
 s 299 305 306 308 309 310 311 312
 s 313 315 317 318 328 331 333 336
 s 337 340 341 343 344 345 346 347
 s 348 349 355 358 362 363 364 365
 s 371 373 374 375 376 377 379 381
 s 383 387 390 393 400 401 402 403
 s 404 405 412 413 422 424 436 444
 s 445 446 447 449 464 466 467 469
 s 470 471 473 474 475 476 477 478
 s 479 480 481 482 483 484 485 486
 s 487 488 489 490 491 492

Restrfnum file:

#JPREDDES62.restr
 51 57 8.5 9.5 0.5 CA CA
 79 67 9.8 10.8 0.5 CA CA
 116 342 2.5 3.5 0.5 CA CA
 119 337 4.3 5.3 0.5 CA CA
 337 355 2.5 3.5 0.5 CA CA
 399 407 2.5 3.5 0.5 CA CA
 142 326 3.8 4.8 0.5 CA CA
 148 160 4.4 5.4 0.5 CA CA
 148 320 6.3 7.3 0.5 CA CA
 223 164 2.8 3.8 0.5 CA CA
 226 142 4.7 5.7 0.5 CA CA
 244 258 4.2 5.2 0.5 CA CA
 258 275 2.5 3.5 0.5 CA CA
 270 263 7.8 8.8 0.5 CA CA

Sstrfnm file:

```
ALPHA 38 51
# 5
ALPHA 57 67
# NO 6 OR 7
# 10 + 25 + 26 + 30
SHEET
STRAND 116 119
STRAND 337 342 ANTI 342 116
STRAND 350 355 ANTI 350 342
STRAND 428 433 PAR 428 350
END
# 8 +9
ALPHA 79 91
# 24 + 13 + 14 + 17
SHEET
STRAND 320 326
STRAND 142 148 ANTI 142 326
STRAND 160 164 ANTI 164 142
STRAND 219 223 PAR 219 164
END
# 15
ALPHA 174 187
# 16
ALPHA 190 197
# 18
ALPHA 226 234
# NO 19
# 20 + 21 + 22
SHEET
STRAND 238 244
STRAND 258 263 ANTI 263 238
STRAND 270 275 ANTI 270 263
END
# 23
ALPHA 298 307
# 27
ALPHA 376 389
# 28 + 29
SHEET
STRAND 395 399
STRAND 407 412 ANTI 407 399
END
# 31
ALPHA 448 467
```